Chlorinated Very Short-Lived Substances: Modelling their global emissions and impact on stratospheric ozone

Tom Claxton MSci, MA, MSc

Lancaster Environment Centre, Lancaster University, UK

September 2020

This dissertation is submitted for the degree of Doctor of Philosophy

Abstract

Chlorinated Very Short-Lived Substances: Modelling their global emissions and impact on stratospheric ozone

Tom Claxton MSci, MA, MSc

Lancaster Environment Centre, Lancaster University, UK

September 2020

Since the discovery of the damaging effects of chlorofluorocarbons, stratospheric ozone has been studied extensively in the last 50 years. While the Montreal Protocol and amendments have largely nullified the threat from long-lived ozone-depleting gases, emerging evidence suggests uncontrolled chlorinated compounds, Very Short-Lived Substances (Cl-VSLS), present a barrier to timely ozone recovery. This thesis extends scientific understanding of Cl-VSLS emissions and impacts, combining observations, inversion methods and a 3-D chemistry transport model.

This work calculates policy-relevant *ozone depletion potentials* (ODPs) of four Cl-VSLS (CH_2Cl_2, $CHCl_3$, C_2Cl_4, $C_2H_4Cl_2$) using a troposphere-stratosphere modelling system. The influence of emission location and season on the ODPs is investigated. Whilst little seasonal variability exists, the location of emissions exerts a strong influence, with the largest ODPs due to Tropical Asian emissions. Chloroform ($CHCl_3$) and dichloromethane (CH_2Cl_2) have the largest ODPs (up to ~0.02-0.03), comparable to some long-lived halocarbons restricted by the Montreal Protocol.

A synthesis inversion is used to calculate regional Cl-VSLS fluxes based on minimising differences between modelled and observed abundances with prior constraints. Over 2007-2017, global CH_2Cl_2 emissions increase significantly due to increasing Asian emissions, while C_2Cl_4 emissions decrease, from diminishing uses in Europe and North America. The emissions are evaluated and provide a good match to assimilated observations and those independent to the inversion.

Stratospheric impacts of Cl-VSLS are investigated using time-varying emissions. The stratospheric input of chlorine from Cl-VSLS and products increased by 43% between 2007 and 2017, from 92.3 ± 5.0 ppt Cl to 132.1 ± 8.9 ppt Cl. Stratospheric model simulations show marked decrease in lower stratospheric ozone due to Cl-VSLS. In 2017, over Antarctica, Cl-VSLS reduced lower stratospheric ozone by 1.2% and the global mean column reduction was 0.4% (-1.2 DU). Increasing Asian emissions indicate potential for greater future impacts. Hence, Cl-VSLS should continue to be monitored.

Acknowledgements

Firstly, I would like to sincerely thank my supervisors Dr Ryan Hossaini and Prof Oliver Wild throughout the duration of my studies. Ryan's advice and direction have been invaluable week in week out, and Oliver has always been there if required. In addition to their guidance, there has always been a supporting network from the wider atmospheric and climate modelling community at Lancaster, especially Dr Ewa Bednarz and Dr Amber Leeson, and all my fellow PhD researchers/post docs.

Additionally, I was externally supervised by Dr Chris Wilson and Prof Martyn Chipperfield from the University of Leeds, whose expertise have been invaluable, particularly Chris' knowledge on synthesis inversion. I would like to give a large thank you to all whom I have collaborated with over the last 4 years, and to colleagues I would never have met otherwise.

A PhD isn't just about academia, and a big part of my life has been on the frisbee pitch, perhaps when I should have been spending more time doing research. I couldn't have made it to this point without all the love from the Fish, and it's sad that global circumstances have ruptured the chance for us to spend more of my last year together, and to say farewell. Another thank you to my parents for supporting me and housing me during these last few months. And a final thanks to Simon, the best and most patient boyfriend one could ever hope for!

Contents

List of Figures

List of Tables

Chapter 1

Introduction and Thesis Aims

The work in this thesis concerns chlorinated very short-lived substances (Cl-VSLS), gases which have not been included in the regulation of ozone-depleting substances (ODSs) by the UN Montreal Protocol and its amendments. This work includes investigation into the time-varying regional and global emissions of Cl-VSLS, the transport of these gases to the stratosphere, and their impact on stratospheric ozone.

The Earth's atmosphere is separated into multiple different layers, with the two lowest layers, the troposphere and stratosphere, the most vital for life. The troposphere is closest to the surface and comprises ~80% of the total mass of the atmosphere [Pandis et al., 1995]. At roughly 10-17 km, depending on latitude, the troposphere ends and the stratosphere begins, with the boundary between the two layers known as the tropopause [Gettelman et al., 2011]. Tropospheric chemistry and composition are strongly influenced by emissions from the surface. These emissions can come from a range of natural sources; however, in the last several centuries anthropogenic emissions have played an increasingly important role in contributing to several environmental issues, including air pollution and climate change. Although the stratosphere is not as *directly* impacted by surface emissions, its composition has been vastly altered by the production and emission of ODSs, such as chlorofluorocarbons (CFCs), in the mid-20th Century.

The ozone layer, which lies between 19-30 km in altitude [Sivasakthivel and Reddy, 2011], wholly in the stratosphere, forms a protective shield around the planet from damaging high energy UV solar radiation. The ozone layer absorbs 93-99% of this radiation [WMO, 1998], which means that should this layer disappear or be seriously depleted, life on Earth will be severely affected. Most long-lived ODSs (e.g. CFCs) are inert in the troposphere. However, in the stratosphere they photolyse to produce chlorine (Cl) and/or bromine (Br) atoms

[Molina and Rowland, 1974; Yung et al., 1980]. Significant global ozone depletion throughout the middle of the 20th Century led to increased springtime Antarctic ozone loss, known as the “ozone hole” phenomenon. As a consequence, the Montreal Protocol was enacted to prevent the production and consumption of CFCs and similarly destructive compounds. Due to this widely successful legislation, ozone levels are expected to recover to pre-depletion levels towards the end of this century [Dhomse et al., 2018]. However, Cl-VSLS may alter the predicted recovery time by at least several years, but possibly much longer [Hossaini et al., 2017].

Cl-VSLS are substances with short tropospheric lifetimes, defined as less than 6 months [Carpenter et al., 2014]. This is in contrast with the much longer lifetimes, of the order of decades, of most gases synonymous with ozone depletion (e.g. CFCs). However, transport from the troposphere to the stratosphere can be sufficiently rapid such that Cl-VSLS can reach the lower stratosphere despite their short tropospheric lifetimes, as evidenced by aircraft measurements [e.g. Leedham Elvidge et al., 2015; Oram et al., 2017]. Although relative ozone concentrations are greatest at around 25 km, due to atmospheric mass decreasing with pressure the greatest absolute ozone concentrations are at 15-20 km [Jia et al., 2015]. Therefore, Cl-VSLS – which are thought to breakdown in the lowermost stratosphere – may pose a greater potential to destroy ozone than previously thought. Since the Montreal Protocol does not regulate these substances, their increased atmospheric emissions in recent years could lead to increased significance as sources of stratospheric chlorine, despite currently only contributing 3% of total tropospheric chlorine [Carpenter et al., 2014; Leedham Elvidge et al., 2015].

The regional distribution and magnitude of Cl-VSLS emissions are not well understood, despite steady increases over the last decade [Engel et al., 2018]. Important Cl-VSLS include dichloromethane (CH_2Cl_2), chloroform ($CHCl_3$) and perchloroethylene (C_2Cl_4). These are all used industrially as solvents, in a variety of applications; however, 50-90% of $CHCl_3$ emissions are thought to be natural [McCulloch, 2003; Worton et al, 2006], as opposed to mainly anthropogenic sources for CH_2Cl_2 and C_2Cl_4. Global emissions of Cl-VSLS have previously been categorised and quantified by source type [Keene et al.,

1999; Khalil et al., 1999]; however, there has been little concerted effort to quantify global Cl-VSLS emissions since these older studies. Regionally, there have been select studies on European [Simmonds et al., 2006] and East Asian [Feng et al., 2019; Oram et al., 2017; Say et al., 2019] emissions, but these do not paint a global picture. In addition, the impacts of Cl-VSLS on ozone are poorly quantified.

The **overarching aim** of this thesis is to provide new scientific understanding and policy-relevant information on the sources of Cl-VSLS and their impact on stratospheric ozone. The **specific thesis aims** are to:

- **Quantify the ozone-depletion potential (ODP) of key Cl-VSLS as a function of emission location and season.** ODP is an important metric for discussing policy implications for halogenated compounds, as each halocarbon can be compared and ranked based on their ability to destroy stratospheric ozone. For short-lived compounds, such as Cl-VSLS, ODPs are not well known, despite being thought to cause ozone destruction.

- **Investigate regional and global trends in Cl-VSLS emissions using atmospheric observations and an inverse modelling framework.** This framework, known as "synthesis inversion", uses a chemical transport model to determine the sensitivity of the Cl-VSLS abundance at global measurement sites to regional surface emissions. Posterior emissions are generated based on minimising the difference between the model and assimilated observations, within prior emission constraints. An inversion results in a series of optimised transient emission fields that accurately captures trends in Cl-VSLS and can be used as input in models for further Cl-VSLS studies.

- **Quantify the contribution of Cl-VSLS to stratospheric chlorine and assess their impact on stratospheric ozone in the present day and recent past.** Using the newly optimised emissions, perform an end-to-end model study to determine how the stratospheric injection of chlorine

from Cl-VSLS and their products has changed over time. Particular emphasis will be placed on comparing recent ozone depletion based on scenarios with and without the influence of transient Cl-VSLS emissions.

The remainder of this thesis is organised as follows. Chapter 2 presents the background to this thesis and our current understanding. It describes the main chemistry schemes present in both the stratosphere and troposphere, and the impacts chlorine have on stratospheric ozone. It also provides an introduction to several Cl-VSLS studied during my PhD, and our current understanding of their emissions, chemistry, and projected impacts on ozone. There is also a brief description of chemistry transport models and previous use of the synthesis inversion process.

Chapter 3 is chiefly adapted from my lead-author paper [Claxton et al., 2019] that quantifies new ODP values for four Cl-VSLS; CH_2Cl_2, $CHCl_3$, C_2Cl_4 and ethylene dichloride ($C_2H_4Cl_2$). These are quantified using (a) the TOMCAT model to assess the transport of chlorine to the stratosphere due to surface Cl-VSLS emissions and (b) SLIMCAT to investigate the impact of these chlorine perturbations on column ozone levels. Particular attention is given to understanding how the location and season of Cl-VSLS emission may affect the ODP.

Chapter 4 presents results from a synthesis inversion to calculate optimised CH_2Cl_2 and C_2Cl_4 emissions for the period 2006-17, chiefly adapted from my lead-author paper [Claxton et al., 2020]. The chapter details the inputs to the inversion, including (a) prior emission fields derived from bottom-up industry estimates and the Reactive Chlorine Emissions Inventory (RCEI), (b) assimilated observations of Cl-VSLS from two separate global measurement networks, and (c) TOMCAT model output to determine the gridded sensitivity of Cl-VSLS concentrations to emissions from different geographical regions. The performance of posterior emissions is evaluated using a range of datasets and the success of the inversion is discussed. This study is also subjected to various sensitivity tests, including the addition of an uncertain CH_2Cl_2 ocean source and an added chemical loss reaction for C_2Cl_4 (C_2Cl_4 + Cl).

Chapter 5 assesses the impacts of Cl-VSLS on stratospheric ozone. It is chiefly adapted from my in-preparation lead-author paper [Claxton et al., in prep]. The chapter uses the optimised CH_2Cl_2 and C_2Cl_4 emissions from Chapter 4. It further develops a simple gridded 12-year $CHCl_3$ emission field based on industry emission estimates and literature values for natural emissions. These $CHCl_3$ emissions are evaluated using observational data. The chapter then quantifies (a) the transient stratospheric chlorine injection from all 3 Cl-VSLS (CH_2Cl_2, C_2Cl_4 and $CHCl_3$) and their product gases ($COCl_2$, Cl_y) using TOMCAT, and (b) the resulting impact these compounds have had on ozone in the recent past, using SLIMCAT.

Finally, the thesis is summarised and evaluated in a concluding chapter (Chapter 6), which discusses the overall success of the thesis, the scientific impact the thesis has on current understanding of Cl-VSLS, what could have been improved upon, and any future work that the thesis could lead to.

Chapter 2

Literature Review

To investigate the impact chlorinated Very Short-Lived Substances (Cl-VSLS) have on the atmosphere requires an understanding of the effect of chlorine on both stratospheric and tropospheric chemistry, and how Cl-VSLS add to the total chlorine budget. Transport and other dynamical processes affecting Cl-VSLS also need to be understood, as the impact of chlorine from Cl-VSLS on stratospheric ozone depends on the prevalence of transport from the surface into the stratosphere. Current scientific knowledge of Cl-VSLS emissions is unfortunately sparse; a primary goal of this thesis is to expand on that knowledge. Despite limited global coverage, observational records of a few Cl-VSLS have been established with records covering a few decades in some locations. Adding to this data, numerical models are able simulate historical Cl-VSLS concentrations using emission inventories as input, as well as making projections of what concentrations are likely to be in the future. This thesis provides new insight into Cl-VSLS emissions and atmospheric impacts by combining both atmospheric measurement data and model experiments.

In this chapter, I introduce the current understanding behind the above topics, which will prove useful for the experiments in later chapters. **Section 2.1** presents the background to the key chemistry and dynamical processes that affect the stratosphere, particularly discussing ozone and the impact of halogens, with a small aside to tropospheric ozone chemistry. In **Section 2.2**, I introduce Cl-VSLS, covering their abundances in the atmosphere, their chemistry, and their impacts, before I discuss the current knowledge of Cl-VSLS emissions in **Section 2.3**. In **Section 2.4** I briefly introduce chemistry transport models and “synthesis inversion”, an analysis technique I will be using in subsequent chapters to aid with my thesis. Finally, **Section 2.5** summarises the chapter.

2.1 Stratospheric Ozone

This section contains a background to some of the key processes affecting stratospheric ozone. **Section 2.1.1** introduces the stratospheric ozone layer and ozone distribution, and **Section 2.1.2** discusses basic stratospheric ozone chemistry. **Section 2.1.3** adds to the discussion by introducing the impact of chlorine on stratospheric ozone. In **Section 2.1.4**, processes influencing the Antarctic ozone hole are discussed. Ozone layer recovery is discussed in **Section 2.1.5**. **Section 2.1.6** briefly covers the main chemistry that governs ozone production and loss in the troposphere.

2.1.1 Stratospheric Ozone

The stratosphere begins at roughly 10-17 km, depending on latitude, and extends to about 50 km above the surface. The tropopause, the lower boundary of the stratosphere, is found at lower altitudes in higher latitude regions compared to the tropics. The stratosphere is characterised by steadily increasing temperatures with altitude, due to the absorption of high energy UV radiation by ozone, O_3 [Hartley, 1880]. A layer of relatively high ozone abundance in the stratosphere is observed (**Figure 2.1**) and is called the ozone layer. This layer forms a vital protective shield for Earth's surface from UV radiation, and is a reason why varied life on Earth can exist above water [Matsumi and Kawasaki, 2003]. Although **Figure 2.1** highlights that the relative ozone concentrations are greatest at about 25 km, since the mass of the atmosphere exponentially decays from the surface, the largest absolute ozone concentrations are in the lower stratosphere (15-20 km) [Jia et al., 2015]. **Figure 2.1** also shows that outside the stratosphere there is significant abundance of ozone in the troposphere, particularly near Earth's surface.

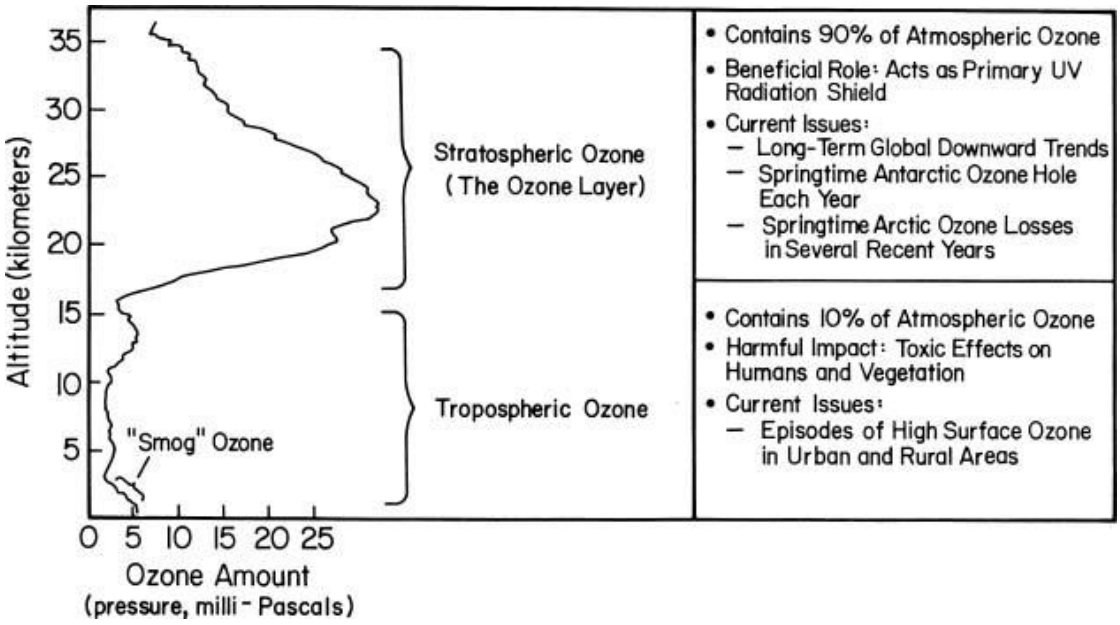

Figure 2.1. Schematic of the vertical profile of ozone in the atmosphere. Taken from Figure 1 in Frequently Asked Questions About Ozone in the 1998 WMO Ozone Assessment Report [WMO, 1998].

The ozone layer is vital for life as it absorbs high energy UV-B radiation, which otherwise has the potential to damage DNA. The ozone layer absorbs 93-99% of this radiation [WMO, 1998], therefore it is important that ozone levels in the stratosphere are unaffected by human activity. Column ozone is an important measure when considering UV fluxes and it is typically expressed in Dobson Units (DU) [Dobson, 1968]. This is defined as the thickness of atmospheric ozone over a point on Earth's surface if it were brought down to surface temperature and pressure, such that 1 DU = 0.01 mm at 298 K and 1 atm of pressure, or rather 1 DU = 2.69×10^6 molecules cm^{-2} of ozone. Observations of column ozone were traditionally made using spectrometers, which can be taken from the surface, or more recently from satellite platforms, which supplements high-resolution surface calculations with extensive global coverage [Davis et al., 2016]. Such measurements have allowed a fairly long historical ozone record to be established spanning over 50 years. A typical column ozone abundance is roughly 300-350 DU [Sivasakthivel and Reddy, 2011], though can vary between 200-500 DU based on location and season [McPeters and Labow, 1996]. Since Dobson Units are a measure of an entire column of ozone, from

surface to the top of the atmosphere, measurements also include tropospheric ozone, which comprises 10% of total ozone [WMO, 1998].

Generally, air enters the stratosphere through the tropical tropopause, and descends back into the troposphere in mid-latitude regions [Butchart, 2014]. For the distribution of stratospheric ozone, this overriding circulation pattern is called Brewer-Dobson Circulation, and transports ozone formed in the tropics towards the polar regions [Brewer, 1949; Dobson, 1956]. As ozone cannot be created without sunlight, poleward transport of ozone is necessary for keeping the ozone layer intact. **Figure 2.2** highlights the distribution of ozone in the stratosphere as a result of Brewer-Dobson circulation. However, just as Brewer-Dobson circulation governs how stratospheric ozone is distributed, it also acts to distribute many of the compounds that have the ability to deplete it. These circulatory movements can take several months or even years to complete. This is more than enough time for many long-lived compounds, such as CFCs, with mean lifetimes of the order of several decades [Carpenter et al., 2014], and their products, to reach the polar stratosphere. In addition to large-scale circulations, tropical convective systems are vitally important to injecting air quickly into the stratosphere [Levine et al., 2007].

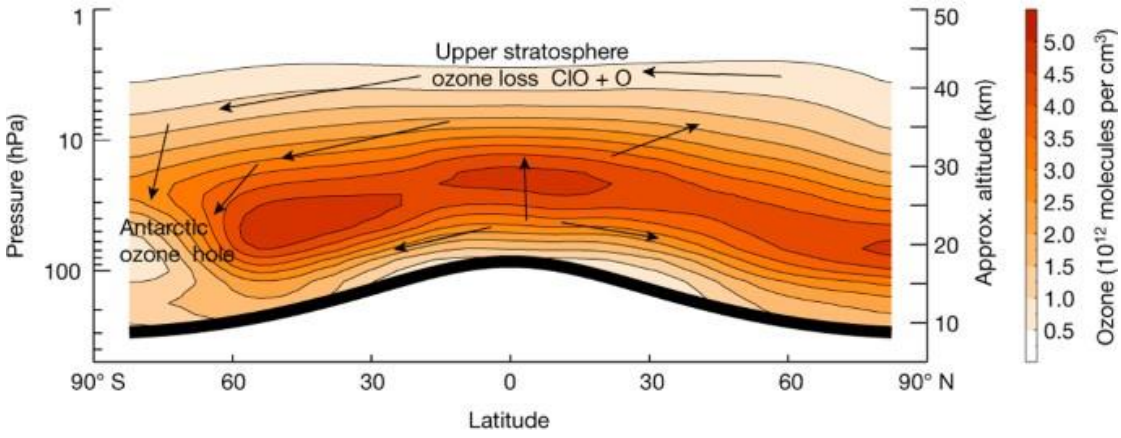

Figure 2.2. Latitude-pressure cross section schematic of stratospheric ozone distribution (satellite data October 2004-2016). Black arrows indicate Brewer-Dobson circulation, indicating an enhanced flow of ozone towards the winter pole. Taken from Figure 1 of Chipperfield et al. [2017].

2.1.2 Ozone Photochemistry

Ozone is produced and destroyed in the stratosphere by a series of photochemical reactions. The original reaction sequence (Equations 2.01-2.04), proposed by Chapman [1930] involves just oxygen-containing species. It begins with the photolysis of O_2:

$$O_2 + hv\ (\lambda < 242\ nm) \rightarrow O(^3P) + O(^3P) \qquad (2.01)$$

where hv is a photon, and $O(^3P)$ represents the ground electronic state of an oxygen atom, in which the four 2p electrons are arranged such that two are paired in one 2p orbital, and two are unpaired in each of the other 2p orbitals. This reaction can only occur with high energy (short wavelength) UV radiation present. One of the resultant oxygen atoms can rapidly react with O_2, in presence of a third body (M), to form ozone, O_3. This third body stabilises the reaction by absorbing the excess energy produced.

$$O(^3P) + O_2 + M \rightarrow O_3 + M \qquad (2.02)$$

However, ozone photolysis by high energy UV radiation is also rapid, which gives the products O_2 and $O(^1D)$, the first excited state of an oxygen atom.

$$O_3 + hv\ (\lambda < 340\ nm) \rightarrow O_2 + O(^1D) \qquad (2.03)$$

This excited state differs from the ground state by pairing the two previously unpaired electrons, and can relax into the ground state by quenching with a third body M. The resulting energy released contributes to the overall temperature increase in the stratosphere. Alternatively, $O(^3P)$ can be directly produced from the photolysis of ozone, at wavelengths larger than 340 nm [Matsumi and Kawasaki, 2003]. $O(^3P)$ and O_3 are usually categorised as O_x, or the odd oxygen family, as the interconversion between them in the above two reactions (Equations 2.02 and 2.03) is very fast. However, O_3 and $O(^3P)$ can also react together to form two O_2 molecules.

$$O_3 + O(^3P) \rightarrow 2O_2 \qquad (2.04)$$

Although Equation 2.04 occurs at a much slower rate than the preceding reactions, this leads to a stable system in which O_3 is both produced and destroyed to reach a steady state.

2.1.3 Chlorine in the Stratosphere

The Chapman reaction scheme was found to overestimate the correct observed concentrations of ozone in the stratosphere. It was later discovered that there are numerous other species that can react to primarily destroy ozone (or O_x in general). In the stratosphere, common species include oxidised hydrogen-containing species (HO_x, created from stratosphere methane and water vapour) [Bates and Nicolet, 1950], oxidised nitrogen-containing species (NO_x, created from stratospheric N_2O) [Crutzen, 1970], and halogen-containing species (chlorine - ClO_x, and bromine - BrO_x) [Stolarski and Cicerone, 1974; Yung et al., 1980].

These species form catalytic cycles with O_x, aiding in the destruction of O_x by way of Equations 2.05 and 2.06, without the need of the slow direct reaction between $O(^3P)$ and O_3 in Equation 2.04.

$$XO + O(^3P) \rightarrow X + O_2 \quad (2.05)$$

$$X + O_3 \rightarrow XO + O_2 \quad (2.06)$$

$$\text{Net: } O(^3P) + O_3 \rightarrow 2O_2$$

X represents the possible different molecules involved in the cycle (X = H, OH, NO, Cl, Br). This combination of reactions (Equations 2.01-2.06) forms the basis of contemporary stratospheric ozone loss and production. Since the advent of the industrial age, sources of stratospheric HO_x and NO_x compounds have changed, in particular due to increases in methane emissions for the former [Hartmann et al., 2013], and increases in N_2O for the latter [Portmann et al., 2012]. However, the major impact on stratospheric ozone in recent decades is due to halogens, particularly chlorine.

The ClO_x catalytic cycle was not described until the 1970s [Stolarski and Cicerone, 1974], and discoveries at roughly the same time linked emissions of chlorofluorocarbons (CFCs) to increased atmospheric chlorine, and hypothetically to increased ozone destruction [Molina and Rowland, 1974]. CFCs were used as relatively cheap, inert, nontoxic and non-flammable refrigerants and propellants, and their use expanded dramatically worldwide post late 1950s. Although they are inert at Earth's surface and throughout the

troposphere, in the stratosphere UV radiation carries sufficient energy to photolyse CFCs and release Cl atoms.

In addition, HO_x and NO_x cycles can interact with ClO_x and BrO_x to lead to increased ozone destruction, by the following reaction scheme, in which generally X represents either HO or NO, and Y represents Cl or Br [Johnson et al., 1995]:

$$X + O_3 \rightarrow XO + O_2 \quad (2.06)$$

$$XO + YO \rightarrow XY + O_2 \quad (2.07)$$

$$XY + hv \rightarrow X + Y \quad (2.08)$$

$$Y + O_3 \rightarrow YO + O_2 \quad (2.09)$$

$$\text{Net: } 2O_3 \rightarrow 3O_2$$

The above cycle avoids the requirement of having O atoms present to react with the initial XO molecule. Lower down in the stratosphere the photolysis of O_2 is less efficient because of absorbing molecules overhead reducing transmission of high energy UV radiation. What is important to note is that these reaction cycles are catalytic with respect to both X and Y, and one atom of chlorine, for example, can destroy many molecules of ozone before the cycle terminates [Lary, 1997]. Termination reactions for chlorine atoms in the stratosphere include reaction with HO_2 or CH_4 to form HCl, or ClO can react with NO_2 to form $ClONO_2$. These are examples of chlorine reservoir compounds, as they themselves do not directly destroy ozone. However, they can photolyse to re-release reactive Cl, or form other photolabile gas-phase compounds following heterogenous chemistry. Certain chlorine reservoirs, e.g. HCl, are also water soluble and can physically leave the stratosphere by way of water vapour and deposition processes. Such processes act to cycle chlorine out of the stratosphere and into the troposphere.

2.1.4 Antarctic Ozone Hole

Even though the above cycles lead to global ozone destruction, it was observed that there were comparatively very large local reductions of ozone

concentrations in the Antarctic spring [Farman et al., 1985; Solomon et al., 1986]. This phenomenon became known as the “ozone hole”. The ozone hole is generally defined as the region where column ozone falls to under 220 DU [Sivasakthivel and Reddy, 2011]. It was proposed that the explanation for these large ozone reductions involved heterogeneous reactions occurring on high altitude polar stratospheric clouds (PSCs) [Molina and Molina, 1987]. These clouds require very cold temperatures (below 200 K), cold enough to freeze both water vapour and nitric acid, which constitute the two main types of PSCs [Solomon, 1999]. Examples of heterogeneous reactions facilitated by PSCs are listed below [von Clarmann, 2013]:

$$HCl_{(s)} + ClONO_{2(g)} \rightarrow Cl_{2(g)} + HNO_{3(s)} \quad (2.10)$$

$$ClONO_{2(g)} + H_2O_{(l,s)} \rightarrow HOCl_{(g)} + HNO_{3(s)} \quad (2.11)$$

$$HCl_{(l,s)} + HOCl_{(g)} \rightarrow H_2O_{(s)} + Cl_{2(g)} \quad (2.12)$$

The chlorinated end-reaction product, Cl_2, is far more photoreactive than the reservoir species HCl and $ClONO_2$. This allows for more effective release of Cl under sunlight. Once Cl is generated, the reaction cycle in Equations 2.06-2.09 is possible; however, a dimeric cycle is more common at lower altitudes:

$$2Cl + 2O_3 \rightarrow 2ClO + 2O_2 \quad (2.13)$$

$$ClO + ClO + M \rightarrow Cl_2O_2 + M \quad (2.14)$$

$$Cl_2O_2 + h\nu \rightarrow Cl + ClO_2 \quad (2.15)$$

$$ClO_2 + M \rightarrow Cl + O_2 + M \quad (2.16)$$

Just as with Equations 2.06-2.09, the net result is the same, converting two O_3 molecules into three O_2 molecules. The reason why enhanced ozone destruction occurs during springtime is that any photolysis reaction (Equation 2.15, and the conversion of Cl_2 formed from Equations 2.10 and 2.12 into Cl) cannot occur until the polar night is over. A dimer reaction cycle can also occur with ClO and BrO species interacting with one another [McElroy et al., 1986], and the general coupling of ClO_x and BrO_x reaction cycles is important in depleting Antarctic ozone [Sinnhuber et al., 2009]. The meteorology of the polar regions is able to sustain the low temperatures required to form PSCs by the

generation of strong polar vortices, which isolate the poles from the rest of the stratosphere, resulting in a sharp temperature gradient between the poles and mid-latitudes [Solomon, 1999]. The above processes explain why polar ozone is most impacted by halogen chemistry, compared to ozone in the tropics and mid-latitudes.

2.1.5 Montreal Protocol and Ozone Recovery

Molina and Rowland [1974] first hypothesised a possible link between CFCs and ozone depletion, a year before CFCs were found to be present in the stratosphere. As such the global scientific community began investigating this growing threat to the ozone layer. In 1985 the Vienna Convention for the Protection of the Ozone Layer was the first unified government response to tackle ozone depletion, crucial as Farman et al. [1985] and Solomon et al. [1986] had reported significant depletion over Antarctica [Salawitch et al., 2018]. In 1987 the Montreal Protocol on Substances that Deplete the Ozone Layer, an international treaty to control the use of CFCs and other ozone depleting substances, was enacted. **Figure 2.3** shows the evolution of equivalent effective stratospheric chlorine due to the original Protocol and subsequent amendments. At first CFC production was only partially limited with phased out timetables for CFCs and halon use. Subsequent amendments, for instance in London and Copenhagen expanded the Protocol to cover additional ozone depleting compounds, including methyl chloroform and carbon tetrachloride, with an eventual ban on all CFC production [Salawitch et al., 2018].

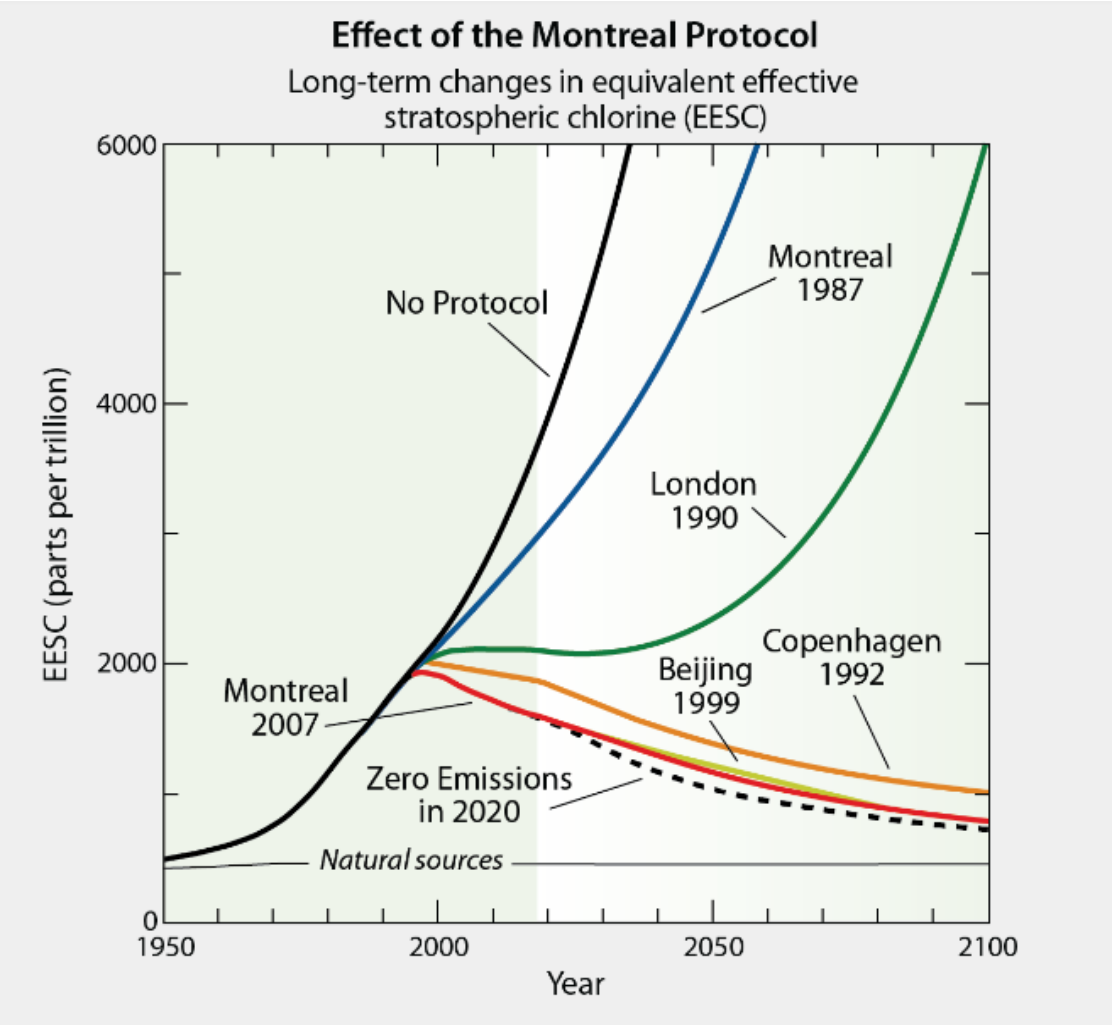

Figure 2.3. Time series of the implementation of the Montreal Protocol and its subsequent amendments. Each key amendment shown depicts their projected impacts on EESC (equivalent effective stratospheric chlorine), trending towards the ideal scenario of zero emissions (dashed line). Taken from Figure Q14-1 from WMO Ozone Assessment Report, 2018 [Salawitch et al., 2018].

Alternatives, such as HCFCs (Hydrochlorofluorocarbons), were the first generation of alternatives for CFCs brought in by industry as a response to the earlier Montreal Protocol amendments. HCFCs are more reactive in the troposphere as they contain weaker C-H bonds. This means that their tropospheric lifetimes are shorter than for CFCs, approximately 5-20 years [Harris et al., 2014]. But HCFCs still transport into the stratosphere, and can contribute to ozone destruction [Engel et al., 2013]. Therefore, the Montreal

Protocol has started placing restrictions on the production of HCFCs [Engel et al., 2018], with a complete phase out scheduled by 2030. The most recent amendment of the Montreal Protocol, agreed in Kigali in 2016, sought to phase down global production of many common HFCs (hydrofluorocarbons) from 2019. These are the second generation of CFC replacements introduced that contain no chlorine or bromine and hence have zero ozone depletion potential. However, their large Global Warming Potential has led to restrictions introduced to minimise their contribution towards climate change [Salawitch et al., 2018].

Many studies have been undertaken to investigate ozone recovery in lieu of the success of the Montreal Protocol [Pawson et al., 2014]. Observations of extra-polar (mid-latitudes and tropics) total column ozone show a positive trend in ozone from 2000-2013, of 1 ± 1.7% [Pawson et al., 2014], and present-day ozone levels are only 2% lower than 1960-1980 levels. However, these values do not include polar ozone changes and focus on the changes primarily in mid-latitude ozone. For polar ozone, total column ozone over Antarctica during October, when the ozone hole is at its greatest extent, has decreased by over 50% from the 1960s to the 1990s [Montzka, Reimann, et al., 2011]. The majority of this depletion occurs in the lower stratosphere (15-20 km), where PSCs are most commonly found. The characteristics (e.g. size and strength) of the Antarctic ozone hole in recent years are still within the same ranges observed since the 1990s, subject to interannual variation, indicating a plateau in Antarctic ozone depletion [Langematz et al., 2018].

As CFC concentrations continue to decrease (**Figure 2.3**), the ozone hole is expected to close gradually, with total springtime column ozone recovering to 1980 levels by around 2060 [WMO, 2018], and global ozone levels are expected to reach their previous levels in the coming decades [e.g. Dhomse et al., 2018]. Dhomse et al. [2018] estimate that column ozone levels return to their 1980 concentrations by 2032 for northern hemisphere mid-latitudes, 2045 for southern hemisphere mid-latitudes, 2059 for the tropics, and 2049 globally. In the upper stratosphere specifically, ozone has increased by 1-3% decade^{-1} since 2000, with the greatest confidence in the northern mid-latitudes between 35 and 45 km [WMO, 2018]. However only half of this increase is attributable to decline in ozone depleting substances, with the other half because of upper

stratospheric cooling slowing down the reactions destroying ozone (e.g. Equation 2.04). Due to the gradual decrease of chlorine due to the Montreal Protocol, the biggest drivers of future ozone changes are the main greenhouses gases CO_2 and CH_4, whose increases act to increase stratospheric ozone production via stratospheric cooling, and N_2O, the primary source of stratospheric NO_x, whose increase contributes to ozone depletion [WMO, 2018].

Although the Montreal Protocol has been very successful in reducing stratospheric chlorine, this progress could be under threat. One possibility is by returning emissions of CFCs [Montzka et al., 2018], and another is by the influx of traditionally less-important chlorine containing substances capable of destroying ozone. A series of such compounds are Chlorinated Very Short-Lived Substances, or Cl-VSLS [e.g. Hossaini et al., 2017; Laube et al., 2008; Sturges et al., 2000; Wales et al., 2018].

2.1.6 Tropospheric Ozone Chemistry

As well as ozone forming an integral part of stratospheric composition, it is present in the troposphere. About 10% of total planetary ozone lies in the troposphere (**Figure 2.1**). Here it acts as a greenhouse gas, absorbing IR radiation, and as a surface pollutant, with approximately 1 million people estimated to be killed every year from the polluting effects of ozone [Malley et al., 2017]. A large source of tropospheric ozone comes from descent of stratospheric air [e.g. Butchart, 2014]; however, tropospheric ozone can be produced photochemically, particularly near the surface. This production (and loss) is governed by a series of photochemical reactions that link volatile organic compounds (VOCs), NO_x, and HO_x [Crutzen, 1974; Liu et al., 1987]. The main difference between tropospheric ozone production and stratospheric ozone production is that O_2 photolysis (Equation 2.01) is not easily achieved in the troposphere. This is because the required high energy UV radiation ($\lambda < 242$ nm) is very unlikely to pass through into the troposphere. Two reaction paths are available, however. The first involves the photolysis of NO_2, which can occur at wavelengths below 400 nm:

$$NO_2 + hv\ (\lambda < 400\ nm) \rightarrow O(^3P) + NO \quad (2.17)$$

This yields oxygen atoms able to form ozone as in Equation 2.02. The ozone formed can react with NO to complete this cycle, a null cycle in which there is no net ozone created or destroyed.

$$O(^3P) + O_2 + M \rightarrow O_3 + M \quad (2.02)$$

$$O_3 + NO \rightarrow O_2 + NO_2 \quad (2.18)$$

In the additional presence of organic compounds, e.g. VOCs, methane (CH_4), a second reaction path is available. The following sequence of reactions (Equations 2.19-2.22) show a small selection of possible reactions, which in this example starts with the reaction of methane with the hydroxyl radical OH [e.g. Ravishankara, 1988]:

$$CH_4 + OH \rightarrow CH_3 + H_2O \quad (2.19)$$

OH is far more abundant in the troposphere than in the stratosphere, with an average concentration of 11 x 10^5 molecules cm^{-3}, a whole order of magnitude greater than the average 1.1 x 10^5 molecules cm^{-3} in the stratosphere [Li et al., 2018]. It is primarily sourced by the reaction between $O(^1D)$ and H_2O, and $O(^1D)$ is created by the photolysis of tropospheric ozone (i.e. Equation 2.03). The stratosphere does not block all UV radiation with wavelengths shorter than 340 nm, allowing $O(^1D)$ formation [e.g. Hofzumahaus et al., 2002]. However, at wavelengths longer than 310 nm, the $O(^1D)$ quantum yield is no greater than 0.1, resulting in $O(^3P)$ as the dominant photolysis product [Matsumi and Kawasaki, 2003]. In addition, the reaction of $O(^1D)$ with H_2O is competed for by the quenching of $O(^1D)$ with a third body M to form $O(^3P)$. In the marine boundary layer, where H_2O is abundant, only 10% of $O(^1D)$ reacts to form OH [Monks, 2005]. Due to the interconversion between HO_x and NO_x compounds (Equation 2.23), higher OH concentrations are also correlated with higher concentrations of NO [Ren et al., 2008].

The primary photochemical sinks of OH are CH_4, as in Equation 2.19, and CO, carbon monoxide. Therefore, the global distribution of OH is dependent on many factors. **Figure 2.4** shows a modelled surface distribution of OH, where it is possible to highlight the influence of the key sources and sinks. Low OH

occurs where photolysis rates are low, over polar regions, and where CO concentrations are high, over tropical rainforests. Common ship routes in the Atlantic Ocean, Indian Ocean, and South China Sea show regions where both NO and H_2O concentrations are high, leading to noticeably elevated OH. Large OH concentrations over land can be linked to main sources of surface ozone, e.g. over Asia. **Figure 2.5** depicts the importance of convection towards OH production with an example modelled vertical distribution of OH concentration from Lieleveld et al. [2016]. The largest convective systems occur over the Northern Tropics, particularly the Maritime Continent [Levine et al., 2007], injecting both O_3 and H_2O throughout the troposphere, providing a column of high OH concentrations.

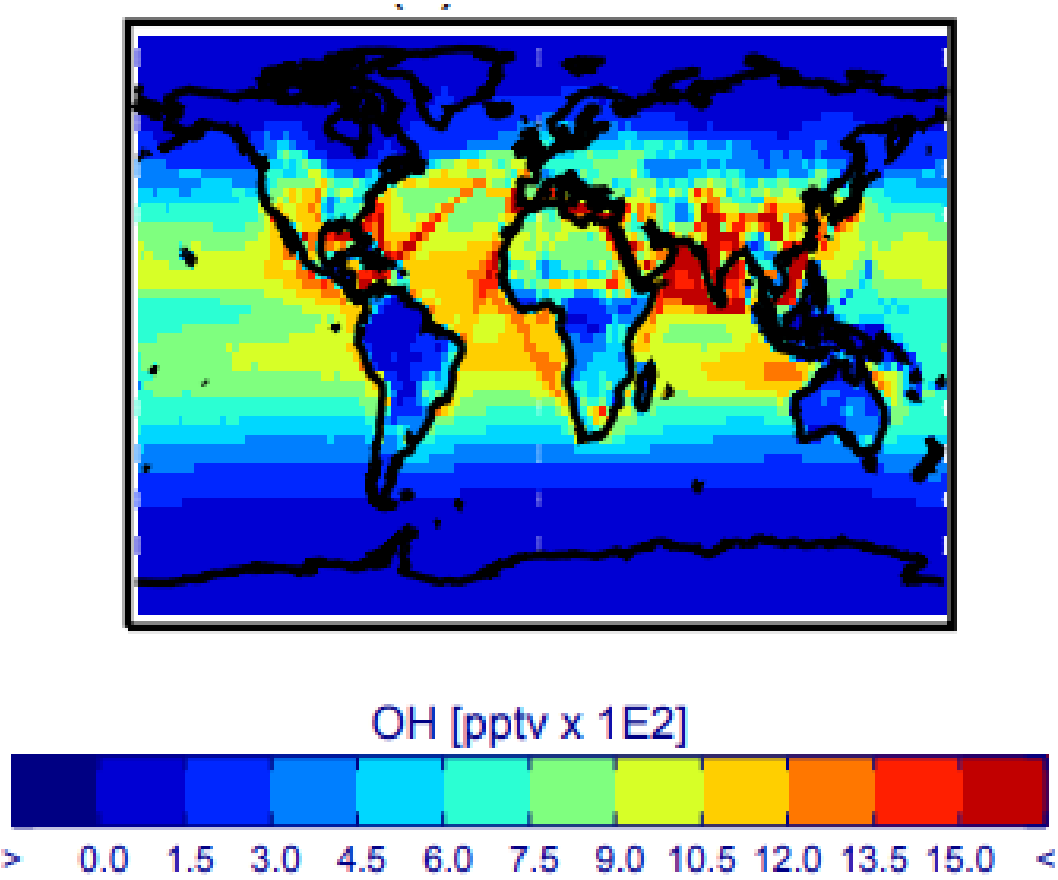

Figure 2.4. Modelled global distribution of annual surface mean OH concentrations, for 2008. Taken from Figure 3 of Monks et al. [2017].

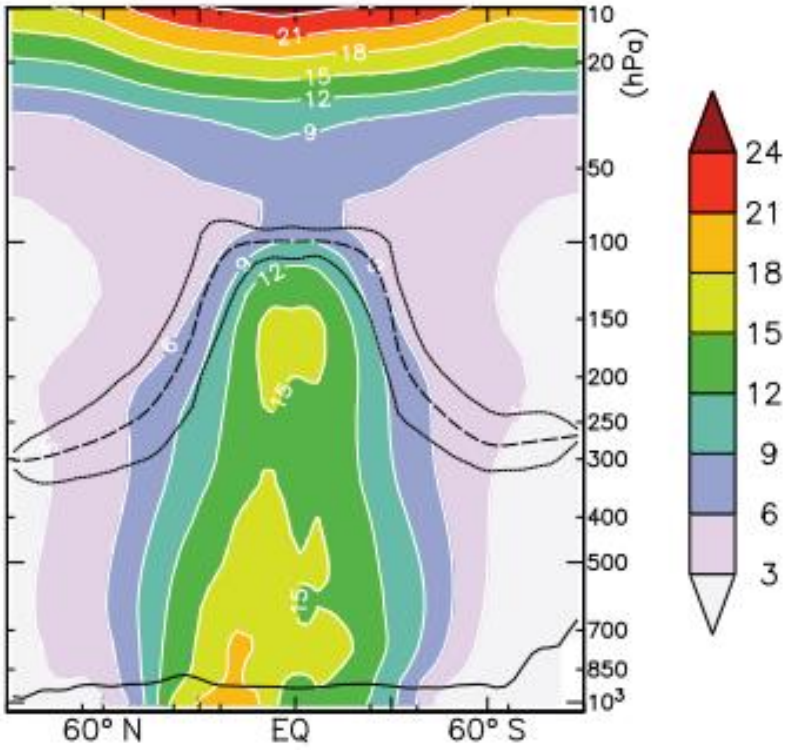

Figure 2.5. Modelled annual zonal mean OH concentrations, in units of 10^5 molecules cm^{-3}. Taken from Figure 1 of Lieleveld et al. [2016].

As a radical species OH is very reactive, and will oxidise most organic compounds. This occurs primarily by hydrogen abstraction, as in Equation 2.19. The resulting CH_3 from this reaction can combine with O_2 rapidly to form a methylperoxy radical:

$$CH_3 + O_2 + M \rightarrow CH_3O_2 + M \quad (2.20)$$

$$CH_3O_2 + NO \rightarrow CH_3O + NO_2 \quad (2.21)$$

$$CH_3O + O_2 \rightarrow CH_2O + HO_2 \quad (2.22)$$

Peroxy radicals are reactive, and in the presence of NO_x can react instead of O_3 in Equation 2.18 to form NO_2, in Equation 2.21. The presence of a large amount of NO_x implies a polluted atmosphere, with significant sources of NO_x primarily from industrial and agricultural sources, such as traffic emissions and fertiliser. Without NO_x, ozone production is not favourable from VOCs alone,

and CH_3O_2 can convert into CH_2O via cycling with just HO_x species, without involving O_x (i.e. ozone) [Ravishankara, 1988]. The HO_2 product from Equation 2.22 can also react with NO, in Equation 2.23. This generates two molecules of NO_2, which can lead to two molecules of ozone formed, as shown below. Unlike the null cycle from Equations 2.17-2.18, the terminating reaction of O_3 with NO to reform NO_2 (Equation 2.18) is bypassed.

$$HO_2 + NO \rightarrow OH + NO_2 \quad (2.23)$$

$$2NO_2 + 2hv \rightarrow 2O(^3P) + 2NO \quad (2.17)$$

$$2O(^3P) + 2O_2 + 2M \rightarrow 2O_3 + 2M \quad (2.02)$$

$$\text{Net: } CH_4 + 4O_2 \rightarrow CH_2O + H_2O + 2O_3$$

The net reaction from adding up Equations 2.16 through to 2.02 above uses up NO_x catalytically. Formaldehyde (CH_2O) is a toxic compound, and can wash out and deposit onto the surface. In addition to chemical sinks, dry deposition is a key loss process for ozone, and plants are able to uptake it through stomata, where it can be chemically converted [Cho et al., 2011], damaging plant physiology. Over water, ozone can deposit onto oceans where it dissolves [Hardacre et al., 2015].

2.2 Chlorinated VSLS: An Overview

This section presents an overview of the current scientific understanding of Chlorinated Very Short-Lived Substances (Cl-VSLS), introducing the most abundant compounds and their uses in **Section 2.2.1**. **Section 2.2.2** focuses on the chemical processes and **Section 2.2.3** on the transport processes that most affect these compounds, in both the stratosphere and troposphere. **Section 2.2.4** discusses the impact Cl-VSLS have on stratospheric ozone. In **Section 2.2.5**, similar impacts but due to Brominated VSLS are briefly discussed. Finally, **Section 2.2.6** introduces the concept of 'ozone depletion potential' with regards to Cl-VSLS, an important metric for policymakers when considering different compounds that can impact stratospheric ozone.

2.2.1 Chlorinated VSLS Uses and Concentrations

Halogenated VSLS are defined as substances with surface lifetimes below 6 months [Ko et al., 2003]. They include chlorinated (Cl-VSLS), brominated (Br-VSLS) and iodinated compounds, all of which have both natural and anthropogenic sources and the potential to destroy stratospheric ozone if transported to the stratosphere [Chipperfield et al., 2018; Hossaini et al., 2017]. In this thesis, I am mostly concerned with Cl-VSLS, which include many compounds commonly used as industrial solvents, owing to their high volatility [IARC, 2016; Ko et al., 2003; Simmonds et al., 2006]. VSLS have been widely thought throughout previous decades to not impact stratospheric ozone. For instance, the US Environmental Protection Agency (EPA) in 1995 listed dichloromethane (CH_2Cl_2, a key Cl-VSLS), amongst other Cl-VSLS, as a compound not in consideration to deplete stratospheric ozone [EPA, 1995].

Of the numerous different Cl-VSLS that are emitted to the atmosphere, there are only a handful whose abundances are routinely monitored. Chloroform ($CHCl_3$) is a VSLS which is emitted significantly by natural sources, with estimates of the natural component of total global $CHCl_3$ emissions ranging from ~90% [McCulloch, 2003] to ~50% [Trudinger et al., 2004], but with few recent up-to-date studies. Natural sources include ocean and soil emissions [Khalil et al., 1999; Xiao, 2008]. The oceanic source is not well understood or quantified, but it is thought to be of a biological nature; e.g. emissions from seaweed have been found to be the primary source of coastal $CHCl_3$ emissions [McCulloch, 2003]. Soil emissions are also estimated to be from biological activity.

Anthropogenic $CHCl_3$ emissions arise due to its use in the production of HCFC-22 (a use that is thought to dominate $CHCl_3$ production [ATSDR, 1997]), from industrial manufacture of pulp and paper [Worton et al., 2006], and from generic industrial and commercial use as a solvent (at least historically in the Western hemisphere). Its historic use as one of the first anaesthetics has been banned in several countries [WHO, 1994]. Anthropogenic sources tend to occur over industrialised countries, in the Northern Hemisphere [Aucott et al., 1999], which is evidenced from long-term surface measurements of chloroform that exist via

the AGAGE (Advanced Global Atmospheric Gases Experiment) network [Carpenter et al., 2014]. Since the turn of the century, $CHCl_3$ atmospheric concentrations and emissions have mostly remained fairly constant [Carpenter et al., 2014; Worton et al., 2006]; however, since 2010 emissions have increased over East Asia [Fang et al., 2019]. This has led to a relatively sharp increase in the observed atmospheric $CHCl_3$ concentration at numerous sites, as seen in **Figure 2.6**. There is a significant hemispheric divide between $CHCl_3$ measurements, reflecting greater industrialisation in the north. Over the last decade there has been a steady increase at northern mid-latitude measurement sites from ~12 ppt on average in 2010 to ~17 ppt in 2018. There is no such rise for southern stations though, and $CHCl_3$ levels there have remained relatively constant at ~6 ppt for the last 20 years.

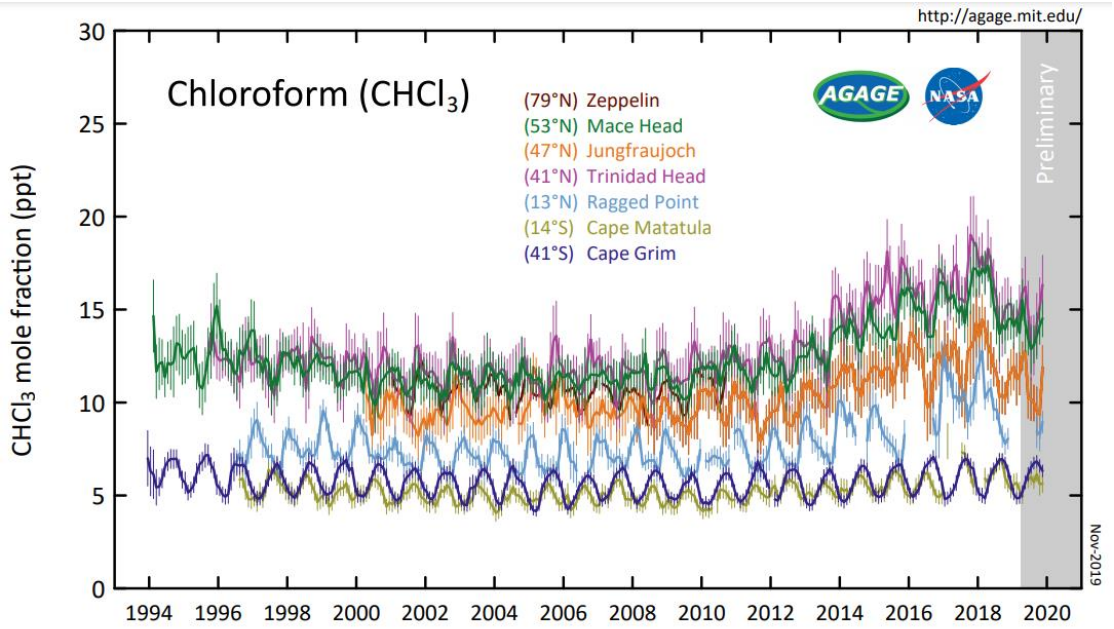

Figure 2.6. Recent observed trends in the atmospheric $CHCl_3$ mole fraction (ppt) at global surface sites of the AGAGE monitoring network. The data are available from: https://agage.mit.edu/data/agage-data. Accessed September 2020.

Another widely emitted Cl-VSLS and one that has attracted significant recent attention is dichloromethane (CH_2Cl_2). Unlike chloroform, most (~90%) global CH_2Cl_2 emissions are thought to arise from anthropogenic rather than natural sources [Montzka, Reimann, et al., 2011]. It is commonly used as an industrial

solvent in a wide variety of applications [IARC, 1999; Montzka, Reimann, et al., 2011]. For instance, historically through solvent applications, CH_2Cl_2 has been used in paint stripper (23-50% of use), aerosol solvents and propellants (10-25%), process solvents in chemical industry (10-20%), and in metal degreasing (8-13%, all c. 1990s) [IARC, 1999; WHO, 1996]. Use of CH_2Cl_2 had been decreasing in Europe and the USA from the 1970s [EPA, 2014; Holbrook, 1993], possibly related to concern over the compound's toxicity. However in recent years, global concentrations are observed to have increased rapidly [**Figure 2.7**; also Leedham Elvidge et al., 2015]. As a mainly anthropogenic emitted species, countries which have recently become more heavily industrialised, such as China and India, may have increased their emissions far more rapidly compared to other regions [e.g. Leedham Elvidge et al., 2015]. For instance, Feng et al. [2019] estimated that Chinese CH_2Cl_2 emissions increased by a factor of 3 between 2005 and 2016, with further increases projected until 2030. Similarly, Say et al. [2019] estimated that Indian CH_2Cl_2 emissions increased 5-fold between 2008 and 2016. Measurements of CH_2Cl_2 exist with both the AGAGE and the NOAA (National Oceanic and Atmospheric Administration) long-term surface networks. **Figure 2.7** shows the recent observed concentration trends for CH_2Cl_2. Similarly to $CHCl_3$, there is a clear hemispheric divide, with northern hemisphere observations several times higher than those in the south, reflecting industrial sources in the north. Concentrations of CH_2Cl_2 have risen on average from ~30 ppt in the early 2000s to ~60 ppt in the late 2010s, at northern measurement sites, with proportionally similar increases at southern sites.

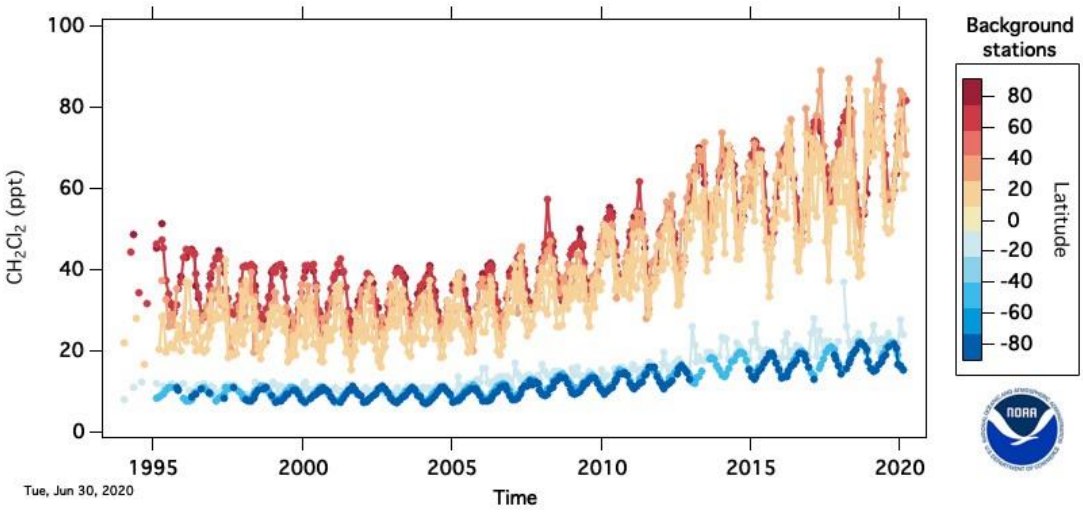

Figure 2.7. Recent observed trends in the atmospheric CH_2Cl_2 mole fraction (ppt) as a function of latitude. Observed data are based on measurements at global surface sites from the NOAA long term monitoring network. The data are available from: https://www.esrl.noaa.gov/gmd/hats/gases/CH2Cl2.html. Accessed September 2020.

Although they are less abundant than CH_2Cl_2 and $CHCl_3$, perchloroethylene (C_2Cl_4), ethylene dichloride ($C_2H_4Cl_2$), and trichloroethylene (C_2HCl_3) are prevalent in the atmosphere. Abundances of C_2Cl_4 are of the order of 3 ppt in the northern hemisphere, and 0.5 ppt in the southern hemisphere, estimated by the NOAA and AGAGE networks [Engel et al., 2018]. Dry-cleaning represents the main traditional use of C_2Cl_4 (80% in the 1950s); however, this has shifted more towards use as a chemical feedstock for HCFCs (50% as chemical feedstock, 15% in dry-cleaning, in the 1990s) [IARC, 2014]. Other uses include metal degreasing and as a textile processing solvent. $C_2H_4Cl_2$ and C_2HCl_3 are not routinely measured at the surface; however, limited boundary layer aircraft data shows $C_2H_4Cl_2$ abundances of 12.8 ppt, similar to that of $CHCl_3$ (10.3 ppt), and C_2HCl_3 has a boundary layer abundance of around 0.2 ppt [Engel et al., 2018]. Like other Cl-VSLS, these compounds have found use as industrial solvents [Montzka, Reimann et al., 2011]. For $C_2H_4Cl_2$, a major use is a chemical feedstock in the production of vinyl chloride (C_2H_3Cl), the precursor to PVC (poly vinyl chloride) plastics [IARC, 1999].

The global average lifetimes of $CHCl_3$, CH_2Cl_2, C_2Cl_4, C_2HCl_3, and $C_2H_4Cl_2$, have been estimated to be 149, 144, 90, 5, and 65 days, respectively [Harris et al., 2014]. In recent years, the safety of using several of these compounds in commercial and/or domestic settings (e.g. C_2Cl_4 as a dry-cleaning solvent) has been debated, due to possible adverse health effects, and less harmful alternatives have been sought. For instance, even CH_2Cl_2, as the least toxic of the three mainly anthropogenic Cl-VSLS, has had regulations passed to limit its use as a possible carcinogen [IARC, 1999]. In 2011 the EU banned use of CH_2Cl_2 in paint strippers [European Commission, 2010], with the US EPA in 2019 announcing its own ban.

Overall, global tropospheric chlorine from CH_2Cl_2, $CHCl_3$ and C_2Cl_4 combined was measured in 2016 at 92-100 ppt Cl equivalent, a 4.0 ± 1.5 ppt Cl yr^{-1} increase from 2012 [Engel et al., 2018]. This is driven by the increase in CH_2Cl_2 by 60% in the last decade, as can be seen in the observed surface measurements in **Figure 2.7**, yet mitigated slightly by decreases in C_2Cl_4 (not shown). VSLS still only provide a small fraction of the total chlorine in the troposphere, at 3.3%, compared with CFCs that still provide 60% of Cl, in 2016 [Engel et al., 2018]. However, CFCs and CCl_4, the largest contributors to tropospheric chlorine, at 60% and 10% contribution, respectively, are both decreasing, which means that in the future Cl-VSLS will become more important for tropospheric chlorine. In 2008 the relative contribution of VSLS to total chlorine was only 2.4% [Engel et al., 2018]. Methyl chloride, CH_3Cl, with a lifetime of approximately a year, longer than the definition for a VSLS, contributes 17% to tropospheric chlorine, and is also not regulated by the Montreal Protocol [Engel et al., 2018]. However, it is mainly emitted by natural sources [Khalil et al., 1999].

2.2.2 Cl-VSLS Chemistry

Figure 2.8 shows various processes that affect VSLS in the atmosphere. These processes are both chemical and dynamical, and occur throughout the troposphere and stratosphere. Once they are emitted, the Cl-VSLS source gases (SG) can be destroyed through reactions with the hydroxyl radical (OH)

or through photolysis. Oxidation by OH is the major sink in the troposphere, due to the lack of high energy UV radiation able to easily photolyse Cl-VSLS. Common product gases (PG) from these reactions include hydrogen chloride (HCl) and phosgene ($COCl_2$). Oxidation by Cl represents a fairly minor sink for Cl-VSLS. For CH_2Cl_2, the reaction scheme for its degradation starts as follows [Hossaini et al., 2019]:

$$CH_2Cl_2 + OH + O_2 \rightarrow CHCl_2O_2 + H_2O \quad (2.24)$$

$$CH_2Cl_2 + Cl + O_2 \rightarrow CHCl_2O_2 + HCl \quad (2.25)$$

The binding of the $CHCl_2$ intermediate with oxygen occurs very readily [Catoire et al., 1996; Hossaini et al., 2019]. The resulting peroxy radical, $CHCl_2O_2$, can react as follows:

$$CHCl_2O_2 + NO \rightarrow CHCl_2O + NO_2 \quad (2.26)$$

$$CHCl_2O + M \rightarrow CHClO + Cl + M \quad (2.27)$$

$$CHCl_2O_2 + HO_2 \rightarrow COCl_2 + H_2O + O_2 \quad (2.28)$$

$$CHClO + OH \rightarrow Cl + CO + H_2O \quad (2.29)$$

CHClO is also an alternate product from the reaction between $CHCl_2O_2$ and HO_2 in Equation 2.28, and can itself react with OH, Cl, NO_3 and hv to form Cl. The stable chlorinated end products of this reaction sequence are HCl (rapidly formed from reactions between VOCs and Cl) and $COCl_2$. These products are water soluble, and are able to washout from clouds as precipitation, removing the chlorine from the atmosphere. They could also transport into the stratosphere, contributing to Product Gas Injection (PGI), and become a secondary source of chlorine in the stratosphere.

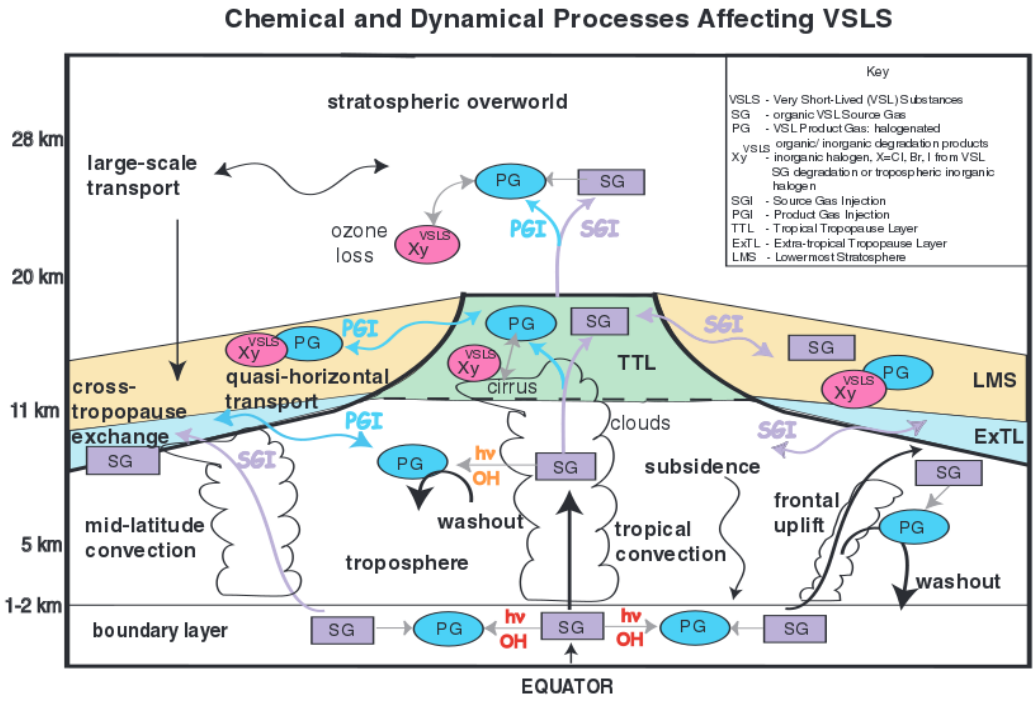

Figure 2.8. Chemical and dynamical processes affecting VSLS, in both the troposphere and stratosphere. Taken from Figure 2-1 of the WMO 2006 Ozone Assessment Report [Law et al., 2006].

Alternatively, Cl atoms can react directly with tropospheric O_3 to form ClO. This ClO can then compete with O_2 for the reaction with O atoms (Equation 2.02) to prevent ozone from regenerating. In the troposphere however, there is a greater tendency for self-reaction between ClO molecules, by the following two reaction pathways [Saiz Lopez and von Glasow, 2012]:

$$O_3 + Cl \rightarrow ClO + O_2 \qquad (2.06)$$

$$ClO + ClO \rightarrow Cl_2 + O_2 \qquad (2.30)$$

$$ClO + ClO \rightarrow OClO + Cl + M \rightarrow Cl_2O_2 + M \qquad (2.31)$$

For chlorine, Equation 2.31 is more effective than Equation 2.30. OClO can instead photolyse to form ClO and O, the latter rapidly forming O_3 as per Equation 2.02, which decreases the efficiency of ozone depletion. OClO and ClO can feed into HOx and NOx cycles to contribute to further ozone loss, in reactions analogous to Equations 2.06-2.09. In the troposphere, chlorine atoms

are primarily lost from reacting with CH_4, contributing 3-15% towards the global methane sink [Lawler et al., 2011; Platt et al., 2004]. In highly polluted hydrocarbon environments, Cl can facilitate the formation of peroxy radicals (e.g. CH_3O_2), which lead to the production of O_3 from Equations 2.20-2.23 in presence of NO_x [Saiz Lopez and von Glasow, 2012].

2.2.3 Cl-VSLS Transport

Despite the relatively short lifetimes of these substances, **Figure 2.8** shows that Cl-VSLS can enter the stratosphere, mainly by convection. In the tropics, this can occur rather readily, which means that the tropical regions are often studied for upper troposphere/lower stratosphere (UTLS) concentrations of Cl-VSLS. The Indian and Western Pacific Oceans, along with the Maritime Continent (e.g. Indonesia, Malaysia, Philippines) are regions of regular deep convection, and are thought to be key regions for stratospheric injections [Levine et al., 2007]. The tops of tropical convective systems can reach up to 15 km, into the tropical tropopause layer (TTL), where injection into the stratosphere is possible. Relatively slow vertical ascent within the TTL allows for the possible increased photochemical degradation of SGs and organic PGs to release inorganic chlorine, also due to the increased proximity to higher energy UV light.

Outside of the tropics, deep convection extending into the UTLS is less common, but not impossible, and SGs are able to be injected into the lower stratosphere at higher latitudes. In addition to convection, frontal systems are able to uplift air masses into the extratropical upper troposphere, allowing transport into the stratosphere [Gettelman et al., 2011]. As well as vertical motion of SGs and PGs via small scale systems, large scale meridional transport is possible. This can transport gases from the TTL into the extratropical lower stratosphere via meridional circulation as shown in **Figure 2.8**.

Towards the surface, the transport of Cl-VSLS from industrialised emitting regions into areas experiencing vertical uplift (e.g. convective regions) is important. Numerous studies have shown that the co-location of surface hotspots with high VSLS mixing ratios leads to greater stratospheric SGI

compared to the zonal average [e.g. Aschmann et al., 2011; Levine et al., 2007; Tegtmeier et al., 2013]. Recently, so called “cold surges” have been discovered to play an important role in transporting Cl-VSLS meridionally on a regional basis from East Asia, where Cl-VSLS abundances are high, to the tropics [Ashfold et al., 2015]. However global scale transport of SGs is difficult due to the short lifetimes of these species, which can lead to large spatially variability of VSLS. **Figure 2.7** highlights this with the lack of inter-hemispherical transport of CH_2Cl_2 leading to northern hemisphere concentrations of the order of three times larger than southern concentrations.

2.2.4 Impacts of Cl-VSLS

As **Figure 2.8** shows, both Cl-VSLS and their product gases are able to be transported into the lower stratosphere via the TTL through Source Gas Injection (SGI) and Product Gas Injection (PGI). Once in the stratosphere, Cl-VSLS are readily photolysed to release chlorine [e.g. Hossaini et al., 2017]. Photolysis of Cl-VSLS occurs almost entirely in the lower stratosphere; however, the resulting chlorine can mix throughout the entire stratosphere. As Cl-VSLS are fairly reactive in the troposphere, it can be assumed that a significant proportion will have also reacted before reaching the tropopause. Several chlorinated product gases (e.g. HCl and $COCl_2$) are water-soluble, therefore the efficiency of stratospheric chlorine PGI depends on the vertical level at which the product gases are produced (i.e. whether they are subject to wet deposition). Stratospheric chlorine SGI (due to the VSLS themselves) is possible to observe from measuring near-tropopause abundances (e.g. from aircraft) and hence is relatively well constrained. But PGI attributed to Cl-VSLS cannot be measured directly, as the expected major stable product gases are also produced from the oxidation of other chlorocarbons. Phosgene ($COCl_2$) is a product of not only $CHCl_3$ and CH_2Cl_2, but also the long-lived gases CH_3CCl_3 (methyl chloroform) and CCl_4 [Fu et al., 2007]. The current best estimate of stratospheric chlorine SGI from all Cl-VSLS is 100 ppt Cl (83-117), for the year 2016 [Engel et al., 2018]. Stratospheric chlorine PGI due to product gases Cl_y (inorganic chlorine, which typically constitutes HCl) and $COCl_2$, can be

estimated from modelling studies, with a current best estimate of 8-50 ppt Cl in 2016 [Engel et al., 2018].

In terms of impacts on ozone, there have been very few modelling studies concerned with Cl-VSLS to date. However, the impact of CH_2Cl_2 specifically has been investigated due to its status as a rapidly increasing compound [Hossaini et al., 2017]. It was found that if growth of CH_2Cl_2 continues at the rate observed between 2004 and 2014, the time it takes for stratospheric Cl_y levels to return to 1980 levels (a sign of ozone recovery) is at least 17 years longer than if no CH_2Cl_2 was present in the stratosphere. As a consequence, annual mean Antarctic lower stratosphere ozone could decrease by ~6% in 2050 compared to a scenario with no CH_2Cl_2 [Hossaini et al., 2017].

2.2.5 Impacts of Brominated VSLS

Although the focus of this thesis is on Chlorinated VSLS, Brominated VSLS (Br-VSLS) have been undergoing more investigation in recent years. This is partly due to the overwhelming contribution of natural sources to global emissions, thought to be impacted by climate change [e.g. Ziska et al., 2017]. The common Br-VSLS are analogous to the common Cl-VSLS, including dibromomethane (CH_2Br_2) and bromoform ($CHBr_3$). Global emissions of these compounds have been estimated at 79 and 470 Gg Br yr^{-1}, respectively [Engel et al., 2018], and typical abundances are of the order of 0.4-4.0 and 0.6-1.7 ppt in the marine boundary layer. Other relatively minor Br-VSLS also contain a chlorine atom; e.g. $CHBr_2Cl$, CH_2BrCl and $CHBrCl_2$. The important natural sources of the above Br-VSLS are ocean plankton and microalgae in coastal waters [Moore et al., 1996], similar to the proposed natural sources of Cl-VSLS.

Compared to Cl-VSLS, whose contribution to total stratospheric Cl is relatively small, Br-VSLS represent a much larger relative proportion of total bromine injected to the stratosphere [Carpenter et al., 2014; Falk et al., 2017]. Although CH_3Br and long-lived halons have provided the bulk of the stratospheric bromine budget, at around 75%, the rest is from Br-VSLS [Falk et al., 2017]. This is in steep contrast to the total stratospheric chlorine budget, for which Cl-VSLS only contribute about 3% at present [Carpenter et al., 2014], albeit this is

likely to increase in coming years. Once in the stratosphere, bromine from VSLS causes decreases in stratospheric ozone, particularly in the lower stratosphere where Br-VSLS have short lifetimes against photolysis [Salawitch et al., 2005]. On a per atom basis, bromine is relatively efficient at destroying ozone, with modelling studies suggesting an 'α-factor', a metric that describes the relative chemical effectiveness of bromine compared to chlorine, of 64 [Sinnhuber et al., 2009].

Increases in Br-VSLS emissions have been postulated as a result of a changing climate [Ziska et al., 2017], as a result of changing sea surface temperatures, ocean salinity, and/or surface wind speeds. Under an RCP6.0 climate scenario (the second highest CO_2 scenario) combined CH_2Br_2 and $CHBr_3$ fluxes are expected to increase on average by 8-10% by the end of the 21st century [Falk et al., 2017]. Under an RCP8.0 scenario, the highest scenario, increases in 6.4% and 9.0% of CH_2Br_2 and $CHBr_3$ emissions, respectively, are projected in the same timeframe [Ziska et al., 2017]. It is plausible that oceanic sources of Cl-VSLS are impacted similarly due to changing climate, although natural oceanic Cl-VSLS sources are less well understood and any such changes are likely to be dwarfed by the sharper changes in industrial emissions, e.g. CH_2Cl_2 emissions have been estimated to have increased by approximately 18% between 2012 and 2016, just a 4-year period [Engel et al., 2018].

2.2.6 Ozone Depletion Potentials

Methods to quantify and communicate the impacts of chlorine on stratospheric ozone have been of crucial importance, especially when considering CFCs and other long-lived compounds. The Ozone Depletion Potential (ODP) metric was developed as a simple measure to assess a compound's relative ability to destroy ozone [Solomon & Albritton, 1992; Wuebbles, 1981, 1983]. It is calculated for a compound X according to Equation 2.32 [Wuebbles et al., 2011]:

$$\mathrm{ODP(X)} = \frac{\text{Global mean column ozone change due to unit emissions of X}}{\text{Global mean column ozone change due to unit emissions of CFC}-11} \quad (2.32)$$

CFC-11 (CCl_3F) is used as the reference compound and therefore has an ODP of 1. Most compounds have an ODP lower than 1, due to CFC-11's high potency to deplete ozone (e.g. owing to the 3 chlorine atoms in the molecule, and its lifetime). In the past, ODPs have been calculated using simple one-dimensional or two-dimensional models [Solomon & Albritton, 1992], but the advent of three-dimensional models has allowed for more accurate calculations of stratospheric ozone changes in response to chlorine perturbations, and hence ODPs. These models have also allowed consideration of spatial variability of emissions, which is especially important for compounds not uniformly mixed in the troposphere, such as VSLS [Brioude et al., 2010].

The ODPs of some important compounds, including Cl-VSLS so far studied, are given in **Table 2.1**. Since Cl-VSLS have only been recently considered as compounds that could potentially deplete ozone, not many studies have been performed to calculate their ODPs. $CHCl_3$ has been studied on one occasion by a now old study [Kindler et al., 1995], yielding an ODP of 0.01. Cl-VSLS make up the lower end of ODPs; however, there are substances with ODPs of a similar order of magnitude to Cl-VSLS which are being phased out under the Montreal Protocol, such as HCFC-22 ($CHCl_2F$).

Although ODPs are a useful metric, they are only a measure of the potential a compound has to deplete ozone, and on their own they cannot be used to identify impacts. They have to be used in tandem with global emissions, as a compound that is emitted more from the surface will be more dangerous towards ozone than one with fewer emissions. HCFC-22 emissions are roughly 0.4 Tg yr^{-1}, which is of a similar order to the estimated emissions of $CHCl_3$, 0.3 Tg yr^{-1} [Engel et al., 2018]. However only the former has been enveloped into the Montreal Protocol, despite similar ODPs.

The restrictions of HCFC-22 production by the Montreal Protocol may impact Cl-VSLS in two ways. Firstly, as Cl-VSLS, (i.e. $CHCl_3$) are used as feedstock compounds for HCFC-22 [Fang et al., 2019], their production may also decrease in turn. The phasing out of HCFC-22 has however led to the introduction of an alternative compound, HFC-32 (CH_2F_2), which is also synthesised using Cl-VSLS (i.e. CH_2Cl_2). Secondly, since the compounds have

similar orders of ODP, there is the possibility that Cl-VSLS themselves will be regulated in the future. To determine if this is necessary, new and updated ODPs of Cl-VSLS will need to be calculated, especially for CH_2Cl_2.

Table 2.1. ODPs and surface lifetimes of a selected few chlorinated compounds, including key CFCs (grey), Cl-VSLS (light blue), and three other chlorocarbons: methyl chloroform (CH_3CCl_3), an industrial solvent; HCFC-22, a key CFC replacement compound, both of which are also regulated by the Montreal Protocol; and naturally occurring methyl chloride (CH_3Cl). Table adapted from Harris et al. [2014].

Compound	ODP	Lifetime (years)
CFC-11	1.0	52
CFC-12	0.73	102
CFC-113	0.81	93
CH_3CCl_3	0.14	5
HCFC-22	0.034	12
CH_3Cl	0.015	0.9
$CHCl_3$	0.01	0.4
C_2Cl_4	0.005 (a)	0.25
C_2HCl_3	0.0001-0.0041 (b)	0.013

Note: No ODPs have been calculated for CH_2Cl_2 or $C_2H_4Cl_2$. The double line represents the boundary between substances controlled (top) and uncontrolled (bottom) by the Montreal Protocol.

(a) Wuebbles et al., 2011.

(b) Brioude et al., 2010.

2.3 Emissions of Cl-VSLS

Although the ODP metric gauges the potential relative impact of Cl-VSLS on stratospheric ozone, information regarding emissions is needed to assess the true impact. Global emissions of Cl-VSLS were first investigated by the Reactive Chlorine Emissions Inventory (RCEI) project, back in the late 1990s [Keene et al., 1999]. A significant outcome was that a 1° by 1° grid of estimated emissions was developed, based on the knowledge of Cl-VSLS sources and the distribution of emissions of the day. **Section 2.3.1** delves more into the contents

of the RCEI, including the accompanying natural emission estimates originally supplied by Khalil et al. [1999] in **Section 2.3.2**. **Section 2.3.3** then addresses any new estimates of industrial Cl-VSLS emissions that have since been calculated on a regional basis.

2.3.1 RCEI Emissions

Keene et al. [1999] separated global Cl-VSLS emissions by their different sources and calculated their relative emission strengths. The Cl-VSLS studied included CH_2Cl_2, $CHCl_3$, C_2Cl_4, and C_2HCl_3, in addition to methyl chloride CH_3Cl, and other slightly longer-lived compounds. The RCEI categorised the sources into industrial, soil, ocean, and biomass burning, and **Figure 2.9** shows the relative contributions for each Cl-VSLS. In compiling the RCEI, industry emissions were calculated on a country by country level using 1990 regional emission data for select countries and extrapolating to other countries using a relationship between emissions and GDP [McCulloch and Midgley, 1996]. Ocean emissions were estimated from a limited number of ship cruise missions that measured sea-to-air fluxes of chlorinated compounds, reinforced by modelling studies, and soil emissions were estimated from direct flux measurements [Khalil et al., 1999]. These three sources represent the principal contributions to total global Cl-VSLS emissions, with the natural components considered to be particularly uncertain.

As can be seen from **Figure 2.9**, for CH_2Cl_2 industry is the greatest source, at 0.49 Tg Cl yr^{-1}, roughly triple the contribution from ocean emissions. This is corollary to $CHCl_3$, in which oceans are by far the greatest source (with 0.32 Tg Cl yr^{-1}), with industry providing only 0.062 Tg Cl yr^{-1}. For the other two VSLS of interest in the inventory, C_2Cl_4 and C_2HCl_3, industrial emissions are an order of magnitude greater than ocean emissions. It is important to stress that these estimates are applicable to the 1990s and so are now outdated, especially considering recent trends in these compounds (**Figures 2.6** and **2.7**). **Figure 2.9** also shows that by far the greatest loss of tropospheric Cl-VSLS is from reaction with OH; however, for $CHCl_3$ and CH_2Cl_2 injection to the stratosphere is a nominal loss.

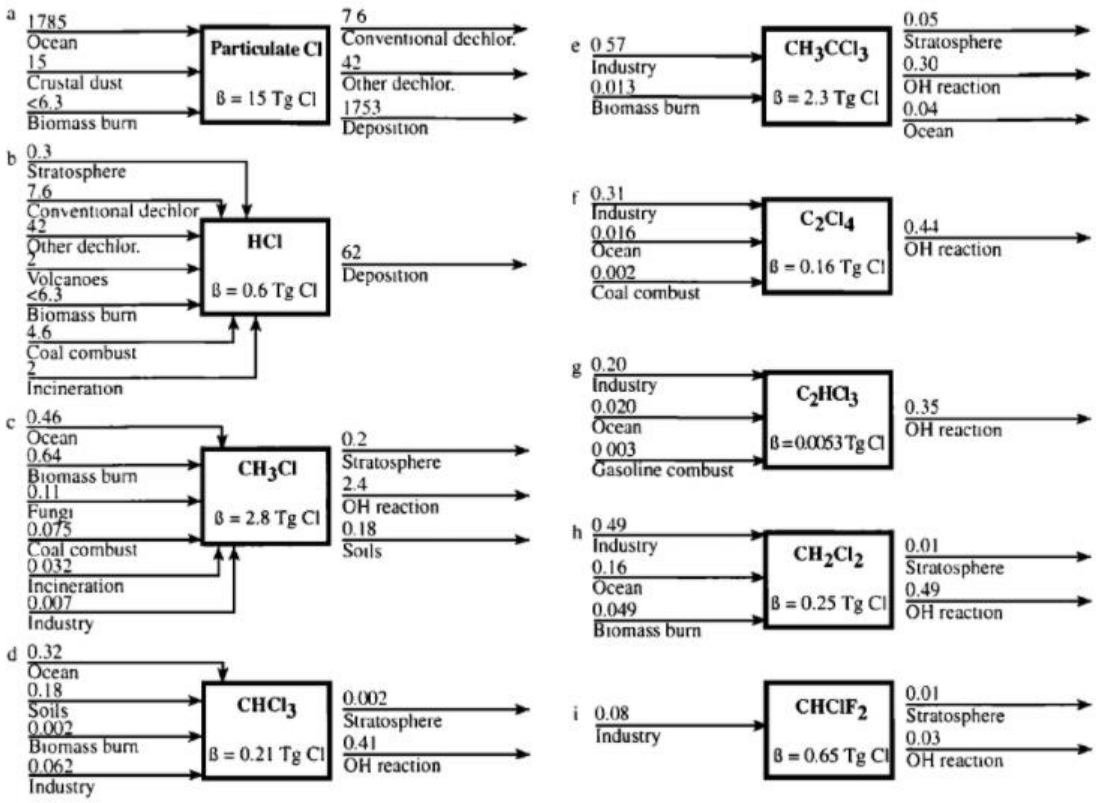

Figure 2.9. Figure taken from Keene et al. [1999] showing the emissions (in Tg Cl yr^{-1}) of various chlorine containing compounds separated into different tropospheric sources and sinks. The Cl-VSLS of interest are (d) $CHCl_3$, (f) C_2Cl_4, (g) C_2HCl_3, and (h) CH_2Cl_2.

2.3.2 Natural Emissions

Although the RCEI includes natural emission estimates for various Cl-VSLS, the global ocean flux and regional distribution is far more uncertain than for industrial emissions. Khalil et al. [1999] described the RCEI natural emission estimates, separating Cl-VSLS emissions into four different bands, 0-30° and 30-90° latitude, for both the northern and southern hemispheres. **Figure 2.10** shows the Cl-VSLS ocean emissions from each of these bands, along with land (soil) emissions for $CHCl_3$.

	S_n (90°N-30°N)[a]	S_{nt} (30°N-0°)	S_{st} (0°-30°S)	S_s (30°S-90°S)	Total [b]
CH_3Cl					
Oceanic	-13	200	280	-7	460 [c]
Land	0	50	50	0	100 [d]
$CHCl_3$					
Oceanic	18	134	134	36	320 [e]
Land	60	60	50	10	180 [f]
CH_2Cl_2					
Oceanic	20	42	42	60	160 [g]
C_2HCl_3	10	4	4	4	20 [g]
C_2Cl_4					
Oceanic	3	3	5	5	16 [g]

Figure 2.10. Figure taken from Khalil et al. [1999], showing the natural emissions (Gg Cl yr^{-1}) of several Cl-VSLS (and CH_3Cl), split into different latitude bands. These emission values are used to generate the ocean and land (soil) contributions for **Figure 2.9**.

Xiao [2008] optimised the RCEI emissions of two Cl-VSLS, with a particular focus on the seasonal cycle of natural emissions. Using a synthesis inversion process (see **Section 2.4.2**), Xiao [2008] calculated mean global natural $CHCl_3$ emissions between 2000 and 2004 of 370 Gg (of source gas) yr^{-1}, markedly smaller than the RCEI estimate of 630 Gg yr^{-1}. The sole cause of this difference was from natural emissions, which suggests that the earlier RCEI inventory overestimated natural emissions, though full verification is difficult. For CH_2Cl_2, a similar inversion was performed that included industrial emissions. This resulted in global CH_2Cl_2 emissions of 629 Gg yr^{-1} (averaged between 2000 and 2004), compared to the RCEI estimate of 836 Gg yr^{-1}. Here, the RCEI overestimated both industrial and oceanic emissions, although since the Xiao [2008] study, CH_2Cl_2 concentrations have increased dramatically [Carpenter et al., 2014; Hossaini et al., 2017], and this industrial estimate now would be brought into question.

More recent determinations of oceanic Cl-VSLS emissions can be used to compare to the RCEI and Xiao [2008] estimates, although such comparisons must be treated with caution due to limited data. Kolusu et al. [2016] inferred CH_2Cl_2 sea-to-air fluxes during ship cruises of the Tropical South Atlantic Ocean in 2009. They calculated the average flux of CH_2Cl_2 as 81 ± 81.72 nmol m^{-2} d^{-1},

corresponding to averages of 6.87 μg m^{-2} d^{-1} and 197 Gg Cl yr^{-1}. Moore [2004] hypothesised that sea-to-air fluxes vary seasonally, and it is entirely possible that averaged out over a year, the oceanic flux of CH_2Cl_2 is negligible. Ooki and Yokouchi [2011] took into account these possible interannual variations in sea-to-air fluxes, calculating just the biogenic CH_2Cl_2 contribution as 0.29 μg m^{-2} d^{-1} - 0.43 μg m^{-2} d^{-1}, or 8.3-12.5 Gg Cl yr^{-1}. No such study has been performed for C_2Cl_4, another Cl-VSLS whose ocean sources, whilst minimal, were also based on a small amount of data during compilation of the RCEI [Khalil et al., 1999]. Without reliable estimates for Cl-VSLS ocean emissions, especially given the large variability in observed fluxes, total Cl-VSLS emission estimates are likely to be increasingly uncertain.

2.3.3 Regional Industrial Estimates

Despite the RCEI providing the most recent (1990s) concerted attempt to quantify global emissions of Cl-VSLS from different sectors, smaller scale studies have since been performed. As a result, some of the RCEI estimates have been called into question. For instance, it was found that the original RCEI estimate of a global biomass burning CH_2Cl_2 source of 59 Gg yr^{-1} [Lobert et al, 1999] may have been overestimated [Lawson et al., 2015; Simpson et al., 2011]. In addition, global natural $CHCl_3$ sources may have also been overestimated, for both soil and ocean sources [Worton et al, 2006], confirmed by Xiao [2008]. Regional estimates of C_2Cl_4 emissions are rare, with Simmonds et al. [2006] providing an industrial estimate of European C_2Cl_4 emissions in 2004 of 60 Gg yr^{-1}, and 30 Gg yr^{-1} based on modelling studies. The RCEI estimates European C_2Cl_4 emissions of 140 Gg yr^{-1}. Indian C_2Cl_4 emissions have been estimated to be 2.9 Gg yr^{-1} in 2016 [Say et al., 2019]. For CH_2Cl_2 and $CHCl_3$ multiple regional studies have been performed, which are detailed below.

CH_2Cl_2

Some industrial regional estimates have been calculated for CH_2Cl_2 from China [Feng et al., 2019, Oram et al., 2017], India [Leedham Elvidge et al., 2015; Say et al., 2019], and Europe [Simmonds et al., 2006]. Feng et al. [2019] calculated Chinese emissions using bottom-up industry information covering 2005 to 2016, with future projections towards 2030. Between 2005 and 2016, Chinese CH_2Cl_2 emissions increased from 101 to 318 Gg yr^{-1}, with the 2005 value of 101 Gg yr^{-1} similar to the RCEI estimate of 130 Gg yr^{-1} for the Asian continent as a whole [Keene et al., 1999]. Oram et al. [2017] used a combination of industry estimates and verification from observations to calculate 2016 CH_2Cl_2 Chinese emissions as 455 Gg yr^{-1}, 1.5 times greater than the Feng et al. [2019] estimate in the same year. Oram et al. [2017] also estimates Chinese $C_2H_4Cl_2$ emissions in 2016 of 203 Gg yr^{-1}, based on the observed ratio of $C_2H_4Cl_2$ with CH_2Cl_2. Alongside Chinese emissions, Japanese CH_2Cl_2 emissions were reported from industrial estimates as ~15 Gg yr^{-1} in 2011, a decrease from 90 Gg yr^{-1} in 2001 [Hase and Kitano, 2013]. Note that in the RCEI, Asian emissions are more heavily distributed over Japan than over China, and the vast opposing shifts in emissions in these two countries [Feng et al., 2019; Hase and Kitano, 2013] contributes to the overall obsolescence of the RCEI. Finally, in India, CH_2Cl_2 emissions were estimated in 2016 to be 96.5 Gg yr^{-1}, using atmospheric measurements to drive an inversion [Say et al., 2019]. This is a 5-fold increase since the previous estimate of 20.3 Gg yr^{-1}, in 2008 [Leedham-Elvidge et al., 2015]

Simmonds et al. [2006] used both industrial and model estimates to investigate European CH_2Cl_2 emissions in the early 2000s. Industrial calculations provide a European emission estimate of 160 Gg yr^{-1}, roughly two times the size of the 70 Gg yr^{-1} calculated from model estimates. Both however depict a significant decrease from the RCEI European estimate of 220 Gg yr^{-1}. This decrease is in line with theorised global changes in CH_2Cl_2 use over the last two decades due to increased industrialisation over China, and phasing out of CH_2Cl_2 use over Europe and North America in line with EU and EPA regulations.

Alternatively to the RCEI, which has estimated CH_2Cl_2 emissions, the IARC (International Agency for Research on Cancer) has documented long-term changes in global CH_2Cl_2 *production*. Production has increased from 93 Gg yr^{-1} in 1960 to 570 Gg yr^{-1} in 1980 [IARC, 1986], with further increases to 764-814 Gg yr^{-1} over the years 2005-2010 [IARC, 2016; OECD, 2011]. On a regional manufacturing basis, CH_2Cl_2 production and imports in the USA were estimated as 45-227 Gg yr^{-1} between 1996 and 2006 [NTP, 2011], and European production and imports in 2016 are estimated between 100 and 1000 Gg yr^{-1} [ECHA, 2016]. In addition, Japanese production in 2011 was reported at 56 Gg yr^{-1} [METI, 2012]. It is important to note that not all uses of CH_2Cl_2 are emissive in nature e.g. for use as a chemical feedstock, and therefore production and import numbers are not a direct equivalent to emissions. For example, Japanese emissions of CH_2Cl_2 were reported as ~15 Gg yr^{-1} in 2011 [Hase and Kitano, 2013], which is 3.5 times lower than the production and import estimate in the same year [METI, 2012]; however, production histories do allow insights into CH_2Cl_2 trends.

$CHCl_3$

For $CHCl_3$, Fang et al. [2019] used inversion processes to determine emissions for East Asia, based on long-term surface observations in the region. The study found that $CHCl_3$ emissions increased at a rate of 2.5% yr^{-1} between 2010 and 2015, primarily due to increases of Eastern Chinese emissions by 41-59 Gg yr^{-1} over this time period. The average regional total for 2015 is estimated as 95 Gg yr^{-1}, larger than the estimate of *global* industrial $CHCl_3$ emissions in the RCEI and the Xiao [2008] inversion study (69 Gg $CHCl_3$ yr^{-1}) [Keene et al., 1999]. Additionally, emissions of $CHCl_3$ from just North Central India were estimated to be 32 Gg yr^{-1} in 2016 [Say et al., 2019]. Average $CHCl_3$ Japanese emissions of 4.9 Gg yr^{-1} were estimated from inverse modelling between 2007 and 2011 [Fang et al., 2019]. However, industry-based emission estimates for Japan over this same time period are approximately only 0.8 Gg yr^{-1} [Hase and Kitano, 2013]. Simmonds et al. [2006] also estimates $CHCl_3$ emissions for Europe as 50 Gg yr^{-1} from industrial calculations and 35 Gg yr^{-1} from model calculations,

compared to 14.5 Gg y^{-1} estimated from the RCEI [Keene et al., 1999]. On a production basis, global production of chloroform amounted to 440 Gg yr^{-1} in 1987, with a significant proportion (>200 Gg yr^{-1}) from the United States [IARC, 2016]. However, unlike CH_2Cl_2, $CHCl_3$ is primarily used in the production of HCFC-22, and not for emissive purposes, which results in low production/emission ratios [WHO, 1994].

2.4 Numerical Models and Techniques

Numerical models have been vital over recent decades in aiding our understanding of chemical and physical processes in the atmosphere. Their computational ability can quickly calculate the distribution and atmospheric impact of a wide range of compounds, and have been instrumental for informing us about the past, present and future of atmospheric composition. In particular, the details of ozone layer destruction and recovery have been greatly improved using models [e.g. Chipperfield et al., 2018; Pawson et al., 2014; Steinbrecht et al., 2018]. Numerical models however come in a variety of different types, each tailored towards achieving specific goals. **Section 2.4.1** will go into further detail about Chemistry Transport Models (CTMs), the subset of models I will be utilising in my thesis. In order to calculate optimised emissions of Cl-VSLS, one of the main aims of this thesis, a mathematical technique called synthesis inversion will be used. **Section 2.4.2** will present the mathematical background to this process, and how it has been used in previous studies.

2.4.1 Chemistry Transport Models

Chemistry transport models (CTMs) are 3-D (latitude, longitude, altitude) global atmospheric models that couple chemistry schemes with transport processes, driven by meteorological conditions (e.g. temperature, wind, and humidity). These conditions are typically calculated “offline” i.e. by a separate model simulation that calculates meteorology, or by reanalysis products, and are then inputted into the CTM at regular intervals. At every time step, CTMs calculate various chemical and dynamical processes that affect the distribution of emitted

source gases and any products gases arising as a result of chemical reactions. The more common setup of CTM involves the model calculating fluxes within grid boxes (Eulerian), as opposed to calculating the fluxes of parcels of air through time (Lagrangian) [Jacob, 1999].

A key focus of a CTM is to study a wide range of environmental issues by using very detailed chemistry schemes. Ozone is a common compound to model in a CTM [e.g. Vautard et al., 2007] because of its environmental importance in both the troposphere and stratosphere. For modelling air pollution and climate, aerosol schemes are often added to the model [Cuvelier et al., 2007]. The end products of CTMs are usually gridded concentration outputs of the target compounds, these can be compared to observations to test how well the model has performed [e.g. Brunner et al., 2003]. Intercomparison between models is common to identify strengths and weaknesses an individual model may have relative to others, and this also allows an average value to be presented, that minimises the effects of individual model biases [e.g. Chipperfield, 2006; Kuhn, 1998; Vautard et al., 2007]. Running multiple different models in a single study is time and resource expensive, so generally intercomparisons are performed just periodically.

In the early stages of CTMs, they were used for investigating short time periods, of the order of months to a few years [Lefèvre et al., 1994; Rood et al., 1989]; however, increasing computing power has led to long multi-year global simulations. The CTM that will be extensively used in subsequent chapters of this thesis is the TOMCAT/SLIMCAT model [Chipperfield, 2006]. This model is separated into tropospheric (TOMCAT) and stratospheric (SLIMCAT) configurations, driven by meteorology from the European Centre for Medium-Range Weather Forecasting's (EMCWF) reanalysis product [Dee et al., 2011]. The model has been used extensively to study many different compounds, including NO_2 [Savage et al., 2004], acetone [Arnold et al., 2005], lead [Giannakopoulos et al., 1999], and several chlorinated and brominated compounds [e.g. Chipperfield et al., 1997; Hossaini et al., 2010, 2013, 2017; Yang et al., 2005].

The TOMCAT/SLIMCAT model typically has a horizontal resolution of 2.8° x 2.8°. With a fairly coarse resolution, many dynamical processes occur on a sub-grid scale and therefore cannot be accurately resolved. Therefore, these processes are parameterised using the variables that can be modelled, such as humidity, temperature, wind speed and direction, etc. In TOMCAT, various convective systems are parameterised by a mass flux scheme from Tiedtke [1989]. This scheme combines thermodynamic representations of convective updrafts and downdrafts with equations dictating cloud formation. Boundary layer turbulent mixing is parameterised by Holtslag and Boville [1993], determining local eddy diffusivity using potential temperature and vertical wind gradient, generally describing boundary layer convection, and hence can be used in tandem with the Tiedtke [1989] parameterisation. Other linked processes that TOMCAT parameterises include rainfall and wet deposition [Giannakopoulos et al., 2004].

As discussed in Section 2.1.6., OH is an integral component of tropospheric chemistry, and has to be accurately described by a model. CTMs such as TOMCAT can read in offline concentration fields of OH, instead of having to include and calculate every key chemical process that affects OH. An OH field commonly used in TOMCAT is originally based on a climatology derived field by Spivakovsky et al. [2000], computed based on observed concentrations of related variables (including O_3, CO, NO_x, temperature). In the TransCom-CH_4 model intercomparison, Patra et al. [2011] adapted this field so that it provided optimal agreement to CH_3CCl_3 (methyl chloroform) trends [Huijnen et al., 2010]. **Figure 2.11** depicts the latitude-pressure profile of this distribution. Similarly to **Figure 2.5**, there is a greater OH concentration over the Northern Hemisphere Tropics, where convective uplift is strongest. However, unlike **Figure 2.5**, the TOMCAT OH field depicts a concentration at 600 hPa twice as large than at the surface. Multi-model global OH concentration models can deviate by as much as 20% from the mean [Zhao et al., 2019].

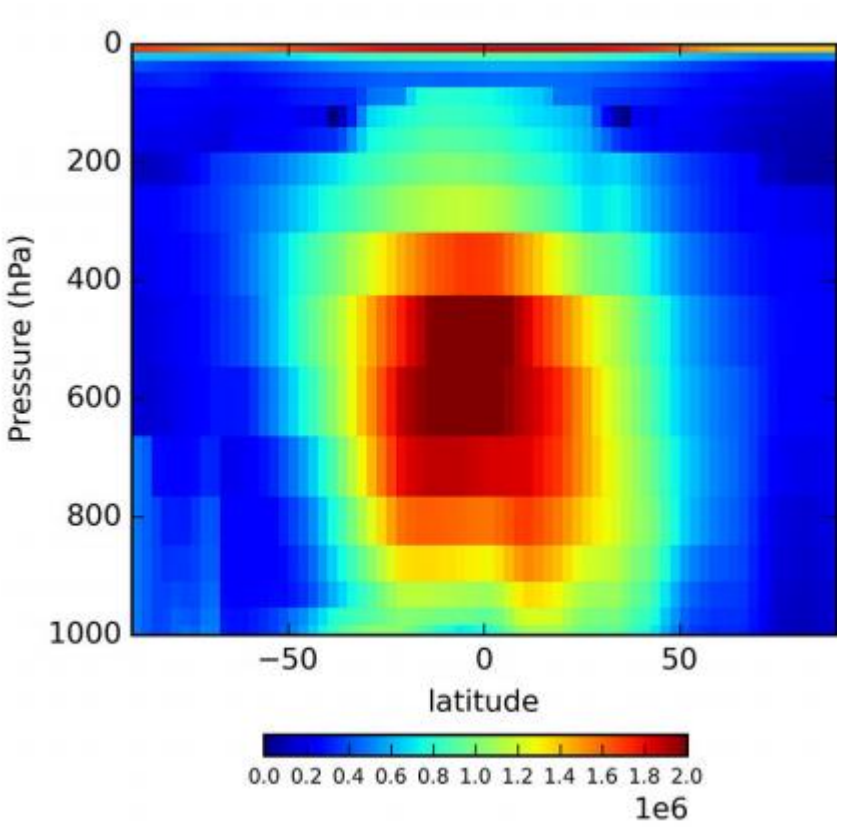

Figure 2.11. Annual zonal mean OH distribution (10^6 molecules cm^{-3}) commonly used in TOMCAT simulations. The field is described by Patra et al. [2011] and was originally derived from Spivakovsky et al. [2000]. Taken from Figure 3 of Yin et al. [2015].

2.4.2 Synthesis Inversion

Synthesis inversion is a mathematical technique that is used to optimise emissions of a given compound, based on knowledge of: (a) a prior estimate of emissions, (b) modelled concentrations calculated from these prior emissions, and (c) a network of observational data over the time period studied [Enting et al., 1995]. The mathematical process works on minimising the "cost function", a variable (J) that weighs the mismatches between two pairs of variables: (a) the assimilated observations and the optimised emissions estimate, against (b) both the optimised and prior emissions estimates [Baker et al., 2006; Wang et al., 2018]. An example of the cost function equation is given in Equation 2.33 below:

$$\boldsymbol{J}(x) = \frac{1}{2}(\boldsymbol{x} - \boldsymbol{x_b}).\ \boldsymbol{B}^{-1}.(\boldsymbol{x} - \boldsymbol{x_b}) + \frac{1}{2}(\boldsymbol{y} - \boldsymbol{G}.\boldsymbol{x}).\ \boldsymbol{R}^{-1}.(\boldsymbol{y} - \boldsymbol{G}.\boldsymbol{x}) \qquad (2.33)$$

where $\boldsymbol{x}$ represents a new posterior emission estimate, $\boldsymbol{x_b}$ the prior emissions, $\boldsymbol{G}$ a model concentration output calculated from the prior emissions, co-located with the corresponding observations, $\boldsymbol{y}$, and **R** and **B** represent the observational and prior emission error covariance matrices, respectively. Observational errors provide information on how effective each observation is in constraining the optimised emissions, with the smaller the error, the more constraint there is on the inversion process. This is similarly the case for the errors in the prior emissions. The goal of synthesis inversion is to find the smallest least-squares Bayesian solution for $\boldsymbol{x}$, which is achieved by minimising Equation 2.33, i.e. setting $\frac{d\boldsymbol{J}}{d\boldsymbol{x}} = 0$, and then solving for $\boldsymbol{x}$**.**

Synthesis inversion is popular for long-lived atmospheric gases, such as CO_2 [Enting et al., 1995; Wang et al., 2018], H_2 [Bousquet et al., 2011], and CH_4 [McNorton et al., 2018; Patra et al., 2011]. The process works best with large observational networks, which allows emissions estimates to be more finely tuned. Synthesis inversions are performed using regional tracers, as this allows each region to be individually finely tuned by incremental amounts to optimise emissions. Therefore, the more regions there are, the more effective the inversion, given there are enough observations to constrain each region successfully.

2.5 Summary

In this chapter, I have presented an overview of the main topics that will be investigated in the subsequent chapters. I have introduced stratospheric chemistry and processes, with the focus of chlorine chemistry (**Section 2.1**), and a small overview of tropospheric ozone chemistry. With Cl-VSLS as the primary subject of this thesis, I have then presented background scientific information we have on their uses, observed concentrations, and impact (**Section 2.2**), before discussing the current knowledge regarding emissions (**Section 2.3**). Finally, I have briefly discussed chemistry transport models and the synthesis inversion procedure, both of which will be widely used in later chapters (**Section 2.4**).

Chapter 3

On the Regional and Seasonal Ozone Depletion Potential of Chlorinated Very Short-Lived Substances

Tom Claxton[1], Ryan Hossaini[1], Oliver Wild[1], Martyn P. Chipperfield[2,3], Chris Wilson[2,3]

[1]Lancaster Environment Centre, Lancaster University, Lancaster, UK
[2]School of Earth and Environment, University of Leeds, Leeds, UK
[3]National Centre for Earth Observation, University of Leeds, Leeds, UK

The following work has been published in Geophysical Research Letters on 19 April 2019 (citation: On the regional and seasonal ozone depletion potential of chlorinated very short-lived substances, *Geophysical Research Letters*, **46**, 5489-5498, doi:10.1029/2018GL081455, 2019). The authors and their contributions are listed below:

Tom Claxton: Processed the data, analysed the data, and wrote the manuscript. **Ryan Hossaini, Martyn P. Chipperfield, and Chris Wilson:** Helped with the synthesis and interpretation of results and compilation of the manuscript. **Oliver Wild:** Helped to compile the manuscript, providing scientific comments.

Abstract

Chloroform ($CHCl_3$), dichloromethane (CH_2Cl_2), perchloroethylene (C_2Cl_4), and 1,2-dichloroethane ($C_2H_4Cl_2$) are chlorinated Very Short-Lived Substances (Cl-VSLS) with a range of commercial/industrial applications. Recent studies highlight the increasing influence of Cl-VSLS on the stratospheric chlorine budget and therefore their possible role in ozone depletion. Here we evaluate the ozone depletion potential (ODP) of these Cl-VSLS using a three-dimensional chemical transport model and investigate sensitivity to emission location/season. The seasonal dependence of the ODPs is small, but ODPs vary by a factor of 2-3 depending on the continent of emission: 0.0143-0.0264 ($CHCl_3$), 0.0097-0.0208 (CH_2Cl_2), 0.0057-0.0198 (C_2Cl_4), and 0.0029-0.0119 ($C_2H_4Cl_2$). Asian emissions produce the largest ODPs owing to proximity to the tropics and efficient troposphere-to-stratosphere transport of air originating from industrialised East Asia. The Cl-VSLS ODPs are generally small, but the upper ends of the $CHCl_3$ and CH_2Cl_2 ranges are comparable to the mean ODP of methyl chloride (0.02), a longer-lived ozone-depleting substance.

Plain Language Summary

Anthropogenic emissions of long-lived chlorinated substances (e.g. chlorofluorocarbons) have led to global ozone layer depletion since the 1970s/1980s, including the Antarctic Ozone Hole phenomenon. The 1987 Montreal Protocol was enacted to ban production of major ozone-depleting gases, and in consequence, there are signs that the ozone layer is recovering. However, emissions of so-called very short-lived substances, such as dichloromethane, have increased in recent years. Historically, these compounds have not been considered a major threat to stratospheric ozone, due to relatively short lifetimes, and they are not controlled by the Protocol. Given that production of these compounds is projected to increase, it is important to determine their ability to affect stratospheric ozone. We quantify the ozone depletion potential (ODP) of chloroform and perchloroethylene and, for the first time, dichloromethane and 1,2-dichloroethane, the main chlorinated very short-lived substances. We show that their ODPs vary depending on where

the emission occurs. For example, the ODP from Asian dichloromethane emissions is up to a factor of two greater than that from European emissions. This reflects the relative efficiency of troposphere to stratosphere transport between different geographical areas; the transport of polluted boundary layer air from continental East Asia being one relatively efficient route.

3.1 Introduction

Chlorinated Very Short-Lived Substances (Cl-VSLS), including chloroform ($CHCl_3$) and dichloromethane (CH_2Cl_2), are a significant source of stratospheric chlorine [e.g. Hossaini et al., 2015; Laube et al., 2008] and therefore contribute to ozone depletion [e.g. Chipperfield et al., 2018; Hossaini et al., 2017]. These compounds have surface atmospheric lifetimes of ~6 months or less [e.g. Ko et al., 2003] and are used in a variety of commercial and industrial applications. CH_2Cl_2 is a common solvent [e.g. Simmonds et al., 2006], used as a paint stripper and in foam production, among other applications [e.g. Feng et al., 2019; Montzka, Reimann, et al., 2011]. $CHCl_3$ has historically been used in the production of HCFC-22 and is a by-product of paper manufacturing. Other Cl-VSLS include perchloroethylene (C_2Cl_4) and 1,2-dichloroethane ($C_2H_4Cl_2$), both of which also have significant anthropogenic sources, though shorter atmospheric lifetimes [Montzka, Reimann, et al., 2011].

Owing to increasing emissions, tropospheric CH_2Cl_2 mixing ratios have approximately doubled since the early 2000s, evidenced by long-term surface monitoring data [e.g. Hossaini et al., 2015, 2017] and measurements in the upper troposphere [Leedham Elvidge et al., 2015]. Although the influence of CH_2Cl_2 on ozone has been modest in the recent past [Chipperfield et al., 2018], if sustained CH_2Cl_2 growth continues in coming decades, ozone layer recovery could be delayed [Hossaini et al., 2017]. A substantial portion of CH_2Cl_2 emissions, estimated globally at ~0.8 Tg/year in 2012 [Carpenter et al., 2014], is believed to occur in Asia [Oram et al., 2017]. CH_2Cl_2 emissions from China, for example, are thought to have increased by a factor of ~3 between 2005 and 2016, with further increases projected until 2030 [Feng et al., 2019].

The ozone depletion potential (ODP) concept [Solomon & Albritton, 1992; Wuebbles, 1981, 1983] was introduced as a relative means to assess a compound's ability to destroy stratospheric ozone. ODP assessment is integral to policy frameworks, notably the Montreal Protocol, which prohibits the production of numerous ozone-depleting substances. For long-lived gases that are well mixed in the troposphere (e.g. chlorofluorocarbons [CFCs]), ODPs are generally independent of emission location and season. However, for VSLS, owing to their short lifetimes, emission location and season have been shown to be important factors [e.g. Brioude et al., 2010; Ko et al., 2003; Pisso et al., 2010]. For particularly short-lived VSLS (e.g. CH_3I, lifetime of days-weeks), the ODP can vary by a factor of ~30 depending on where the emission occurs [Brioude et al., 2010; Harris et al., 2014].

Despite recent interest in Cl-VSLS, very little information on their ODP is present in the literature, and there are no estimates for CH_2Cl_2 and $C_2H_4Cl_2$, to our knowledge. In this study we use a three-dimensional (3-D) chemical transport model (CTM) to quantify the ODP of four Cl-VSLS ($CHCl_3$, CH_2Cl_2, C_2Cl_4, and $C_2H_4Cl_2$). We consider how their ODPs vary with emission location (and season) from five major industrialised geographical areas. **Sections 3.2** and **3.3** describe the CTM setup and the ODP procedure. Results are presented in **Section 3.4** and conclusions in **Section 3.5**. We also calculate the ODP of methyl chloride, a longer-lived chlorocarbon, with a lifetime of ~1 year [Montzka, Reimann, et al., 2011].

3.2 TOMCAT/SLIMCAT 3-D CTM

We performed a series of experiments with the TOMCAT/SLIMCAT 3-D CTM [Chipperfield, 2006; Monks et al., 2016], widely used in VSLS-related studies [e.g. Hossaini, Chipperfield, et al., 2016, Hossaini, Patra, et al., 2016]. The CTM is forced by wind and temperature fields from the European Centre for Medium-Range Weather Forecasts ERA-Interim reanalysis [Dee et al., 2011]. Simulations were performed at a horizontal resolution of 2.8° × 2.8°, with 60 vertical levels extending from the surface to ~60 km. The CTM exists in both tropospheric and stratospheric configurations. In tropospheric mode, convective

transport is parameterised based on Tiedtke [1989] and turbulent boundary layer mixing follows Holtslag and Boville [1993]. This model configuration was used to quantify the stratospheric chlorine input due to Cl-VSLS and their product gases, phosgene ($COCl_2$) and inorganic chlorine (Cl_y). $COCl_2$ is an oxidation product of CH_2Cl_2, $CHCl_3$, and C_2Cl_4 (**Table 3.S1**, Supporting Information), with an assumed tropospheric lifetime of 58 days [Kindler et al., 1995] due to wet deposition. For Cl_y, the assumed lifetime is 5 days [Sherwen et al., 2016].

The stratospheric configuration of TOMCAT/SLIMCAT contains a detailed chemistry scheme covering all major processes relevant to stratospheric ozone loss (e.g. heterogeneous reactions on sulfate aerosols and polar stratospheric clouds). The model version employed here was used by Chipperfield et al. [2018] to investigate long-term ozone trends. Here it is used to determine the response of ozone to stratospheric chlorine perturbations from Cl-VSLS (and products) and to therefore evaluate ODPs. The Cl-VSLS chemistry is consistent between both CTM configurations, with kinetic data mostly from Burkholder et al. [2015].

3.3 ODP Calculation

The steady-state ODP (Equation 3.01) of a compound, X, is defined as the global column ozone change due to a unit emission of X, relative to the global column ozone change due to a unit emission of CFC-11 at equilibrium [e.g. Wuebbles et al., 2011]. The ODP of X can therefore be calculated from a reference stratospheric model run, a model run with X perturbed relative to the reference, and a run with CFC-11 perturbed relative to the reference.

$$\mathrm{ODP(X)} = \frac{\text{Global mean column ozone change due to unit emissions of X}}{\text{Global mean column ozone change due to unit emissions of CFC}-11} \qquad (3.01)$$

The tropospheric TOMCAT/SLIMCAT configuration was first used to calculate the steady-state stratospheric input of CH_2Cl_2, $CHCl_3$, C_2Cl_4, and $C_2H_4Cl_2$ and their products. These steady-state chlorine perturbations were determined using five different years of model meteorology (2013-2017) to assess the influence of interannual tropospheric transport variability on our results. As we

are principally interested in how chlorine perturbations vary with emission location, a series of tagged Cl-VSLS tracers was emitted from five geographical areas, each at a continuous rate of 1 Tg/year. The regions (**Figure 3.1**) are based on the TRANSCOM project [e.g. Gurney et al., 2003; Patra et al., 2011] and broadly correspond to major industrialised areas: Temperate North America (TemNA), Europe (Eur), Temperate Latin America (TemLA), Temperate Asia (TemAs), and Tropical Asia (TroAs). A 1-Tg/year emission was chosen as it is similar to current global estimates of CH_2Cl_2 emissions [Hossaini et al., 2017].

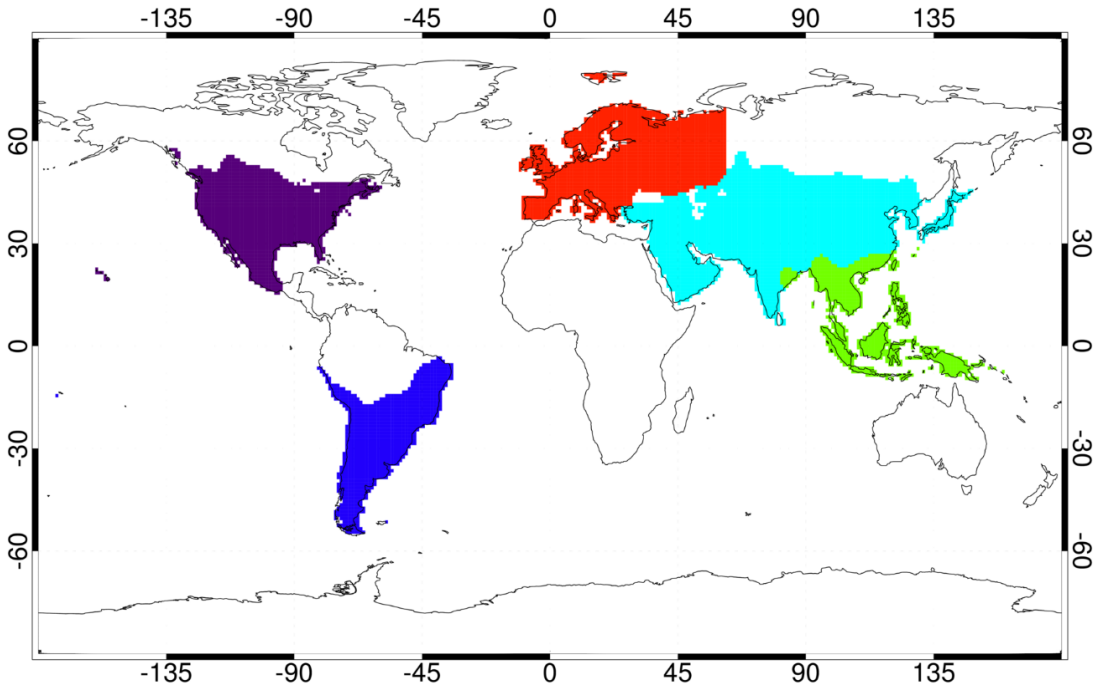

Figure 3.1. The 5 regions for the ODP analysis, regions based on the TRANSCOM project: Purple = Temperate NA, Blue = Temperate LA, Red = Europe, Light Blue = Temperate Asia, Lime Green = Tropical Asia. (Note: Originally included in the Supporting Information)

Within regions, the Cl-VSLS emission distribution followed the industrial scenario [Keene et al., 1999; McCulloch et al., 1999] of the Reactive Chlorine Emissions Inventory (RCEI). For $C_2H_4Cl_2$, not considered by the RCEI, the same distribution as CH_2Cl_2 was assumed—reasonable given their observed

correlation [Oram et al., 2017]. Although the RCEI was undertaken over 20 years ago, the broadscale industrial emission distribution within our regions is unlikely to have changed to such a degree to significantly affect our results. This is particularly true of Europe and North America, though Asian regions may have seen larger changes to the distribution. To test the influence of emission distributions, we also considered Cl-VSLS tracers emitted with uniformly distributed fluxes within each region; that is, an extreme departure from the RCEI case.

The above approach was also used to calculate the steady-state CFC-11 stratospheric perturbation following a continuous 50-Gg/year surface emission. This moderate emission rate was chosen to (a) avoid any possible nonlinearities in the ozone response for large chlorine perturbations and (b) give a response above the model's numerical noise [e.g. Wuebbles et al., 1998]. The resulting stratospheric CFC-11 perturbation (~100 ppt) produces a global mean column ozone decrease of ~1%, consistent with previous work [Wuebbles et al., 1998]. The calculated range (due to different emission locations/distribution) of stratospheric Cl-VSLS perturbations (and the CFC-11 perturbation) were used as input to the detailed stratospheric chemistry model (**Section 3.2**). For each chlorine perturbation, the ozone response was calculated relative to a reference unperturbed stratosphere, allowing ODPs to be quantified from Equation 3.01.

3.4 Results

3.4.1 Hemispheric and Zonal Source Gas Distributions

A key consideration is whether anthropogenic emissions from Northern Hemisphere (NH) midlatitudes and subtropics (including major Asian economies) can sustain significant Cl-VSLS mixing ratios in the tropics, where troposphere-to-stratosphere transport takes place. **Figure 3.2** compares the modelled CH_2Cl_2 abundance at the surface and at 90 hPa (~17 km, location of tropical tropopause), resulting from a 1-Tg/year emission from four of the five regions considered. Note Temperate North America, not shown for clarity, shows a similar hemispheric distribution to Europe. Similar figures for other Cl-VSLS are given in **Figures 3.S1-3.S3** (Supporting Information).

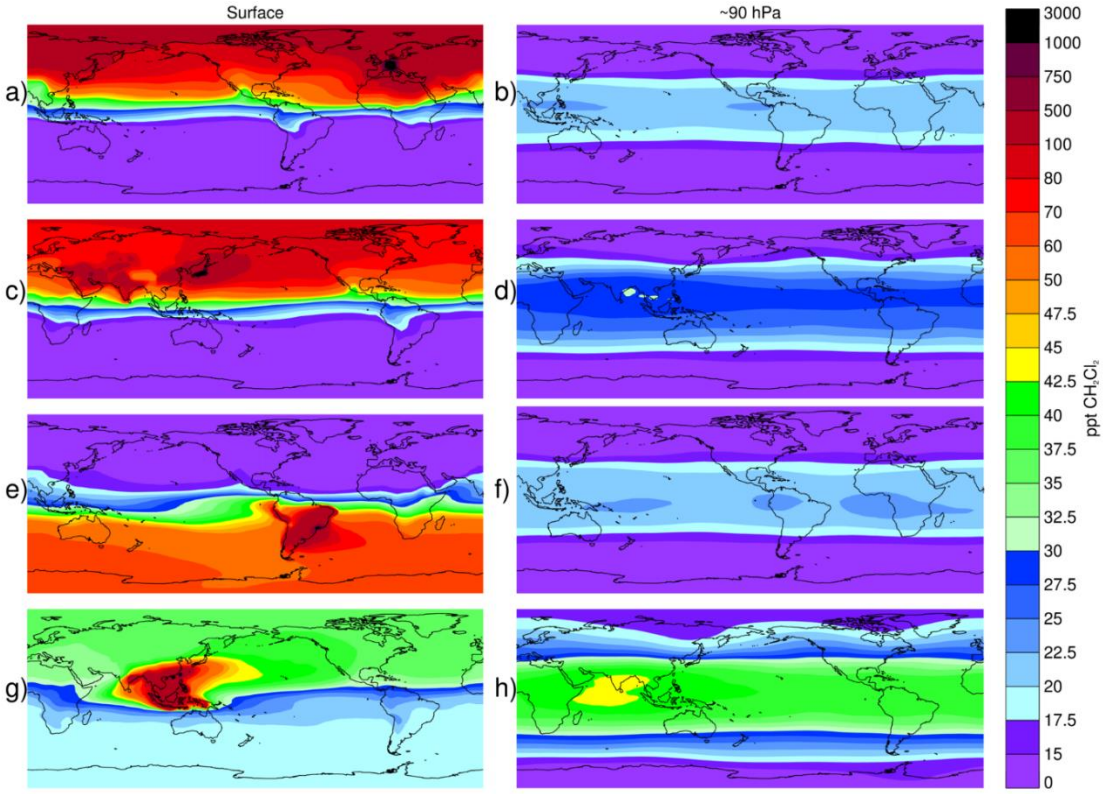

Figure 3.2. Modelled 5-year annual mean steady-state mixing ratio (ppt) of CH_2Cl_2 at the surface (left) and at 90 hPa (right) based on a 1-Tg/year emission from (a, b) Europe, (c, d) Temperate Asia, (e, f) Temperate Latin America, and (g, h) Tropical Asia.

Emissions from midlatitude and subtropical regions establish a strong CH_2Cl_2 hemispheric gradient at the surface (**Figure 3.2**, left column). Zonally, surface CH_2Cl_2 is relatively well mixed away from main industrialised areas where clear maxima occur. The tropical (±20°) 5-year mean surface CH_2Cl_2 mixing ratios at steady state are 29 ppt (emission from TemNA), 26 ppt (Eur), 30 ppt (TemAs), 39 ppt (TroAs), and 37 ppt (TemLA). Proximity to the tropics is clearly a large influence on these values, with TroAs emissions sustaining the largest tropical CH_2Cl_2 levels. The spread in these values is ~40%, with Eur and TemNA emissions resulting in similar tropical surface CH_2Cl_2 abundances that are a factor of 1.5 lower than that resulting from TroAs emissions. While transport of Cl-VSLS to the stratosphere will be relatively inefficient over these regions, the CH_2Cl_2 lifetime is sufficiently long to allow meridional transport to sustain nonnegligible CH_2Cl_2 abundances in the tropical boundary layer (e.g. **Figure**

3.2a). Once in the tropical troposphere, vertical gradients in zonally averaged CH_2Cl_2 are generally small [Hossaini, Chipperfield, et al., 2016; also **Figure 3.3**].

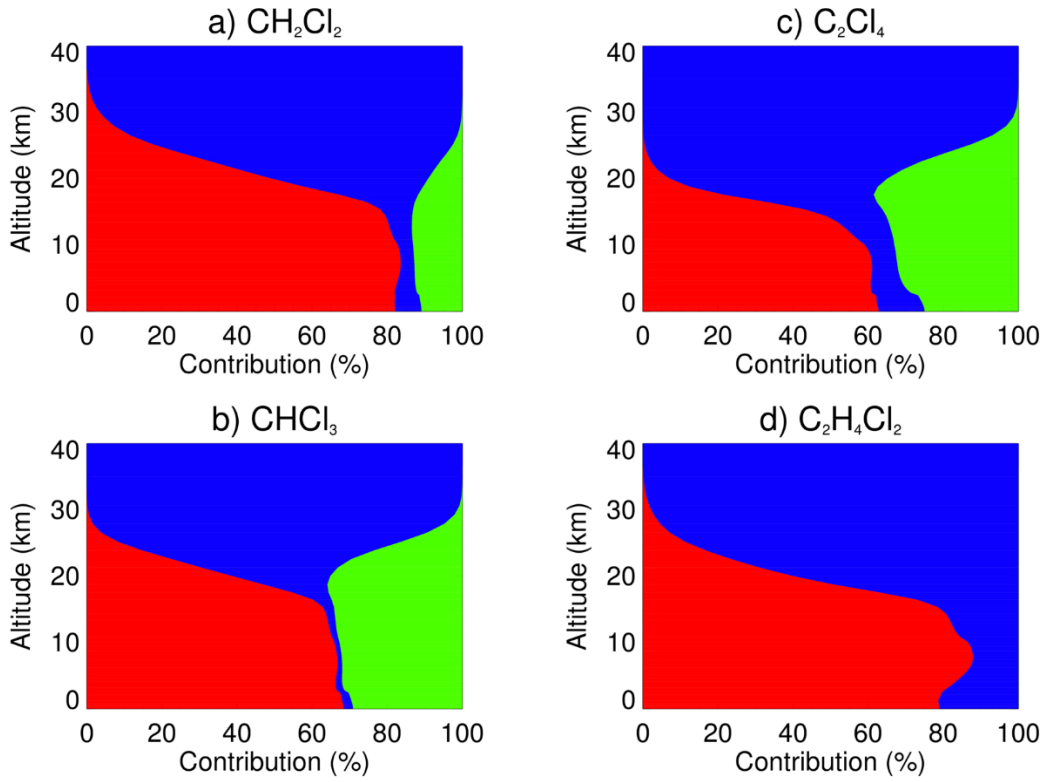

Figure 3.3. Vertical profile of the contribution (%) of source and product gases to total chlorine from (a) CH_2Cl_2, (b) $CHCl_3$, (c) C_2Cl_4, and (d) $C_2H_4Cl_2$. Contributions are tropical (20°N-20°S) 5-year means calculated at steady state following a continuous 1-Tg/year emission from Europe. Red is the proportion for source gases, blue for Cl_y, and green for $COCl_2$ (see text in Supporting Information).

Tropical CH_2Cl_2 is reasonably well mixed at 90 hPa, the approximate tropical tropopause. Compared to analogous brominated compounds such as $CHBr_3$ (24-day lifetime in tropical boundary layer) and CH_2Br_2 (94 days), Cl-VSLS are relatively long-lived, thus subgrid scale transport processes (e.g. convection) are a less important influence for their troposphere-to-stratosphere transport. For $CHBr_3$, for example, previous model studies highlighted strong zonal variability in its tropical near-tropopause abundance [e.g. Aschmann et al., 2011; Hossaini, Patra, et al., 2016]. The largest levels have been predicted in

strong convective regions, including the Indian Ocean, Central America, and the Maritime Continent [e.g. Aschmann et al., 2011; Gettelman et al., 2009; Hosking et al., 2010; Liang et al., 2014]. Such strong zonal variability is less apparent for CH_2Cl_2 apart from in the case of Asia emissions (particularly tropical) which co-located with such transport processes (**Figure 3.2h**).

3.4.2 Stratospheric Chlorine Perturbations

A summary of modelled stratospheric Cl perturbations from Cl-VSLS is given in **Table 3.1**. These steady state perturbations are calculated as the sum of chlorine in both source and product gases, expressed as annual/seasonal means over a 5-year period, 2013-2017. Due to the latter, these values are more representative than considering a single year of meteorology. Regardless of emission location, the Cl perturbation is greatest for $CHCl_3$ (91.9 ppt Cl), followed by CH_2Cl_2 (69.4 ppt Cl), C_2Cl_4 (33.7 ppt Cl), and $C_2H_4Cl_2$ (23.6 ppt Cl). Recall these perturbations are based on a 1-Tg/year source gas emission, with the values quoted above being all-region averages, assuming the RCEI emission distribution. For a given region, differing Cl perturbations across species reflects the different chlorine atomicity and tropospheric lifetimes of the compounds. In the tropical boundary layer, local lifetimes of $CHCl_3$, CH_2Cl_2, C_2Cl_4, and $C_2H_4Cl_2$ were assessed to be 112, 109, 67, and 47 days, respectively [Carpenter et al., 2014], consistent with the relative importance of each compound described above and in good agreement to our model estimates (**Table 3.S2**, Supporting Information).

Table 3.1. Modelled Stratospheric Cl Perturbations (ppt Cl) Due to 1-Tg/ year VSLS Emission from Different Regions.

		Annual mean stratospheric Cl perturbation (ppt Cl)		Seasonal mean (RCEI distr.) stratospheric Cl perturbation (ppt Cl)				
Species	Emission region	Evenly distributed emission	RCEI distributed emissions	DJF	MAM	JJA	SON	SGI (%; RCEI distr.)
$CHCl_3$	Eur	79.2 ± 1.0	79.1 ± 1.0	73.6 ± 0.7	75.2 ± 2.2	82.7 ± 1.5	84.9 ± 0.9	61.6
	TemAs	97.6 ± 2.1	99.5 ± 2.0	93.7 ± 1.7	89.8 ± 2.9	102.1 ± 2.7	112.4 ± 3.4	65.3
	TemLA	79.1 ± 0.6	78.7 ± 0.6	82.0 ± 0.8	84.2 ± 0.9	74.5 ± 1.0	74.0 ± 1.2	60.8
	TemNA	84.1 ± 0.9	82.0 ± 0.8	77.4 ± 0.7	78.6 ± 1.8	85.1 ± 1.2	86.9 ± 1.1	61.9
	TroAs	130.5 ± 5.5	120.0 ± 4.8	118.9 ± 4.5	113.3 ± 7.3	120.3 ± 5.7	127.3 ± 6.4	68.4
CH_2Cl_2	Eur	59.1 ± 0.9	55.8 ± 0.8	51.2 ± 0.7	54.3 ± 1.8	59.4 ± 1.0	58.3 ± 0.7	76.5
	TemAs	75.3 ± 1.7	71.0 ± 1.3	67.8 ± 0.8	66.4 ± 2.2	72.5 ± 1.5	77.2 ± 2.2	77.6
	TemLA	59.6 ± 0.5	58.9 ± 0.5	60.9 ± 0.7	62.6 ± 1.1	56.0 ± 0.8	56.1 ± 1.1	75.1
	TemNA	63.3 ± 0.8	61.8 ± 0.8	57.8 ± 1.0	60.6 ± 1.8	65.0 ± 0.8	63.6 ± 1.2	76.6
	TroAs	105.5 ± 4.9	99.3 ± 4.8	99.9 ± 4.5	95.0 ± 7.3	99.4 ± 5.9	102.8 ± 6.2	80.0
C_2Cl_4	Eur	24.0 ± 0.5	22.6 ± 0.5	20.7 ± 0.5	22.4 ± 1.2	23.9 ± 0.6	23.4 ± 0.4	38.2
	TemAs	37.7 ± 1.5	34.3 ± 1.1	32.8 ± 0.7	30.4 ± 1.6	34.3 ± 1.3	39.7 ± 2.1	42.5
	TemLA	25.5 ± 0.4	24.8 ± 0.4	25.7 ± 0.6	27.2 ± 0.9	22.9 ± 0.5	23.4 ± 0.8	38.5
	TemNA	27.1 ± 0.6	25.9 ± 0.6	24.7 ± 0.9	25.8 ± 1.4	26.7 ± 0.4	26.3 ± 0.8	39.3
	TroAs	66.1 ± 4.6	60.7 ± 4.6	62.9 ± 4.1	56.8 ± 6.7	59.3 ± 5.7	64.0 ± 6.0	48.1
$C_2H_4Cl_2$	Eur	16.8 ± 0.5	15.7 ± 0.4	13.8 ± 0.6	17.0 ± 1.1	17.5 ± 0.4	14.4 ± 0.4	75.7
	TemAs	27.1 ± 1.1	24.0 ± 0.8	23.0 ± 0.5	22.5 ± 1.4	24.1 ± 0.8	26.4 ± 1.6	76.8
	TemLA	16.5 ± 0.3	15.8 ± 0.4	16.1 ± 0.5	17.0 ± 0.7	14.8 ± 0.4	15.2 ± 0.7	75.7
	TemNA	18.8 ± 0.5	17.8 ± 0.5	16.5 ± 0.8	19.2 ± 1.2	19.2 ± 0.3	16.5 ± 0.7	76.1
	TroAs	49.8 ± 3.9	44.9 ± 3.7	46.5 ± 3.4	41.7 ± 5.4	43.9 ± 4.5	47.7 ± 5.0	78.5

Note: Steady-state perturbations derived as sum of chlorine from source and product gases at the tropical (±20° latitude) tropopause (16.5-17.5km). Perturbations are annual 5-year means (2013-2017 meteorology, ±1σ) and are presented for the evenly distributed and the RCEI-distributed emissions. Seasonal values (5-year mean ±1σ) assume RCEI distribution. Final column gives annual total Cl perturbation due to SGI (%). DJF=December-January-February; MAM=March-April-May; JJA=June-July-August; SON=September-October-November; TemNA=Temperate North America; Eur=Europe (Eur); TemLA=Temperate Latin America; TemAs=Temperate Asia; TroAs=Tropical Asia; RCEI=Reactive Chlorine Emissions Inventory; SGI =source gas injection.

Table 3.1 reveals that differences between tracers with the RCEI emission distribution and those evenly distributed are small; for example, the all-region mean Cl perturbation from CH_2Cl_2 is 69.4 ppt Cl (RCEI) and 72.6 ppt Cl (even), agreeing to within 4.6%. We focus herein on the RCEI case, noting that small differences between the scenarios are likely caused by how close the emissions are distributed to the tropics, where troposphere-to-stratosphere transport takes place. Indeed, for this reason, calculated Cl perturbations exhibit significant sensitivity to the continental scale location of emission, consistent with the known dependence of VSLS emission location on their ODPs [e.g. Bridgeman et al., 2000; Brioude et al., 2010]. The spread in stratospheric Cl perturbations due to emission location is 52% ($CHCl_3$), 78% (CH_2Cl_2), 169% (C_2Cl_4), and 186% ($C_2H_4Cl_2$), with longer-lived compounds exhibiting a lower sensitivity. The seasonal dependence of stratospheric Cl perturbations is far smaller. For example, for a given region of CH_2Cl_2 emission, the seasonal spread is ~10% or less. Therefore, we do not overinterpret our findings in terms of seasonality, though note that seasonal differences reflect the complex interaction of (a) seasonality in transit times for NH air reaching the tropics [Orbe et al., 2016], low level flow into areas of convection [Pisso et al., 2010], seasonality in vertical transport efficiency through the tropical tropopause layer [e.g. Bergman et al., 2012; Hosking et al., 2010; Krüger et al., 2009], and interaction of such processes with region-dependent Cl-VSLS lifetimes [Brioude et al., 2010].

Tropical Asia emissions lead to the largest stratospheric Cl injections, coinciding with efficient troposphere-to-stratosphere transport over the Maritime Continent [e.g. Hosking et al., 2010; Wright et al., 2011]. Temperate Asia is the second most efficient region, most likely due to its locality toward tropical Asia and reflecting the efficient transport of polluted airmasses originating from continental East Asia to the deep tropics and tropical upper troposphere [Ashfold et al., 2015; Oram et al., 2017; Orbe et al., 2015]. Note our stratospheric chlorine perturbations are somewhat, but not strongly, influenced by the year of meteorology under consideration, as evident by the ±1σ values in **Table 3.1**. These standard deviations (σ) are calculated on the 5-year mean Cl perturbations and in relative terms (the ratio of σ to the mean) range from 0.8-8%. The two Asian regions are impacted the largest by interannual

variability, indicating that transport processes have greater leverage to influence VSLS troposphere-to-stratosphere transport from these regions compared to others.

3.4.3 SGI Versus PGI

Table 3.1 also shows the percentage of total chlorine that enters the stratosphere via source gas injection (SGI). For a given species, the regional spread in these values is generally small, with emissions from tropical Asia resulting in the largest SGI components. CH_2Cl_2 has the largest proportion of SGI (75-80%) and C_2Cl_4 (38-48%) the least. The relative importance of SGI versus Product Gas Injection (PGI) depends on both the lifetime of the source gases and the different combination of product gases ($COCl_2$ and Cl_y) produced. **Figure 3.3** shows vertically resolved tropical mean profiles of the contribution of SGI versus PGI, using European emissions as an example.

In terms of the total tropospheric chlorine budget arising from $CHCl_3$ and CH_2Cl_2, source gases are the most important component (accounting for ~60-80% at the tropical tropopause, **Table 3.1**), followed by phosgene. $CHCl_3$ and CH_2Cl_2 have similar lifetimes, and the larger phosgene component in the budget of the former reflects the larger phosgene yield from the $CHCl_3$ + OH sink, compared to that from CH_2Cl_2 oxidation (see Supporting Information, **Section 3.6**). For C_2Cl_4, delivery of chlorine to the stratosphere via SGI and PGI is comparable, with the latter slightly larger. This reflects the shorter C_2Cl_4 lifetime compared to $CHCl_3$ and CH_2Cl_2 and the significant phosgene yield from C_2Cl_4 oxidation [Tuazon et al., 1988]. Note a source of uncertainty (see also **Section 3.4.4**) in our model is the assumed tropospheric washout lifetimes of phosgene and Cl_y products (**Section 3.6**). This uncertainty is more relevant to the two shortest-lived compounds under consideration (C_2Cl_4 and $C_2H_4Cl_2$).

3.4.4 ODP Calculations

The stratospheric chlorine injections discussed in **Section 3.4.2** were added as tropopause boundary conditions in the stratospheric TOMCAT/SLICMAT model

configuration. For each Cl-VSLS, three stratospheric simulations were performed, the first with the mean Cl perturbation from the five (RCEI-distributed) regions (**Table 3.1**). The second and third experiments were designed to represent the lower and upper bounds of the Cl perturbations, incorporating the regional/seasonal spread. Thus, the mean Cl perturbations were multiplied by 0.5 and 1.5 to approximate the lower and upper bounds, respectively (**Table 3.S3**, Supporting Information). Each perturbation experiment was run for 25 years to allow a new ozone steady state to be established with respect to the reference run (**Figure 3.S4**, Supporting Information).

There is a strong linearity ($|R|>0.999$) between stratospheric Cl from Cl-VSLS and the resulting global mean column ozone change (Dobson Units; see **Figure 3.S5**, Supporting Information). For each Cl-VSLS considered, the linear ozone responses allow the ozone change due to any chlorine perturbations in **Table 3.1** to be calculated. Note that the global average loss of ozone due to the CFC-11 perturbation was -3.8 Dobson Units, based on a 50-Gg/year surface emission. As the ozone responses are proportional to the emissions, the corresponding ozone change for a 1-Tg/year CFC-11 emission is readily calculated, allowing ODPs to be derived using Equation 3.01. An example latitude-height cross section of ozone changes due to VSLS and due to CFC-11 is given in **Figure 3.S6** (Supporting Information). Chlorine derived from either compound depletes ozone in the same regions that is where ozone loss cycles involving chlorine are efficient; that is, notably the polar lower stratosphere and upper stratosphere.

Figure 3.4 shows the range of ODPs for each Cl-VSLS grouped by emission location and season (see also **Table 3.S4,** Supporting Information). Our results are in qualitative agreement with previous studies, highlighting an emission location and seasonal dependence of VSLS ODPs in general [e.g. Brioude et al., 2010; Pisso et al., 2010]. However, as those previous studies have largely focused on particularly short-lived VSLS, it is notable that the spread in derived ODPs for Cl-VSLS assessed here is generally smaller, particularly for seasonal variations. For example, Pisso et al. [2010] showed that the ODP of n-propyl bromide (~20-day lifetime), when emitted from NH midlatitudes (30-60°N),

varied by a factor of ~2.5 between NH summer and winter. In contrast, the seasonal spread in Cl-VSLS here is far smaller, and a factor of ~2.5 is more similar to the total ODP spread taking into account the larger variability introduced by emission location.

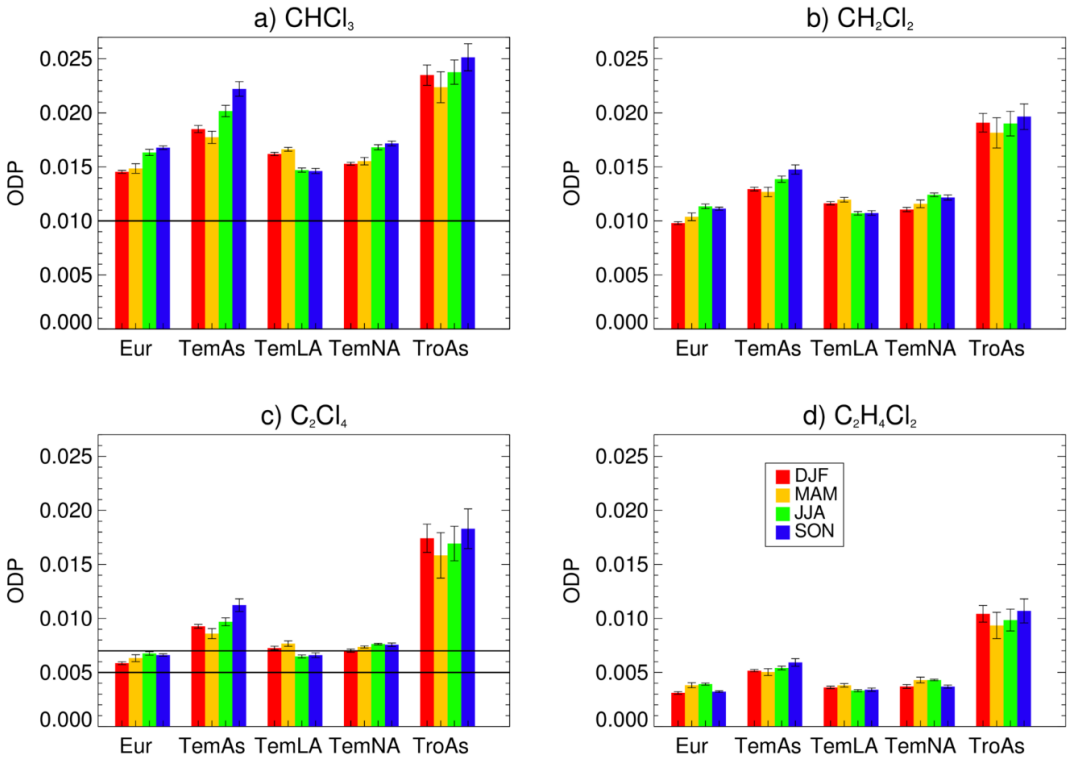

Figure 3.4. Calculated ODPs for (a) $CHCl_3$, (b) CH_2Cl_2, (c) C_2Cl_4, and (d) $C_2H_4Cl_2$, as a function of emission region and season. Horizontal lines represent literature values: $CHCl_3$ from Kindler et al. [1995] and C_2Cl_4 from Kindler et al. [1995; upper] and Wuebbles et al. [2011; lower]. Error bars incorporate uncertainty due to tropospheric and stratospheric interannual variability. ODP=ozone depletion potential; DJF=December-January-February; MAM=March-April-May; JJA=June-July-August; SON=September-October-November; TemNA=Temperate North America; Eur=Europe (Eur); TemLA=Temperate Latin America; TemAs =Temperate Asia; TroAs =Tropical Asia.

Few ODP estimates for Cl-VSLS are available in the literature. For $CHCl_3$ and C_2Cl_4, Kindler et al. [1995] reported values of ~0.01 and ~0.006, respectively. Our $CHCl_3$ ODP range (0.0143-0.0264) is larger than these semiempirical Kindler et al. [1995] estimates, though our C_2Cl_4 range (0.0057-0.0198) incorporates their estimate at the lower limit. Our lower ODP limit for C_2Cl_4 is also 14% larger than the 0.005 reported by a previous 3-D model study [Wuebbles et al., 2011]. However, that work assumed that all chlorine released from tropospheric C_2Cl_4 oxidation was in the form of Cl_y, which is subject to deposition. Our study also considered phosgene as an intermediate, which is expected to have a longer tropospheric lifetime versus deposition [Kindler et al., 1995] and is thus a relatively efficient carrier of chlorine to the stratosphere.

Our derived ODP range for CH_2Cl_2 is 0.0097-0.0208, and to the best of our knowledge, this is the first estimate for this compound. The range is skewed by the larger values from the Asian emission scenarios, particularly tropical Asia, as is the case for each Cl-VSLS considered. For example, CH_2Cl_2 ODPs are a factor of two larger when emissions are concentrated in tropical Asia as opposed to Europe, with emissions from the latter resulting in the lowest ODPs. The CH_2Cl_2 ODPs from the temperate Asia emission scenario (**Figure 3.4**) are also larger with respect to the all-region all-season mean (**Table 3.S4**); significant as (a) efficient troposphere-to-stratosphere transport routes exist for emissions from this region [Ashfold et al., 2015; Oram et al., 2017; **Figure 3.2**], and (b) regional CH_2Cl_2 emissions are expected to further increase in coming years [Feng et al., 2019]. The derived ODPs for $C_2H_4Cl_2$ are in the range 0.0029-0.0119 and are the lowest of the species considered.

Our study shows Cl-VSLS have generally small ODPs. For context, the ODPs of some major substances controlled by the Montreal Protocol [Harris et al., 2014] are 1.0 (CFC-11), 0.73 (CFC-12), and 0.81 (CFC-113). We also calculated the ODP of methyl chloride (CH_3Cl) using the same experimental setup as for Cl-VSLS (**Table 3.S4**). The CH_3Cl ODP range is 0.0188-0.0262, with an average ODP of 0.02. This is in good agreement with previous estimates of ~0.02 [Harris et al., 2014] and shows that, at the upper limit, $CHCl_3$ and CH_2Cl_2 have comparable ODPs to CH_3Cl despite their shorter atmospheric lifetimes (reflecting the multiple Cl atoms of these Cl-VSLS). It is important to

note that product gases account for a significant portion of the chlorine injected into the stratosphere from VSLS (**Table 3.1**). As details of product chemistry are uncertain, we also quantified ODPs under the assumption that no product gases reach the stratosphere. Naturally, these ODPs are smaller and represent lower limits (**Table 3.S4**). Finally, while ODPs for Cl-VSLS are not strongly influenced by interannual variability in our model, details of tropospheric transport can vary greatly between models, including those running with the same reanalysis meteorology [Orbe et al., 2016]. On this basis, we recommend other modelling groups quantify VSLS ODPs to corroborate our findings.

3.5 Concluding Remarks

A 3-D CTM was used to quantify the ODPs of $CHCl_3$, CH_2Cl_2, C_2Cl_4, and $C_2H_4Cl_2$ and to investigate sensitivity to emissions location and season. Determining the ability of these compounds to influence stratospheric ozone is important given recently reported increases in CH_2Cl_2 emissions and projections of further increases [Feng et al., 2019]. The derived ODP ranges reveal a small but significant potential for Cl-VSLS to influence ozone, particularly if emissions are located in close proximity to the tropics: $CHCl_3$ (0.0143-0.0264), CH_2Cl_2 (0.0098-0.0208), C_2Cl_4 (0.0057-0.0198), and $C_2H_4Cl_2$ (0.0029-0.0119). Our simulations indicate (a) relatively efficient transport of Cl-VSLS originating from continental east Asia to the lower stratosphere, in support of recently proposed transport pathways, and (b) that VSLS emissions resulting from the industrialisation of South East Asia have up to a factor of 3 times greater potential to influence stratospheric ozone than emissions from Europe.

Acknowledgements

This work was supported by R.H.'s NERC Fellowship (NE/N014375/1) and the SISLAC project (NE/ R001782/1). M.P.C. is supported by a Wolfson Merit Award. We thank Wuhu Feng for TOMCAT/SLIMCAT model development. Model data are available at the Lancaster University data repository

(doi:10.17635/lancaster/researchdata/283). The supporting information consists of six figures and four tables.

3.6 Supporting Information

This supporting information includes some text describing the Cl-VSLS chemistry in TOMCAT/SLIMCAT. The chemical reactions, including rate constants used in the scheme, are summarised in **Table 3.S1**. The modelled Cl-VSLS lifetimes are compared to literature values in **Table 3.S2**. A summary of stratospheric model experiments that used different chlorine perturbations calculated by the tropospheric model configuration, is given in **Table 3.S3**. The derived ODP for the four Cl-VSLS are given in **Table 3.S4**. The modelled surface and near-tropopause abundance of $CHCl_3$, C_2Cl_4 and $C_2H_4Cl_2$ is shown in **Figures 3.S1-3.S3**. **Figure 3.S4** shows the transient stratospheric ozone response to CH_2Cl_2 and CFC-11 perturbations before a steady state is reached. The (linear) relationship between stratospheric Cl loading from VSLS and column ozone change is given in **Figure 3.S5**. **Figure 3.S6** shows latitude-height maps detailing the differences in ozone change between the control experiment and CFC11 and CH_2Cl_2 perturbations.

Description of Cl-VSLS chemistry

The tropospheric configuration of TOMCAT/SLIMCAT includes a simple chemistry scheme to calculate loss of Cl-VSLS via OH, Cl and photolysis, and conversion into two product gases, Cl_y (a generic representation of all inorganic chlorine), and phosgene ($COCl_2$). In all tropospheric simulations, a climatological field of OH concentration from the TransCom-CH_4 project was used [Patra et al., 2011] and the tropospheric Cl concentration was assumed as 1.3×10^3 atoms cm^{-3} [Hossaini, Chipperfield, et al., 2016]. The chemical loss reactions of Cl-VSLS are given in **Table 3.S1**.

The ratio between production of phosgene and Cl_y from CH_2Cl_2 oxidation varies according to a parametrisation of the detailed chemical mechanism described by Hossaini, Chipperfield, et al. [2016]. See notes to **Table 3.S1**. The phosgene

yield from $CHCl_3$ and C_2Cl_4 are taken from the literature [Tuazon et al., 1988; Kindler et al., 1995], while $C_2H_4Cl_2$ oxidation only produces Cl_y.

Table 3.S1. Summary of reactions/removal processes involving VSLS and their products.

Reaction	**Rate constant[1], *k***	**Notes**
$CHCl_3 + OH \rightarrow COCl_2 + Cl_y$	$k(T) = 2.2\times10^{-12} \exp(-920/T)$	**4**
$CHCl_3 + Cl \rightarrow COCl_2 + Cl_y$	$k(T) = 3.3\times10^{-12} \exp(-990/T)$	**5**
$CHCl_3 + hv \rightarrow 3Cl_y$	**-**	**-**
$CH_2Cl_2 + OH \rightarrow Y\ COCl_2 + (2-2Y)\ Cl_y$	$k(T) = 1.92\times10^{-12} \exp(-880/T)$	**6**
$CH_2Cl_2 + Cl \rightarrow Y\ COCl_2 + (2-2Y)\ Cl_y$	$k(T) = 7.4\times10^{-12} \exp(-910/T)$	**5, 6**
$CH_2Cl_2 + hv \rightarrow 2Cl_y$	**-**	**-**
$C_2Cl_4 + OH \rightarrow 0.47COCl_2 + 3.06Cl_y$	$k(T) = 4.7\times10^{-12} \exp(-990/T)$	**7**
$C_2Cl_4 + Cl + M \rightarrow 0.47COCl_2 + 3.06Cl_y$	$k_0(T) = 1.4\times10^{-28} (T/300)^{-8.5}$ $k_{inf}(T) = 4.0\times10^{-11} (T/300)^{-1.2}$	**5, 8**
$C_2Cl_4 + hv \rightarrow 4Cl_y$	**-**	**-**
$C_2H_4Cl_2 + OH \rightarrow 2Cl_y$	$k(T) = 1.14\times10^{-12} \exp(-1150/T)$	**-**
$C_2H_4Cl_2 + Cl \rightarrow 2Cl_y$	$k(T) = 1.3\times10^{-12}$	**2, 5**
$C_2H_4Cl_2 + hv \rightarrow 2Cl_y$	**-**	**-**
$COCl_2 + OH \rightarrow$ products	$k(T) = 5\times10^{-15}$	**3**
$COCl_2 + hv \rightarrow 2Cl_y$	**-**	**-**
$COCl_2 \rightarrow$ washout	**-**	**9**
$Cl_y \rightarrow$ washout	**-**	**10**

Notes:

[1]Units of bimolecular rate constants are cm^3 $molecules^{-1}$ s^{-1}. Units of termolecular rate constants: $\mathbf{k_0}$ (cm^6 $molecules^{-2}$ s^{-1}) and $\mathbf{k_{inf}}$ (cm^3 $molecules^{-1}$ s^{-1}). All rate constants from Burkholder et al. [2015] unless noted.

[2]Wallington et al. [1996]

[3]Ko and Poulet et al. [2003]

[4]Assumed $COCl_2$ yield of 1 [Kindler et al., 1995].

[5]In the troposphere, [Cl] assumed as 1.3×10^3 molecules cm^{-3} based on the tropospheric mean calculated by Hossaini, Chipperfield, et al. [2016].

[6]The $COCl_2$ yield (Y) from CH_2Cl_2 oxidation was calculated in a semi-explicit manner from a parametrisation based on Hossaini, Chipperfield, et al. [2016]. Y is calculated as: $0.7\ k(HO_2\text{-}CHCl_2O_2)\ [HO_2] + 0.4\ k(RO_2\text{-}CHCl_2O_2)\ [RO_2]/\{k(HO_2\text{-}CHCl_2O_2)\ [HO_2] + k(RO_2\text{-}CHCl_2O_2)\ [RO_2] + k(NO\text{-}CHCl_2O_2)\ [NO] + k(NO_3\text{-}CHCl_2O_2)\ [NO_3]\}$, where k(X-

$CHCl_2O_2$) is the rate constant of the reaction between X and the intermediate $CHCl_2O_2$, which itself is formed from the reaction of CH_2Cl_2 and OH/Cl in the presence of O_2.

[7]Assumed $COCl_2$ yield of 0.47 [Tuazon et al., 1988; Kindler et al., 1995].

[8]k_0 and k_{inf} are the low pressure limiting and high-pressure limiting rate constants [Burkholder et al., 2015].

[9]Assumed 58-day washout lifetime in troposphere based on Kindler et al. [1995].

[10]Assumed 5-day washout lifetime in troposphere based on Sherwen et al. [2016].

Table 3.S2. Comparison of calculated Cl-VSLS lifetimes (days) compared with the literature. Tropical lifetimes reported with the seasonal range in brackets, mid-latitude seasonal lifetimes reported individually.

Local lifetime (days) with respect to OH oxidation						
Source	**VSLS**	**Tropics (25°S to 25°N)**	**Mid-latitudes (25°N to 65°N)**			
		Annual mean	***JJA***	***SON***	***DJF***	***MAM***
This work	$CHCl_3$	107 (97-119)	94	261	829	205
	CH_2Cl_2	107 (97-119)	93	259	820	204
	C_2Cl_4	63 (58-71)	56	157	502	124
	$C_2H_4Cl_2$	45 (41-50)	40	114	372	91
WMO [2014]	$CHCl_3$	112 (100-136)	97	240	750	160
	CH_2Cl_2	109 (98-133)	95	235	725	155
	C_2Cl_4	67 (60-81)	58	145	450	96
	$C_2H_4Cl_2$	47 (42-58)	41	103	320	69

Table 3.S3. Summary of stratospheric CTM experiments used to calculate ODPs. Also shown are the stratospheric Cl perturbations from each experiment and the resulting ozone change. Note, all Cl perturbations and ozone changes are based on a 1 Tg/yr surface emission apart from the CFC-11 which was based on a 50 Gg/yr emission.

Experiment No.	Description	Stratospheric Cl perturbation (ppt Cl)	Global mean column ozone change (DU)
0	Control Run	-	-
1	CFC-11 perturbation	306.9	-3.78
2	CH_2Cl_2 perturbation	69.4	-1.00
3	CH_2Cl_2 perturbation $\times$ 0.5	34.7	-0.50
4	CH_2Cl_2 perturbation $\times$ 1.5	104.0	-1.50
5	$CHCl_3$ perturbation	91.9	-1.38
6	$CHCl_3$ perturbation $\times$ 0.5	45.9	-0.69
7	$CHCl_3$ perturbation $\times$ 1.5	137.8	-2.06
8	C_2Cl_4 perturbation	33.7	-0.72
9	C_2Cl_4 perturbation $\times$ 0.5	16.8	-0.36
10	C_2Cl_4 perturbation $\times$ 1.5	50.5	-1.09
11	$C_2H_4Cl_2$ perturbation	23.6	-0.40
12	$C_2H_4Cl_2$ perturbation $\times$ 0.5	11.8	-0.20
13	$C_2H_4Cl_2$ perturbation $\times$ 1.5	35.5	-0.60
14	CH_3Cl perturbation	165.0	-1.62
15	CH_3Cl perturbation $\times$ 0.5	82.5	-0.82
16	CH_3Cl perturbation $\times$ 1.5	247.4	-2.42

Table 3.S4. ODPs of the four Cl-VSLS**,** showing minimum, maximum, mean, mean only considering source gas (SG) contributions, and median values from the 20 region-season combinations (see also **Figure 3.4** in main text). The final column is the conversion factor between chlorine loading and ODP, calculated from the slope for each species in **Figure 3.S5**, divided by the ozone loss due to 1 Tg/yr emission of CFC-11 (-75.6 DU).

		ODP				
Cl-VSLS	**Min**	**Max**	**Mean**	**Mean, SG only**	**Median**	**Cl-ODP conversion (ppt^{-1})**
$CHCl_3$	0.0143	0.0264	0.0181	0.0117	0.0168	1.98E-4
CH_2Cl_2	0.0097	0.0208	0.0133	0.0103	0.0121	1.91E-4
C_2Cl_4	0.0057	0.0198	0.0095	0.0041	0.0075	2.83E-4
$C_2H_4Cl_2$	0.0029	0.0119	0.0053	0.0041	0.0041	2.24E-4
CH_3Cl	0.0188	0.0262	0.0215	/	0.0209	1.29E-4

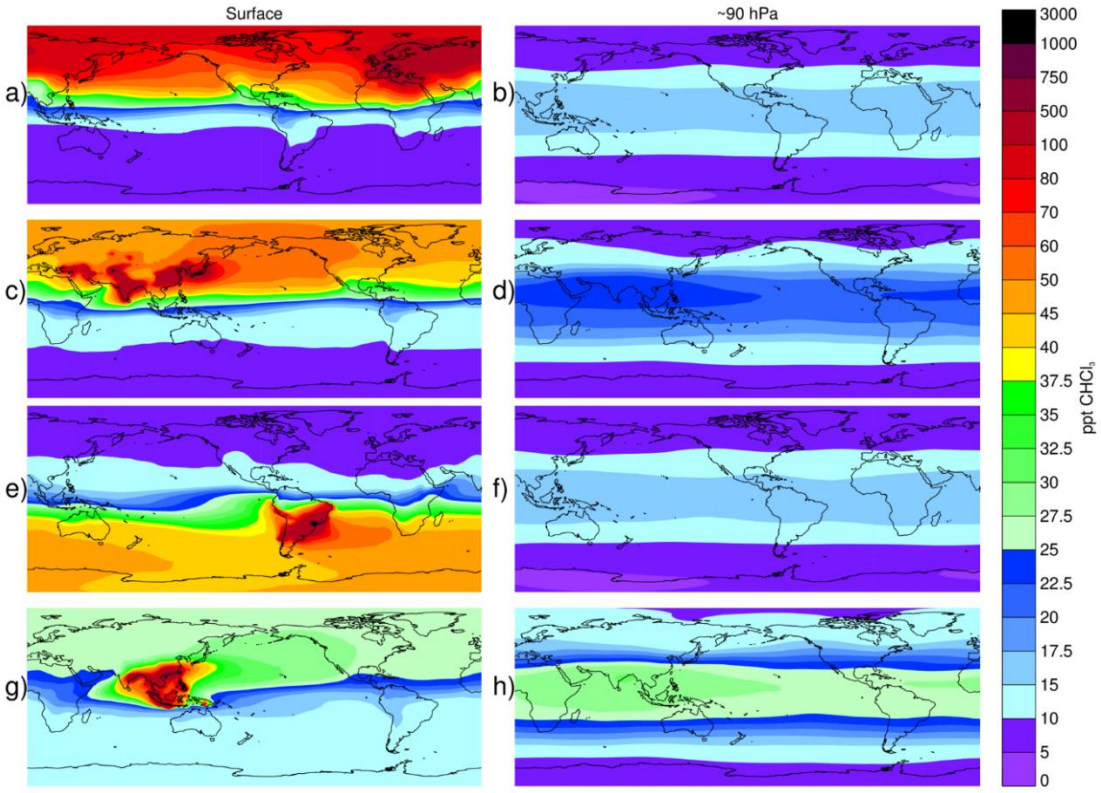

Figure 3.S1. Modelled 5-year annual mean steady-state mixing ratio (ppt) of $CHCl_3$ at the surface (left) and at 90 hPa (right) based on a 1-Tg/year emission from (a, b) Europe, (c, d) Temperate Asia, (e, f) Temperate Latin America, and (g, h) Tropical Asia.

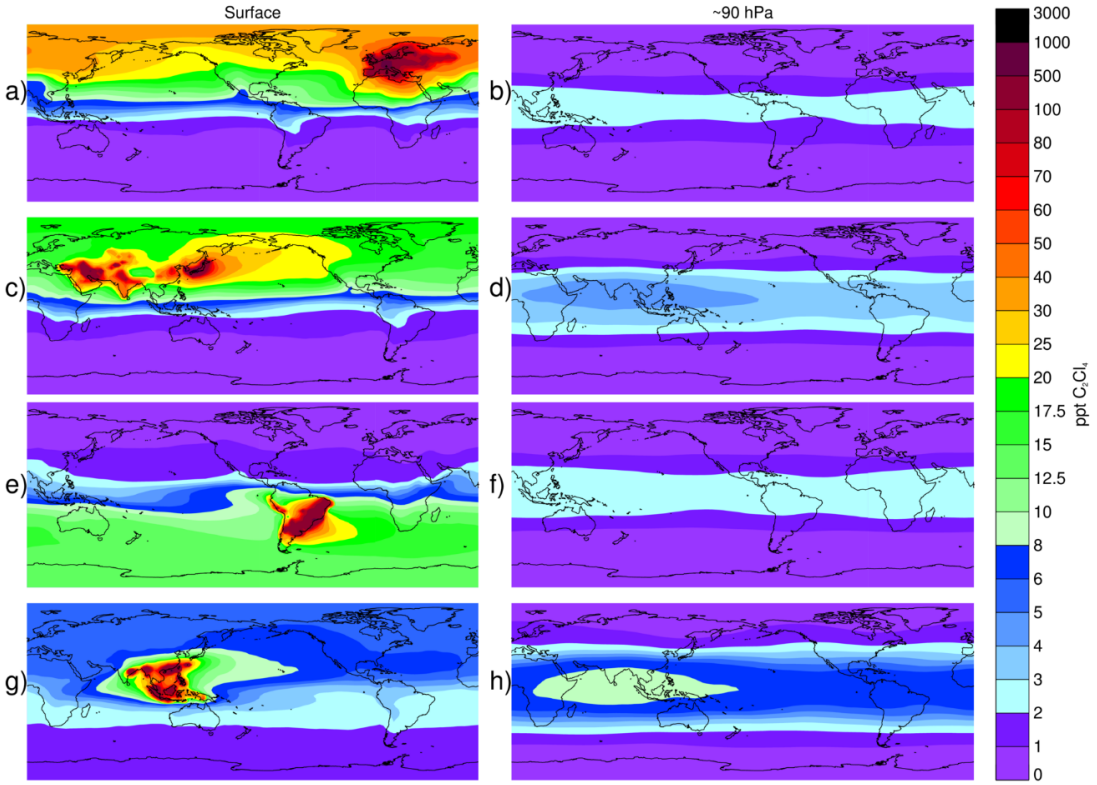

Figure 3.S2. As **Figure 3.S1** but for C_2Cl_4**.**

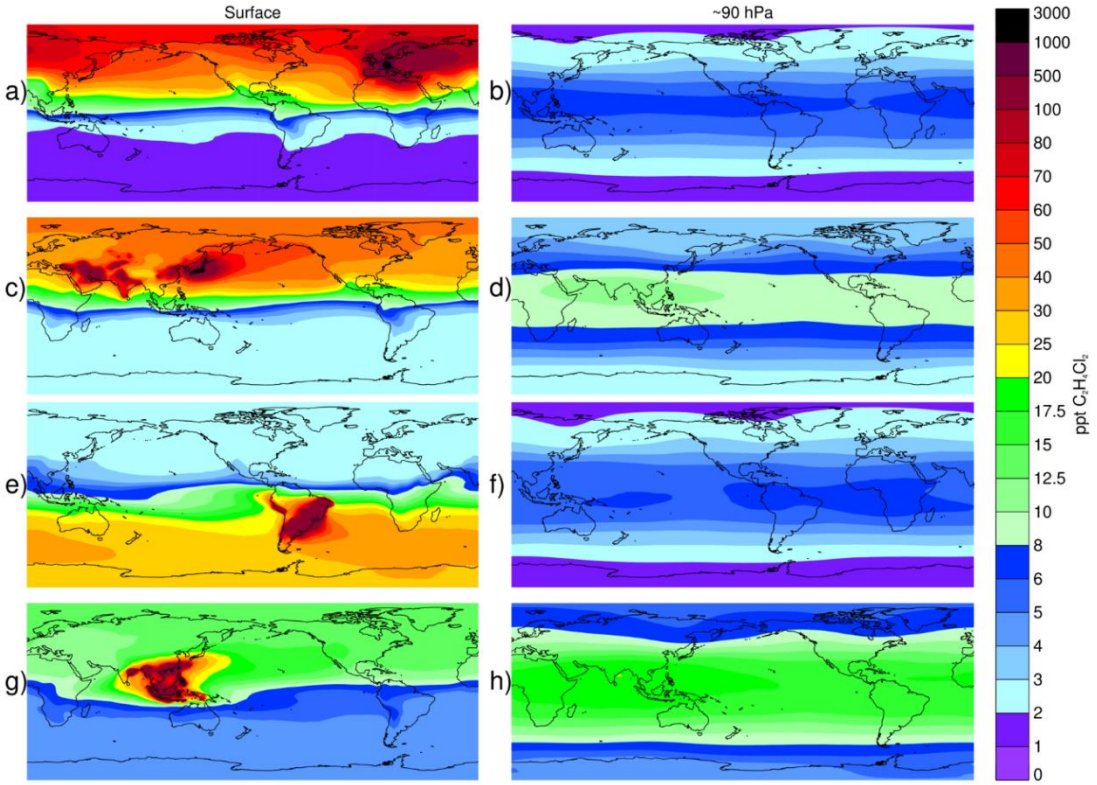

Figure 3.S3. As **Figure 3.S1** but for $C_2H_4Cl_2$.

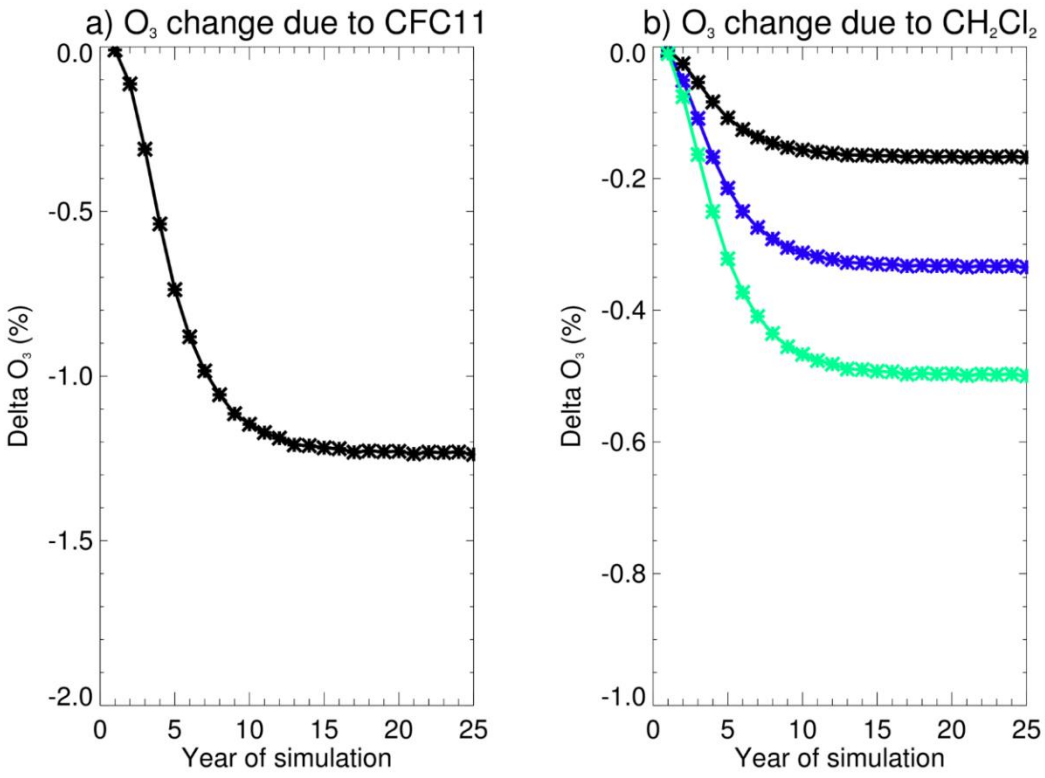

Figure 3.S4. The percentage change of ozone due to a) 50 Gg CFC-11 and b) the three 1 Tg CH_2Cl_2 experiments as a function of simulation year. In panel b) EXP2 is the blue line, EXP3 in the black line, and EXP4 is the green line. See **Table 3.S3** for the list of experiments.

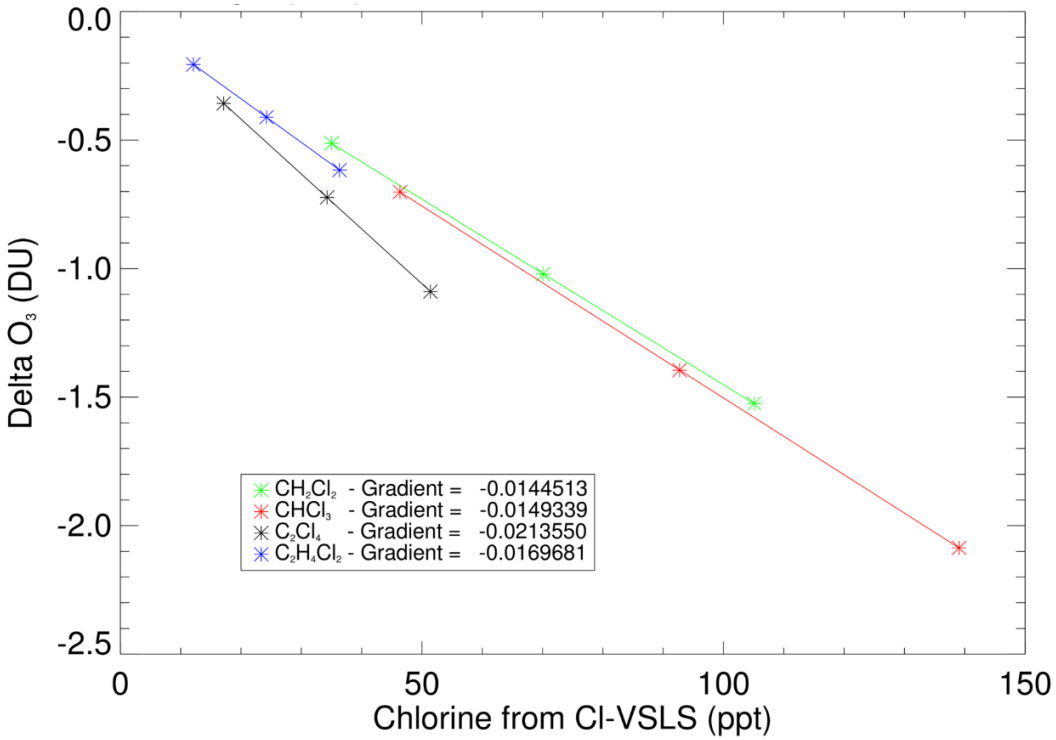

Figure 3.S5. The relationship between absolute ozone change in Dobson Units (DU) and the chlorine loading (ppt) for the four Cl-VSLS, which contain the values for the final column of **Table 3.S4**.

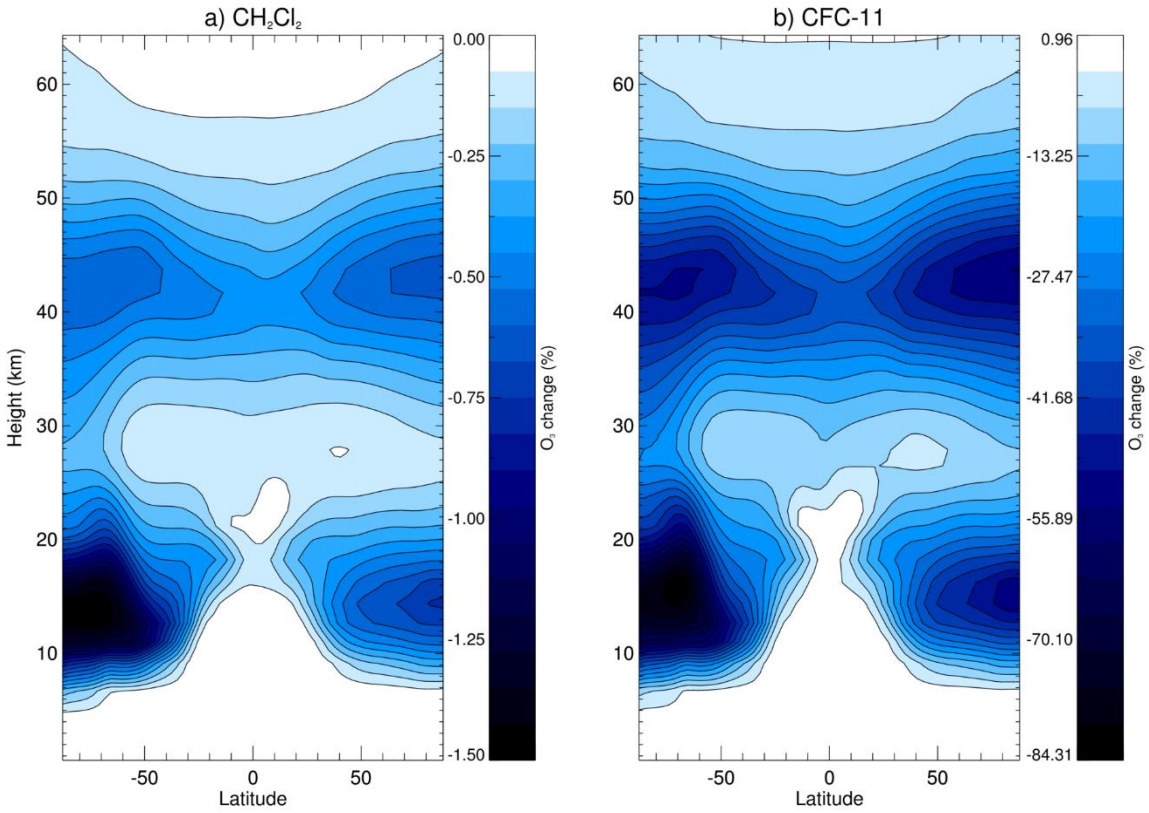

Figure 3.S6. Latitude-height plot of annual zonal mean percentage ozone change between the control experiment EXP0 and: a) EXP2, the CH_2Cl_2 base perturbation in **Table 3.S3**, and b) EXP1, CFC-11, weighted to 1 Tg/yr emissions.

Chapter 4

A Synthesis Inversion to Constrain Global Emissions of Two Very Short Lived Chlorocarbons: Dichloromethane, and Perchloroethylene

Tom Claxton[1], Ryan Hossaini[1], Chris Wilson[2,3], Stephen A. Montzka[4], Martyn P. Chipperfield[2,3], Oliver Wild[1], Ewa M. Bednarz[1], Lucy J. Carpenter[5], Stephen J. Andrews[5], Sina C. Hackenberg[5,19], Jens Mühle[6], David Oram[7], Sunyoung Park[8], Mi-Kyung Park[8], Elliot Atlas[9], Maria Navarro[9,20], Sue Schauffler[10], David Sherry[11], Martin Vollmer[12], Tanja Schuck[13], Andreas Engel[13], Paul B. Krummel[14], Michela Maione[15], Jgor Arduini[15], Takuya Saito[16], Yoko Yokouchi[16,21], Simon O'Doherty[17], Dickon Young[17], and Chris Lunder[18].

[1]Lancaster Environment Centre, Lancaster University, Lancaster, UK
[2]School of Earth and Environment, University of Leeds, Leeds, UK
[3]National Centre for Earth Observation, University of Leeds, Leeds, UK
[4]National Oceanic and Atmospheric Administration, Boulder, Colorado, USA
[5]Wolfson Atmospheric Chemistry Laboratories, Department of Chemistry, University of York, York, UK
[6]Scripps Institution of Oceanography, University of California, San Diego, CA, USA
[7]National Centre for Atmospheric Science, School of Environmental Sciences, University of East Anglia, Norwich, UK

[8]Kyungpook Institute of Oceanography, Kyungpook National University, Daegu, South Korea
[9]Rosenstiel School of Marine and Atmospheric Science, University of Miami, Miami, FL, USA
[10]National Centre for Atmospheric Research, Boulder, CO, USA
[11]Nolan Sherry & Associates, London, UK
[12]Laboratory for Air Pollution and Environmental Technology, Empa, Swiss Federal Laboratories for Materials Science and Technology, Duebendorf, Switzerland
[13]Institute for Atmospheric and Environmental Sciences, Goethe University Frankfurt, Frankfurt, Germany
[14]Climate Science Centre, CSIRO Oceans and Atmosphere, Aspendale, Australia
[15]Department of Pure and Applied Sciences, University of Urbino, Urbino, Italy
[16]National Institute for Environmental Studies, Tsukuba, Japan
[17]School of Chemistry, University of Bristol, Bristol, UK
[18]Norwegian Institute for Air Research, Kjeller, Norway
[19]now at Eurofins Dr. Specht International GmbH, Am Neuländer Gewerbepark 2, Hamburg
[20]Deceased 19th December 2017
[21]Deceased 1st January 2020

The following work has been accepted in the Journal of Geophysical Research: Atmospheres on the 4th Match 2020 (A synthesis inversion to constrain global emissions of two very short lived chlorocarbons: dichloromethane, and perchloroethylene, *Journal of Geophysical Research: Atmospheres*, **125**, https://doi.org/10.1029/2019JD031818). The authors and their contributions are listed below:

Tom Claxton: Performed TOMCAT model simulations, processed and analysed the data, and wrote the manuscript. **Ryan Hossaini:** Helped initial set up of TOMCAT model simulations, supervised interpretation of results and compiled the manuscript. **Chris Wilson:** Provided expertise on synthesis

inversion methods, assisted with analysis and interpretation, and compiled the manuscript. **Stephen A. Montzka:** Provided NOAA surface and tall tower observational data, helped to interpret results, and compiled the manuscript. **Martyn P. Chipperfield:** Supported TOMCAT model simulations, and helped compile the manuscript. **Oliver Wild and Eva M. Bednarz:** Provided comments on the manuscript. **Lucy J. Carpenter, Stephen J. Andrews, and Sina C. Hackenberg:** Provided CH_2Cl_2 ocean cruise fluxes comments on the manuscript. **Jens Mühle:** Provided information of data calibration and comments on the manuscript. **David Oram**: Provided CH_2Cl_2 observational insight and input towards the manuscript. **Sunyoung Park, Mi-Kyung Park, Martin Vollmer, Paul B. Krummel, Michela Maione, Jgor Arduini, Takuya Saito, Yoko Yokouchi, Simon O'Doherty, Dickon Young, and Chris Lunder:** Responsible for observational data collected at AGAGE and AGAGE-affiliated network stations. Facilitated access to these data. **Elliot Atlas, Maria Navarro, and Sue Schauffler:** Provided observational data for CONTRAST and ATTREX flight campaigns. **David Sherry:** Provided industrial emission estimates for Cl-VSLS. **Tanja Schuck and Andreas Engel:** Provided observational data for Taunus Observatory.

Abstract

Dichloromethane (CH_2Cl_2) and perchloroethylene (C_2Cl_4) are chlorinated very short lived substances (Cl-VSLS) with anthropogenic sources. Recent studies highlight the increasing influence of such compounds, particularly CH_2Cl_2, on the stratospheric chlorine budget and therefore on ozone depletion. Here, a multiyear global-scale synthesis inversion was performed to optimise CH_2Cl_2 (2006-2017) and C_2Cl_4 (2007-2017) emissions. The approach combines long-term surface observations from global monitoring networks, output from a three-dimensional chemical transport model (TOMCAT), and novel bottom-up information on prior industry emissions. Our posterior results show an increase in global CH_2Cl_2 emissions from 637 ± 36 Gg yr^{-1} in 2006 to 1,171 ± 45 Gg yr^{-1} in 2017, with Asian emissions accounting for 68% and 89% of these totals, respectively. In absolute terms, Asian CH_2Cl_2 emissions increased annually by

51 Gg yr^{-1} over the study period, while European and North American emissions declined, indicating a continental-scale shift in emission distribution since the mid-2000s. For C_2Cl_4, we estimate a decrease in global emissions from 141 ± 14 Gg yr^{-1} in 2007 to 106 ± 12 Gg yr^{-1} in 2017. The time-varying posterior emissions offer significant improvements over the prior. Utilising the posterior emissions leads to modelled tropospheric CH_2Cl_2 and C_2Cl_4 abundances and trends in good agreement to those observed (including independent observations to the inversion). A shorter C_2Cl_4 lifetime, from including an uncertain Cl sink, leads to larger global C_2Cl_4 emissions by a factor of ~1.5, which in some places improves model-measurement agreement. The sensitivity of our findings to assumptions in the inversion procedure, including CH_2Cl_2 oceanic emissions, is discussed.

Plain Language Summary

The 1987 Montreal Protocol banned production for dispersive uses of major ozone-depleting gases, such as chlorofluorocarbons, due to their role in depletion of the stratospheric ozone layer. In consequence, the ozone layer is expected to recover in coming decades, as stratospheric chlorine from banned substances slowly declines. However, chlorinated very short lived substances (Cl-VSLS), not controlled by the Montreal Protocol, represent a small, but growing, source of atmospheric chlorine that could potentially slow ozone recovery. It is thus important that the magnitude of emissions of these compounds, their spatial distribution, and changes with time are quantified. Here, we combined observations of Cl-VSLS, prior estimates of their emissions, and a chemical transport model to produce an optimised set of emission estimates on a region-by-region basis between 2006 and 2017. We show that industrial emissions of dichloromethane, the most abundant Cl-VSLS, increased by ~84% within this period, predominately due to an increase in Asian emissions, while European and North American emissions decreased. Over 2007-2017, emissions of perchloroethylene, a less abundant Cl-VSLS, decreased, particularly in Europe and North America. We show that our new

emission estimates lead to better agreement with observational data compared to previous estimates.

4.1 Introduction

Halogenated very short lived substances (VSLS) are organic compounds with annual mean atmospheric lifetimes at the planetary surface of ~6 months or less [Engel et al., 2018]. These lifetimes are short compared to the principal gases synonymous with ozone depletion, such as chlorofluorocarbons (CFCs), which were banned under the terms of the 1987 Montreal Protocol and its later amendments. However, despite their short lifetimes, over the last two decades, a wealth of research has shown that VSLS of both natural and anthropogenic origin can reach the stratosphere, where they contribute to stratospheric bromine and chlorine and thus ozone depletion [e.g., Claxton et al., 2019; Fernandez et al., 2014; Hossaini et al., 2017; Laube et al., 2008; Sturges et al., 2000; Wales et al., 2018]. Brominated VSLS (e.g., bromoform and dibromomethane) are predominately of natural oceanic origin [e.g., Quack & Wallace, 2003; Ziska et al., 2013], while chlorinated VSLS (Cl-VSLS) have significant anthropogenic sources [e.g., Engel et al., 2018; McCulloch et al., 1999]. At present, these compounds account for a small, but growing, portion of atmospheric chlorine, and they are not controlled by the Montreal Protocol. In 2016, Cl-VSLS were estimated to provide 115 (75-160) ppt of chlorine to the stratosphere, which represents 3.5% of total chlorine in the stratosphere from all sources [Engel et al., 2018; Hossaini et al., 2019].

The most abundant Cl-VSLS, dichloromethane (CH_2Cl_2), is of particular interest owing to an observed rapid increase in its global concentration since the mid-2000s [Hossaini et al., 2017, 2019; Leedham Elvidge et al., 2015]. As a versatile solvent, CH_2Cl_2 has a range of industrial applications and roughly 90% of total emissions have been estimated to be anthropogenic [Montzka, Reimann, et al., 2011]. Annual global CH_2Cl_2 emissions have been estimated at ~1,000 Gg yr^{-1} in 2016, with a global mean surface mole fraction of 33-39 ppt observed from monitoring networks, a factor of ~2 larger compared to the early part of the century [Engel et al., 2018]. Biogenic CH_2Cl_2 sources have also been

hypothesised from the ocean [Jones & Carpenter, 2005; Ooki & Yokouchi, 2011] and from mangrove forests [Kolusu et al., 2018], though the magnitudes of these sources are poorly constrained and are expected to be small. A less abundant Cl-VSLS is perchloroethylene, C_2Cl_4, which is almost solely anthropogenic and historically has found use, for example, in dry-cleaning applications. Unlike CH_2Cl_2, the abundance of C_2Cl_4 has continually decreased over the last few decades [Carpenter et al., 2014; Simpson et al., 2004], due to phasing out in favour of less-toxic alternatives. In 2016, the global mean C_2Cl_4 mole fraction was 1.1-1.2 ppt, with global emissions estimated at 83-103 Gg yr^{-1} [Engel et al., 2018]

Claxton et al. [2019] recently quantified the ozone-depletion potential (ODP) of several Cl-VSLS, highlighting a strong dependence of the ODP on the location of emission. They reported ODP ranges for CH_2Cl_2 and C_2Cl_4 of 0.0097-0.0208 and 0.0057-0.0198, respectively, with emissions from Southern Asia having the largest ODPs. This is significant for Cl-VSLS, as Asian emissions (a) likely account for a large fraction of present-day global total emissions, having grown in importance over the last decade [Fang et al., 2019; Leedham Elvidge et al., 2015; Oram et al., 2017], and (b) may continue to increase in coming years [Feng et al., 2019]. On the above basis, it is important that the geographical distribution and strength of Cl-VSLS emissions are investigated and that accurate, up-to-date inventories are available as input for global modelling studies. Such modelling studies examining the stratospheric input of Cl-VSLS have thus far relied on simple surface mixing ratio boundary conditions to constrain surface abundances of CH_2Cl_2 and other compounds based on measurements in the remote atmosphere. While these are observationally based and have been implemented so that time trends and latitudinal gradients are captured [Hossaini et al., 2019], zonal variability is not represented by the approach. This includes any potential colocation of large surface emissions with regions of efficient transport pathways to the upper troposphere/stratosphere, such as from continental East Asia [e.g., Ashfold et al., 2015], which are likely relevant to determining accurate ODPs [Claxton et al., 2019].

Despite a growing interest in Cl-VSLS, there have been few recent studies examining their emissions at the global scale. Keene et al. [1999] established

the Reactive Chlorine Emissions Inventory (RCEI) framework in which global emissions were estimated using a bottom-up approach for a wide range of chlorocarbons. Within that framework, industrial emissions of 583 ± 32 Gg yr^{-1} CH_2Cl_2 and 366 ± 20 Gg yr^{-1} C_2Cl_4 were estimated [McCulloch et al., 1999]. These values, based on analysis relevant to the 1990s, likely underestimate present CH_2Cl_2 emissions and overestimate C_2Cl_4 emissions, based on recent trends [Engel et al., 2018]. Khalil et al. [1999] added to the RCEI framework by estimating total oceanic emissions of 191 Gg yr^{-1} CH_2Cl_2 and 19 Gg yr^{-1} C_2Cl_4. However, Cl-VSLS fluxes from the ocean are highly spatially variable [e.g., Kolusu et al., 2016] and a significantly lower CH_2Cl_2 source (<90 Gg yr^{-1}) has been inferred in later work [Trudinger et al., 2004]. Furthermore, while some evidence for in situ CH_2Cl_2 production (related to biological activity) has been reported [Ooki & Yokouchi, 2011], the ocean may also take up atmospheric CH_2Cl_2 and re-emit it elsewhere [Moore, 2004]. This possibly confounds the interpretation of observational results that were used to infer the magnitude of natural emissions in earlier work. In addition, Lobert et al. [1999] estimated a biomass burning CH_2Cl_2 source of 59 Gg yr^{-1}, though evidence for the existence of this source is missing from more recent analyses [Lawson et al., 2015; Leedham Elvidge et al., 2015; Mühle et al., 2007; Simpson et al., 2011].

There are two core objectives of this study: first, to investigate global and regional changes in CH_2Cl_2 and C_2Cl_4 emission magnitudes and distributions on a multiannual timescale; second, to generate and evaluate a set of up-to-date global emissions for both compounds, suitable for use as input to atmospheric models. To accomplish this, we performed a global synthesis inversion to optimise Cl-VSLS emissions over the period 2006-2017. Briefly, this approach combines long-term observations from global monitoring networks, prior information on emissions, and a chemical transport model. The paper is structured as follows. The 3-D chemical transport model is described in **Section 4.2**. The inversion procedure is outlined in **Section 4.3**, including both the theory and a description of the different observations used. Our main inversion results, including various sensitivity analyses, are presented in **Section 4.4**. These include the addition of ocean sources of CH_2Cl_2 and an

added Cl sink of C_2Cl_4. Conclusions and recommendations for future work are given in **Section 4.5**.

4.2 Description of the TOMCAT Chemical Transport Model

TOMCAT is an offline 3-D Chemistry Transport Model (CTM) [Chipperfield, 2006; Monks et al., 2017] that has been widely used to investigate tropospheric chemistry and transport, including several VSLS-focused studies [e.g., Hossaini et al., 2010, 2019; Claxton et al., 2019]. The CTM is forced by six-hourly wind, temperature, and humidity fields taken from the European Centre for Medium-Range Weather Forecasts (ECMWF) ERA-Interim meteorological reanalyses [Dee et al., 2011]. The TOMCAT configuration used had a horizontal resolution of 2.8° × 2.8°, with a vertical resolution of 60 levels, up to an altitude of ~64 km. Our model configuration also employs a simplified tropospheric chemistry scheme, reading an offline monthly varying field of the tropospheric hydroxyl radical (OH) concentration [Spivakovsky et al., 2000; Huijnen et al., 2010]. The OH field was used in the Atmospheric Tracer Transport Model Intercomparison Project (TransCom) study of CH_4 [Patra et al., 2011] and leads to an average methyl chloroform lifetime (1992-2007) of 4.71 (±0.18) years in TOMCAT, in reasonable agreement with recent estimates of ~5 years obtained from inverse methods [e.g., Rigby et al., 2013]. Although the model OH field here is fixed in time, we note that evidence for interannual OH variability, for instance, due to ENSO activity, exists [e.g., Montzka, Krol, et al., 2011; Prinn et al., 2005; Turner et al., 2018].

Both CH_2Cl_2 and C_2Cl_4 are subject to OH oxidation and photolysis sinks in the model. An additional inversion experiment (see ensuing discussion) was performed for C_2Cl_4 in which the competing three-bodied loss reaction of C_2Cl_4 with Cl atoms was also included. The inclusion of this reaction in models has been shown to be important to reproduce atmospheric C_2Cl_4 observations in the upper troposphere [Hossaini et al., 2019; Rudolph et al., 1996]. In this case, the model assumes a fixed tropospheric mean Cl concentration of 1.3×10^3 atoms cm^{-3} globally, based on model estimates from Hossaini, Chipperfield, et al. [2016]. In practice, the spatial distribution of tropospheric Cl would be

nonuniform, and given this uncertainty, this model run is treated as a sensitivity. Reaction rate constants were taken from the 2015 Jet Propulsion Laboratory (JPL) report [Burkholder et al., 2015]. For the purposes of this study which investigates source gas emissions, product gas chemistry was not required.

4.3 Description of the Inversion Technique

4.3.1 Synthesis Inversion

The “synthesis inversion” technique optimises model prior emissions of a given compound by minimising differences between modelled and observed mixing ratios [e.g., Baker et al., 2006]. This top-down technique is well established and has been used to investigate surface emissions of several compounds, including CH_4 [McNorton et al., 2018], CO_2 [Law et al., 2008; Wang et al., 2018], CO [Pétron et al., 2002], and H_2 [Bousquet et al., 2011]. Here, we apply the technique to CH_2Cl_2 and C_2Cl_4 to optimise their emissions for 12-year (2006-2017) and 11-year (2007-2017) periods, respectively, over which a wide range of tropospheric observations are available (**Section 4.3.2**). Prior surface CH_2Cl_2 and C_2Cl_4 emissions (**Section 4.3.4**) were aggregated over a possible 14 source regions (**Figure 4.1(a)**). Boundaries for these source regions (10 land and four ocean), which are continental in scale, are adapted from previous TransCom inversion studies [e.g., Baker et al., 2006]. The four ocean regions are defined by the following latitude bands: Extratropical Northern Ocean (30-90°N), Tropical Northern Ocean (0-30°N), Tropical Southern Ocean (0-30°S), and Extratropical Southern Ocean (30-90°S). Given the large uncertainty surrounding oceanic CH_2Cl_2 emissions (see discussion in **Section 4.3.2.3**), for this compound, two different inversions were performed as part of our sensitivity analysis. The first did not include any oceanic CH_2Cl_2 emission (i.e., it assumed industry sources only), while the second also considered emissions from the ocean regions.

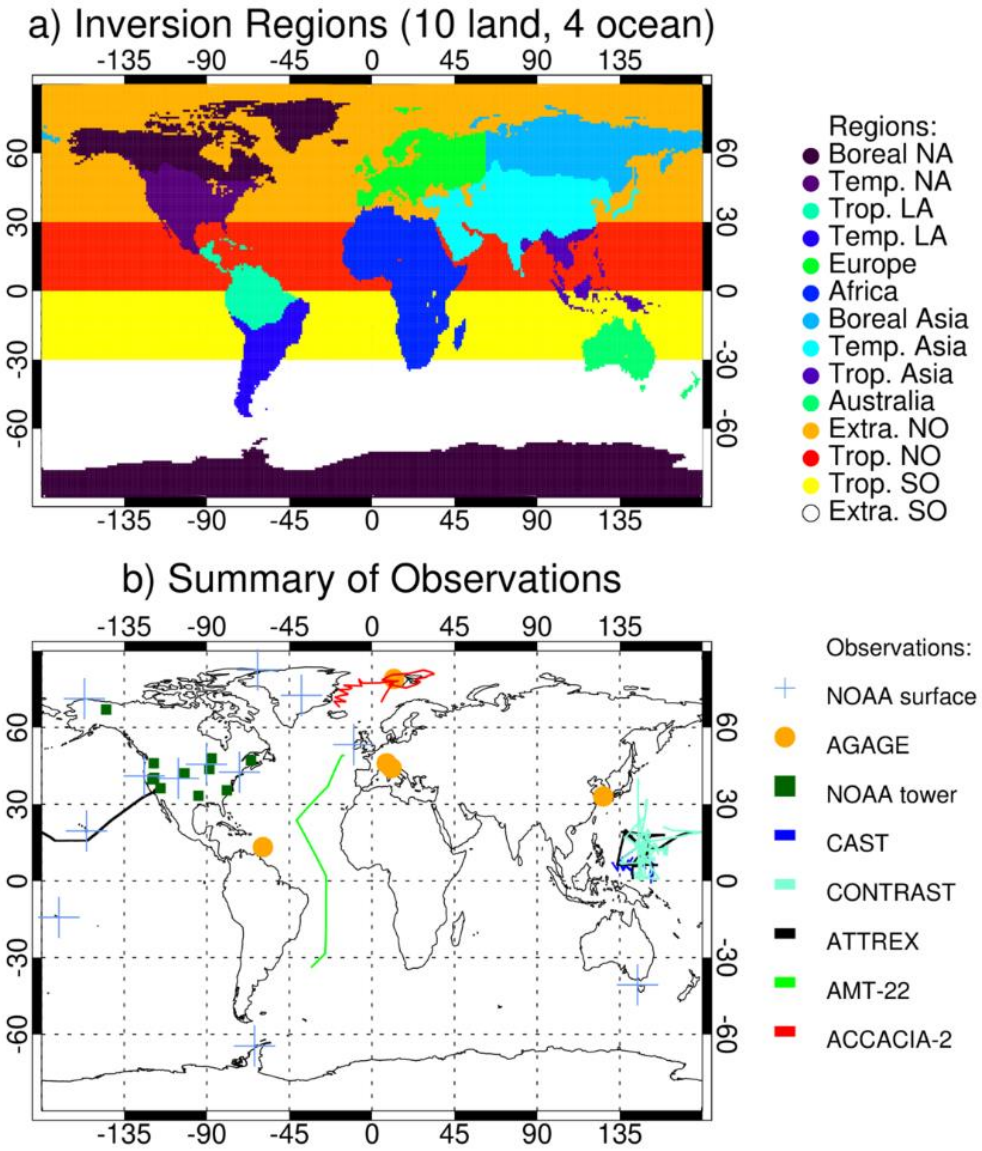

Figure 4.1. (a) Map showing the 14 regions (10 land and 4 ocean) used in the inversion. NA = North America, LA = Latin America, NO = Northern Ocean, SO = Southern Ocean, Extra. = Extratropical, Trop. = Tropical, Temp. = Temperate. (b) Summary of the various observations used in this study: weekly flasks at NOAA surface sites (blue plusses); on-site high-frequency measurements at AGAGE surface sites (orange circles); approximately daily flasks at NOAA tall tower sites (green squares). Flight campaigns: CAST (purple); ATTREX (black); CONTRAST (light blue). Ocean campaigns: AMT-22 (green); ACCACIA-22 (red).

Within each source region, the distribution of emission is fixed (see **Section 4.3.4**), and the inversion optimises the total emission from each region on an annual basis.

The technique is based on minimising the cost function, J:

$$J(\boldsymbol{x}) = \frac{1}{2}(\boldsymbol{x} - \boldsymbol{x_b}).\boldsymbol{B}^{-1}.(\boldsymbol{x} - \boldsymbol{x_b}) + \frac{1}{2}(\boldsymbol{y} - \boldsymbol{G}.\boldsymbol{x}).\boldsymbol{R}^{-1}.(\boldsymbol{y} - \boldsymbol{G}.\boldsymbol{x}) \qquad (4.01)$$

where $\boldsymbol{x}$ is an emission estimate, $\boldsymbol{x_b}$ are the prior emissions, $\boldsymbol{B}$ is the covariance matrix for the errors in emissions, $\boldsymbol{y}$ are the observations, $\boldsymbol{R}$ is the covariance matrix for the errors in observations, and $\boldsymbol{G}$ is the normalised model output concentration Jacobian matrix. It maps the emission field on to the observation vector $\boldsymbol{y}$ via the transport model. The cost function is at a minimum at $\boldsymbol{x} = \boldsymbol{x_a}$, where $\boldsymbol{x_a}$ is given as [Tarantola & Valette, 1982]:

$$\boldsymbol{x_a} = \boldsymbol{x_b} + [\boldsymbol{G}^T.\boldsymbol{R}^{-1}.\boldsymbol{G} + \boldsymbol{B}^{-1}]^{-1}.\boldsymbol{G}^T.\boldsymbol{R}^{-1}.(\boldsymbol{y} - \boldsymbol{G}.\boldsymbol{x_b}) \qquad (4.02)$$

Since all the other quantities are known, the posterior emissions for each of the 14 regions analysed in the inversion can be solved on a year-by-year basis. Note that our justification for estimating annual emissions (e.g., as opposed to monthly resolved) is based on several factors that are outlined in **Section 4.3.2.1** below. This solution of $\boldsymbol{x_a}$ gives the best match to the observations, while reducing the likelihood of straying unrealistically from the prior emissions $\boldsymbol{x_b}$. A successful inversion is indicated by a significant reduction in the posterior emission errors compared to the prior emission errors.

4.3.2 Observations

4.3.2.1 Surface Observations of CH_2Cl_2 and C_2Cl_4

Most of the CH_2Cl_2 and C_2Cl_4 observational data considered in this study come from remote surface sites, as summarised in **Tables 4.1** and **4.2**. We consider monthly mean measurements of both compounds over the 12-year period obtained from a total of 29 unique surface locations, 19 used as input into the inversion, and 10 held back for independent verification. These data are from the National Oceanic and Atmospheric Administration (NOAA) and Advanced Global Atmospheric Gases Experiment (AGAGE) long-term monitoring

networks, which have been described extensively in the literature [e.g., Montzka et al., 2018; Prinn et al., 2018]. AGAGE network monthly mean measurements include pollution events, while NOAA measurements are mostly obtained at remote sites. Observations obtained from the sites in **Table 4.1** were used directly in the inversion. Between the two networks, a reasonable level of geographical coverage is achieved (see **Figure 4.1(b)**). Critically, this includes sites in each of the main industrialised regions where Cl-VSLS emissions are expected to be greatest, such as the continental USA (four sites), Europe (four sites), and East Asia (one site). A conversion factor of 1.1038 was applied to the AGAGE CH_2Cl_2 record to account for a known calibration difference between the NOAA-2003 and AGAGE SIO-14 calibration scales of ~10% [Carpenter et al., 2014; Engel et al., 2018]. Note that four measurement sites are shared between the two networks; for this study, we use both measurements; however, we convert AGAGE data to NOAA calibration scales. For C_2Cl_4, NOAA and AGAGE use NOAA-2003 and NOAA-2003B calibration scales, respectively, which have been found to agree to within <1%. We additionally considered NOAA measurements of both compounds in 2015 from the USA-based tall tower network (**Table 4.2**). These data were not assimilated in the inversion but rather were used to provide an independent assessment of the prior versus posterior emissions over the USA (at 10 sites).

The availability and abundance of Cl-VSLS measurement data was a principal factor in our decision to estimate annual mean emissions as opposed to monthly resolved emissions. The 19 unique observational sites (**Table 4.1**) provide a maximum of 228 monthly mean measurements in a given year. Solving emissions for 14 different regions would, in a monthly resolved inversion, require 168 (14 × 12) model Cl-VSLS tracers for each year of our study period. This number of tracers (168) is comparable to the number of observations we have available to us in a year (maximum of 228 monthly means, assuming no missing data) and would lead to a less well constrained inversion process, as each month's emissions would only be constrained on average by 1.4 observations. In addition, we believe that the large computational expense of running with such a large number of tracers is not warranted on the basis of (1) our study is primarily interested in long-term interannual emission trends and

(2) the seasonal cycle of Cl-VSLS is found to be reproduced well using our non-seasonal posterior emissions (see **Sections 4.4.6** and **4.4.7**). Finally, we note that there is little information in the literature with which to inform any prior emission seasonality in our model. Furthermore, for CH_2Cl_2, no significant seasonal variation in industrial emissions has been reported [McCulloch & Midgley, 1996].

Table 4.1. Summary of Surface Observational Sites Used as Input to the Inversion (Arranged North to South).

Code	Station Name, Location	Lat (°)	Lon (°)	Elevation (m)	Network
ALT	Alert, Canada	82.5	-62.5	190.0	NOAA
ZEP	Zeppelin, Svalbard, Norway	78.9	11.9	490.0	AGAGE
SUM	Summit, Greenland	72.6	-38.4	3209.5	NOAA
BRW	Barrow, AK, USA	71.3	-156.6	11.0	NOAA
MHD	Mace Head, Ireland	53.3	-9.9	5.0	NOAA, AGAGE
JFJ	Jungfraujoch, Switzerland	46.3	8.0	3580.0	AGAGE
LEF	Park Falls, WI, USA	45.9	-90.3	472.0	NOAA
CMN	Monte Cimone, Italy	44.2	10.7	2165.0	AGAGE
HFM	Harvard Forest, MA, USA	42.5	-72.2	340.0	NOAA
THD	Trinidad Head, CA, USA	41.1	-124.2	107.0	NOAA, AGAGE
NWR	Niwot Ridge, CO, USA	40.1	-105.6	3523.0	NOAA
GSN	Gosan, Jeju, South Korea	33.3	126.2	89.0	AGAGE
MLO	Mauna Loa, HI, USA	19.5	-155.6	3397.0	NOAA
KUM	Cape Kumukai, HI, USA	19.5	-154.8	3.0	NOAA
RPB	Ragged Point, Barbados	13.2	-59.5	42.0	AGAGE
SMO	Tutuila, American Samoa	-14.2	-170.6	42.0	NOAA, AGAGE
CGO	Cape Grim, Australia	-40.7	144.7	94.0	NOAA, AGAGE
PSA	Palmer Station, Antarctica	-64.9	-64.0	10.0	NOAA
SPO	South Pole, Antarctica	-90.0	-24.8	2810.0	NOAA

Table 4.2. Summary of Surface Observational Sites Available in 2015 from the NOAA Tall Tower Network (Arranged North to South), not used as Input in the Inversion.

Code	Station Name, Location	Lat (°)	Lon (°)	Elevation (m)	Network
CRV	CARVE, AK, USA	65.0	-147.6	611.4	NOAA
AMT	Argyle, ME, USA	45.0	-68.7	53.0	NOAA
MBO	Mt. Bachelor, OR, USA	44.0	-121.7	2731.0	NOAA
WBI	West Branch, IA, USA	41.7	-91.4	241.7	NOAA
BAO	Boulder, CO, USA	40.1	-105.0	1584.0	NOAA
WGC	Walnut Grove, CA, USA	38.3	-121.5	0.0	NOAA
STR	Sutro Tower, CA, USA	37.8	-122.5	254.0	NOAA
MWO	Mt. Wilson, CA, USA	34.2	-118.1	1728.0	NOAA
SCT	Beech Island, SC, USA	33.4	-81.8	115.2	NOAA
WKT	Moody, TX, USA	31.3	-97.3	251.0	NOAA

4.3.2.2 Aircraft Observations of CH_2Cl_2 and C_2Cl_4

We also considered measurements of both Cl-VSLS from three different flight campaigns: the 2014 Co-ordinated Airborne Studies in the Tropics (CAST) mission [Andrews et al., 2016; Harris et al., 2017], the 2014 Convective Transport of Active Species in the Tropics (CONTRAST) mission [Pan et al., 2017], and the 2014 Airborne Tropical Tropopause Experiment (ATTREX) mission [Navarro et al., 2015]. The locations of these campaigns are shown in **Figure 4.1(b)**. The CAST mission (January-February) centred around Guam in the tropical West Pacific and made extensive measurements in the marine boundary layer during 22 flights, with vertical profiles extending up to ~10 km. Likewise, the CONTRAST (January-February) and ATTREX (January-March) missions also sampled the tropical West Pacific in a region centred around Guam. However, these campaigns sampled air from higher altitudes, with ATTREX extending into the lower stratosphere. Data from these three flight campaigns are not used as input to the inversion; instead they are used as independent observations to test the posterior results (in the relevant months of 2014).

4.3.2.3 Ocean Emission Data

As noted in **Section 4.1**, the ocean is a potential source of CH_2Cl_2 and C_2Cl_4. However, there are large uncertainties and several important confounding issues that require attention. Given that oceanic emissions have been proposed to be relatively more important for CH_2Cl_2 than C_2Cl_4 [Keene et al., 1999], we focus most of the following discussion on CH_2Cl_2, which provides a rationale for performing an inversion with and without an ocean CH_2Cl_2 source.

First, there is very limited observational data with which to draw any firm conclusions regarding the strength of any oceanic emission. Khalil et al. [1999] estimated a total oceanic CH_2Cl_2 source of ~196 Gg yr^{-1} distributed in four latitude bands: 30-90°N (~24 Gg yr^{-1}), 0-30°N (~50 Gg yr^{-1}), 0-30°S (~50 Gg yr^{-1}), and 30-90°S (~72 Gg yr^{-1}). Khalil et al. [1999] acknowledged that the data available to them to calculate fluxes, including measured seawater and atmosphere concentrations of CH_2Cl_2 (and C_2Cl_4), were limited. The calculated fluxes were thus deemed to be “extremely uncertain” and later work inferred a significantly smaller upper limit to total ocean CH_2Cl_2 emissions (<90 Gg yr^{-1}) based on analysis of firn air samples [Trudinger et al., 2004].

Second, in addition to a paucity of measurements, observational results and expectations suggest the possibility for very large spatiotemporal variability in ocean CH_2Cl_2 fluxes. For example, based on data collected during a cruise in the tropical Atlantic, Kolusu et al. [2016] calculated a mean CH_2Cl_2 flux of 81 (±82) nmol m^{-2} day^{-1}. Given this large variability, short-term observational studies likely lack sufficient spatial and seasonal coverage to provide adequate estimates of annual net emissions over large domains. Extrapolation to infer regional or global emission totals, while common practice, can be problematic. Extrapolating the Kolusu et al. [2016] flux to a tropical ocean band gives ~236 (±237) Gg yr^{-1} and to the entire ocean gives a total of ~915 (±468) Gg yr^{-1}. This is a similar order to our prior global emission of 1,011.5 Gg yr^{-1}, that includes both land and ocean sources.

Third, another major confounding issue related to the above and relevant to drawing inference on the nature of any ocean CH_2Cl_2 source related to in situ production was discussed by Moore [2004]. Due to seasonal changes in CH_2Cl_2

ocean solubility (a decrease in warmer waters) and large seasonal changes in the CH_2Cl_2 concentration, summertime measurements may show ocean supersaturations that are unrelated to in situ production. In consequence, seasonally resolved data (or analyses accounting for temporary fluxes arising from physical effects, e.g., Ooki & Yokouchi, [2011]) are needed to determine the degree to which fluxes derived from measured ocean-water saturation are a result of in situ production or simply seasonal changes in solubility and atmospheric concentration. Moore [2004] also provided strong evidence that dissolved CH_2Cl_2 persists for extended periods (possibly years to decades) in intermediate and deep ocean waters. In consequence, observed CH_2Cl_2 supersaturations in seawater may be caused by its transport from colder waters at higher latitudes. Based on the above, the inferred oceanic CH_2Cl_2 source reported in previous studies [Keene et al., 1999; Khalil et al., 1999] may reflect re-equilibration processes and does not necessarily provide evidence for marine production.

A plausible mechanism by which CH_2Cl_2 may be produced in the ocean has been proposed and involves the photolysis and subsequent reaction of biogenic precursors, such as CH_2ICl, in seawater [Jones & Carpenter, 2005]. To our knowledge, the only observational study that provides some evidence of marine CH_2Cl_2 production (related to phytoplankton) is that of Ooki and Yokouchi [2011]. That study accounted for the physical factors discussed above to derive a marine CH_2Cl_2 in situ source from the Indian Ocean (between 10°S and 40°S) of 0.29-0.43 μg m^{-2} day^{-1}. When extrapolated zonally across the globe, a CH_2Cl_2 source of 10-15 Gg yr^{-1} was derived for this latitude band. In summary, considering the uncertainties mentioned above, we performed inversions with and without ocean CH_2Cl_2 sources.

For the inversion performed allowing net CH_2Cl_2 emissions from the ocean, we compare posterior emissions from our inversion to novel measurements from two recent ship cruises: (a) AMT-22 (Atlantic Meridional Transect, RRS James Cook) and (b) ACCACIA-2 (Aerosol-Cloud Coupling And Climate Interactions in the Arctic, JR288, RRS James Clark Ross). These campaigns took place in October/November 2012 and July/August 2013, respectively. AMT-22 covered a track through the Atlantic Ocean from 45°N to 30°S and ACCACIA-2 covered

the North Atlantic/Arctic Oceans from 70°N to 80°N, including a navigation around the archipelago of Svalbard, Norway (**Figure 1(b)**). Along these cruise tracks, sea-to-air flux estimates of CH_2Cl_2 (only) were derived based on in situ automated measurements of CH_2Cl_2 concentrations in surface seawater (from the ships' clean underway seawater supply inlets; nominal depth 5-6 m) and in air from a continuously pumped air inlet [Hackenberg et al., 2017]. Details of the GC-MS measurement systems are given in Andrews et al. [2015]. The CH_2Cl_2 sea-to-air flux was calculated following the approach of Johnson [2010] but would reflect the combination of both physical effects and any in situ production as discussed above. Average fluxes within the latitude limits of our ocean regions (**Figure 4.1** and **Section 4.3.1**) were calculated and an estimate of the global ocean emission from each latitude band was obtained through a simple extrapolation. These integrated fluxes are a starting point to compare to our posterior ocean emissions for CH_2Cl_2 in **Section 4.4.4**.

4.3.3 Observation Errors

The covariance matrix for errors in observations (e.g., R in Equation 4.01) is made up of various error sources. Our approach to quantifying these follows the framework described by Xiao [2008], which considers (1) “sampling frequency” errors, (2) “measurement” errors, and (3) “mismatch” errors [Chen & Prinn, 2006]. Each of these terms are used to define the total observational error and are detailed in turn below.

4.3.3.1 Sampling Frequency

The first error source arises due to the sampling frequency of the observational networks. That is, how well the observed monthly mean CH_2Cl_2 or C_2Cl_4 mole fractions are described by a finite number of measurements [Xiao, 2008]. For each site, and each month, the total sampling frequency error, $\boldsymbol{\sigma}_{sf}$, for an observational monthly mean is given as

$$\sigma_{sf} = \sqrt{\frac{\sigma_{mon}^2}{m}} \tag{4.03}$$

where σ_{mon}^2 is the variance of the reported mole fractions over the month and m is the number of observations in that month. For AGAGE surface sites, where measurements are obtained at relatively high frequency (order of 200 measurements per month), the sampling frequency error is calculated according to Equation 4.03. As it is difficult to assess the independence of successive measurements, Equation 4.03 assumes uncorrelated observations. This might lead to an underestimation in $\boldsymbol{\sigma}_{sf}$, but this is likely to be small compared to the overall error. For the NOAA surface sites, mole fractions are obtained based on paired flask samples obtained approximately weekly (i.e., relatively low frequency). Therefore, following Xiao [2008] sampling frequency errors for the NOAA data points were generated from the TOMCAT model, using 30-min averaged output at each of the NOAA locations.

4.3.3.2 Measurement Error

A second source of error arises from errors in the measurements. These can result from instrument precision or other uncertainties in the measuring techniques, such as calibration imperfections. Every observation will have a measurement error, although these are often difficult to fully estimate. In terms of precisions, the AGAGE network reports 0.5% for both CH_2Cl_2 and C_2Cl_4 based on the measurement precisions of the working standard used [Prinn et al., 2018], while the NOAA network reports precision for each individual measurement, which is aggregated over each month (typically around 0.7%). In this study, we assume a minimum overall 5% measurement error ($\boldsymbol{\sigma}_{meas}$) for both compounds. This value is based on the study of Andrews et al. [2016] who performed an intercomparison of CH_2Cl_2 mole fractions obtained by four different instruments, operated by four different groups, using the same standards. The results indicated that the mean absolute percentage error between the four instruments was ~5% in the troposphere.

4.3.3.3 Mismatch Error

An additional source of error is the mismatch between the observations and the model. This arises when comparing relatively low spatial resolution model output to point observations. An observational site could be unrepresentative of the model grid cell that it is located in. For example, the Harvard Forest (HFM) surface site is in the same TOMCAT grid cell as New York and other parts of the US Eastern seaboard. However, the site lies in the middle of a forest with presumably lower emissions and concentrations more characteristic of other rural observations. To take this into account, a mismatch error can be defined using the neighbouring grid cells [Chen & Prinn, 2006]. This is defined in Equation 4.04:

$$\sigma_{mismatch} = \sqrt{\frac{1}{9}\sum_{i=1}^{9}(c_i - \bar{c})^2} \quad (4.04)$$

where c_i is the model concentration output for each of the eight neighbouring grid cells, taken as an annual mean, and $\bar{c}$ is the mean model output over the nine cells. The mismatch error equation is a measure of the spatial variance, and although it is not a perfect metric, it helps to place uncertainty on observations with significant variation in their locality.

The three sources of error are combined in Equation 4.05 to give a total observational error:

$$\sigma_{total} = \sqrt{{\sigma_{sf}}^2 + {\sigma_{meas}}^2 + {\sigma_{mismatch}}^2} \quad (4.05)$$

Of the three error terms contributing in Equation 4.05, the sampling frequency term is typically small (<0.1% relative to observations) compared to, for example, the measurement error (5%). The size of the mismatch error is on average 2% but can vary strongly across sites. For some sites, particularly ones that neighbour urban locations, it can be as large as 15%, or even up to 150% at one site in particular (GSN). For more remote sites (e.g., in the Arctic), the mismatch error could be as low as 0.5%, 10 times lower than the measurement error.

4.3.4 Prior Emissions: Magnitude and Errors

Our prior emission estimates for CH_2Cl_2 and C_2Cl_4 are summarised in **Tables 4.3** and **4.4**, respectively. Note that these annual priors are held constant over each year of the inversion period. For CH_2Cl_2, prior estimates of Asian, European, and North American emissions (i.e., the expected three most significant industrialised regions) are 671, 50, and 55 Gg yr^{-1}, respectively (based on data from Nolan Sherry Associates, NSA). These bottom-up estimates (see also **Table 4.S1** in Supporting Information) were commissioned for this study and represent expected industrial emissions in 2016, based on a global industry database of chloromethane production and production capacity available to NSA. Production figures are calculated and refined by a combination of this extensive database, industry dialogue, trade data, and back-calculations based on known feedstock applications and quantities. These are entered into a chloromethanes mass balance scheme which is checked against industry capacity and closely calculated production ratios. Of the 671 Gg yr^{-1} industry estimate of total Asian CH_2Cl_2 emissions from NSA, 621 Gg yr^{-1} (~93%) is set as the inversion prior estimate for our Temperate Asia region (incorporating the NSA data for China, India, Japan, and Korea). The remaining 50 Gg yr^{-1} is taken as the prior for our Tropical Asian region (where NSA analysis shows the major markets for CH_2Cl_2 are Thailand, Indonesia, Singapore, Malaysia, and Vietnam). For the other six land regions, in the absence of more recent up-to-date data, prior industry CH_2Cl_2 emissions are taken from the RCEI, as summarised by Keene et al. [1999].

Recall that for CH_2Cl_2, two inversions are performed, one without ocean emissions and one with. For the without ocean case, our global total CH_2Cl_2 prior is ~815 Gg yr^{-1} (**Table 4.3**), that is, considering industrial emissions only. For the with ocean case, prior estimates of ocean CH_2Cl_2 emissions from four different ocean regions (see also **Sections 4.3.1** and **4.3.2**) are taken from Khalil et al. [1999], also part of the RCEI framework. The total ocean CH_2Cl_2 prior is 197 Gg yr^{-1}, increasing the global total prior to 1,012 Gg yr^{-1} in the "with ocean" inversion case (**Table 4.S2,** Supporting Information). Note that the original RCEI inventory also included a small biomass burning CH_2Cl_2 source of 59 Gg yr^{-1} [Lobert et al., 1999]. However, this estimate was based on an

assumed single global CH_2Cl_2/CO emission ratio for all fuel types. Subsequent studies have reported a lower (by two orders of magnitude) CH_2Cl_2/CO ratio [Simmonds et al., 2006] or have found no evidence for significant CH_2Cl_2 enhancements in biomass burning plumes [Lawson et al., 2015; Leedham Elvidge et al., 2015; Mühle et al., 2007; Simpson et al., 2011]. On this basis, a biomass burning CH_2Cl_2 source was not considered in the present work.

Table 4.3. A Summary of Prior (2016 Best Estimate) and Posterior CH_2Cl_2 Emissions (Gg yr^{-1}) and their Uncertainties, from the Synthesis Inversion not Allowing for an Oceanic CH_2Cl_2 Source.

Region		2006		2017	
	Prior Emissions	**Posterior Emissions**	**Error Reduction**	**Posterior Emissions**	**Error Reduction**
Europe	50.0	112.0 ± 9.1	81.9%	75.1 ± 11.4	77.3%
Africa	9.18	16.6 ± 8.4	8.0%	19.2 ± 8.7	5.2%
Australia	4.85	3.90 ± 2.22	54.2%	3.41 ± 2.62	45.9%
Boreal Asia	6.81	-19.8 ± 5.4	20.5%	-21.8 ± 6.2	9.3%
Boreal NA	1.11	0.002 ± 1.08	3.0%	0.14 ± 1.11	1.1%
Temperate Asia	621.0	89.9 ± 22.8	96.3%	590.7 ± 28.4	95.4%
Temperate LA	8.43	-2.57 ± 4.68	44.5%	0.96 ± 5.62	33.4%
Temperate NA	55.0	71.1 ± 4.9	91.1%	32.1 ± 5.9	89.3%
Tropical Asia	50.0	341.4 ± 22.7	54.5%	454.2 ± 28.7	42.6%
Tropical LA	8.67	24.1 ± 7.8	10.1%	17.1 ± 8.1	7.0%
Combined Asia	**671.0**	**431.3 ± 32.2**	**-**	**1044.9 ± 40.4**	**-**
Global Total	**815.1**	**636.6 ± 36.5**	**-**	**1171.2 ± 44.9**	**-**

Note. See the main text for a description of the prior emissions. NA = North America; LA = Latin America. Combined Asia = Temperate + Tropical.

For C_2Cl_4, a similar approach was adopted whereby prior industry emission estimates for our Asia, Europe, and North American regions are adapted from 2016 bottom-up estimates obtained from NSA (**Tables 4.4** and **4.S1**). Similarly to CH_2Cl_2, the Asia estimate is distributed among our Temperate and Tropical Asian regions as 93.3 and 15.0 Gg yr^{-1}, respectively. For the other six land regions, prior C_2Cl_4 emissions were formulated by reducing industrial emissions

from the RCEI inventory by a factor of 2. This reduction was performed because tropospheric C_2Cl_4 mixing ratios have been observed to be declining since 2000 or earlier [e.g., Simpson et al., 2004; Simmonds et al., 2006], meaning the older RCEI estimates (formulated in the 1990s) are very likely to overestimate present-day emissions. The magnitude of our resultant global total C_2Cl_4 prior emission (207 Gg yr^{-1}), of which 9% is from the ocean, is therefore in closer agreement to more recent independent global estimates [e.g., Engel et al., 2018].

Table 4.4. A Summary of Prior (2016 Best Estimate) and Posterior C_2Cl_4 Emissions (Gg yr^{-1}) and their Uncertainties, from the Synthesis Inversion.

Region		2007		2017	
	Prior Emissions	**Posterior Emissions**	**Error Reduction**	**Posterior Emissions**	**Error Reduction**
Europe	48.0	65.2 ± 4.4	90.9%	36.6 ± 2.6	94.6%
Africa	2.30	3.77 ± 2.20	4.5%	3.65 ± 2.09	9.2%
Australia	0.62	1.44 ± 0.33	47.1%	0.52 ± 0.25	59.7%
Boreal Asia	1.80	-2.34 ± 1.66	7.6%	-2.69 ± 1.60	10.9%
Boreal NA	0.50	-0.06 ± 0.48	5.3%	0.52 ± 0.47	6.7%
Temperate Asia	93.3	1.92 ± 8.80	90.6%	6.47 ± 7.35	92.1%
Temperate LA	1.06	2.00 ± 1.03	2.8%	2.04 ± 0.97	9.1%
Temperate NA	24.0	44.8 ± 2.7	88.6%	33.5 ± 1.8	92.3%
Tropical Asia	15.0	38.1 ± 8.0	45.1%	35.0 ± 7.9	46.1%
Tropical LA	1.58	2.73 ± 1.55	2.1%	2.29 ± 1.53	3.3%
Extratropical NO	3.51	-16.5 ± 2.2	37.8%	-12.6 ± 1.7	51.2%
Extratropical SO	5.85	-0.50 ± 0.79	86.4%	-0.14 ± 0.65	89.0%
Tropical NO	3.51	-0.63 ± 1.66	52.7%	1.06 ± 1.59	54.5%
Tropical SO	5.85	0.93 ± 1.25	78.7%	-0.09 ± 1.25	78.7%
Combined Asia	**108.3**	**40.0 ± 11.9**	**-**	**41.4 ± 10.8**	**-**
Global Total	**206.5**	**140.8 ± 13.8**	**-**	**106.1 ± 12.0**	**-**

Note: Results are based on inversion that did not include the C_2Cl_4 + Cl sink.

In addition to the observational errors necessary to the inversion procedure (**Section 4.3.3**), there are also errors in the prior emission estimates discussed above. As these are generally poorly quantified in inversion studies, they are set to ±100% for all regions as default. The sensitivity of our results to assumptions about prior errors is discussed in **Section 4.4.3**.

4.3.5 Prior Emissions: Distribution

Within the continental-scale regions considered in this study (**Figure 4.1(a)**), CH_2Cl_2 emissions are distributed according to a recent 1° × 1° global HCFC-22 emissions inventory reported by Xiang et al. [2014]. The rationale behind this choice is that CH_2Cl_2 is coproduced by industry with $CHCl_3$ [Oram et al., 2017], and the latter is used almost exclusively as a feedstock in the production of HCFC-22 and fluoropolymers [Fang et al., 2019; Mühle et al., 2019; Tsai, 2017], despite CH_2Cl_2 emissions likely being primarily associated with use, not production. On this basis, the use of the HCFC-22 emission distribution can be used as a reasonable proxy for CH_2Cl_2 and is a desirable alternative to the far older RCEI distribution. We understand that HCFC-22 is also likely to be emitted where it is used, not where it is produced, which makes this a rough approximation. In the similar absence of more recent data, the HCFC-22 distribution was used as a proxy for C_2Cl_4. It is important to stress that (a) these distributions only affect fluxes within regions (**Figure 4.1(a)**) and (b) that the inversion procedure adjusts the integrated regional total emissions, on a region-by-region basis. The distribution of our prior CH_2Cl_2 emissions is presented in **Figure 4.S1** (Supporting Information). It is assumed that the within-region distribution does not change over our study period (2006-2017).

4.4 Results and Discussion

4.4.1 Posterior CH_2Cl_2 Emissions and Trends

The synthesis inversion produces regional emission estimates, on an annual basis, for each of the 12 years studied. We investigated the degree to which our inversion was able to differentiate between emissions arising from one region

over another. A strong negative covariance was found for the closely located regions, Temperate Asia and Tropical Asia, which implies a difficulty in differentiating between these two regions. On this basis, in the ensuing discussion results from these regions are combined and referred to as "combined Asia." We first consider results from the "no ocean" CH_2Cl_2 inversion. **Table 4.3** compares prior and posterior CH_2Cl_2 emissions for 2006 and 2017, the first and last years of our study, highlighting an increase in posterior global total CH_2Cl_2 emissions from 637 ± 37 Gg yr^{-1} (2006) to 1,171 ± 45 Gg yr^{-1} (2017). This 84% increase is largely due to increasing emissions from combined Asia, estimated to rise from 431 ± 32 Gg yr^{-1} in 2006 to 1,045 ± 40 Gg yr^{-1} in 2017. Our results thus imply that combined Asian emissions more than doubled during the study period and account for ~70% of global total CH_2Cl_2 emissions in 2006 and ~90% in 2017. The latter is a similar relative proportion to that derived from the bottom-up information from NSA presented in **Table 4.S1**.

While there are no other estimates of total Asian CH_2Cl_2 emissions in the literature, to our knowledge, some country-specific estimates have been reported. Oram et al. [2017] roughly estimated Chinese CH_2Cl_2 emissions of 455 (410-500) Gg yr^{-1} in 2015 from bottom-up information from NSA. However, significantly smaller Chinese CH_2Cl_2 emissions in 2016 of 318 (254-384) Gg yr^{-1} have also been reported, apparently also based on bottom-up information [Feng et al., 2019], thus highlighting the uncertainty in the regional budget. Our estimate of total Asian emissions (1,045 Gg yr^{-1} in 2017) includes emissions from other major economies, such as India, expected to be significant emitters of CH_2Cl_2 [e.g., Leedham Elvidge et al., 2015]. The sensitivity of the above findings to inclusion of ocean emissions in our inversion is discussed in **Section 4.4.4**.

For other major industrialised regions, North America and Europe, our posterior emissions show a decrease over the 12-year study period (2006-2017). CH_2Cl_2 emissions from North America decreased from 71 ± 5 to 32 ± 6 Gg yr^{-1} (−55%) and from Europe decreased from 112 ± 9 to 75 ± 11 Gg yr^{-1} (−33%). Again, there is limited information in the literature to compare these findings to. Combining surface observations, model calculations, and CO ratio methods, Simmonds et al. [2006] derived European top-down CH_2Cl_2 emissions of 51-61

Gg yr^{-1} over the 2002-2004 period. Our estimate of European CH_2Cl_2 emissions, for the closest year to their study (2006), is larger at 112 Gg yr^{-1}. Simmonds et al. [2006] also reported a bottom-up estimate of industrial CH_2Cl_2 emissions of 139 Gg yr^{-1} from Europe, based on industry sales, in 2002/2003. We note that this is a very similar figure to our bottom-up estimate from NSA (albeit for 2007, **Table 4.S1**).

Figure 4.2 presents a time series of annual posterior CH_2Cl_2 emissions for a selection of the most important regions. The top panel shows the global total CH_2Cl_2 emission over the 12-year study period, the middle panel the contribution from our combined Asian region, and the bottom panel European and North American emissions. Also shown in the top panel are independent estimates of global CH_2Cl_2 emissions (2006-2016 only) calculated from a 12-box model forced by either NOAA or AGAGE long-term surface measurements [e.g., Cunnold et al., 1983; Rigby et al., 2013]. These annual emission data were prepared for the 2018 WMO/UNEP Scientific Assessment of Ozone Depletion and show CH_2Cl_2 emissions increasing from 442-759 Gg yr^{-1} in 2006 to 698-1,256 Gg yr^{-1} in 2016, with the ranges in each period reflecting results obtained considering the two different observational networks analysed by the 12-box model [Engel et al., 2018]. Good agreement between results from this study and those of the 12-box model is found, particularly when the latter assimilates NOAA data, which is plausible as our model also incorporates CH_2Cl_2 data on the NOAA calibration scale. For example, our global total CH_2Cl_2 emission in 2006 (637 ± 37 Gg yr^{-1}) and 2016 (1,117 ± 41 Gg yr^{-1}) fall within the 12-box model ranges noted above. In the most recent years, our posterior emissions fall towards the upper bound of the full uncertainty range of the 12-box model calculations (**Figure 4.2**). The relative increase in global CH_2Cl_2 emissions between 2006 and 2016 is 61% (12-box model average) and 75% (this work), and the mean annual differences (±1 SD) between our total emissions and the 12-box model AGAGE and NOAA estimates are 159 ± 51 and 42 ± 36 Gg yr^{-1}, respectively.

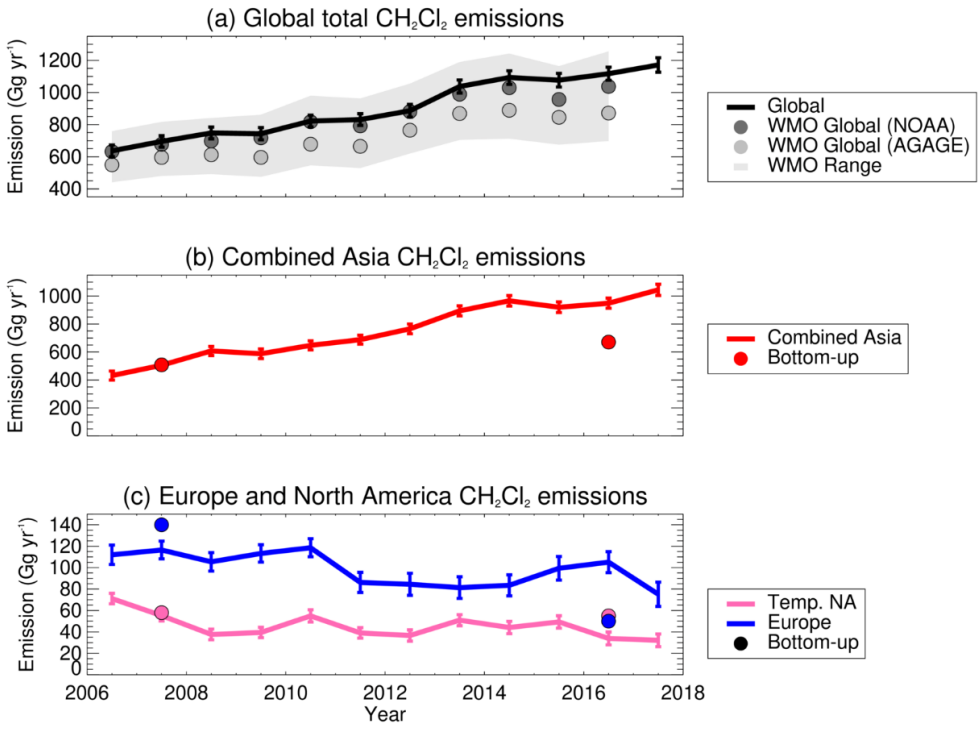

Figure 4.2. Timeseries of posterior CH_2Cl_2 emissions (Gg yr^{-1}) over the 12-year (2006-2017) study period. (a) Global total emissions from the inversion (black line, this work) alongside estimates from a 12-box model (circles) forced by NOAA (dark grey) and AGAGE (light grey) observations, as reported in Engel et al. (2018). The full 12-box model uncertainty range is represented by pale grey shading. (b) Asian emissions from the inversion showing Combined Asia (Temperate + Tropical), alongside bottom-up estimates from NSA (circles). (c) European and North American emissions, alongside bottom-up estimates from NSA (circles). See **Section 4.3.4** for a description of the bottom-up data. Note that the CH_2Cl_2 results shown here are for the no oceanic emission scenario. Error bars represent uncertainty ranges included in **Table 4.3**.

Our inversion approach allows us to examine the regional drivers of the increase in global CH_2Cl_2 emissions, which—as apparent from **Figure 4.2(b)**—are strongly driven by increasing emissions from Asia. In contrast, the relative changes in emissions from Europe and North America over the study period are relatively small. As previously noted, both these latter regions experienced an overall decrease in emissions, though the time series is also characterised by

significant interannual variability (**Figure 4.2(c)**). **Figure 4.2** also includes, on a regional basis, the bottom-up estimates of CH_2Cl_2 emissions from NSA for Asia, Europe, and North America in the years 2007 and 2016 (**Table 4.S1**). Recall that these 2016 inventory-based estimates were used as the prior emissions for these three respective regions in our inversion (see **Section 4.3.4**). Like top-down estimates, any bottom-up inventory-based emission data is subject to uncertainty. Therefore, we do not overinterpret these data, though note (a) that they imply a striking decrease in European CH_2Cl_2 emissions between 2007 and 2016 that is larger than predicted by our posterior emissions and (b) that discrepancies between top-down CH_2Cl_2 emissions (from Europe) and bottom-up estimates have been previously reported [Simmonds et al., 2006]. Our North American posterior emissions in 2007 more closely relate to the bottom-up estimate; however, our posterior emissions in 2016 are slightly lower than the bottom-up estimate but agree within the uncertainty range of the inversion (**Figure 4.2(c)**).

4.4.2 Posterior C_2Cl_4 Emissions and Trends

The posterior C_2Cl_4 emissions are summarised in **Table 4.4** and **Figure 4.3**. The tabulated results are based on an inversion that only included loss of C_2Cl_4 by OH and photolysis, ignoring the C_2Cl_4 + Cl sink. Correlations between regions were analysed in the same manner as for CH_2Cl_2, and a strong negative covariance was found between the Temperate and Tropical Asia regions. Therefore, we also employ the same "Combined Asia" for the ensuing discussion. Based on this inversion setup, global total C_2Cl_4 emissions decreased from 141 ± 14 Gg yr^{-1} in 2007 to 106 ± 12 Gg yr^{-1} in 2017. Both are significant reductions compared to our prior estimate of 207 Gg yr^{-1}. Also shown in **Figure 4.3** are (a) emission estimates prepared using a 12-box model as reported by Engel et al. [2018] and (b) regional bottom-up estimates of C_2Cl_4 emissions commissioned for this work (**Table 4.S1**). The 12-box model results show global C_2Cl_4 emissions decreasing from 95-199 Gg yr^{-1} in 2007 to 66-160 Gg yr^{-1} in 2016. The ranges in these values reflect the two different observational datasets used to force the model. Our posterior emissions show

similar absolute decreases, from 141 ± 14 to 104 ± 10 Gg yr^{-1} over the same period. Similarly, the relative decrease in global C_2Cl_4 emissions (2007-2016) is 24% (12-box model average) and 26% (this work), and the mean annual differences (±1 SD) between our total emissions and the 12-box model AGAGE and NOAA estimates are 26 ± 6 and 13 ± 7 Gg yr^{-1}, respectively. As described above, there is very good agreement between global C_2Cl_4 emissions derived in this work and those from Engel et al. [2018], which used primarily the same observations, though analysed with a simpler (12-box) model.

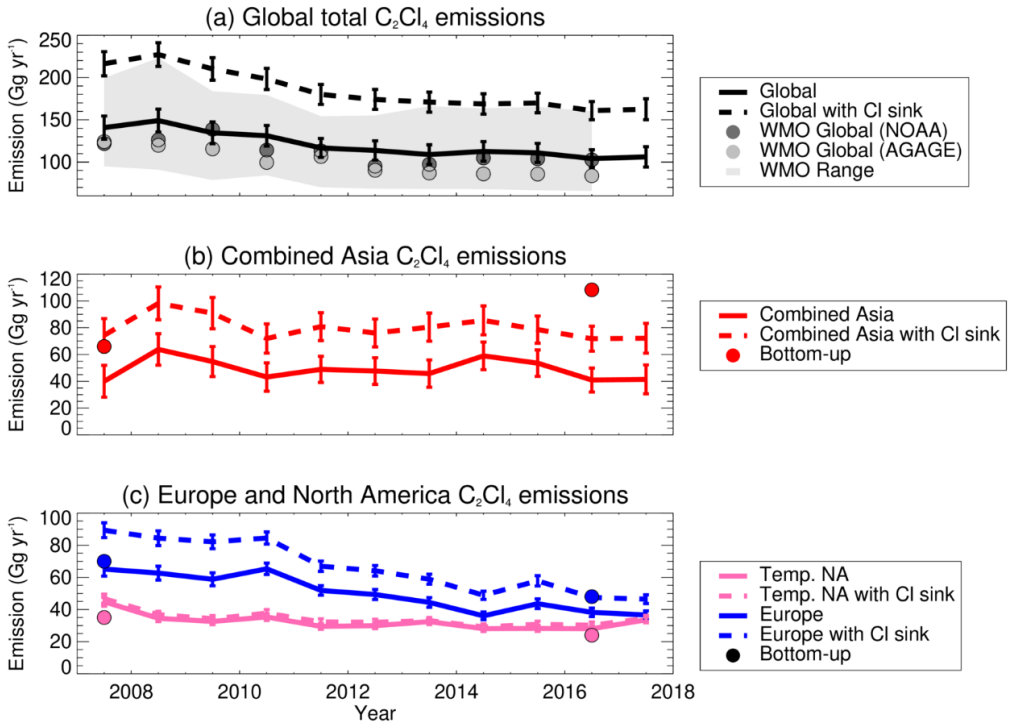

Figure 4.3. As **Figure 4.2** but for C_2Cl_4**.** Results are shown for simulations with (dashed line) and without (solid line) the C_2Cl_4 + Cl sink reaction.

However, there are clear discrepancies between our regional posterior emissions and the regional bottom-up estimates from NSA shown in **Figure 4.3**. First, our posterior results for Europe show declining emissions over the study period. While a decline is consistent with the bottom-up data, the magnitude of emissions is not in agreement, with the inversion showing lower C_2Cl_4 emissions in both 2007 and 2016 (in 2016 by a factor of ~2.2 lower). Second,

our inversion produces far lower Asian emissions than implied from the bottom-up data. The latter show an increase in Asian C_2Cl_4 emissions from 66 Gg yr^{-1} in 2007 to 108 Gg yr^{-1} in 2016. For comparison, our posterior combined Asian emissions in the same years are 40 ± 12 and 41 ± 9 Gg yr^{-1}, respectively. The bottom-up Asian 2016 estimate (108 Gg yr^{-1}) is larger than the 2016 global total emissions calculated from both our inversion and from the average of the 12-box model estimates [Engel et al., 2018]. Better agreement is found for North American emissions (**Figure 4.3**).

Unlike for CH_2Cl_2, tropospheric loss of C_2Cl_4 via Cl radicals (in addition to OH oxidation) can be a significant sink, although its magnitude is not well constrained as the concentration of tropospheric Cl radicals is uncertain. Its inclusion in global models has been shown to lead to better agreement with C_2Cl_4 observations, particularly in the upper troposphere [e.g., Hossaini et al., 2019]. The main inversion results discussed above did not consider this sink, nor did the 12-box model estimates [Engel et al., 2018]. A second inversion was performed that did include this additional C_2Cl_4 sink. The posterior results from that inversion are presented in **Table 4.S3** (Supporting Information) and shown with dashed lines in **Figure 4.3**. It is evident that inclusion of the Cl atom sink for C_2Cl_4 significantly changes the predicted global total C_2Cl_4 emissions. As would be expected, emissions are larger in the presence of an additional atmospheric loss process. For example, we estimate global total C_2Cl_4 emissions of 106 ± 12 Gg yr^{-1} in 2017 without the Cl sink (**Table 4.4**) and 162 ± 12 Gg yr^{-1} with it (**Table 4.8**, i.e., 53% larger). On a regional basis, Asian emissions provide the bulk of this increase, with 90% larger combined Asian C_2Cl_4 in 2017 when the C_2Cl_4 + Cl sink is included compared to without it. Inclusion of the sink reduces the discrepancy between our posterior Asian emissions and the NSA bottom-up estimates (**Figure 4.3(b)**), though our emissions are still lower in the present day. Better agreement is also obtained for Europe, while North American emissions are broadly unchanged. It is expected that agreement between our posterior C_2Cl_4 emissions and the 12-box model are poorer in absolute magnitude when the Cl sink is included, as this sink is absent in the 12-box model study. However, we note that the trends remain similar.

4.4.3 Posterior Errors

Our inversion procedure calculates the error in the posterior emissions from the terms in Equation 4.01, using the relationship in Equation 4.06:

$$\text{Posterior error matrix, } \boldsymbol{A} = [\boldsymbol{G}^T.\boldsymbol{R}^{-1}.\boldsymbol{G} + \boldsymbol{B}^{-1}]^{-1} \qquad (4.06)$$

To find the regional emission error, the square root of the leading diagonal elements of ***A*** is taken. **Tables 4.3** and **4.4** show the regional posterior errors for CH_2Cl_2 and C_2Cl_4, respectively. The percentage reductions between the prior error and the posterior errors are also given in these tables. A large error reduction implies more confidence in the posterior solution, and for CH_2Cl_2, the largest reductions occur for the main emitting regions where observations are available, for example, Temperate North America (89% error reduction for CH_2Cl_2 in 2017), Temperate Asia (95%), and Europe (77%). Note that these values should be considered in tandem with the posterior errors themselves. For example, although Europe has a significant error reduction (e.g., in 2017 a reduction of 77%), this results in a posterior error of ±11 Gg yr^{-1}, which is 15% of the actual posterior CH_2Cl_2 emission from this region. The inverse is true for Temperate Asia, where relatively large posterior emissions (591 Gg yr^{-1} in 2017) and a large error reduction (95%) lead to a very small (5%) error in the posterior emission. The C_2Cl_4 errors generally show a similar behaviour, with the largest prior versus posterior error reduction achieved for the main industrial regions where large emissions are derived.

A small error reduction corollary is a sign of less confidence in the posterior emissions. For both compounds, these generally apply to regions that are minimally constrained by local observations, such as Africa and tropical Latin America. Fortunately, as it is assumed that these regions do not contribute much to the total global emissions, relatively large uncertainty in their regional posterior emissions have minimal impact on our findings. That said, we highlight Boreal Asia, a region that is a small net source in our prior emissions (6.8 Gg yr^{-1} for CH_2Cl_2, 1.8 Gg yr^{-1} for C_2Cl_4) but becomes a net sink for both compounds in our posterior solution. In 2017, our posterior emissions for Boreal Asia are -22 (±6) Gg yr^{-1} for CH_2Cl_2 and -2.7 (±1.6) Gg yr^{-1} for C_2Cl_4. For this region, the percentage reductions between the prior error and the posterior error

are small (**Tables 4.3** and **4.4**). While some chlorocarbons are taken up by terrestrial ecosystems [e.g., Khalil & Rasmussen, 1999], no terrestrial sinks of CH_2Cl_2 have been reported, and the lack of observational constraints in this region could point towards a small inversion artifact. An analysis of covariances did not reveal a strong coupling between Boreal Asia and another region.

4.4.4 Ocean Emissions

Thus far, we have largely focused on our posterior emissions from land (in the "no ocean" inversion for CH_2Cl_2). In this section, we examine ocean emissions. A summary of posterior CH_2Cl_2 emissions with the ocean source included is given in **Table 4.S2** (Supporting Information) and can be compared to the equivalent no ocean case (**Table 4.3**). In the inversion in which net emissions from the ocean are allowed, oceanic CH_2Cl_2 emissions (sum from all four ocean bands) account for 197 Gg yr^{-1} (19%) of our prior global total emission, decreasing to 162 Gg yr^{-1} (14%) in our posterior solution in 2017. The global total CH_2Cl_2 emission is relatively insensitive to the inclusion of the ocean source, 1,171 ± 45 Gg yr^{-1} (no ocean) versus 1,166 ± 64 Gg yr^{-1} (with ocean) for 2017. However, inclusion of the ocean decreases the combined Asia posterior emissions by ~18%, from 1,045 ± 40 Gg yr^{-1} (no ocean) in 2017 to 886 ± 53 Gg yr^{-1} (with ocean). This effect is largely explained by the inversion placing emissions of CH_2Cl_2 in the tropical Northern Ocean (0-30°N latitude). As was the case in the "no ocean" inversion, **Figure 4.S2** (Supporting Information) highlights increasing Asian emissions over our study period, while European and North American emissions decrease. With the ocean included, the Combined Asian emissions provide a closer match to the bottom-up NSA estimates of industrial Asian emissions (i.e., our prior) in 2016 (**Figure 4.S2**). However, as mentioned later in **Section 4.4.6**, there is no discernible difference in performance between the inversions with and without the ocean source, when compared with observations (even independent data), despite these changes in Asian emissions.

Table 4.5. Optimised CH_2Cl_2 Oceanic Emissions (Gg yr^{-1}) Derived from Positive Prior Fluxes for this Inversion, a Previous Inversion [Xiao, 2008], and Measurements from Four Observational Studies.

Ocean band	This work[a]	Xiao [2008][b]	AMT-22 Campaign[c]	ACCACIA-2 Campaign[c]	Kolusu et al. [2016][c]	Ooki and Yokouchi [2011][d]
Extratropical NO	-64.4 ± 10.9	3.5 ± 3.0	14.7 ± 26.9	-47.9 ± 32.7		
Tropical NO	111.8 ± 43.1	88 ± 29	70.9 ± 63.6		236 ± 237	
Tropical SO	9.9 ± 12.7	31 ± 24	64.0 ± 43.3			12.5 ± 2.5
Extratropical SO	4.3 ± 3.9	2 ± 5				

Note: All measurements converted into Gg yr^{-1}. Reported uncertainties for inversion calculations and campaign ocean tracks of 1 SD. NO = Northern Ocean; SO = Southern Ocean.

[a]Twelve-year average posterior emission.

[b]Five-year average posterior emission from 2000-2005.

[c]Atlantic Ocean sea-to-air flux measurements, originally reported as nmol m^{-2} day^{-1}, and converted into Gg $band^{-1}$ yr^{-1} for the relevant ocean latitude bands. AMT-22 campaign measurements took place in October-November 2012, ACCACIA-2 campaign measurements in July-August 2013, and Kolusu et al. [2016] measurements in April-May 2009.

[d]Indian Ocean biogenic production from phytoplankton, reported between 10°S and 40°S in µg m^{-2} day^{-1}. These measurements were taken from November 2009 to January 2010 and account for physical effects that are the likely principal source in the sea-to-air flux measurements.

The geographical distribution of our posterior ocean CH_2Cl_2 emissions differs significantly from the prior in the inversion that allows nonzero ocean fluxes. For example, when averaged over the entire 12-year study period, the Extratropical Northern Ocean represents a net sink of CH_2Cl_2 (**Table 4.5**). In the extratropical Southern Ocean, the derived net flux is significantly lower than the prior but remains positive. Also shown in **Table 4.5** are results from the inversion study of AGAGE and NOAA observations by Xiao [2008], who allowed nonzero fluxes from the ocean and tabulated ocean CH_2Cl_2 emissions from these same latitude bands. Posterior emissions for the Tropical Northern and Extratropical Southern Oceans from our study fall within the Xiao [2008] uncertainty ranges. However,

notably the significant mean CH_2Cl_2 sink we derive to the Extratropical Northern Ocean is not apparent in the Xiao [2008] study for the observations during 2000-2005, a period before the large atmospheric increase in CH_2Cl_2 occurred.

It is also possible to perform a basic comparison of our posterior ocean CH_2Cl_2 emissions to observed estimates based on (limited) cruise data. As noted in **Section 4.3.2.3**, ocean CH_2Cl_2 sea-to-air fluxes from the AMT-22 and ACCACIA-2 ship cruises (see tracks in **Figure 4.1(b)**) were derived based on concentration measurements without consideration of the potential influence of physical effects on the derived fluxes. These cruises sampled in three out of the four ocean bands used in our inversion and the integrated flux from each ocean band is presented in **Table 4.5**. Broadly, the sign of the emissions agrees in all three regions observed; however, it is important to note that this comparison is potentially confounded by considering annual average inversion results to cruise data that we expect could be influenced by seasonally varying sea-to-air fluxes based on seasonal changes in solubility and atmospheric concentrations [Moore, 2004].

Xiao [2008] reports a large seasonal cycle in ocean emissions, and for the 30-90°N region, there is a maximum of approximately 20 Gg yr^{-1} in the summer and a minimum of −10 Gg yr^{-1} in the winter. We note that ACCACIA-2 took place during July-August, and reported an average flux of −48 Gg yr^{-1}, which is contrary to what the seasonal cycle states. However, neither our inversion nor that of Xiao [2008] can resolve between 60° and 80°N, where ACCACIA-2 took place. AMT-22, measuring from 30° to 50°N in autumn, calculates an average flux of 15 Gg yr^{-1}, which is close to the average autumnal values from Xiao [2008]. In the original RCEI estimates, none of the ocean tracks used to infer CH_2Cl_2 fluxes took place above 60°N [Khalil et al., 1999]; therefore, the large summer sink observed by ACCACIA-2 at these very high latitudes could be evidence for the significant interregional variation we see in our inversion results.

Also presented in **Table 4.5** is an estimate of an ocean CH_2Cl_2 source based on measurements in the tropical Atlantic from April to May in 2009 [Kolusu et al., 2016]. This source is very uncertain and is generally much higher than any

single ocean band emission derived from the inversion. As with the cruises previously discussed, these data do not necessarily support marine CH_2Cl_2 production because of the strong potential for changes in sea-to-air flux related to seasonality in solubility and atmospheric concentrations. Rather, this data simply highlights an ocean region where a significant quantity of CH_2Cl_2 may enter the atmosphere (at least during the period of the campaign of April-May). Due to the large uncertainty, it is difficult to say how representative the observations are, as the study showed there was a strong latitudinal gradient, especially when crossing the Equator [Kolusu et al., 2016]. Lastly, in **Table 4.5**, are estimated biogenic CH_2Cl_2 emissions reported by Ooki and Yokouchi [2011] based on data collected in the tropical Southern Indian Ocean (10-40°S). Factoring in the uncertainty ranges, our inversion emissions from the tropical Southern Ocean are comparable.

In summary, our posterior CH_2Cl_2 net ocean source (11% of the global total from all sources in 2017 or 125 Gg yr^{-1}) is comparable to previous inversion estimates and to a small set of available oceanic observations. However, while the total source magnitude is comparable, the distribution shifts the majority of the emissions into the Tropical NO region and very few emissions into the Tropical SO region. This distribution is likely a consequence of the large driving force of Combined Asian land emissions; practically, it is plausible that the tropical distribution is more even, as observations suggest. For C_2Cl_4, the posterior ocean source is negligible and often negative (**Table 4.4**). For both compounds, our inversion does not distinguish between ocean re-emission and, if it exists, “true” marine production.

4.4.5 Sensitivity to Prior Uncertainty

Our prior emission errors were set to ±100% for all regions (**Section 4.3.4**), and we tested the sensitivity of our posterior emissions to this value. **Figure 4.4** illustrates this by presenting posterior CH_2Cl_2 and C_2Cl_4 emissions for seven of the most important inversion regions under different prior error assumptions applied to each region simultaneously. Note that for this analysis, a 0% error simply represents the prior emission. As errors are progressively increased,

each of the inversion regions is given a greater degree of freedom to reach a target.

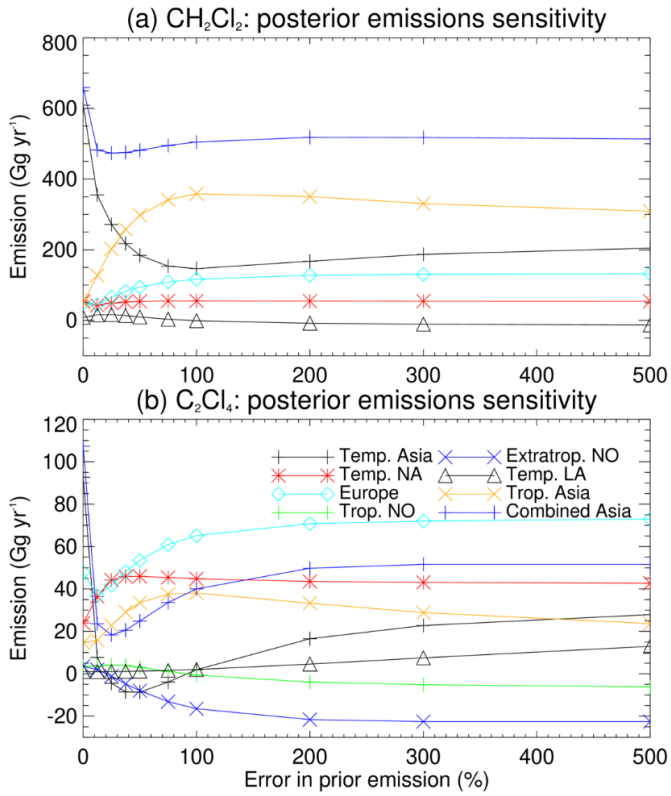

Figure 4.4. Summary of results testing the sensitivity of posterior emissions to the assumed error in the prior emissions for (a) CH_2Cl_2 and (b) C_2Cl_4. Results are shown indicatively for the year 2007 and for seven different regions (five for CH_2Cl_2), including a Combined Asian result. Note that a 0% prior emission error equates to the prior emissions. For CH_2Cl_2, results are shown for the no ocean inversion scenario.

There are several features apparent in **Figure 4.4** that warrant attention. For CH_2Cl_2, Temperate North America and Europe are examples of regions whose emission magnitudes are insensitive to the uncertainty assumed for the prior when it is above ~50%. The Temperate and Tropical Asian regions were found to vary more with the assumed prior uncertainty, and the derived emissions are slightly anticorrelated. However, our Combined Asia region is insensitive to prior error when assumed to be equal or larger than ±100% (**Figure 4.4(a)**). Temperate Latin America is an example of a region that reaches its optimum

emission value at a larger emissions error than ±100%, and at further increased error drifts negatively. As previously noted, our posterior CH_2Cl_2 emissions from this region are negative, possibly reflecting a small inversion artifact due to the lack of data, but are also very small and thus of limited global importance: -0.96 (±5.62) Gg yr^{-1} in 2017. A similar sensitivity analysis to prior errors for the with ocean CH_2Cl_2 case was also performed (**Figure 4.S3**, Supporting Information).

For C_2Cl_4, the posterior emissions are generally stable beyond ±100% prior error. Again, Temperate and Tropical Asia have a small tendency to drift towards each other, though likewise, the Combined Asia region is insensitive to prior error, justifying our initial assumption, but only at errors beyond ±200% (**Figure 4.4(b)**).

4.4.6 Posterior Versus Prior Emissions Performance

With prior and posterior CH_2Cl_2 and C_2Cl_4 emissions calculated, their performance can be evaluated by comparing modelled mixing ratios obtained with each to observations. We first focus on a single year (2016) and consider how well the posterior emissions reproduce background NOAA and AGAGE surface observations. Both the NOAA and AGAGE data used in these comparisons were assimilated by the inversion (i.e., to construct the posterior emissions). Comparisons to independent observational data are considered in **Section 4.4.7**. Modelled monthly mean CH_2Cl_2 ("no ocean" inversion) and C_2Cl_4 are compared to NOAA measurements in **Figures 4.S4** and **4.S5**, respectively.

For CH_2Cl_2, **Figure 4.S4** reveals generally very good agreement between the model (posterior emissions) and the observations. At several sites, particularly those at midlatitude and high latitude in the Northern Hemisphere (NH), the prior and posterior emissions perform similarly. However, a clear improvement is obtained when using the posterior emissions in the tropics and in the Southern Hemisphere (SH). For C_2Cl_4, posterior improvements at NOAA sites are more striking. **Figure 4.S5** shows that our prior C_2Cl_4 emissions were too large, leading to a significant overestimation of observed mole fractions.

Similar comparisons but for AGAGE observations (converted to the NOAA calibration scale) are shown in **Figures 4.S6** and **4.S7**. These comparisons are also for the year 2016, with the exception of the Gosan (GSN) site in South Korea (2015). For CH_2Cl_2, the measurements are better reproduced using our posterior emissions at most sites, except for ZEP, though as noted above, the differences between prior and posterior results are relatively small in the NH. For C_2Cl_4, again, the posterior emissions lead to much better agreement between the model and observations. A notable feature for CH_2Cl_2 in **Figure 4.S6**, apparent when using both the prior and posterior emissions, is the model overestimation of baseline CH_2Cl_2 observations at Gosan. This site is heavily influenced by several large nearby sources, and the mismatch errors in the inversion are particularly large. However, significantly improved agreement to the Gosan data is obtained when the "raw" measurements are used to construct monthly means (i.e., without filtering out pollution events). Such events are inherently included in the model monthly means.

The comparisons discussed above focused on a single recent year. A more informative approach is to consider the performance of the posterior emissions over the entire study period. To quantify this performance, we calculate the mean absolute deviation (Equation 4.07) over the full study periods at each available NOAA site (14 for CH_2Cl_2 and 12 for C_2Cl_4) based on monthly means:

$$mean\ absolute\ deviation = \frac{\sum_{months}|model - observation|}{n_{months}} \qquad (4.07)$$

For CH_2Cl_2, the posterior emissions provide much improved agreement to the observations at all sites, reducing the model/observation deviation to below ~5 ppt at most NH sites and below ~0.9 ppt at all SH sites (**Figure 4.5(a)**). This is not entirely unexpected given that these observations were included in the inversion itself. However, overall, the reduction of the prior deviations by roughly 60% in the posterior indicates that the inversion procedure has been successful. C_2Cl_4 is equally successful, also with an average deviation reduction of roughly 80% and 40% when the C_2Cl_4 + Cl sink is included (**Figure 4.5(b)**). Evident from the same figure, the magnitude of these improvements is not overly sensitive to inclusion of the +Cl sink, but the decreased reduction is due to the reduction in the prior deviations.

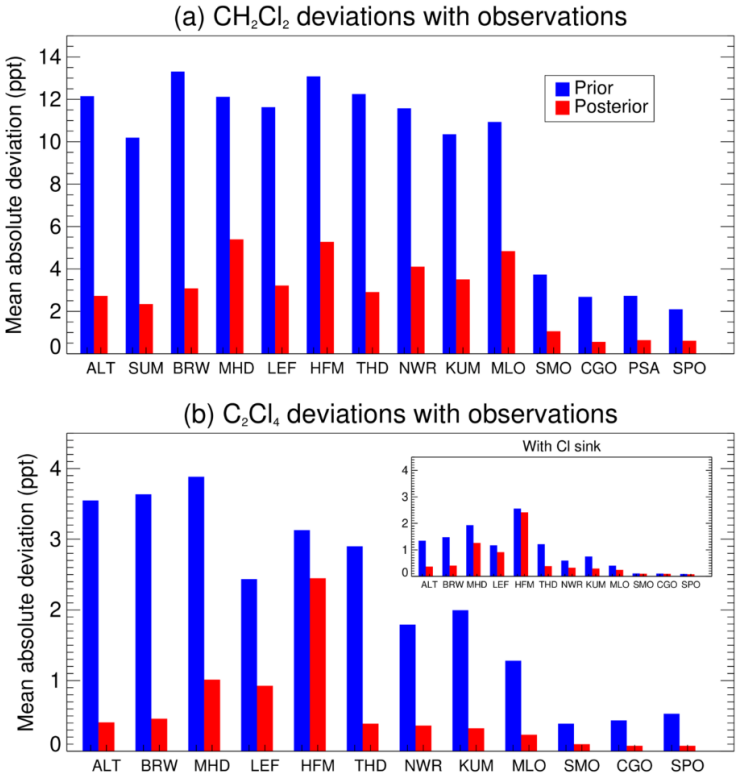

Figure 4.5. Mean absolute deviation (ppt) between modelled and observed (a) CH_2Cl_2 and (b) C_2Cl_4, at NOAA sites. The deviations are averages calculated from monthly mean data over the study periods (2006-2017 for CH_2Cl_2 and 2007-2017 for C_2Cl_4) and are shown for model output generated using the prior emissions and the posterior emissions. The C_2Cl_4 + Cl sink comparisons are inset in (b). For CH_2Cl_2, results are generated using the posterior emissions from the no ocean inversion scenario.

In addition to the above deviations, it is important that the time-dependent posterior emissions adequately capture trends. The four NOAA sites shown in **Figure 4.6** for CH_2Cl_2 are a selection from various geographical locations (**Table 4.1**): a high latitude NH site (ALT), a midlatitude NH site (LEF), a tropical site (KUM), and an SH site (CGO). The posterior CH_2Cl_2 model output is far better at matching with the observations over the 12-year period compared to the prior model output. This is especially true of the earlier parts of our study period given that our prior emissions (for the main industrialised regions) were based on bottom-up data from 2016. Annotated in **Figure 4.6** are the modelled (posterior) and observed CH_2Cl_2 trends over the 2006-2017 period, calculated

using a simple least squares regression. The modelled and observed trends are 3.0 and 2.9 ppt yr^{-1} at ALT, 2.8 and 3.0 ppt yr^{-1} at LEF, 2.6 and 2.9 ppt yr^{-1} at KUM, and 0.7 and 0.7 ppt yr^{-1} at CGO and thus are in excellent agreement. Despite the geographical range of the three NH sites, similar trends, roughly 3 ppt yr^{-1}, are found.

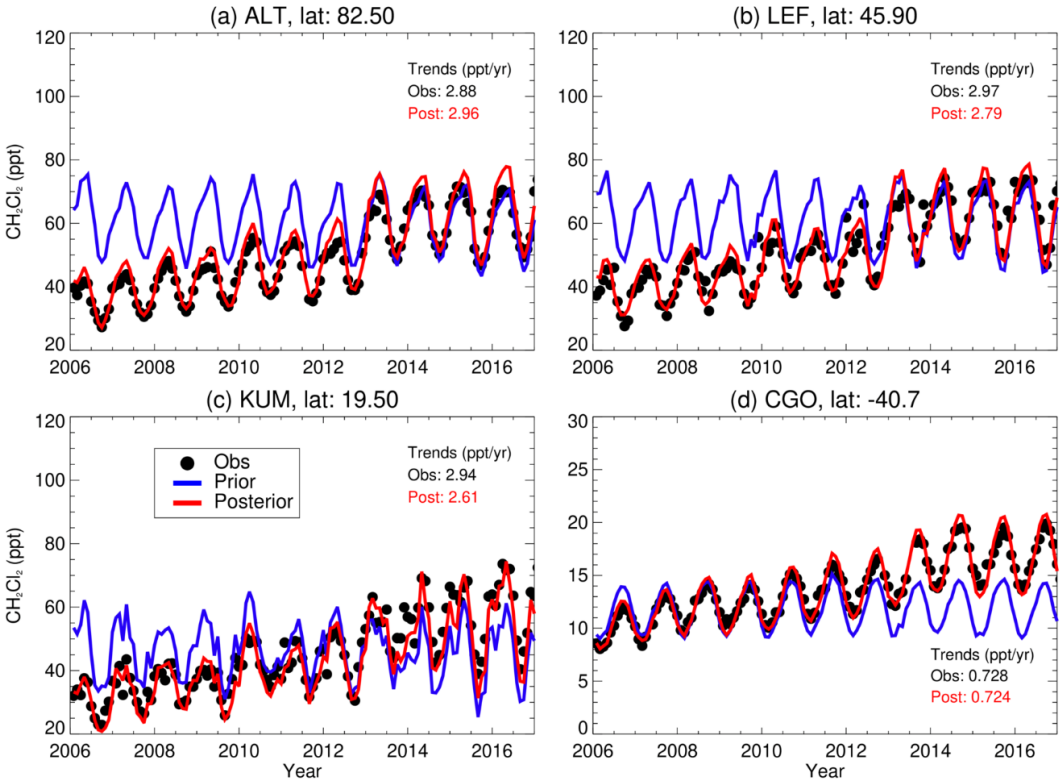

Figure 4.6. Comparison of modelled monthly mean CH_2Cl_2 mixing ratio (ppt) versus NOAA observations (2006-2017) at stations (a) ALT, (b) LEF, (c) KUM, and (d) CGO. Each panel contains model output based on the prior (blue) and the posterior (red) emissions, with annual trends (ppt yr^{-1}) in the model (posterior) and observations annotated. For CH_2Cl_2, results are generated using the posterior emissions from the no ocean inversion scenario.

A similar analysis for C_2Cl_4 was performed at the same four sites, with again good agreement between the model (with posterior emissions) and the observations (**Figure 4.7**). The modelled and observed trends without the C_2Cl_4 + Cl sink reaction included are -0.14 and -0.13 ppt yr^{-1} at ALT, -0.15 and -0.12

ppt yr^{-1} at LEF, -0.07 and -0.08 ppt yr^{-1} at KUM, and -0.02 and -0.01 ppt yr^{-1} at CGO. In addition, **Figure 4.7** includes the Cl sink of C_2Cl_4. The trends are slightly improved in the posterior for three of the sites (except KUM), and the figure shows the stark contrast between the two prior model outputs. The addition of the Cl sink leads to a decreased lifetime of C_2Cl_4 [Hossaini et al., 2019], and therefore, prior concentrations are decreased. The inversion compensates for this by increasing posterior emissions, as shown in **Figure 4.3**. Despite two very different prior positions, the two almost identical C_2Cl_4 posterior outputs (in **Figures 4.5(b)** and **4.7**) indicate how effective the inversion process can be.

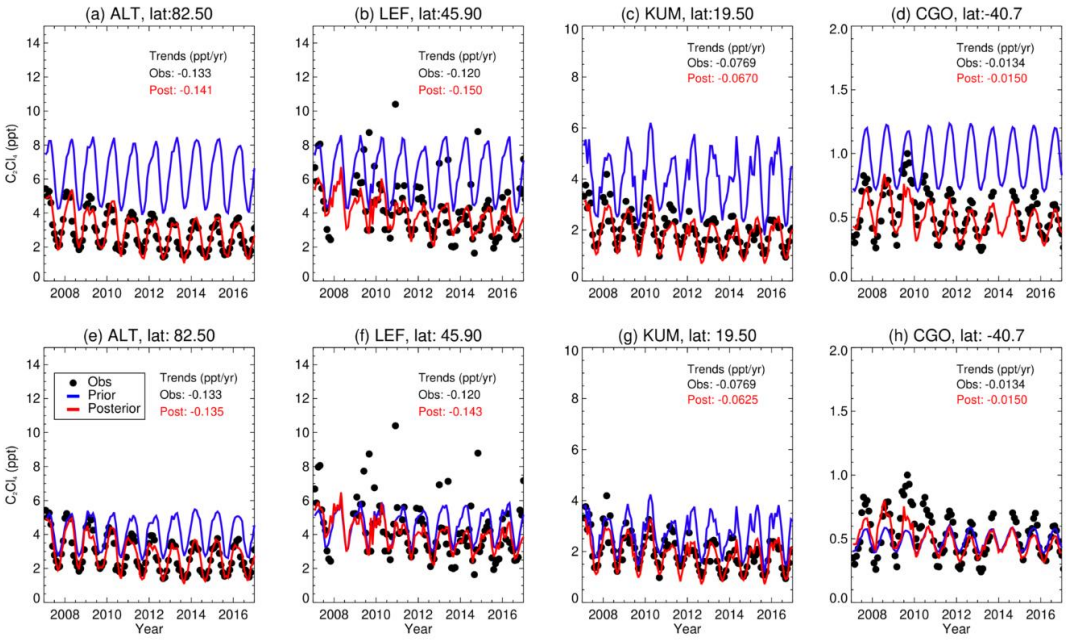

Figure 4.7. Comparison of modelled monthly mean C_2Cl_4 mixing ratio (ppt) versus NOAA observations (2007-2017) at the same stations as in **Figure 4.6**. Panels (a)-(d) are comparisons without the C_2Cl_4 + Cl reaction, and (e)-(h) are with the reaction.

For every year of the model, TOMCAT assumes the same offline OH field. In practice this is not the case, and OH can vary annually on average by 2-3% [Montzka, Krol, et al., 2011]. The cause of this is primarily due to variation in the major source compounds towards OH generation, i.e. NO_x, H_2O, O_3, CO, and CH_4. Periodic phenomena such as the El Nino Southern Oscillation direct

changes in H_2O, for example. As a result of assuming constant OH, the modelled concentrations of CH_2Cl_2 and C_2Cl_4 would not include any interannual variability. If for a given year the model was underestimating OH at a certain location, the resulting inversion would underestimate Cl-VSLS emissions. There has been a general increasing trend in OH concentrations between 1990 and 2010, particularly over East and Southeast Asia, of the order of 1% yr^{-1} [Zhao et al., 2019]. This suggests that Asian Cl-VSLS emissions could in fact be a fraction larger than calculated.

Note that for CH_2Cl_2, the discussion above has focused on the "no ocean" inversion. The posterior modelled CH_2Cl_2 mixing ratios from the with ocean inversion (not shown) are found to be almost identical; thus, the performance of the two inversions is very similar. This implies that it cannot be concluded (or excluded) that a significant ocean CH_2Cl_2 source exists from this analysis.

4.4.7 Independent Observations

In the previous section, we compared modelled CH_2Cl_2 and C_2Cl_4 mixing ratios, generated using our posterior emissions, to observations used in the inversion itself. Here, we examine independent observations, first considering aircraft measurements during the 2014 CAST, CONTRAST, and ATTREX missions over the tropical West Pacific (**Section 4.3.2**). Modelled and observed vertical profiles (surface to ~20 km) are displayed in **Figure 4.8**. For each aircraft observation, the monthly mean concentration in the corresponding model grid cell was extracted. These monthly mean concentrations and observations were then averaged over 1 km vertical bins, providing the blue squares and black lines in **Figure 4.8**, respectively. Throughout the vertical extent of these profiles, there is (a) near-perfect agreement between modelled CH_2Cl_2 using the posterior emissions ("no ocean" inversion) compared to the observations and (b) a significant improvement over the prior. The latter presumably reflects the larger Asian emissions in our posterior model occurring in the vicinity to the measurement campaigns. For C_2Cl_4 (CONTRAST and ATTREX only), **Figure 4.8(b)** shows results from the model both with and without the Cl sink. In both cases, the posterior emissions outperform the prior. The Cl sink case matches

with the observations more effectively at higher altitudes, whereas both cases are similar towards the surface. On average, the model output overestimates C_2Cl_4 by 0.53 ppt for the no Cl sink and by 0.47 ppt for the Cl sink case. This overestimation could be caused by the large Combined Asia emissions, which heavily influence these observations.

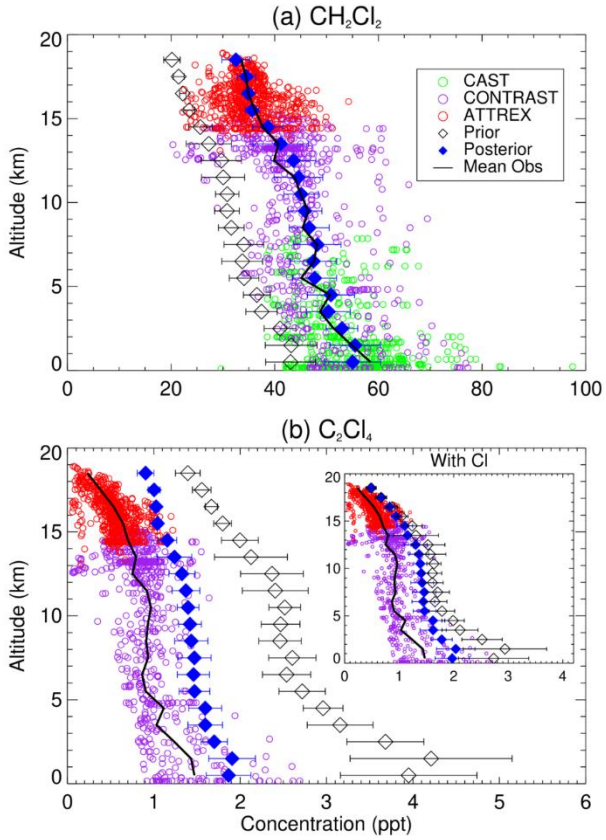

Figure 4.8. Modelled versus observed vertical profiles of (a) CH_2Cl_2 and(b) C_2Cl_4 volume mixing ratio (ppt) during the 2014 CAST/CONTRAST/ATTREX field missions in the West Pacific (see **Section 4.3.2**). Model output has been averaged in 1 km vertical bins and is shown for both the prior and posterior emissions. Note that these aircraft data are "independent" in that they were not used in the inversion to produce the posterior emissions. The C_2Cl_4 + Cl sink data are inset in (b). For CH_2Cl_2, results are generated using the posterior emissions from the no ocean inversion scenario.

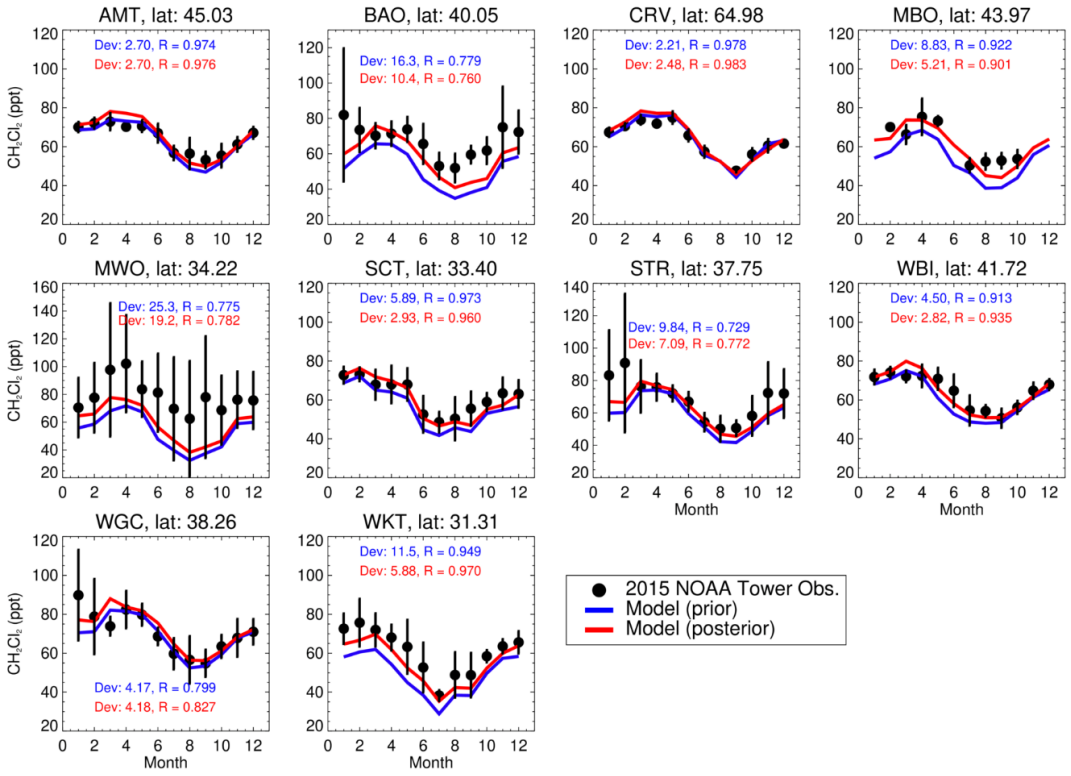

Figure 4.9. Comparison between monthly mean NOAA tall tower observations of CH_2Cl_2 (ppt) in 2015 (independent observations) and modelled values obtained using the prior and posterior emissions. The vertical bars on the observations indicate ±1 SD of all measurements acquired at that site during that month. Annotated for each site are the average annual deviations (Dev) between the two model outputs and the observations, and the correlation coefficient, R. Results are generated using the posterior emissions from the no ocean inversion scenario.

The second test for our inversion is from the independent network of NOAA tall tower sites (USA-based, e.g., see **Figure 4.1**). At each of the 10 sites where CH_2Cl_2 observations are available, the posterior model provides a reasonable representation of the measurements in 2015 (**Figure 4.9**). Annotated on this figure are the mean absolute deviations at each site between the model (with prior and with posterior emissions) versus the observations, in that year. At most sites, the posterior model outperforms the prior, but generally, only small improvements in the CH_2Cl_2 average deviation are achieved. The correlations between model and observations (also annotated) also show a consistent

improvement for the posterior. At certain sites, large standard deviations on the monthly mean observations coincide with poor model-measurement agreement, in some months. For example, the proximity of the MWO site to large urban areas may partly explain why the monthly mean observations are consistently larger than the model outputs, and for the other instances where large standard deviations occur, the model outputs lie at the lower range of the observations.

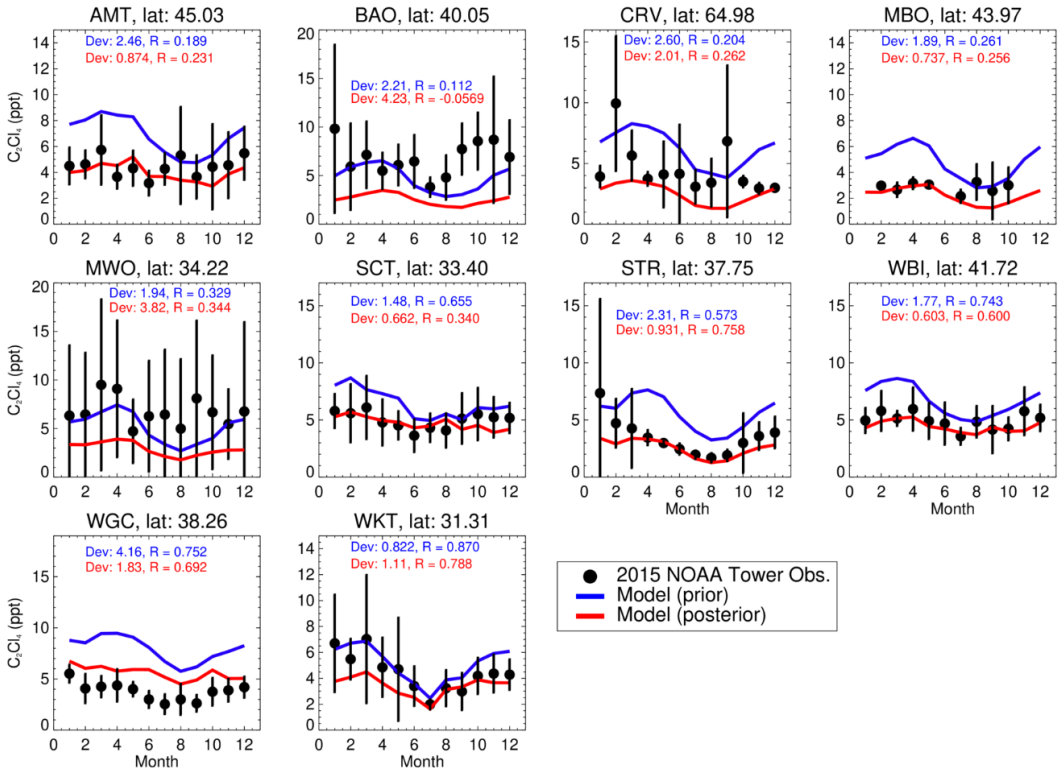

Figure 4.10. As **Figure 4.9** but for C_2Cl_4. Note that the model results here did not include the C_2Cl_4 + Cl sink.

For C_2Cl_4, a similar analysis was performed and reveals a more varied picture (**Figure 4.10**). As prior emissions generally overestimate C_2Cl_4, this leads to large improvements in the posterior output at most sites. However, at some sites the modelled-observed C_2Cl_4 deviations are larger for the posterior compared to the prior (e.g., BAO and MWO). As for CH_2Cl_2, this is largely due to the close proximity of substantial sources influencing observations that are likely not well captured by the model. However, at most sites, we note that our

posterior model output lies within the observed variability. We further note that as with all comparisons of relatively coarse global-scale models with point-based observations, sampling errors in the model can affect such comparisons.

For Europe, beyond the NOAA and AGAGE observational data used in the inversion, there are few long-term surface measurements of CH_2Cl_2 and C_2Cl_4. However, a recent network addition is the establishment of a CH_2Cl_2 record at the Taunus Observatory (50.22°N, 8.44°E, at 825 m) in central Germany [Schuck et al., 2018]. Taunus reports CH_2Cl_2 measurements using the AGAGE SIO-14 scale (here converted to the NOAA scale). **Figure 4.11(a)** compares modelled and observed monthly mean CH_2Cl_2 at the Taunus site between 2014 and 2017. The agreement between the model (with posterior emissions) and observations is reasonable, with the shape of the seasonal cycle generally well captured. The model does overestimate CH_2Cl_2 at this particular site during some periods. Since sampling errors in the model could cause this overestimation, **Figure 4.11** also investigates model variability by including the standard deviation between the eight neighbouring model grid cells, using Equation 4.04. At this particular site, variability introduced from neighbouring model grid cells is reasonably small and does not fully rationalise the small discrepancies between the model and observations, including apparent slight offsets in the seasonal cycle. However, we note that at other NH sites—including from the USA-based tall tower network—the CH_2Cl_2 seasonal cycle is very well captured (e.g., **Figures 4.S4**, **4.S6**, and **4.9**).

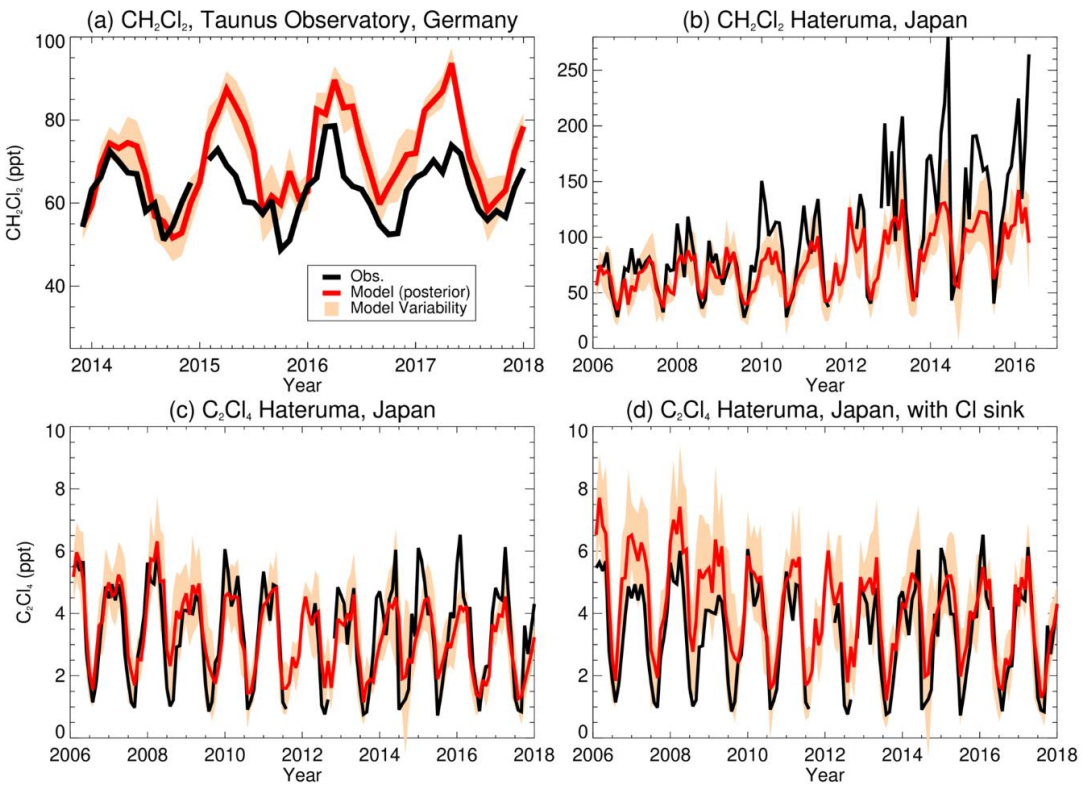

Figure 4.11. A comparison between modelled and observed monthly mean mixing ratios (ppt) of CH_2Cl_2 and C_2Cl_4 at independent measurement sites**.** (a) CH_2Cl_2 at the Taunus Observatory in central Germany [Schuck et al., 2018], (b) CH_2Cl_2 at Hateruma, Japan, (c) C_2Cl_4 at Hateruma (no C_2Cl_4 + Cl sink), and (d) C_2Cl_4 at Hateruma (including +Cl sink). The model output was generated using the posterior emissions from the inversion. In the case of CH_2Cl_2, results from the no ocean inversion scenario are shown (see main text). Model variability (light orange) was calculated from the standard deviation of the surrounding eight model grid cells (Equation 4.04). All observations here are calibrated to NOAA scales.

Also included in **Figure 4.11** are comparisons of modelled CH_2Cl_2 and C_2Cl_4 using our posterior emissions to baseline measurements obtained from the AGAGE-affiliated site in Hateruma, Japan (HAT, 24.1°N, 123.8°E, at 46.5 m). Hateruma is calibrated with the NIES-08 scale and for CH_2Cl_2 can be converted to the AGAGE SIO-14 scale by a factor of 1.066 ± 0.008. The conversion factor between the NIES-08 scale and AGAGE's NOAA-2003B scale for C_2Cl_4 is 0.994 ± 0.010. Given that the number of monitoring stations in Asia is limited and that

this is where the largest Cl-VSLS emissions are predicted to occur, these independent comparisons are particularly useful. For CH_2Cl_2, model-observation agreement is generally good, though in the most recent years of our study period, the model underestimates observed CH_2Cl_2 mixing ratios, particularly in winter. This wintertime disparity could represent a combination of uncaptured seasonality in CH_2Cl_2 emissions and underestimated model CH_2Cl_2 lifetime and is apparent even when considering the model sampling/mismatch issues noted above. For C_2Cl_4, comparisons to the Hateruma data are shown for the model with and without the Cl sink used to construct the posterior emissions. Both cases lead to adequate model-measurement agreement, though including the Cl sink provides far better agreement in the most recent years.

4.5 Summary and Conclusions

Combining long-term surface observations and a chemical transport model, we have performed a global-scale synthesis inversion to (a) constrain regional/global emissions of CH_2Cl_2 and C_2Cl_4, (b) investigate emission trends over the 2006 to 2017 period, and (c) produce a set of evaluated emission inventories for future global modelling studies. Our main findings are the following:

- For an inversion in which only industrial CH_2Cl_2 emissions are considered, we estimate that global CH_2Cl_2 emissions increased from 637 ± 37 Gg yr^{-1} in 2006 to 1,171 ± 45 Gg yr^{-1} in 2017, with reasonably good agreement between our results and those reported in the recent WMO Ozone Assessment with a simplified model and similar data as input [Engel et al., 2018]. This increase is largely attributed to an increase in Asian emissions, while relatively small European and North American emissions decrease over the same period. This geographical shift in the emission distribution is broadly consistent with studies that have highlighted the growing importance of major Asian economies as a CH_2Cl_2 source [e.g., Leedham Elvidge et al., 2015; Feng et al., 2019]. In 2017, we estimate Asian emissions accounted for 89% (1,045 ± 40 Gg

yr^{-1}) of total CH_2Cl_2 emissions, up from 68% (431 ± 32 Gg yr^{-1}) in 2006. CH_2Cl_2 emissions from Europe and North America combined represented 9% of the global total in 2017, down from 29% in 2006. Decreases in these regions may, in part, reflect recent concerns over the compound's toxicity in consumer products.

- For an inversion in which both oceanic and industrial CH_2Cl_2 sources are considered, we estimate global CH_2Cl_2 emissions of 1,166 ± 64 Gg yr^{-1} in 2017, that is, very similar to the no ocean case. However, including the ocean source reduces the estimate of 2017 Asian emissions from 1,045 ± 40 to 886 ± 53 Gg yr^{-1} (a reduction of 15%). A large portion of this difference is explained by the inversion placing a significant emission of CH_2Cl_2 in the tropical Northern Ocean (0-30°N latitude). Averaged over our study period, oceanic CH_2Cl_2 emissions from this latitude band are approximately 123 (±45) Gg yr^{-1}, which is comparable to 88 (±29) Gg yr^{-1} for the same band estimated from a previous inversion study using primarily the same observational data as input but for an earlier time period [Xiao, 2008]. The inclusion of an ocean source does not affect our overarching conclusions on a shift in global CH_2Cl_2 emissions, with an increasing contribution from Asia, and a declining contribution from Europe and North America since the mid-2000s. Additionally, comparisons of atmospheric measurements between this and the “no ocean” inversion lead to no evidence for (or against) an ocean CH_2Cl_2 source.

- Unlike CH_2Cl_2, which has increased in the atmosphere since the early/mid-2000s, C_2Cl_4 has been in long-term decline. Our results indicate a decrease in global emissions from 141 ± 14 Gg yr^{-1} in 2007 to 106 ± 12 Gg yr^{-1} in 2017. These values were obtained from an inversion setup in which the C_2Cl_4 + Cl sink reaction was not included and agree well with estimates produced for the recent WMO Ozone Assessment using a simplified model and similar input data [Engel et al., 2018]. Inclusion of the C_2Cl_4 + Cl reaction, shown to be an important, albeit uncertain, sink of C_2Cl_4 in recent modelling studies [Hossaini et al.,

2019], increases the estimated global C_2Cl_4 emissions to 216 ± 14 Gg yr^{-1} in 2007 and 162 ± 12 Gg yr^{-1} in 2017, that is, around 50% larger. Further work to constrain tropospheric Cl atom concentrations may help to constrain top-down emission estimates for C_2Cl_4. Inclusion of the Cl sink generally leads to slight improvements compared to the default inversion when comparing against atmospheric measurements.

- Using observational data not included in the inversion, the performance of the posterior CH_2Cl_2 and C_2Cl_4 emissions was evaluated. For both compounds, observed surface trends between the mid-2000s and 2017 are well reproduced: ~3 ppt CH_2Cl_2 yr^{-1} and ~−0.1 ppt C_2Cl_4 yr^{-1} at NH sites. Independent measurements from the 2014 CAST/CONTRAST/ATTREX aircraft missions over the tropical West Pacific are also reproduced very well throughout the vertical extent of the troposphere for CH_2Cl_2, but do not allow any constraint on the magnitude of an oceanic source. These independent data are reproduced relatively less successfully for C_2Cl_4. Similarly, the posterior emissions show improvement over the prior at numerous USA-based NOAA tall tower sites in 2015. Comparisons for other surface sites were performed, including Taunus Observatory (Germany) and Hateruma (Japan), and reveal generally good agreement. Our emissions are thus suitable for inclusion in global atmospheric modelling studies.

In conclusion, emissions of CH_2Cl_2—a substance known to cause ozone depletion—have increased significantly since the mid-2000s. Given that Asian emissions lead to a relatively large CH_2Cl_2 ODP compared to emissions from other regions [Claxton et al., 2019], its regional and global abundance should continue to be monitored. As emissions from the Asian continent are by far the largest, a denser set of measurements, from the surface to the tropopause, would be beneficial to distinguish emissions from different subregions and ultimately constrain the troposphere-to-stratosphere input of chlorine from VSLS. A consideration of how emissions are likely to change in coming decades would also help constrain the influence of CH_2Cl_2 on the timescale of stratospheric ozone recovery. Future work should also focus on elucidating the

mechanism by which CH_2Cl_2 is recycled through the ocean and quantifying the magnitude and distribution of biogenic sources.

Acknowledgments

This work was supported by RH's NERC Independent Research Fellowship (NE/N014375/1), the NERC ISHOC project (NE/R004927/1), and the NERC SISLAC project (NE/R001782/1). MPC is supported by a Wolfson Merit Award. We thank Dr. Wuhu Feng for his work developing the TOMCAT/SLIMCAT model. We thank Dr. Prabir Patra and Dr. Bin Xiang for providing the HCFC-22 emission distribution. LJC thanks NERC for funding the CAST and ship observations (NE/J00619X/1, NE/K004980/1, and NE/I028769/1). Data from the NOAA monitoring network are available from https://www.esrl.noaa.gov/gmd/. We thank C. Siso for technical assistance in making the NOAA measurements and Dr B. Miller and Dr A. Andrews for assistance in providing results from NOAA's tall tower network. Gosan measurements were supported by Basic Science Research Program through the National Research Foundation of Korea (NRF) funded by the Ministry of Education (No. 2017R1D1A1B03034034). The operation of the AGAGE station at Ragged Point, Barbados, is supported by the National Aeronautics and Space Administration (NASA, USA; Grant NNX16AC98G to MIT and subaward 5710002970 to the University of Bristol) with additional support from the National Oceanic and Atmospheric Administration (NOAA, USA; contract RA133R15CN0008 to the University of Bristol). Observations at Hateruma were partly supported by the Ministry of the Environment of Japan. Data from the AGAGE monitoring network are available from https://agage.mit.edu/data/ and are supported by the NASA Upper Atmospheric Research Program in the United States with grants NNX16AC96G and NNX16AC97G to SIO and grant NNX16AC98G to MIT. ATTREX and CONTRAST measurements were supported by National Science Foundation Grant AGS1261689 and NASA Grant NNX13AH20G. The model data can be accessed via the Lancaster University data repository at DOI: 10.17635/lancaster/researchdata/353. The Supporting Information to this article consists of seven figures and three tables.

4.6 Supporting Information

This supporting information summarises bottom-up estimates of the two Cl-VSLS studied in **Table 4.S1**. **Table 4.S2** summarises inversion results for a CH_2Cl_2 inversion ran with ocean regions included. **Table 4.S3** summarises inversion results for a C_2Cl_4 inversion with a theorised Cl sink included. An example, for CH_2Cl_2, of the emissions distribution used in the study is given in **Figure 4.S1**. **Figure 4.S2** shows the emissions time series for the aforementioned CH_2Cl_2 including ocean inversion. The sensitivity testing with regards to prior emissions error for this inversion is then shown in **Figure 4.S3**. **Figures 4.S4-4.S5** show a single year comparison over the NOAA observational sites that were used in the inversion process, between the model output based on the prior emissions, and the output based on the resulting optimised posterior emissions, for CH_2Cl_2 and C_2Cl_4 respectively. **Figures 4.S6-4.S7** show the same comparison, but over the AGAGE sites used in the inversion instead.

Table 4.S1. Bottom-up estimates of industrial CH_2Cl_2 and C_2Cl_4 emissions (Gg yr^{-1}) in 2007 and 2016 adapted from Nolan Sherry Associates, NSA analysis (see **Section 4.3.4**).

Region	CH_2Cl_2 (Gg yr^{-1})		C_2Cl_4 (Gg yr^{-1})	
	2007	**2016**	**2007**	**2016**
Europe	140	50	70	48
North America	58	55	35	24
Asia (Temperate)	453	621	52	93.3
Asia (Tropical)	55	50	14	15

Table 4.S2. As **Table 4.3** but based on a CH_2Cl_2 inversion that includes ocean regions. NO = Northern Ocean, SO = Southern Ocean.

Region		2006		2017	
	Prior Emissions	**Posterior Emissions**	**Error Reduction**	**Posterior Emissions**	**Error Reduction**
Europe	50.0	140.6 ± 10.5	79.1%	109.6 ± 12.5	75.1%
Africa	9.18	1.72 ± 8.62	6.0%	9.71 ± 8.95	2.5%
Australia	4.85	5.34 ± 1.99	59.0%	3.64 ± 2.50	48.4%
Boreal Asia	6.81	-3.94 ± 6.10	10.4%	-5.95 ± 6.52	4.3%
Boreal NA	1.11	0.73 ± 1.09	2.3%	0.82 ± 1.11	0.8%
Temperate Asia	621.0	182.9 ± 26.6	95.7%	626.3 ± 36.1	94.2%
Temperate LA	8.43	-10.9 ± 6.9	18.4%	-3.83 ± 7.69	8.8%
Temperate NA	55.0	67.8 ± 4.9	91.0%	32.8 ± 5.9	89.2%
Tropical Asia	50.0	163.7 ± 30.9	38.1%	259.8 ± 38.7	22.6%
Tropical LA	8.67	3.91 ± 8.47	2.4%	7.40 ± 8.53	1.6%
Extratropical NO	24.0	-54.0 ± 8.5	64.3%	-58.3 ± 11.5	52.1%
Extratropical SO	71.9	5.27 ± 2.80	96.1%	6.17 ± 4.09	94.3%
Tropical NO	50.3	71.6 ± 15.6	69.0%	177.5 ± 23.2	53.8%
Tropical SO	50.3	39.4 ± 6.8	86.4%	0.08 ± 9.99	80.1%
Combined Asia	**671.0**	**346.6 ± 40.8**	-	**886.1 ± 52.9**	**-**
Global Total	**1011.5**	**614.2 ± 49.0**	-	**1165.8 ± 63.5**	**-**

Table 4.S3. As **Table 4.4** but based on an inversion that included the C_2Cl_4 + Cl sink reaction.

Region		2007		2017	
	Prior Emissions	**Posterior Emissions**	**Error Reduction**	**Posterior Emissions**	**Error Reduction**
Europe	48.0	89.3 ± 4.6	90.4%	46.4 ± 2.7	94.3%
Africa	2.30	4.93 ± 2.22	3.6%	5.36 ± 2.13	7.5%
Australia	0.62	1.04 ± 0.33	46.3%	0.57 ± 0.26	57.6%
Boreal Asia	1.80	-2.66 ± 1.67	6.9%	-2.33 ± 1.61	10.5%
Boreal NA	0.50	-0.09 ± 0.48	5.3%	0.49 ± 0.47	6.1%
Temperate Asia	93.3	27.6 ± 9.2	90.2%	29.5 ± 7.7	91.8%
Temperate LA	1.06	2.64 ± 1.04	2..2%	3.05 ± 0.99	7.0%
Temperate NA	24.0	46.7 ± 2.8	88.3%	34.4 ± 1.9	92.1%
Tropical Asia	15.0	46.7 ± 8.5	42.1%	42.6 ± 8.1	44.7%
Tropical LA	1.58	2.90 ± 1.55	1.9%	2.49 ± 1.53	3.4%
Extratropical NO	3.51	-14.7 ± 2.1	41.4%	-10.2 ± 1.7	52.6%
Extratropical SO	5.85	4.87 ± 0.82	86.0%	3.22 ± 0.71	87.8%
Tropical NO	3.51	-0.51 ± 1.52	56.7%	1.36 ± 1.40	60.2%
Tropical SO	5.85	7.44 ± 1.12	80.9%	5.47 ± 1.10	81.2%
Combined Asia	**108.3**	**74.3 ± 12.5**	**-**	**72.1 ± 11.2**	**-**
Global Total	**206.5**	**216.3 ± 14.3**	**-**	**162.5 ± 12.4**	**-**

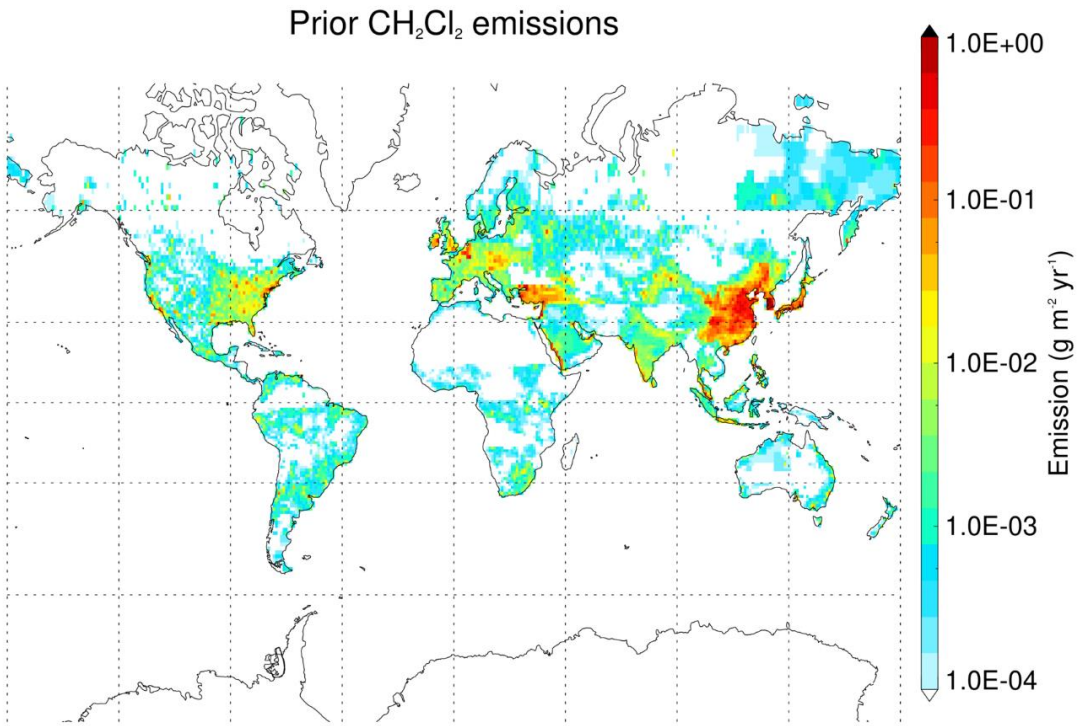

Figure 4.S1. Prior emission distribution of CH_2Cl_2 (g m^{-2} yr^{-1}) used in the inversion. The distribution is based on present day HCFC-22 emissions [Xiang et al., 2014]. Note the logarithmic scale.

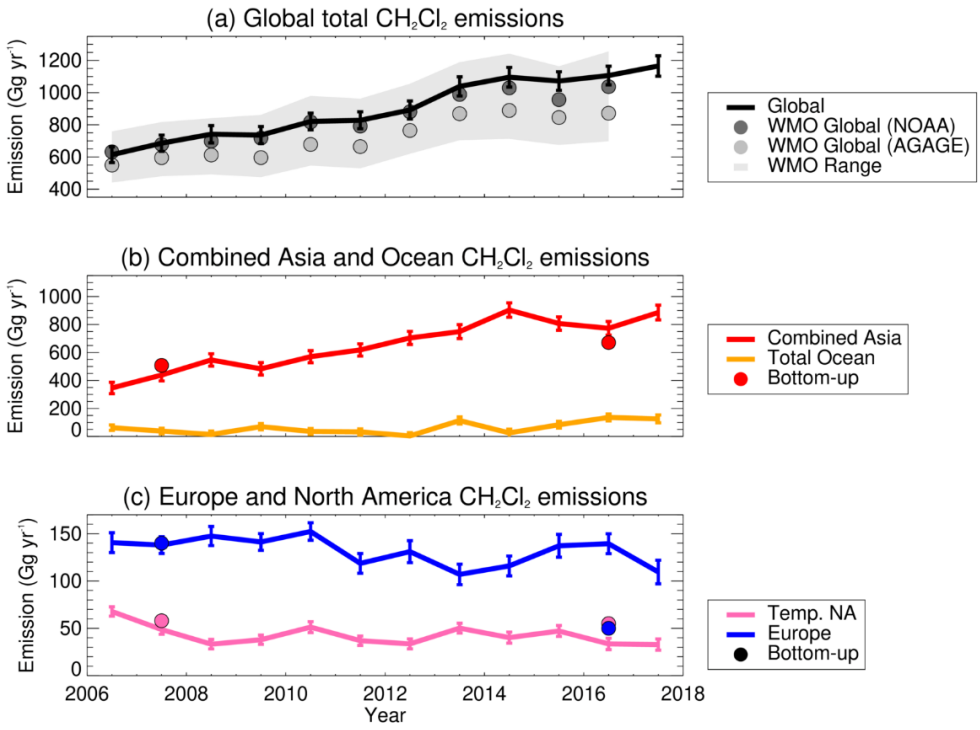

Figure 4.S2. Global and regional emissions for CH_2Cl_2, as **Figure 4.2**, but including the four ocean regions in the inversion. In **(b)** the total ocean emissions are included.

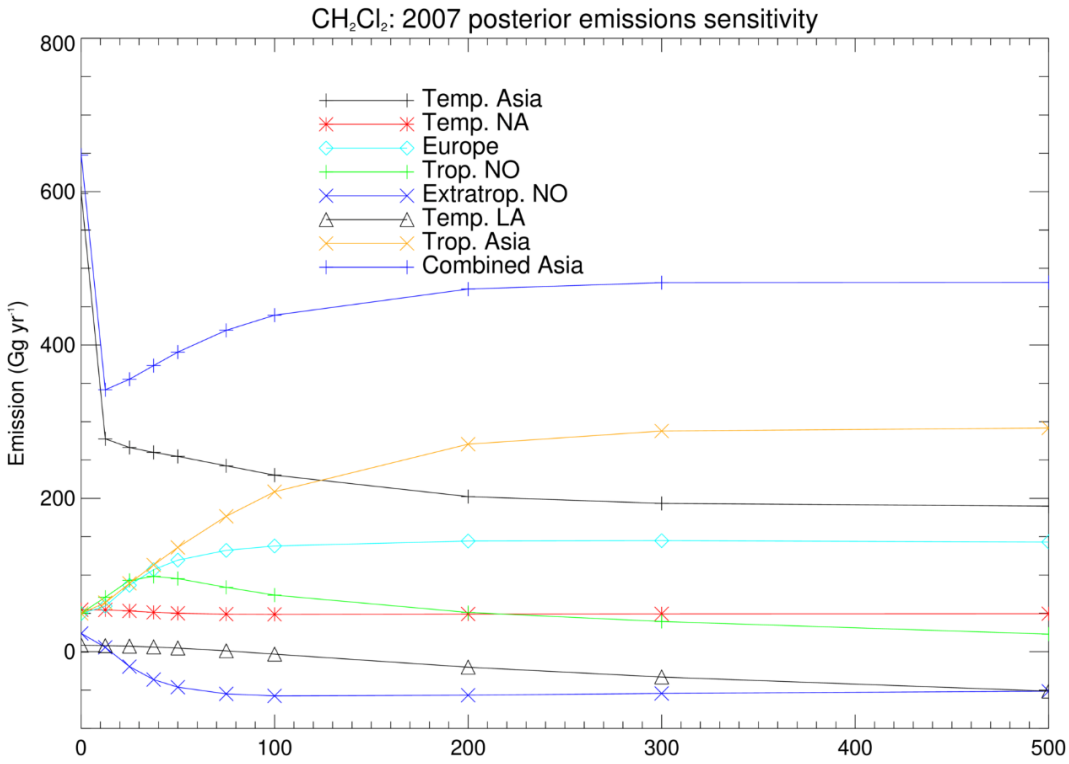

Figure 4.S3. Sensitivity testing of posterior emissions with respect to varying prior emission error for CH_2Cl_2 in 2007, as **Figure 4.4**, but for the "with-ocean" inversion scenario**.**

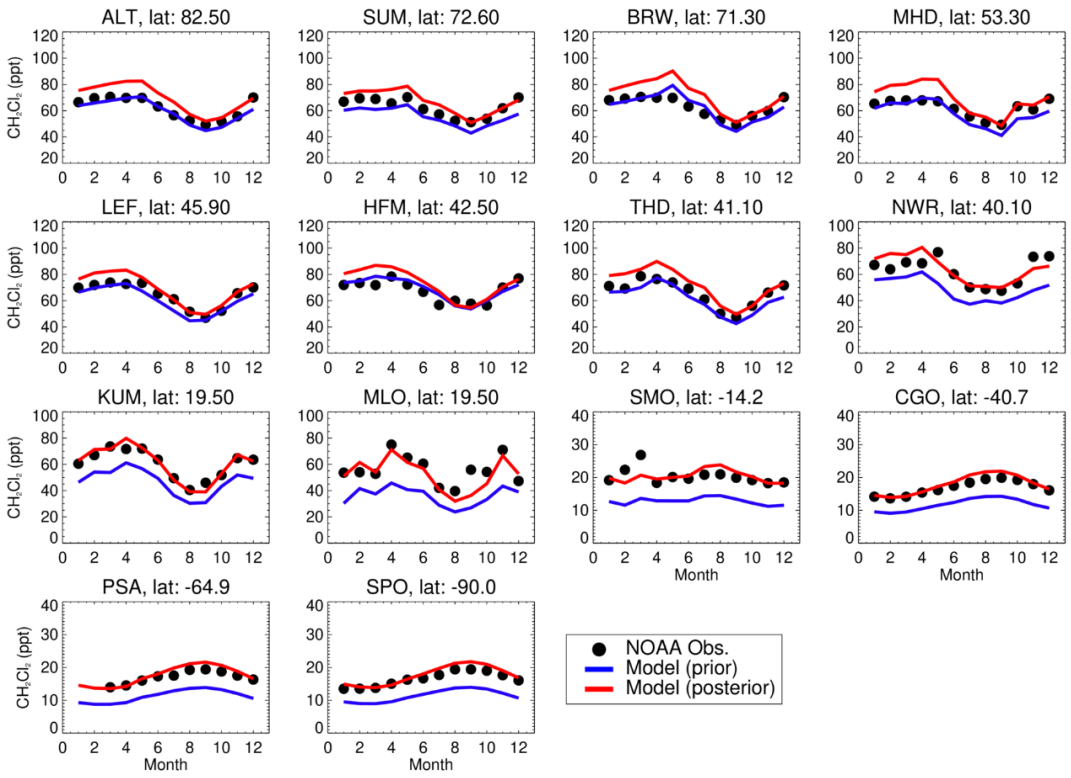

Figure 4.S4. Comparison of modelled monthly mean CH_2Cl_2 mixing ratio (ppt) and observed CH_2Cl_2 using both the prior and posterior emissions. The observational data are from the NOAA global network (see site summary in **Table 4.1**) and the comparisons are for the year 2016.

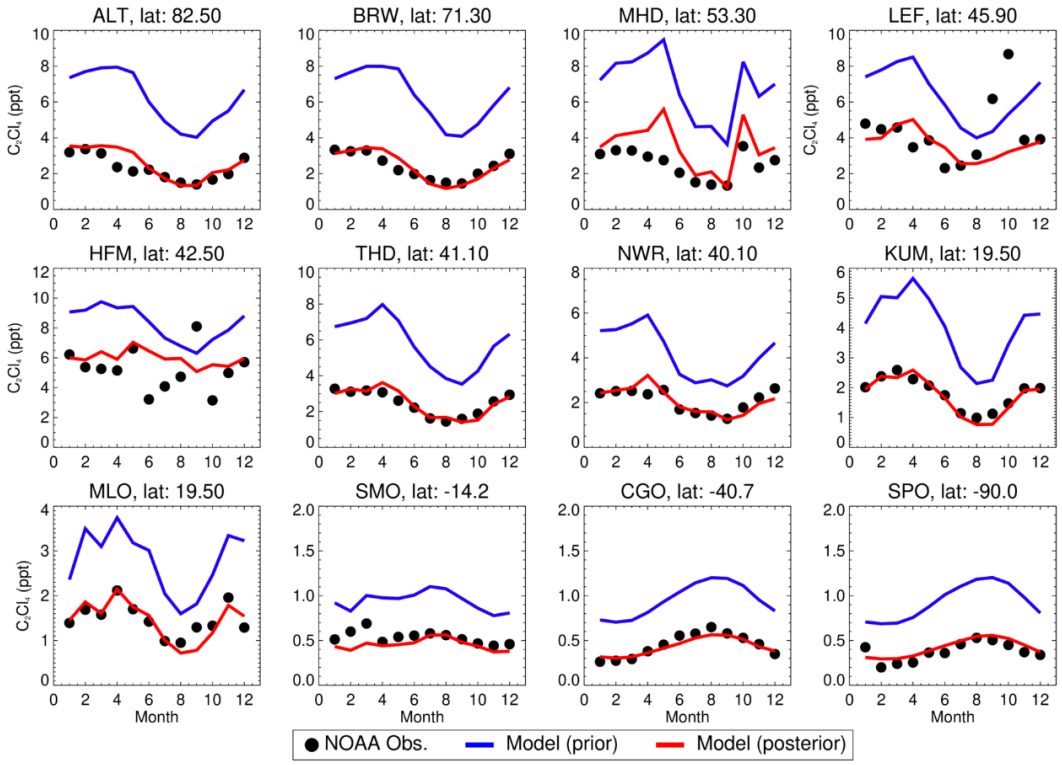

Figure 4.S5. As **Figure 4.S4** but for C_2Cl_4**.** Note, the model results here did not include the C_2Cl_4 + Cl sink.

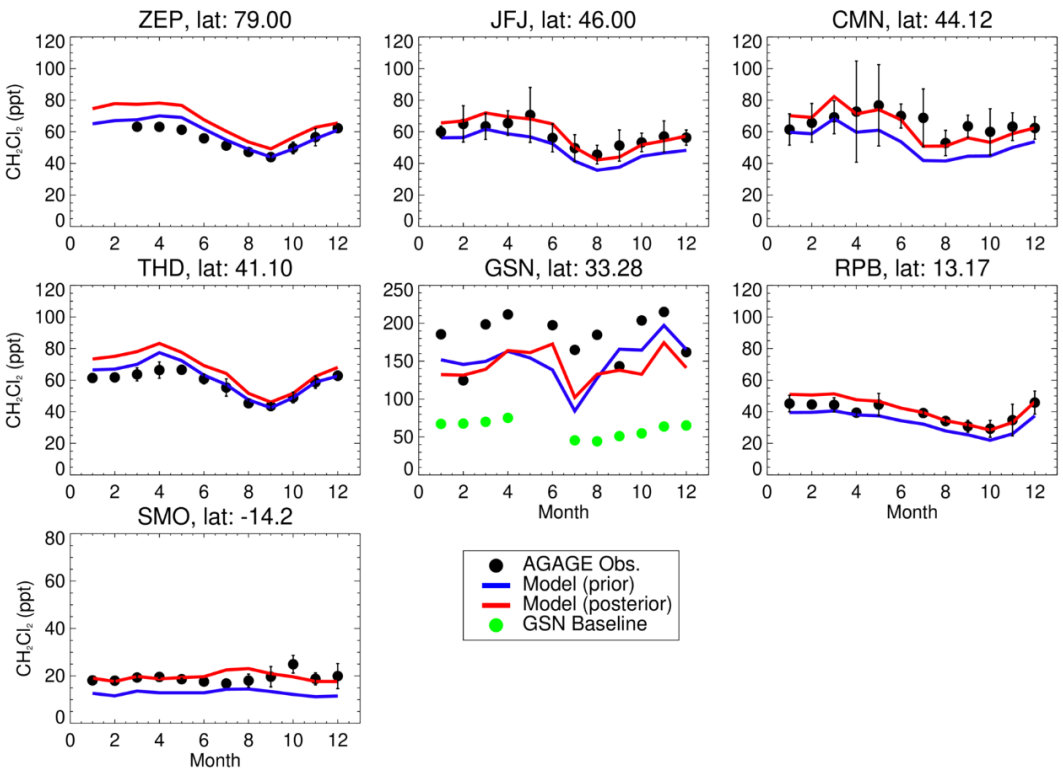

Figure 4.S6. Comparison of observed and modelled monthly mean CH_2Cl_2 mixing ratio (ppt) using both the prior and posterior emissions. The observational data are from the AGAGE global network (see site summary in **Table 4.1**) and vertical bars denote ±1 SD. Comparisons are for the year 2016 for all sites, with exception of GSN (2015). All monthly mean observations are calculated using "raw" pollution events included; for GSN, baseline observations (filtered for pollution events) are also added, in green.

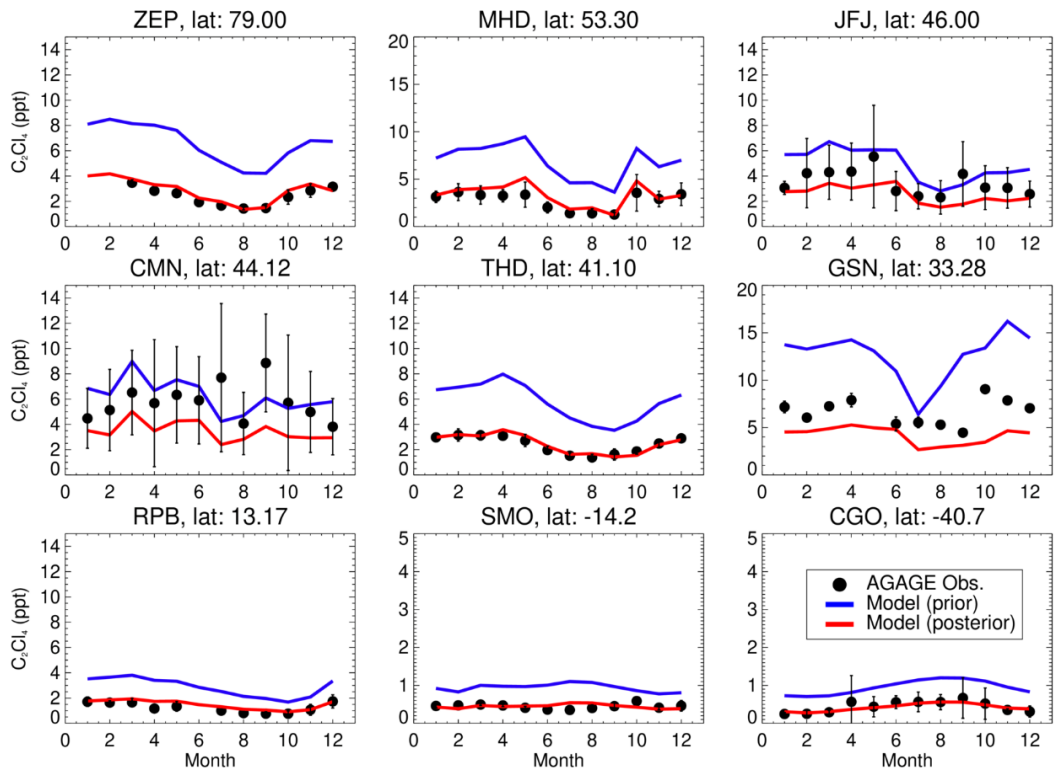

Figure 4.S7. Same as **Figure 4.S6** except for C_2Cl_4.

Chapter 5

Quantifying the Time-Varying Stratospheric Chlorine Injection and Ozone Impact due to Very Short-Lived Substances

Tom Claxton[1], Ryan Hossaini[1], Ewa M. Bednarz[1], Martyn P. Chipperfield[2,3]

[1]Lancaster Environment Centre, Lancaster University, Lancaster, UK
[2]School of Earth and Environment, University of Leeds, Leeds, UK
[3]National Centre for Earth Observation, University of Leeds, Leeds, UK

The current list of authors and their contributions are listed below:

Tom Claxton: Performed model simulations, processed and analysed the data, and wrote the manuscript. **Ryan Hossaini:** Supervised interpretation of results from model simulations, and compilation of the manuscript. **Ewa M. Bednarz:** Assisted with analysis and interpreted results. **Martyn P. Chipperfield:** Supported TOMCAT/SLIMCAT model simulations.

Abstract

Chlorinated Very Short-Lived Substances (Cl-VSLS), such as dichloromethane (CH_2Cl_2) and chloroform ($CHCl_3$), have increasing influence on the stratospheric chlorine budget, and hence possibly ozone depletion. In this study, a gridded 12-year (2006-2017) estimate of global $CHCl_3$ emissions was

aggregated from the literature. Global $CHCl_3$ emissions total 416 ± 120 Gg yr^{-1} in 2017 (of which 73% come from natural emissions), increasing at a rate of 6 Gg yr^{-1} between 2006 and 2017, primarily due to increases in East Asian emissions. Alongside our previously calculated emissions of CH_2Cl_2 and perchloroethylene (C_2Cl_4), emissions of these three Cl-VSLS were implemented into a three-dimensional chemical transport model (TOMCAT/SLIMCAT) to determine surface concentration trends and the stratospheric chlorine injection over an 11-year (2007-2017) period. We find Cl-VSLS contribute 96.9 ± 8.3 ppt Cl to the stratosphere via source gas injection, and through key product gases Cl_y and phosgene, an additional 35.2 ± 3.3 ppt Cl, in 2017. Total stratospheric chlorine from Cl-VSLS in 2017 is estimated at 132.1 ± 8.9 ppt Cl (43% larger than in 2007). The time-varying stratospheric chlorine injections were entered as tropopause boundary conditions in one of two SLIMCAT model runs designed to investigate the impact of Cl-VSLS on ozone, the other assuming zero Cl-VSLS. Comparing the two, we find 2017 annual mean lower stratosphere ozone changes due to Cl-VSLS of -0.56% (globally), with larger changes up to a maximum of about -18% in the Antarctic lower stratosphere during spring. In terms of column changes, 2017 mean column ozone drops by 1.23 DU (-0.4%) globally, and by 3.44 DU over Antarctica. These impacts and their significance in terms of regional mortality are discussed.

5.1 Introduction

Chlorinated Very Short-Lived Substances (Cl-VSLS) are a group of chlorine-containing compounds with tropospheric lifetimes of less than approximately 6 months [e.g. Ko et al., 2003]. Due to the phasing out of CFCs (chlorofluorocarbons) and other long-lived Ozone-Depleting Substances (ODSs) under the Montreal Protocol and its amendments, uncontrolled Cl-VSLS are of increasing policy interest as they provide a growing source of anthropogenic chlorine to the atmosphere [e.g. Claxton et al., 2019; Hossaini et al., 2017; Laube et al., 2008]. Between 2012 and 2016, Cl-VSLS have been estimated to account for around 3.0-3.5% of the total chlorine injected into the stratosphere [Engel et al., 2018; Hossaini et al., 2015]. In absolute terms,

stratospheric injections of Cl-VSLS have increased from 26-77 ppt Cl to 75-160 ppt Cl between 2010 and 2016 [Engel et al., 2018; Montzka, Reimann, et al., 2011]. This increase is primarily due to dichloromethane (CH_2Cl_2) emissions, the most abundant Cl-VSLS, rapidly rising over recent years [Claxton et al., 2020; Hossaini et al., 2017; Leedham Elvidge et al., 2015]. CH_2Cl_2 is commonly used as a versatile industrial solvent and roughly 90% of total emissions are estimated to be anthropogenic [Claxton et al., 2020; Montzka, Reimann, et al., 2011]. The bulk of these emissions have been estimated to occur in Asia, with modelling studies suggesting a contribution of 89% of the global total emission in 2017 [Claxton et al., 2020].

In addition to CH_2Cl_2, chloroform ($CHCl_3$), perchloroethylene (C_2Cl_4), and ethylene dichloride ($C_2H_4Cl_2$) are three other key Cl-VSLS that contribute to the atmospheric chlorine budget [Engel et al., 2018]. Whilst $CHCl_3$ has significant natural sources, such as from oceans and soils [Khalil et al., 1999; McCulloch, 2003], there is an increasing anthropogenic source [Fang et al., 2019]. As well as emissive applications as solvents, $CHCl_3$ and CH_2Cl_2 are involved as chemical feedstocks in HCFC-22 and HFC-32 production, respectively [Feng et al., 2019; McCulloch et al., 1999]. To date, there has only been one modelling study that has quantified the time-varying stratospheric injection of chlorine due to VSLS. Hossaini et al. [2019] found that total stratospheric chlorine from the above four VSLS and their products increased from 69 ± 14 ppt Cl in 2000 to 111 ± 22 ppt Cl in 2017. However, that study used a highly simplified treatment of Cl-VSLS at the model surface, prescribing zonal mean surface mixing ratio boundary conditions (based on surface monitoring network data), as opposed to considering spatially varying emission fluxes (e.g. as diagnosed by Claxton et al. [2020]). It is unlikely that this simple approach is able to capture the co-location of surface emission ‘hot spots’ with areas of rapid vertical uplift, such as convectively active regions.

Claxton et al. [2019] assessed the ozone depletion potential (ODP) of the four aforementioned Cl-VSLS, using a 3D chemistry transport model (CTM). The results showed that ODPs of Cl-VSLS experience regional variation depending on the location of emission, with emissions of Cl-VSLS from Southeast Asia having the greatest ODP, owing to increased vertical transport over the region

[e.g. Aschmann et al., 2011; Gettelman et al., 2009; Liang et al., 2014]. For the three Cl-VSLS, $CHCl_3$ was found to have the largest ODP range of 0.0143-0.0264, CH_2Cl_2 had a range of 0.0097-0.0208, C_2Cl_4 had a range of 0.0057-0.0198, and $C_2H_4Cl_2$ had a range of 0.0029-0.0119. These ODP ranges reflect variability due to both the season and the geographical region of emission, with the latter being more significant [Claxton et al., 2019]. There have yet to be any comprehensive end-to-end studies that link time-varying surface Cl-VSLS emissions to time-varying impacts on ozone. However, Hossaini et al. [2017] explored the impact on stratospheric ozone from possible future changes in surface CH_2Cl_2 in a series of model sensitivity studies. The study found that compared with a scenario with no CH_2Cl_2, holding CH_2Cl_2 concentrations at 2016 levels into the future leads to an increase in the time it takes for Antarctic ozone levels to recover to 1980 levels by 5 years. Increasing CH_2Cl_2 emissions [Claxton et al., 2020; Feng et al., 2019] are likely to extend this period of time further, potentially by several decades if large and sustained emission growth continues throughout the century [Hossaini et al., 2017].

In our previous study, a set of multi-year gridded surface emissions for CH_2Cl_2 (2006-2017) and C_2Cl_4 (2007-2017) were optimised using observations from the NOAA and AGAGE global monitoring networks and a 3D CTM, through 'synthesis inversion' [Claxton et al., 2020]. With these emission fields, calculating injections of Cl-VSLS into the stratosphere is more effective than the simpler approach adopted by Hossaini et al. [2019]. In this study, we first describe and evaluate a simple gridded set of $CHCl_3$ emissions, extending Claxton et al. [2020], though using a more empirical approach. These emissions are then implemented into the TOMCAT/SLIMCAT CTM, in conjunction with the CH_2Cl_2 and C_2Cl_4 emissions from Claxton et al. [2020], to perform an end-to-end study quantifying (a) the time-varying contribution of Cl-VSLS and their products to stratosphere chlorine, and (b) the impact of changes in Cl-VSLS emissions on stratospheric ozone. The paper is structured as follows. **Section 5.2** discusses the CTM set-up, including briefly the assumptions made regarding product gases. **Section 5.3** describes and evaluates a set of global $CHCl_3$ emissions. Our main results are presented in **Section 5.4**, where first we consider trends in the surface concentration of CH_2Cl_2, C_2Cl_4 and $CHCl_3$ from

our forward model runs, before calculating time-varying stratospheric chlorine injections. The sensitivity of total chlorine from Cl-VSLS that reaches the stratosphere to a range of factors (e.g. oxidant concentrations) are discussed and quantified. We then quantify the impact of this chlorine on stratospheric ozone, comparing model scenarios with and without Cl-VSLS. Conclusions and recommendations of further work are given in **Section 5.5**.

5.2 TOMCAT/SLIMCAT 3D CTM

We have used the TOMCAT 3D CTM to (1) develop and test a set of $CHCl_3$ emissions and (2) quantify the time-varying input of chlorine from CH_2Cl_2, C_2Cl_4, and $CHCl_3$, along with their degradation products, into the stratosphere. The model configuration has been extensively used in many VSLS focused studied [e.g. Hossaini et al., 2010, 2019], and the tropospheric configuration used here is identical to that of Claxton et al. [2020] (**Section 4.2**). Briefly, the model uses offline meteorology, including 6-hourly wind, temperature and humidity fields, taken from the European Centre for Medium-Range Weather Forecasts (ECMWF) ERA-Interim reanalyses [Dee et al., 2011]. The model contains treatments of turbulent boundary layer mixing and convective transport, parameterised based on Holtslag and Boville [1993] and Tiedtke [1989], respectively. The model was run at a horizontal resolution of 2.8° x 2.8°, with 60 vertical levels spanning from 7 m to 67 km.

For the purpose of developing and testing the validity of $CHCl_3$ emissions estimates (see **Section 5.3**), only a simple $CHCl_3$ photochemical loss scheme was used and product gas chemistry was not considered. The reaction rate constant for the $CHCl_3$ + OH sink was taken from the Jet Propulsion Laboratory (JPL) report [Burkholder et al., 2015]. An offline monthly-varying tropospheric OH field is implemented in this TOMCAT configuration [Huijnen et al., 2010; Spivakovsky et al., 2000], which has been previously used and evaluated in a TransCom study of CH_4 [Patra et al., 2011].

For the purpose of quantifying stratospheric chlorine injections, an extended version of the above TOMCAT model configuration was used that considers both source gas (CH_2Cl_2, C_2Cl_4, and $CHCl_3$) surface emissions/chemistry and

product gas chemistry [e.g. Claxton et al., 2019]. The two product gases considered are phosgene ($COCl_2$) and a generic inorganic chlorine (Cl_y) tracer. In practice, the latter is representative of HCl as this is the dominant tropospheric inorganic chlorine reservoir [Wang et al., 2019]. All three Cl-VSLS studied are eventually degraded into either $COCl_2$ or HCl; however, the relative proportions of the two products are different for each source gas. CH_2Cl_2 degradation follows a relationship discussed in Hossaini et al. [2019]. For each CH_2Cl_2 molecule oxidised, the amount of $COCl_2$ produced is related to the competing reactions of the initial $CHCl_2O_2$ intermediate. This amount is roughly 0.05-0.1 over industrial regions, and >0.3 over the oceans, with the amount of Cl_y produced equal to 2 – (2Y), where Y is the $COCl_2$ proportion. For $CHCl_3$ oxidation the ratio is simply 1 $COCl_2$: 1 Cl_y [Kindler et al., 1995], and for C_2Cl_4 oxidation the ratio is 0.47 $COCl_2$: 3.06 Cl_y [Tuazon et al., 1988]. Further details of the chemistry scheme are given in the Supporting Information of Claxton et al. [2019] (**Section 3.6**).

The eventual photolysis of $COCl_2$ into Cl_y is considered and a washout lifetime of 58 days in the troposphere is assumed for $COCl_2$ [Kindler et al., 1995]. For Cl_y, there are two different modelled estimates of its tropospheric lifetime in recent literature: 5 days based on Sherwen et al. [2016], and 37 hours based on Wang et al. [2019]. Our forward runs to quantify time-varying stratospheric chlorine injections from VSLS and their products assumed the 5-day lifetime for Cl_y as default, and the 37 hours lifetime was considered in a further sensitivity experiment. An additional sensitivity test was performed to investigate the inclusion of a C_2Cl_4 + Cl sink reaction (in addition to the main C_2Cl_4 + OH sink). Claxton et al. [2020] previously calculated emissions of C_2Cl_4 with and without this sink (see ensuing discussion), assuming a global tropospheric Cl concentration of 1.3 x 10^3 atoms cm^{-3} [Hossaini, Chipperfield, et al., 2016]. Although, in practice the distribution of Cl is very likely to be non-uniform. For the forward run in this study, this Cl concentration was again assumed, therefore propagating the C_2Cl_4 + Cl sink scenario from Claxton et al. [2020]. A final sensitivity test was performed to determine the sensitivity of Cl-VSLS injection to model OH concentration. Global mean tropospheric OH

concentrations can vary by as much as ± 20%, depending on the model [Zhao et al., 2019].

In addition to the TOMCAT model configuration described above, which was used the determine the tropospheric chemistry and transport of Cl-VSLS and their products, the SLIMCAT model configuration was used to investigate the stratospheric impact of Cl-VSLS on ozone. SLIMCAT has been extensively used for assessments of stratospheric composition, including recent studies calculating long-term ozone trends [e.g. Chipperfield et al., 2018]. The base resolution is alike to TOMCAT, with a 2.8° x 2.8° horizontal resolution, but with 32 vertical levels, up to an altitude of 65 km. The model includes a comprehensive treatment of stratospheric processes, with an extensive series of reactions involving ozone creation and destruction, including heterogeneous reactions on aerosols and polar stratospheric clouds relevant for polar ozone loss. Two SLIMCAT experiments were performed. One included a prescribed (at the tropopause) time-varying contribution of Cl-VSLS to stratospheric chlorine, calculated by the forward TOMCAT experiments, and one excluded this 'additional' chlorine. In both experiments, the model contained time-varying treatments of all other major sources of chlorine, such as long-lived anthropogenic (e.g. CFCs, HCFCs) and natural (e.g. CH_3Cl) chlorocarbons, as well as major long-lived bromocarbons (e.g. CH_3Br, halons) and other relevant source gases (e.g. CH_4, N_2O). SLIMCAT simulations were performed over the period 2007 to 2017. The model was "spun up" over sixteen years prior to the start year of the study.

5.3 Description and Evaluation of $CHCl_3$ Emissions (2006-2017)

5.3.1 Background

Unlike CH_2Cl_2 and C_2Cl_4, whose global emissions were recently quantified by Claxton et al. [2020], chloroform ($CHCl_3$) has significant natural sources. Soil and ocean emissions, from biological activity, together represent between 50-90% of total $CHCl_3$ emissions [Khalil et al., 1999; McCulloch, 2003; Trudinger et al., 2004]. Throughout this century, until about 2011, global anthropogenic emissions of $CHCl_3$ have been fairly constant, estimated at 90 Gg yr^{-1}

[Carpenter et al., 2014; Worton et al., 2006]. However, recent increases in Asian emissions have been inferred based on inverse modelling from two East Asian measurement sites [Fang et al., 2019], rising from on average 46.2 ± 2.3 Gg yr^{-1} over 2007-2010 to 95.2 ± 9.1 Gg yr^{-1} in 2016. For other industrialised regions of the world, e.g. Europe and North America, a similar increase has not been found [Fang et al., 2019].

'Synthesis inversion' is a technique that optimises model prior emission estimates by minimising differences between modelled and observed concentrations [e.g. Baker et al., 2006]. The efficacy of synthesis inversion generally improves with an increasing number of observations. For many long-lived gases, such as CH_4 and CO_2, synthesis inversion approaches are very effective due to a relative abundance of surface measurements [Law et al., 2008; McNorton et al., 2017; Wang et al., 2018]. However, for Cl-VSLS, there are limited long term observational data. The NOAA (National Oceanic and Atmospheric Administration) and AGAGE (Advanced Global Atmospheric Gas Exchange) networks provide the bulk of available Cl-VSLS measurement stations. For CH_2Cl_2 and C_2Cl_4, both networks were used to constrain emissions in our previous work [Claxton et al., 2020]. However, for $CHCl_3$, only AGAGE measurements exist.

Spatial coverage is another important aspect for synthesis inversion. Ideally, observations should cover as much of the planet as possible, and at a minimum, observations should exist in key emitting regions. For CH_2Cl_2 and C_2Cl_4, a synthesis inversion was feasible to this regard, as the NOAA and AGAGE networks (including some affiliate sites, e.g. Hateruma, Japan) cover the main industrial regions of East Asia, Europe, and North America [Claxton et al., 2020]. However, the AGAGE network does not individually have enough global coverage, with only 9 long term measurement sites, 4 of which are in Europe, to constrain the regional breakdown of global $CHCl_3$ emissions. As a result, a synthesis inversion approach for addressing $CHCl_3$ emissions was found to be too unconstrained in our exploratory work.

Creation of a gridded set of $CHCl_3$ emissions using a more empirical approach is somewhat simplified by the fact that surface concentrations of $CHCl_3$ were

relatively stable over the period 2002-2010 [Carpenter et al., 2014]. With ~70% of emissions natural, these can be assumed to be fixed from year to year, with the assumption that any land use and oceanic changes have not yielded significant deviations in emissions. For the remaining 30%, industry estimates and literature calculations can be compiled to form a “best guess” of anthropogenic emissions over the recent past. In order to test these emissions, they are run forward in a TOMCAT simulation and the model output is compared to the $CHCl_3$ observations that are available.

5.3.2 Natural $CHCl_3$ Emissions

The $CHCl_3$ emission field is compiled from various different source contributions: soil, ocean, and industrial. The soil and ocean emissions are base-derived from Khalil et al. [1999], which described the natural component of the Reactive Chlorine Emissions Inventory (RCEI) for several Cl-VSLS. The ocean emissions were produced from calculating the average sea-to-air flux from several ocean measurement campaigns, separated into 4 latitudinal bands: 30-90°N, 0-30°N, 0-30°S, and 30-90°S. The associated annual $CHCl_3$ ocean emissions were reported to be 20.2, 150.4, 150.4, and 40.4 Gg yr^{-1}, respectively (totalling 361.3 Gg yr^{-1}) [Khalil et al., 1999]. The RCEI also reported annual soil $CHCl_3$ emissions from the same four latitude bands: 67.3, 67.3, 56.1, and 11.2 Gg yr^{-1}, respectively (totalling 202.0 Gg yr^{-1}). Since these estimates published in the late 1990s, the size of these natural emissions has been called into question [Worton et al., 2006]. Through intercomparison between measurement sites, it was found that the $CHCl_3$ calibration scale used by Khalil et al. [1999] was a factor of 2 greater than used in observations from the AGAGE network [O’Doherty et al., 2001]. Worton et al. [2006] therefore roughly halved the $CHCl_3$ natural emissions from Khalil et al. [1999], providing a revised global ocean estimate of 180 Gg yr^{-1} and a global soil estimate of 100 Gg yr^{-1}.

Xiao [2008] updated and optimised the RCEI natural $CHCl_3$ emissions for the years 2000-2004 using a synthesis inversion, also considering the same four latitude bands (**Table 5.1**). The resulting global ocean emissions, totalling 167.9 ± 106.0 Gg yr^{-1}, were on average 54% smaller compared to Khalil et al. [1999].

The global soil emissions from Xiao [2008], totalling 135.7 ± 56.4 Gg yr^{-1}, were 33% smaller. In addition to this, the Xiao inversion generated monthly emissions, to investigate the seasonal cycle of both the soil and ocean sources. The latitudinally-varying emissions from Xiao [2008] were gridded for this study and form the basis of the natural component of the total $CHCl_3$ emission field in TOMCAT. A soil distribution based on the distribution of methyl bromide soil emissions, developed by Lee-Taylor et al. [1998], was used as a proxy to grid (1°×1°) the $CHCl_3$ soil emissions. The ocean $CHCl_3$ emissions were evenly distributed on this grid across their respective latitude bands.

Table 5.1. $CHCl_3$ emissions (Gg yr^{-1}) from the ocean and soil in 4 latitude bands averaged over the 2000-2004 period. These optimised emissions are from the modelling study of Xiao [2008]. Errors in the global totals are propagated from the 1 s.d. errors in each latitude band.

Latitude	Ocean emission (Gg yr^{-1})	Soil emission (Gg yr^{-1})	Total natural emission (Gg yr^{-1})
30-90°N	11.5 ± 9.7	55.6 ± 34.0	67.1 ± 35.4
0-30°N	62.8 ± 68.4	38.2 ± 34.1	101.0 ± 76.4
0-30°S	70.5 ± 77.8	33.1 ± 28.4	103.6 ± 82.8
30-90°S	23.1 ± 20.3	8.8 ± 7.1	31.9 ± 21.5
Global total	**167.9 ± 106.0**	**135.7 ± 56.4**	**303.6 ± 120.0**

Table 5.2 summarises the seasonal cycle of both natural $CHCl_3$ emission sources inputted into TOMCAT. On average, the soil emission accounts for 45% of the global total natural emissions, with the ocean accounting for the remainder. The sensitivity of the performance of the gridded $CHCl_3$ emissions to emission seasonality was examined. Tests were performed comparing one TOMCAT model run with seasonal ocean and soil emissions, and one with simple annually averaged emissions (i.e. aseasonal). Due to the size of the seasonality found in Xiao [2008], it is expected that the seasonal case would perform better, and particularly for areas more influenced by soil than ocean emissions, as the soil seasonality is stronger.

Table 5.2. Assumed global monthly averaged $CHCl_3$ emissions (Gg yr^{-1}) from soil and ocean sources between 2000-2004 [Xiao, 2008], which repeat annually in our TOMCAT experiments. Note that the uncertainties in the annual average (final column) are the 1 s.d. errors calculated from the 12 months in order to quantify the strength of the seasonality, and not from latitudinal band error propagation as in **Table 5.1**.

Source	Jan	Feb	Mar	Apr	May	Jun	Jul	Aug	Sep	Oct	Nov	Dec	Ave
Ocean	162	194	197	204	157	145	160	187	190	169	124	129	**168 ± 27**
Soil	86	96	100	112	146	233	244	205	153	92	83	80	**136 ± 60**

5.3.3 Industrial $CHCl_3$ Emissions

For the industrial component of $CHCl_3$ emissions, we assembled regional estimates piecewise on an annual basis. The regions used are adapted from previous TransCom inversion studies [e.g. Baker et al., 2006]. We only consider four of these regions, those linked with industrial production of $CHCl_3$. These are Europe, Temperate North America, Temperate Asia, and Temperate Latin America [Claxton et al., 2019; **Figure 3.1**]. Emissions from each region are summarised in **Table 5.3**. For almost every region, estimates are interpolated based on analysis from Nolan Sherry Associates (NSA), a chlorocarbon consultancy, in 2007 and 2016, which calculated production figures by a combination of a global industry database, industry dialogue, trade data, and back-calculations based on known feedstock applications and quantities. For Temperate Asia, the emissions used are adapted from Fang et al. [2019]. They calculated sub-regional estimates from a range of East and Southeast Asian countries using two separate inversion processes, from 2007-2015. We take the average of the two processes, and extrapolate to 2006 and 2016-2017, to form a 12-year record analogous to the length of record for CH_2Cl_2 in Claxton et al. [2020]. The total regional combination of emission is shown in **Table 5.3**. Although the Fang et al. [2019] Asian region and our Temperate Asian region are not identical, data from NSA shows that emissions from Asia are predominantly from East and South Asia, which mostly lie within the Temperate Asia region. NSA data reports emissions of ~13 Gg yr^{-1} for South Asia, and 25-

53 Gg yr^{-1} for East Asia from 2006-2016, compared to the Fang et al. [2019] estimates of 49-95 Gg yr^{-1} from 2007-2015.

Table 5.3. Annual industrial $CHCl_3$ emissions (Gg yr^{-1}) from the main emitting regions of Europe, Temperate Latin America, Temperate North America, and Temperate Asia.

Region	2006	2007	2008	2009	2010	2011	2012	2013	2014	2015	2016	2017
Europe	4.26	4.17	4.07	3.98	3.89	3.79	3.70	3.60	3.51	3.42	3.33	3.23
Temp. LA	1.11	1.10	1.10	1.09	1.08	1.08	1.07	1.07	1.06	1.06	1.05	1.04
Temp. NA	2.26	2.20	2.14	2.08	2.02	1.96	1.90	1.83	1.77	1.71	1.65	1.59
Temp. Asia	43.6	49.3 ± 4.9	51.7 ± 4.7	43.1 ± 4.0	40.6 ±4.9	56.3 ± 5.0	52.3 ± 7.5	60.8 ± 4.5	80.8 ± 5.7	95.2 ± 9.1	100.9	106.6
Tot. industrial	51.2	56.8	59.0	50.3	47.7	63.1	59.0	67.3	87.1	101.4	106.9	112.5
Tot. industrial + natural	354.8	360.4	362.6	353.9	351.3	366.7	362.6	370.9	390.7	405.0	410.5	416.1

Note: Eur, Temp. LA and Temp. NA emissions are adapted from Nolan Sherry Associates (NSA) data, and Temp. Asia emissions are adapted from Fang et al. [2019]. Also shown is the sum of industrial plus annual average natural emissions (see **Table 5.2**). Error values provided for Temperate Asian emissions (2007-2015) are adapted from Fang et al. [2019]. Total emission errors are approximately equal to ±120 Gg yr^{-1} for every year, almost wholly as a result of errors in natural emissions (**Table 5.1**).

The distribution of the industrial $CHCl_3$ emissions follows a proxy distribution of HCFC-22 [Xiang et al., 2014]. This is an identical approach to that employed for industrial CH_2Cl_2 and C_2Cl_4 emissions in Claxton et al. [2020], and is a reasonable assumption based on observed correlations between several Cl-VSLS and HCFC-22 [Wang et al., 2014]. This distribution is up to date compared to the most recent global $CHCl_3$ distribution from the RCEI [Keene et al., 1999], which does not factor in the changing industrialisation of East Asia. The HCFC-22 distribution also retains similar emission patterns over North America and Europe compared to the RCEI. The emission distribution within regions is assumed constant over the full 12-year period. Overall, total $CHCl_3$

emissions from all sources vary from 354.8 Gg yr^{-1} in 2006 to 416.1 Gg yr^{-1} in 2017. The bulk proportion of these emissions are from natural sources (ocean + soil), comprising 303.6 Gg yr^{-1} each year. This represents 73-86% of total $CHCl_3$ emissions from all sources, depending on the year. For industrial emissions only, Temperate Asia accounts for 86-94% of the total. Whilst industrial emissions from other geographical regions not considered in the study are likely to exist, these are estimated to be <0.5 Gg yr^{-1}, several orders of magnitude below regional soil emissions, for instance.

5.3.4 Evaluation of $CHCl_3$ Emissions

AGAGE maintains a long-term network of surface measurements of $CHCl_3$ [e.g. Prinn et al., 2018]. Whilst the number of measurement sites is too low to successfully perform a synthesis inversion [e.g. Claxton et al., 2020], these observations can form a basis to judge the success of our gridded $CHCl_3$ emission field described above. **Table 5.4** lists the AGAGE observation sites that were used to evaluate the emissions, which were implemented in a forward TOMCAT simulation (see **Section 5.2**). The monthly mean raw (i.e. no filtering for 'pollution events') observed $CHCl_3$ mole fractions were compared on a site by site basis to the corresponding TOMCAT model output. **Figure 5.1** shows a timeseries of observed and modelled $CHCl_3$ at each AGAGE site, over the 12-year period 2006-2017. Also annotated on **Figure 5.1** are two statistical metrics used to determine how well matched the observations (obs) and model output (mod) are, mean absolute deviation (MD) and mean percentage error (MPE), shown in Equations 5.01 and 5.02:

$$MD = \frac{\sum_m |mod - obs|}{n_m} \quad (5.01)$$

$$MPE = \frac{\sum_m \frac{100 \times |mod - obs|}{obs}}{n_m} \quad (5.02)$$

At some of the measurement sites, the model output matches very closely to the observations, particularly over North America and Europe, suggesting that the emission estimates are reasonably accurate for these regions. For sites ZEP, JFJ, and THD, the mean 12-year percentage errors between the model

and observations are only 12%, 6.3%, and 10%, respectively. Southern Hemisphere (SH) sites, however, vary greatly from site to site. Whilst CGO has a similar percentage error to Northern Hemisphere (NH) sites, at 11%, the model output at SMO overestimates the observations, with a mean percentage error of 55%. As SMO is heavily influenced by the Pacific Ocean that envelops it, it is possible that ocean emissions in the 0-30°S latitude band are in reality smaller than what we have assumed.

Table 5.4. Summary of AGAGE surface observational sites used to compare with $CHCl_3$ model output.

Code	Station Name, Location	Lat (°)	Lon (°)	Elevation (m)
ZEP	Zeppelin, Svalbard, Norway	78.9	11.9	490.0
MHD	Mace Head, Ireland	53.3	-9.9	5.0
JFJ	Jungfraujoch, Switzerland	46.3	8.0	3580.0
CMN	Monte Cimone, Italy	44.2	10.7	2165.0
THD	Trinidad Head, CA, USA	41.1	-124.2	107.0
GSN	Gosan, Jeju, South Korea	33.3	126.2	89.0
HAT	Hateruma, Japan	24.1	123.8	46.5
RPB	Ragged Point, Barbados	13.2	-59.5	42.0
SMO	Tutuila, American Samoa	-14.2	-170.6	42.0
CGO	Cape Grim, Australia	-40.7	144.7	94.0

Note that Hateruma uses a separate measurement scale (NIES-11) compared to the rest of the AGAGE sites (SIO-98), and Hateruma measurements have been converted by a factor of 1.066 ± 0.005 [Fang et al., 2019].

Gosan, in South Korea, is a key site in determining how effective the emission field is over Asia, where measurements of $CHCl_3$ are generally sparse. Here, the model output underestimates the observations, with a mean 12-year percentage error of 25%. This bias becomes more significant throughout the 12-year period. It is likely that Gosan is heavily influenced by local pollution sources which may not be captured by the model, leading to the underestimation [Claxton et al., 2020]. Although a shorter record (2006-2015), the model versus observation comparison for Hateruma (Japan) reinforces the

Gosan finding, with the model exhibiting a low bias in the most recent years, but with generally good agreement in the mid-2000s. It is possible that both sites are especially influenced by strong local $CHCl_3$ sources and that the Asian emissions estimates, based on Fang et al. [2019], are too low.

The model/measurement comparisons in **Figure 5.1** are based on a model run with seasonally varying natural $CHCl_3$ emissions. Testing the performance of the model with seasonal natural emissions is an important check, as natural sources contribute the majority of the total global $CHCl_3$ emission (**Table 5.3**). Hence, **Figure 5.1** also shows a case in which the annual average natural emissions (the final column of **Table 5.2**) were applied to every month equally throughout the study period (i.e. aseasonal natural emissions in the model). It can be quickly identified that for many sites, particularly in the NH, the seasonal cycles no longer match up, and the intraannual variation in the model with aseasonal natural emissions is far greater than in the observations (for example the mean 12-year percentage errors for ZEP, JFJ and THD are 20%, 13%, and 14%, respectively, for the aseasonal case). For SH sites, the comparisons are fairly unchanged; however, the deviation metrics suggest that seasonal natural emissions provide a slightly better agreement. For Gosan and Hateruma, the aseasonal case performed more successfully than the seasonal one, but the 'improvement' is small. For tropical and SH sites, given the small differences between the two model outputs, it is likely that seasonality is less prominent than for extratropical northern sites. **Tables 5.1** and **5.2** show that soil emissions are the primary source of seasonality, of which 69% are in the NH.

Figure 5.2 further highlights the differences in modelled surface $CHCl_3$ with seasonal and aseasonal natural emissions. This figure compares the monthly $CHCl_3$ anomaly, calculated as the departure of monthly mean $CHCl_3$ from the annual mean, averaged over all 12 years. Here, it is clear how relatively well the seasonal emission scenario performs for NH extratropical sites, although the seasonal cycle still isn't perfectly captured. Despite the large absolute deviations for sites such as HAT, RPB, and SMO in **Figure 5.1** (up to 55%), the seasonal model output matches fairly effectively.

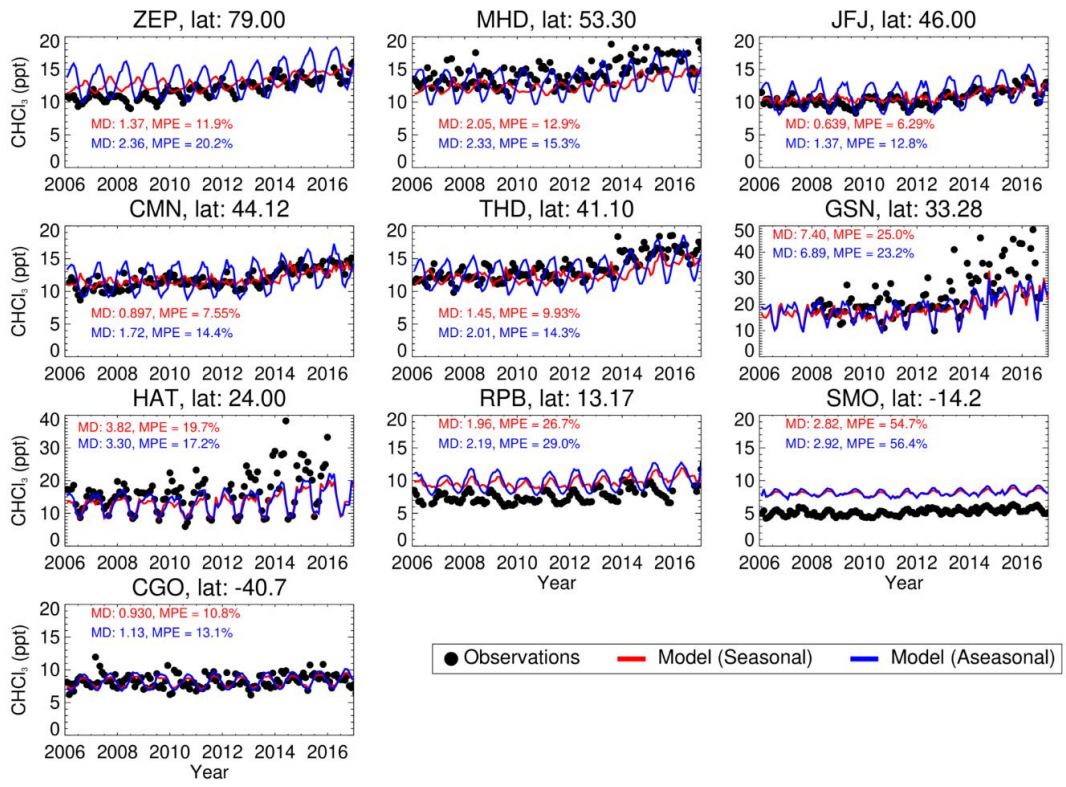

Figure 5.1. Timeseries of observed versus modelled surface $CHCl_3$ (ppt) at AGAGE monitoring sites. Modelled $CHCl_3$ is shown for two different natural (ocean + soil) emission scenarios: where natural emissions have a seasonal cycle (red), and where the annual average natural emissions are used for every month (blue, aseasonal case). Included for every site are the mean 12-year absolute deviations (MD, Equation 5.01) and the mean 12-year percentage errors (MPE, Equation 5.02) between the observations and each model output.

In addition to long term surface observations, aircraft data can be used to assist the evaluation of the $CHCl_3$ emission estimates. ATTREX (Airborne Tropical Tropopause Experiment) [Navarro et al., 2015], CONTRAST (Convective Transport of Active Species in the Tropics) [Pan et al., 2017], and CAST (Co-ordinated Airborne Studies in the Tropics) [Andrews et al., 2016] are three aircraft measurement campaigns that took place in Jan-Mar 2014, over the West Pacific, centred around Guam. As these campaigns sampled close to the key industrial East Asia region, comparisons with the model output provide a valuable supplement to the available Asian surface sites.

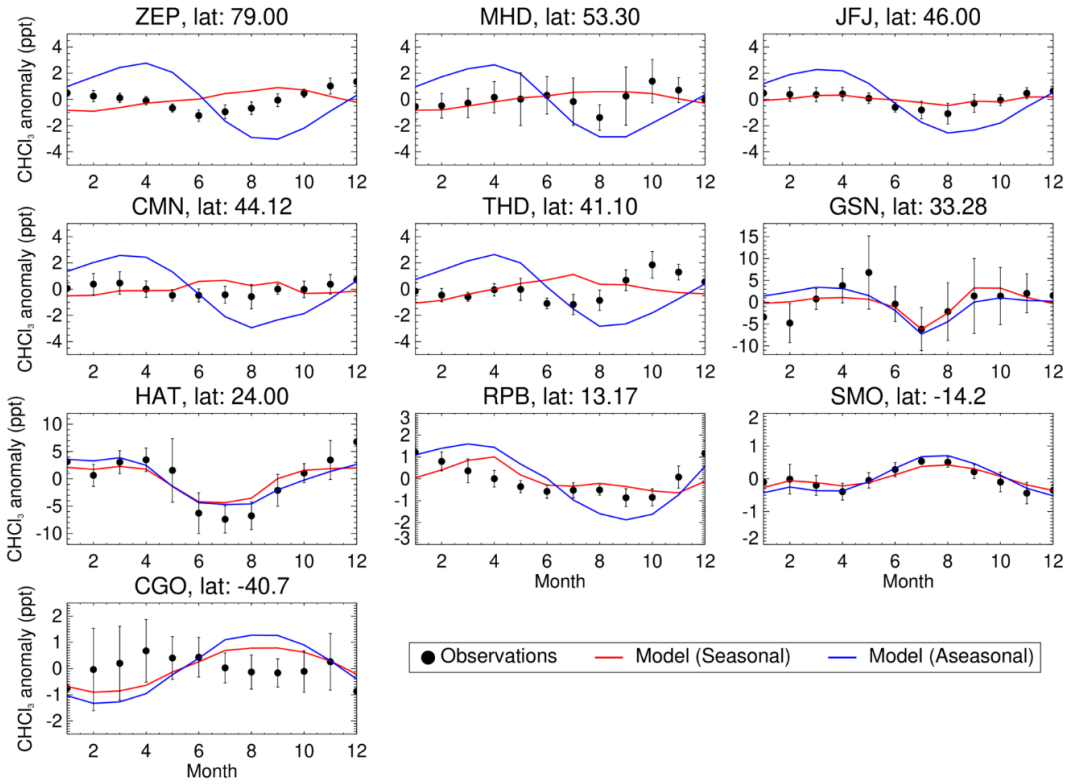

Figure 5.2. 12-year average of monthly anomalies from the annual mean (ppt) at each AGAGE site, comparing observed $CHCl_3$ with seasonal and aseasonal $CHCl_3$ model outputs. Error bars depict ±1 s.d. from the 12-year average observational monthly anomaly.

Figure 5.3 displays all $CHCl_3$ aircraft measurements from the surface into the upper troposphere/lower stratosphere (the ATTREX campaign sampled at a particularly high altitude, above ~14 km). The observations have also been averaged into 1 km bins, as has the corresponding model $CHCl_3$ output. From this, it can be seen that the model overestimates the binned observations slightly, by 0.7 ppt on average throughout the profile. However, the model lies close to the uncertainty range of the observations, and there is good agreement in the boundary later and mid-troposphere. Overall, taking into account both the surface (**Figure 5.1**) and aircraft (**Figure 5.3**) comparisons, our basic estimation of $CHCl_3$ emissions has led to good agreement with observed values, with the performance of the emissions being of a similar order to the results obtained

from the synthesis inversions performed for CH_2Cl_2 and C_2Cl_4 [Claxton et al., 2020].

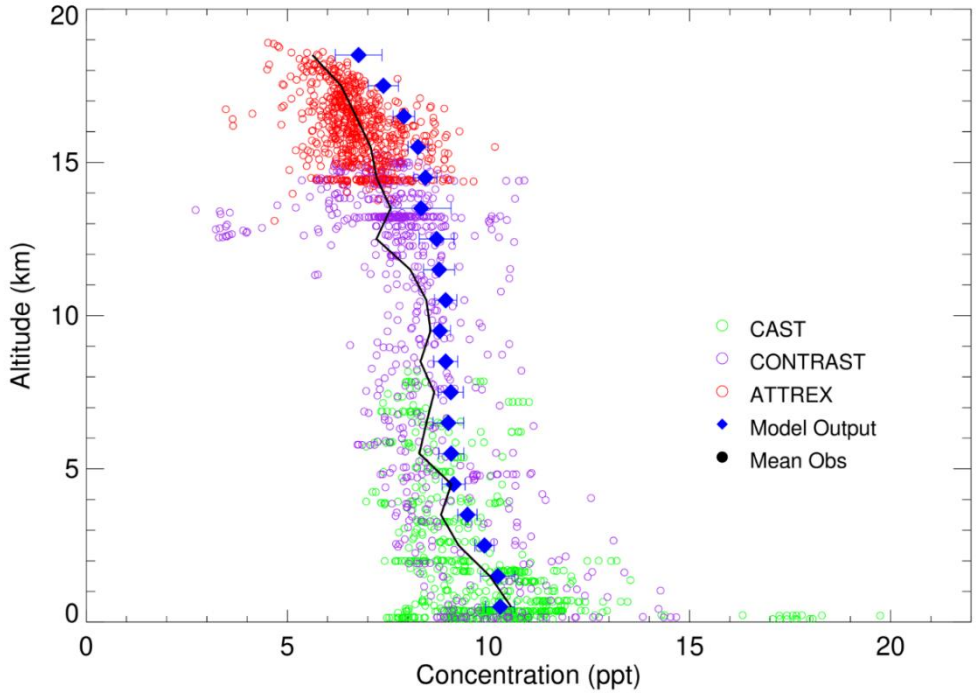

Figure 5.3. Modelled versus observed vertical profiles of $CHCl_3$ (ppt) during the 2014 CAST/CONTRAST/ATTREX field missions. Model output (blue) and the observational mean (black) have been averaged into 1 km vertical bins.

5.4 End-to-End Study of Cl-VSLS Emissions and Impact on Stratospheric Ozone

5.4.1 Surface Trends in Cl-VSLS

With evaluated and reasonably accurate emission fields for the three main Cl-VSLS (CH_2Cl_2 and C_2Cl_4 from Claxton et al. [2020], and $CHCl_3$ from the preceding section), the time-varying atmospheric impacts can be investigated. **Table 5.5** summarises the global source gas emissions for each Cl-VSLS for every year of our 12-year study period (2006-2017). These Cl-VSLS emissions were implemented in a forward TOMCAT model run using a model configuration that contained a simplified treatment of product gas production and removal

(see **Section 5.2**). The TOMCAT model output was first used to investigate changes in surface Cl-VSLS concentrations and to diagnose surface trends. **Figure 5.4** depicts the modelled surface concentration of each species for 2017, the final year of the study.

As Asian CH_2Cl_2 emissions have increased dramatically over the last 10-15 years [Claxton et al., 2020], it is unsurprising that East Asia is the region of greatest CH_2Cl_2 concentrations in **Figure 5.4**. These concentrations reach up to 1 ppb, which is of a similar order to local measurements observed under polluted conditions [Barletta et al., 2006; Oram et al., 2017; Shao et al., 2011]. Background concentrations, e.g. over the NH oceans, are approximately 60 ppt, which represent typical values measured by the NOAA observational network at similar latitudes [e.g. Claxton et al., 2020; also **Figure 2.4**]. There is a large hemispherical gradient across all Cl-VSLS, due to relatively strong NH sources and meridional circulation only occurring at timescales similar to Cl-VSLS lifetimes. For $CHCl_3$, maximum concentrations also occur over East Asia, at approximately 100 ppt. This is again of a similar order to observations recorded in the area (e.g. 232 ppt at Taiwan from polluted air strongly influenced from continental East Asia) [Oram et al., 2017]. Despite natural emissions comprising 80% of total $CHCl_3$ emissions, these industrial peaks are still visible, due to the large proportion of Temperate Asia emissions in **Table 5.3**. For C_2Cl_4, Asian emissions aren't significantly greater than emissions from any other region [Claxton et al., 2020]. As a result, industrial hotspots with concentrations reaching over 40 ppt are scattered throughout Europe, Asia, and North America. Observed background NH concentrations of C_2Cl_4 are typically of the order of 3 ppt [Claxton et al., 2020], which matches the results in **Figure 5.4(c)**. When comparing with observational data, it is important to note that the model grid cells cover a large area, and an observational point may not be representative over the entirety of its surrounding area.

Also included in **Figure 5.4** is the modelled surface concentration of the two main product gases studied, Cl_y and phosgene (expressed as a sum of both compounds and in terms of equivalent chlorine). Concentrations of the two product gases reach up to 60 ppt Cl equivalent in East Asia, though baseline values of 25-30 ppt Cl are estimated between 60°N and 30°S.

Table 5.5. Summary of annual emissions (Gg yr^{-1}) for the 3 Cl-VSLS input into forward TOMCAT simulations. CH_2Cl_2 and C_2Cl_4 emissions are derived from Claxton et al. [2020] (**Tables 4.3**, **4.4**, **4.S3**).

Species	2006	2007	2008	2009	2010	2011	2012	2013	2014	2015	2016	2017
CH_2Cl_2	637	695	748	743	822	832	886	1037	1093	1076	1117	1171
$CHCl_3$	355	360	363	354	351	367	363	371	391	405	411	416
C_2Cl_4	-	141	149	135	131	117	114	109	113	111	104	106
C_2Cl_4 + Cl	-	216	227	210	198	180	174	171	169	170	161	163

Note: C_2Cl_4 + Cl represents the emissions generated with inclusion of a Cl reaction sink. $CHCl_3$ emissions are from **Table 5.3**.

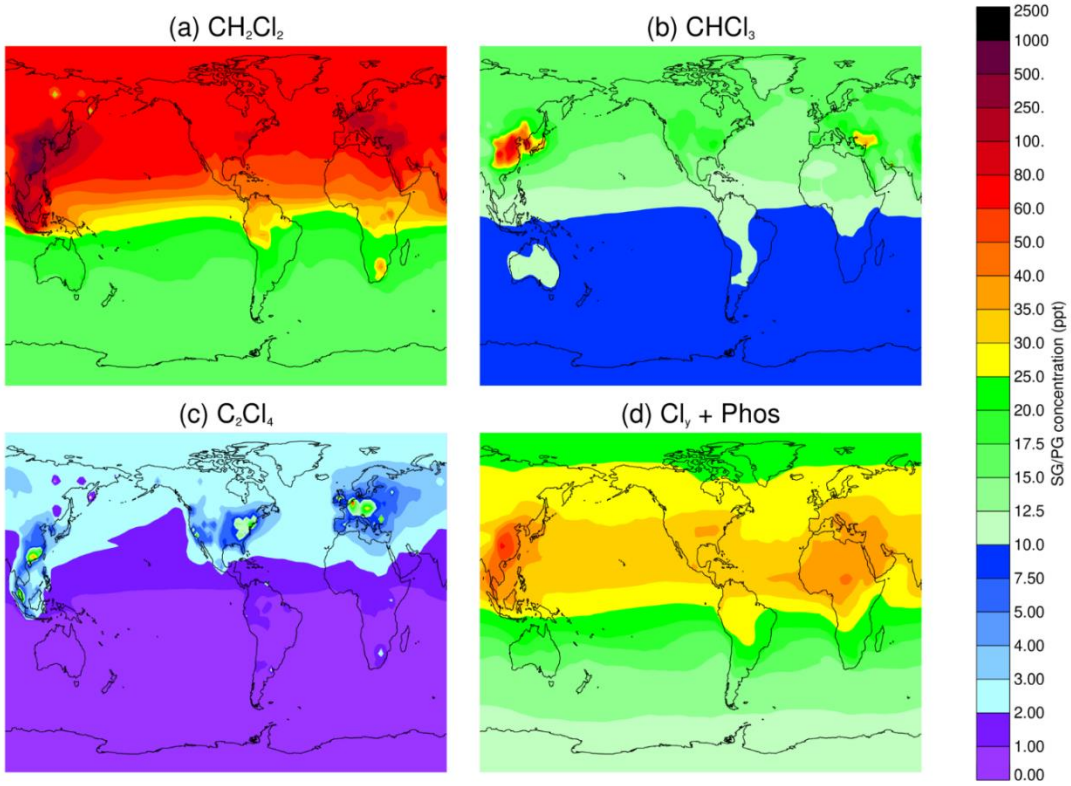

Figure 5.4. Modelled 2017 surface mixing ratios (ppt source gas) of (a) CH_2Cl_2, (b) $CHCl_3$, (c) C_2Cl_4, and (d) sum of product gases Cl_y and phosgene. For (d), units are ppt Cl equivalent.

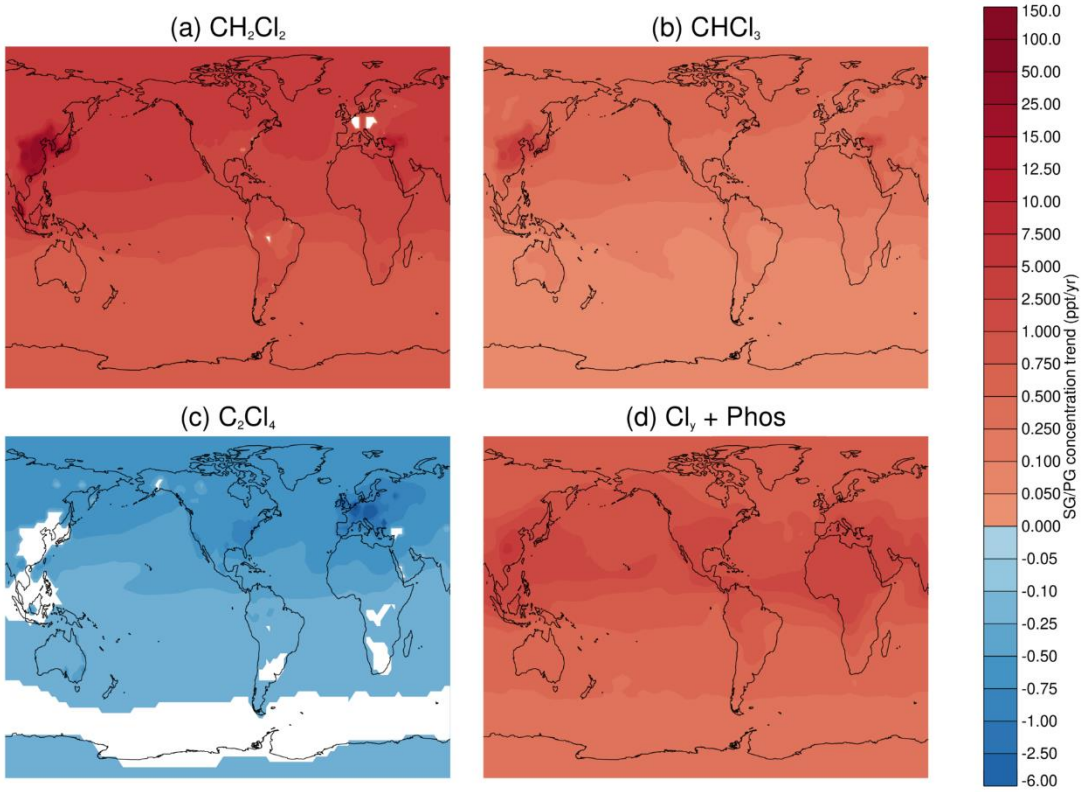

Figure 5.5. Modelled surface mixing ratio trend (ppt source gas yr^{-1}) for (a) CH_2Cl_2, (b) $CHCl_3$, (c) C_2Cl_4, and (d) sum of product gases Cl_y + phosgene. Note that the CH_2Cl_2 and $CHCl_3$ trends are for the period 2006-2017, whilst C_2Cl_4 and product gas trends are for 2007-2017. For (d), units are ppt Cl equivalent yr^{-1}. White areas represent trends that lie below the 95% confidence interval.

Figure 5.5 shows the calculated trend in the surface abundance of all three Cl-VSLS over the study period 2006-2017 (2007-2017 for C_2Cl_4), for each model grid box. There is a clear increasing trend in CH_2Cl_2 surface concentration, including at background locations. This increasing trend ranges from ~100 ± 6 ppt yr^{-1} in areas of East Asia, to 2.5 ± 0.2 ppt yr^{-1} at NH background locations and 0.8 ± 0.04 ppt yr^{-1} at SH background locations, and a positive trend is almost ubiquitous across the globe. The trends in **Figure 5.5** were also tested for their significance. A Student's t-test was performed on the trend correlation, with a null hypothesis assuming zero correlation. The number of degrees of freedom provided was equal to n-2, where n is the number of years for each Cl-VSLS trend calculation. As each trend was performed using annual means, it is

likely that any autocorrelation is minimised. The majority of the CH_2Cl_2 trends lie above the 95% confidence interval, illustrated by the lack of white patches in **Figure 5.5(a)**. These non-significant trends are located in Europe, where high surface concentrations fluctuate annually. Despite regions such as Europe experiencing a negative trend in emissions [Claxton et al., 2020; **Figure 4.2**], the efficient zonal mixing of CH_2Cl_2 still results in a general increase in the surface concentrations over the 12 years.

For $CHCl_3$, there is also a general increasing trend, due to a relatively strong increase in emissions over the later 5 years of the study period (see also **Table 5.5**). This trend is noticeably far lower than that for CH_2Cl_2, with the greatest trend reaching *only* 10.8 ± 1.8 ppt yr^{-1} in some grid boxes. Similarly to CH_2Cl_2, the maximum trends in $CHCl_3$ surface mixing ratio occur over East Asia. C_2Cl_4 experiences a negative trend globally, of up to -2.6 ± 0.5 ppt yr^{-1}, reflecting its generally decreasing emissions. As a consequence of the greater relative error of the C_2Cl_4 trend, less confidence in the trends have been found by the Student's t-test, particularly in the Southern Hemisphere. For both $CHCl_3$ and C_2Cl_4, there are regions which experience changes in emissions contrary to their respective concentration trends [**Table 5.4**; Claxton et al., 2020]. However, these changes are too small compared to the impact of zonal cross-regional transport on surface mixing ratios. The final panel in **Figure 5.5** shows that for the two main product gases, Cl_y and phosgene, the trend follows that expected of a roughly weighted combination from all three Cl-VSLS (i.e. overall positive), with a similar distribution to its analogous surface concentration plot in **Figure 5.4**.

5.4.2 Stratospheric Injection of Cl-VSLS and Products

5.4.2.1 Primary Analysis

An important source of Cl-VSLS and their product gases, Cl_y and phosgene, to the stratosphere, is via the tropical tropopause [Claxton et al., 2019; Gettelman et al., 2009; Hosking et al., 2010]. This is because of efficient transport from large-scale convective systems, which originate over warm ocean waters. Throughout the tropics, the greatest likelihood of these systems occurs over

South East Asia [e.g. Gettelman et al., 2009], and therefore emissions close to this region will lead to the largest chlorine injection [Claxton et al., 2019]. As a result, it is of key importance to determine the amount of chlorine from Cl-VSLS at the tropical tropopause. Here we define the tropical tropopause as between the latitudes 20°N and 20°S, and at an altitude between 16.5 and 17.5 km, consistent with the altitude range from the WMO definition [Engel et al., 2018].

Table 5.6 shows the modelled abundance at the tropical tropopause for each of the three Cl-VSLS, and their products, for each year of our study (similar values are later used as boundary conditions in the stratospheric configuration, SLIMCAT). For C_2Cl_4, results for 2006 have been excluded as the input emission data only starts in 2007. **Table 5.6** categorises the stratospheric chlorine injection from each source gas ("source gas injection", SGI) and the contributions of both major product gases ("product gas injection", PGI), each expressed in ppt of chlorine equivalent. As can be expected, the tropopause abundance is roughly proportional to global emissions, and follows the same trend. For CH_2Cl_2, there is an increase of roughly 3.8 ppt Cl yr^{-1}, resulting in a total stratospheric Cl contribution (SGI + PGI) due to CH_2Cl_2 of 88.0 ± 8.7 ppt Cl in 2017, an increase from 49.4 ± 3.2 ppt Cl in 2006. For $CHCl_3$, the yearly trend is 0.46 ppt Cl yr^{-1}, with a 2017 total chlorine injection of 39.0 ± 2.1 ppt Cl, up from 33.9 ± 1.4 ppt Cl in 2006. Note, a value of 0.84 ppt Cl yr^{-1} is generated when calculating $CHCl_3$ PGI+SGI trend from 2011, the year at which $CHCl_3$ notably increases. Owing to decreasing emissions between 2007 and 2017, there is a negative trend in the stratospheric chlorine injection due to C_2Cl_4, of -0.19 ppt Cl yr^{-1} for its total SGI + PGI contributions, from 6.41 ppt Cl in 2007 to 5.06 ppt Cl in 2017.

Table 5.6. Annual modelled stratospheric Cl injections (ppt Cl) due to Cl-VSLS emissions from **Table 5.5**. Injections are derived as the sum of equivalent ppt chlorine at the tropical (±20° latitude) tropopause (16.5-17.5 km). The final column summaries equivalent data from the most recent WMO/UNEP Ozone Assessment Report, over ±25° latitude (and 16.5-17.5 km) [Engel et al., 2018]. For each Cl-VSLS, SGI (Source Gas Injection) and PGI (Product Gas Injection) from Cl_y and phosgene are calculated. Uncertainties given are ± 1 s.d. from the mean, and do not reflect the uncertainty in the emissions.

		2006	2007	2008	2009	2010	2011	2012	2013	2014	2015	2016	2017	WMO [2018] for 2016
CH_2Cl_2	SGI	38.7 ± 2.7	40.4 ± 4.3	46.0 ± 4.1	46.3 ± 3.8	50.9 ± 6.3	51.3 ± 4.2	55.4 ± 5.3	62.1 ± 7.4	68.6 ± 6.3	65.0 ± 5.4	68.9 ± 8.1	68.5 ± 8.1	52.6-77.0
	Cl_y	5.35 ± 1.55	5.78 ± 1.75	6.64 ± 2.08	6.23 ± 1.61	6.29 ± 1.98	7.15 ± 2.14	7.00 ± 2.04	7.70 ± 2.51	8.93 ± 2.64	8.38 ± 2.43	8.91 ± 2.72	10.1 ± 3.08	
	Phos	5.32 ± 0.24	5.47 ± 0.37	5.85 ± 0.39	6.30 ± 0.40	6.61 ± 0.50	6.90 ± 0.43	7.27 ± 0.42	7.96 ± 0.73	8.83 ± 0.60	9.12 ± 0.50	9.29 ± 0.58	9.35 ± 0.69	
	Total	49.4 ± 3.2	51.6 ± 4.6	58.4 ± 4.6	58.8 ± 4.1	63.8 ± 6.6	65.3 ± 4.7	69.7 ± 5.7	77.7 ± 7.9	86.3 ± 6.8	82.5 ± 5.9	87.1 ± 8.6	88.0 ± 8.7	
$CHCl_3$	SGI	21.9 ± 1.2	22.2 ± 1.5	22.3 ± 1.5	22.3 ± 1.2	22.5 ± 1.3	22.3 ± 1.6	22.9 ± 1.3	23.1 ± 1.5	23.8 ± 1.7	24.6 ± 1.5	25.4 ± 1.6	25.0 ± 1.9	17.1-22.5
	Cl_y	1.37 ± 0.47	1.47 ± 0.52	1.54 ± 0.60	1.40 ± 0.46	1.32 ± 0.52	1.48 ± 0.57	1.36 ± 0.50	1.39 ± 0.57	1.49 ± 0.57	1.47 ± 0.53	1.53 ± 0.55	1.74 ± 0.64	
	Phos	10.6 ± 0.5	10.7 ± 0.5	10.8 ± 0.5	10.8 ± 0.5	10.5 ± 0.5	10.7 ± 0.6	10.8 ± 0.5	10.9 ± 0.7	11.2 ± 0.7	11.6 ± 0.8	12.0 ± 0.8	12.3 ± 0.8	
	Total	33.9 ± 1.4	34.3 ± 1.6	34.7 ± 1.7	34.5 ± 1.4	34.4 ± 1.5	34.5 ± 1.7	35.1 ± 1.5	35.3 ± 1.7	36.4 ± 1.9	37.7 ± 1.7	38.9 ± 1.9	39.0 ± 2.1	
C_2Cl_4	SGI	-	4.24 ± 0.43	4.78 ± 0.53	4.85 ± 0.50	4.38 ± 0.41	3.91 ± 0.37	4.04 ± 0.48	3.97 ± 0.43	4.15 ± 0.49	3.65 ± 0.39	3.47 ± 0.30	3.35 ± 0.42	1.52-2.84
	Cl_y	-	0.84 ± 0.21	0.94 ± 0.26	0.90 ± 0.20	0.78 ± 0.20	0.78 ± 0.21	0.73 ± 0.20	0.71 ± 0.20	0.76 ± 0.21	0.68 ± 0.17	0.65 ± 0.17	0.69 ± 0.19	
	Phos	-	1.33 ± 0.13	1.38 ± 0.15	1.40 ± 0.11	1.29 ± 0.11	1.21 ± 0.09	1.14 ± 0.09	1.10 ± 0.10	1.11 ± 0.10	1.08 ± 0.09	1.04 ± 0.09	1.02 ± 0.11	
	Total	-	6.41 ± 0.49	7.10 ± 0.61	7.15 ± 0.54	6.46 ± 0.47	5.90 ± 0.43	5.90 ± 0.53	5.78 ± 0.48	6.03 ± 0.54	5.40 ± 0.43	5.16 ± 0.35	5.06 ± 0.48	
Total SGI			66.8 ± 4.6	73.1 ± 4.3	73.5 ± 4.0	77.8 ± 6.4	77.5 ± 4.5	82.3 ± 5.5	89.2 ± 7.6	96.6 ± 6.5	93.3 ± 5.6	97.8 ± 8.3	96.9 ± 8.3	71.8-101.2
Total PGI			25.6 ± 1.9	27.2 ± 2.3	27.0 ± 1.8	26.8 ± 2.2	28.2 ± 2.3	28.3 ± 2.2	29.8 ± 2.8	32.2 ± 2.9	32.3 ± 2.7	33.4 ± 2.9	35.2 ± 3.3	8-50
Total SGI + PGI			92.3 ± 5.0	100.2 ± 4.9	100.5 ± 4.4	104.7 ± 6.8	105.7 ± 5.1	110.7 ± 5.9	118.8 ± 8.1	128.7 ± 7.1	125.6 ± 6.2	131.2 ± 8.8	132.1 ± 8.9	89.9-141.1

Table 5.6 also includes best estimates from the most recent WMO/UNEP Ozone Assessment, based on the simple idealised modelling study of Hossaini et al. [2017] and aircraft observations, as reported in Engel et al. [2018]. These values are appropriate for the year 2016 and are calculated at the tropopause between 25°N and 25°S; i.e. a slightly different latitude range to our study. For CH_2Cl_2, our 2016 estimate of SGI (68.9 ± 8.1 ppt Cl) falls within the range of the WMO best estimate (52.6-77.0 ppt Cl). For $CHCl_3$, our 2016 SGI estimate of 25.4 ± 1.6 ppt Cl is just outside the WMO range (17.1-22.5 ppt Cl), and for C_2Cl_4 we calculate SGI of 3.47 ± 0.30 ppt Cl, 1.5× that of the WMO estimate average (1.52-2.84 ppt Cl). The *total* SGI from these three Cl-VSLS is listed in **Table 5.6**. Our value for total SGI of 97.8 ± 8.3 ppt Cl lies within the WMO best estimated range of 71.8-101.2 ppt Cl, but towards the upper limit. Note, this WMO SGI reported estimate is based on the contributions of just these three Cl-VSLS, and other Cl-VSLS, such as $C_2H_4Cl_2$, were not specifically included in the calculation [Engel et al., 2018].

The WMO report also includes estimates of PGI based on the combination of several modelling studies [Engel et al., 2018]. The nature of combining results from different studies leads to large uncertainty in the WMO estimated PGI range of 8-50 ppt Cl. The PGI estimate from this study is 32.2-35.2 ppt Cl (2014-2017) and hence falls within the WMO range. Our estimate of the *total* contribution (SGI + PGI) of Cl-VSLS to stratospheric chlorine is 132.1 ± 8.9 ppt Cl in 2017 which falls towards the upper limit of the equivalent WMO estimate (**Table 5.6**).

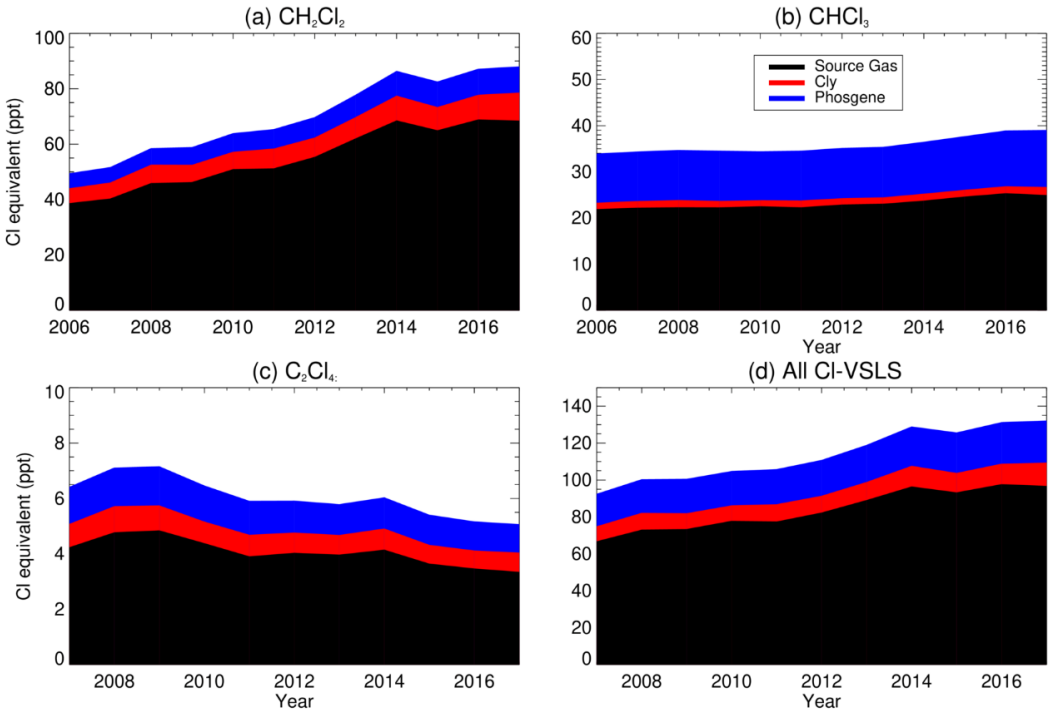

Figure 5.6. Tropical tropopause Cl-VSLS injection timeseries in ppt Cl, 2006-2017. For each Cl-VSLS, the annual contribution from SGI (black), Cl_y (red) and phosgene (blue) is shown. Note for (c) C_2Cl_4, and (d) total from all Cl-VSLS, the timeseries starts at 2007.

Figure 5.6 summarises the results given in **Table 5.6** by visualising the yearly chlorine injections due to each source gas, Cl_y, and phosgene. Here the rise in CH_2Cl_2 concentrations can be more easily identified. What is also apparent is the differing proportions of product gases for each Cl-VSLS. Despite CH_2Cl_2 and $CHCl_3$ having very similar tropospheric lifetimes, of around 110 days [Claxton et al., 2019; Harris et al., 2014], 21% of the *total* stratospheric chlorine injection due to CH_2Cl_2 is from product gases (10.5% Cl_y, 10.5% phosgene), whilst for $CHCl_3$ this proportion is 35%, and concentrations of phosgene are 8 times larger than those of Cl_y. C_2Cl_4 has a PGI proportion of about 32.5%; however, note this value is only based on a scenario in which C_2Cl_4 is oxidised by OH only.

5.4.2.2 Sensitivity Testing

In addition to a sink reaction with OH, there is a likely sink of C_2Cl_4 with Cl radicals [Rudolph et al., 1996]. We tested the effect of this reaction by propagating the C_2Cl_4 + Cl emissions from Claxton et al. [2020], detailed in **Table 5.5**. The results from the inclusion of the C_2Cl_4 + Cl sink reaction are shown in **Table 5.7**. As the inversion results from the C_2Cl_4 + Cl sink experiment were designed to optimise emissions using the same series of observations as the case without the sink, it isn't surprising that the SGI values in **Table 5.7** match those in **Table 5.6** fairly closely, with a maximum deviation from the original case of 11%. However, the PGI estimates vary considerably. The Cl_y injections increase by a factor of 3, and phosgene injections increase by a factor of 2.1, when the C_2Cl_4 + Cl sink is included. The 3× increase of Cl_y cannot be rationalised just by the 50% increased C_2Cl_4 emissions for this scenario. It is probable that this extra Cl_y comes directly from the C_2Cl_4 + Cl sink reaction. Overall, the average PGI proportion has increased from 32.5% to 52%, and total stratospheric Cl equivalent from C_2Cl_4 (SGI + PGI) increased from 5.06 ppt Cl to 7.82 ppt Cl in 2017 (i.e. comparing results from **Table 5.6** to **Table 5.7**). However, although there is reasonable confidence in the existence of the sink [Hossaini, Chipperfield, et al., 2016; Rudolph et al., 1996], the Cl concentration field used in the model is far less certain. Recall, 1.3 x 10^3 atoms cm^{-3} was assumed as a globally uniform troposphere Cl concentration, whereas in practice this is unlikely to be accurate. Therefore, we only include the base case (without the C_2Cl_4 + Cl sink) in our calculation of total tropopause chlorine injection to study ozone impacts.

Table 5.7. As **Table 5.6**, but for the additional C_2Cl_4 + Cl emission scenario.

		2007	2008	2009	2010	2011	2012	2013	2014	2015	2016	2017
C_2Cl_4 + Cl	**SGI**	4.40	5.07	5.36	4.86	4.08	4.40	4.37	4.36	3.86	3.86	3.53
	Cl_y	2.56	2.88	2.76	2.32	2.26	2.13	2.09	2.24	1.94	1.94	2.09
	Phos	2.90	3.00	3.00	2.71	2.52	2.37	2.31	2.36	2.24	2.21	2.20
	Total	9.86	11.0	11.1	9.88	8.86	8.90	8.76	8.96	8.04	8.02	7.82

Table 5.8. As **Table 5.6** but for a model sensitivity experiment assuming a Cl_y lifetime of 37 hours [Wang et al., 2019], rather than 5 days [Sherwen et al., 2016].

		2006	2007	2008	2009	2010	2011	2012	2013	2014	2015	2016	2017
CH_2Cl_2	SGI	38.7	40.4	46.0	46.3	50.9	51.3	55.4	62.1	68.6	65.0	68.9	68.5
	Cl_y	3.60	3.91	4.51	4.14	4.10	4.81	4.55	5.03	5.91	5.54	5.89	6.91
	Phos	5.32	5.47	5.85	6.30	6.61	6.90	7.27	7.96	8.83	9.12	9.29	9.35
	Total	47.6	49.7	56.3	56.8	61.6	62.9	67.2	75.1	83.3	79.7	84.1	84.7
$CHCl_3$	SGI	21.9	22.2	22.3	22.3	22.5	22.3	22.9	23.1	23.8	24.6	25.4	25.0
	Cl_y	0.92	1.00	1.06	0.94	0.87	1.01	0.89	0.92	1.00	0.98	1.02	1.20
	Phos	10.6	10.7	10.8	10.8	10.5	10.7	10.8	10.9	11.2	11.6	12.0	12.3
	Total	33.4	33.9	34.2	34.0	33.9	34.0	34.6	34.9	36.0	37.2	38.4	38.5
C_2Cl_4	SGI		4.24	4.78	4.85	4.38	3.91	4.04	3.97	4.15	3.65	3.47	3.35
	Cl_y		0.51	0.57	0.54	0.45	0.47	0.43	0.42	0.46	0.40	0.39	0.43
	Phos		1.33	1.38	1.40	1.29	1.21	1.14	1.10	1.11	1.08	1.04	1.02
	Total		6.07	6.73	6.78	6.13	5.59	5.61	5.49	5.72	5.13	4.90	4.80
Total SGI			66.8	73.1	73.5	77.8	77.5	82.3	89.2	96.6	93.3	97.8	96.9
Total PGI			22.9	24.2	24.1	23.8	25.1	25.1	26.3	28.5	28.7	29.6	31.2
Total			89.7	97.2	97.6	101.6	102.5	107.4	115.5	125.0	122.0	127.4	128.1

An additional sensitivity experiment was performed by changing the lifetime of Cl_y. The lifetime supplied in the base model, of 5 days, was based on modelling work by Sherwen et al. [2016]. However, an alternative and much lower estimate of 37 hours was found by Wang et al. [2019]. Therefore, the TOMCAT model runs were repeated using this lower lifetime estimate. The SGI and phosgene injections do not change at all, and despite a change in the assumed Cl_y lifetime by a factor of 3.2 in the model, the Cl_y stratospheric injections only change at most by around a factor of 1.4-1.65 (**Table 5.8**). Overall, the decreased Cl_y lifetime leads to decreased total Cl-VSLS contributions (SGI+PGI, all 3 Cl-VSLS) by only ~3% for each year, which are within the error ranges provided in **Table 5.6**. Therefore, the total chlorine injection into the stratosphere due to Cl-VSLS isn't particularly sensitive to current uncertainty in the tropospheric Cl_y lifetime.

A final set of sensitivity tests were performed with varying OH concentrations. Multi-model global tropospheric mean OH concentrations are approximately $10.8 \pm 2.1 \times 10^5$ molecules cm^{-3} [Zhao et al., 2019]. This uncertainty of ±20%

was used to scale our offline OH field in TOMCAT and further forward runs were performed that were otherwise identical to the base case. Focusing on the year 2017, we found from these sensitivity tests that CH_2Cl_2 SGI ranged from 56.6-86.0 ppt Cl when OH was altered by 20%, compared to the base case value of 68.5 ± 8.1 ppt Cl (**Table 5.6**). Similarly, for $CHCl_3$, SGI ranged from 20.4-31.8 ppt Cl (c.f. 25.0 ± 1.9 ppt Cl in **Table 5.6**). Overall, the total SGI from all VSLS considered ranges from 79.7-122.2 ppt Cl, and total SGI+PGI ranges from 114.4-158.1 ppt Cl, compared to 96.6 ± 8.3 and 132.1 ± 8.9 ppt Cl, respectively. These ranges are broadly in line with those provided in the 2018 WMO Ozone Assessment, in **Table 5.6** [Engel et al., 2018]. Compared to changing Cl_y lifetime, Cl-VSLS contributions to stratospheric Cl are far more sensitive to uncertainties in OH. In addition, e.g. for the SGI+PGI total contributions, the range of 114.4-158.1 ppt Cl far exceeds the ± 8.9 ppt Cl estimate of uncertainty from **Table 5.6**. Therefore, it can be concluded that variations and uncertainty in tropospheric OH concentration are significant towards quantifying Cl-VSLS injection into the stratosphere.

5.4.3 Stratospheric Ozone Impacts

5.4.3.1 Ozone Changes due to Cl-VSLS

With tropopause injection values of Cl-VSLS calculated using TOMCAT (e.g. **Table 5.6**), we entered these as boundary conditions into the stratospheric configuration of the model, SLIMCAT. Two simulations were performed with SLIMCAT, one with the time series of Cl-VSLS injections from 2007-2017, and one with zero Cl-VSLS. Therefore, we can determine the transient impact on ozone from Cl-VSLS, assuming accurate levels of Cl-VSLS emissions were included. For the “with Cl-VSLS” scenario, the tropopause injection values are formed from the total contribution from each Cl-VSLS in **Table 5.6**. Both source gas and product gas contributions are included and are considered separately in the model. The evaluation of stratospheric ozone concentrations from the model under each scenario was analysed. **Figure 5.7(a)** shows the annual mean percentage ozone difference between the two scenarios in 2017, the final year of the model runs, as a function of latitude and altitude. As expected,

inclusion of Cl-VSLS leads to a decrease in ozone concentration and this decrease is evident throughout the stratosphere. This decrease is particularly prominent in the Antarctic lower stratosphere, at around -3.5% at its maximum, and in the upper stratosphere, regions where chlorine is relatively efficient at destroying ozone [von Clarmann, 2013]. It has been well established that dynamical changes are a significant driver of lower stratosphere ozone decreases [Shepherd, 2008], and this has also been found to be the case for recent ozone trends [Chipperfield et al., 2018]. However, as our two model scenarios use the same offline dynamics, the ozone decrease in **Figure 5.7** are purely due to chemical processes (i.e. the addition of 'extra' chlorine from Cl-VSLS). Overall, in 2017, global mean lower stratosphere ozone loss due to Cl-VSLS is estimated at -0.56%, which increases to -1.19% when just considering ozone changes over Antarctica (60°-90°S, **Table 5.9**).

The "ozone hole", the phenomenon that arises from the unusual Antarctic meteorological conditions, combined with chlorine from CFCs and other ODSs, is most prominent during the Antarctic spring. The polar winter leads to a build-up of chlorine reservoir species, such as $ClONO_2$ and HCl [e.g. Lowe and MacKenzie, 2008]. These can react inside and on polar stratospheric clouds (PSCs) to form more labile compounds, including HOCl, and Cl_2. When the sun returns in spring, these chlorinated compounds can be readily photolysed, releasing large amounts of Cl rapidly, leading to a dramatic decrease in ozone. **Figure 5.7(b)** calculates the difference in ozone concentrations due to Cl-VSLS during October of 2017, the peak month of the ozone hole [e.g. Orce and Helbling, 1997]. The ozone difference over the Antarctic lower stratosphere reaches a maximum of about -18% (and an average of -3.16% at 50 hPa, see **Table 5.9**), although the ozone loss over the Arctic lower stratosphere is unsurprisingly far smaller in this month.

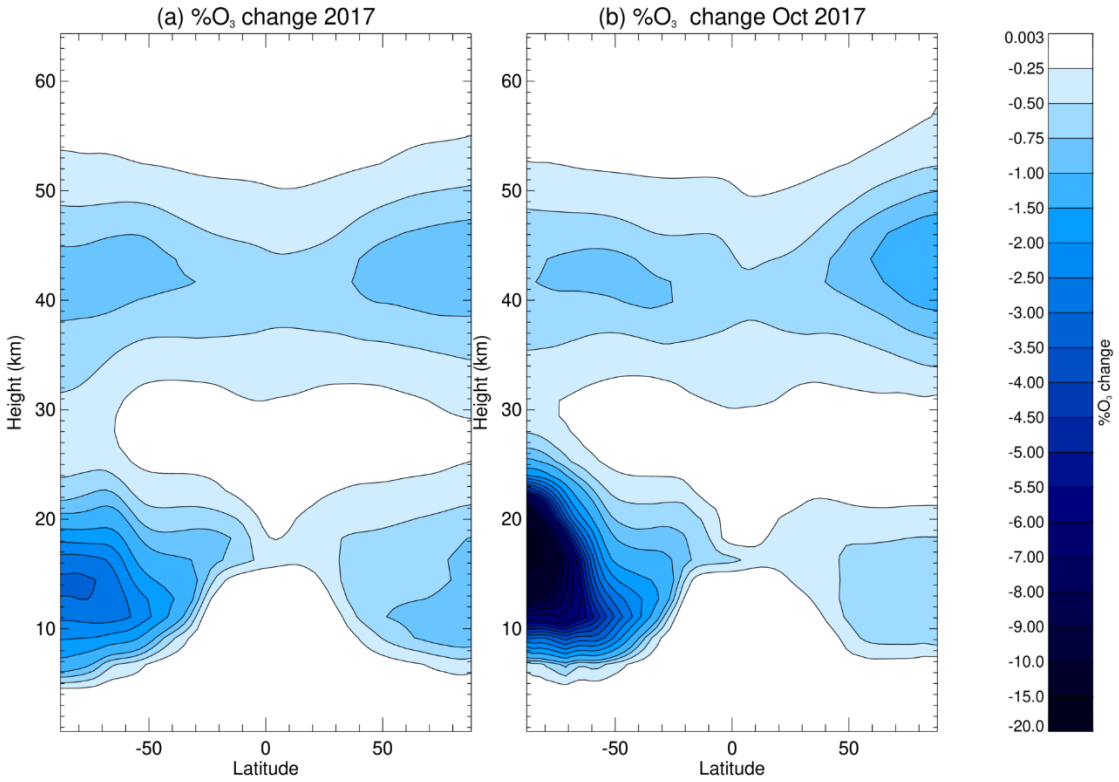

Figure 5.7. Latitude-height ozone difference (%) between SLIMCAT model runs with Cl-VSLS and without. (a) Annual average difference for the final year of the study, 2017; (b) difference during October 2017, the peak month of Antarctic ozone loss.

In addition to purely investigating the final year of the study, we can observe how O_3 concentrations have changed as a result of the changing Cl-VSLS emissions from 2007-2017. **Table 5.9** calculates changes in ozone over various different regions, including the lower stratosphere (50 hPa) [e.g. Eyring et al., 2010], the lower stratosphere just over the Antarctic (60°-90°S), both annually and in October, and the upper stratosphere (5 hPa). As Cl-VSLS are particularly reactive compared to most chlorinated ODS, they decompose relatively rapidly in the lower stratosphere. However, upper stratosphere ozone loss due to Cl-VSLS is not negligible, and ozone decreases at a rate of -0.009 % yr^{-1} at 5 hPa. Throughout the 11 years of the study, ozone loss due to the difference between the two Cl-VSLS scenarios increases with year, as expected from one of the scenarios continually increasing its chlorine injection into the stratosphere. However, the loss is not linear, for example 2008 lower stratosphere ozone loss is greater than in 2010, despite the inverse being true with regards to chlorine

injection from Cl-VSLS in **Table 5.6**. Therefore, other factors must also act to modulate the relative magnitude of Cl-VSLS-induced ozone change, such as interannual variability in stratospheric meteorology.

In the lower stratosphere, Antarctica is more affected by yearly changes in Cl-VSLS. Over 2007-2017, between the two Cl-VSLS scenarios, the global lower stratosphere percentage ozone change decreases at a rate of -0.009 % yr^{-1}, whilst just considering the Antarctic, the trend is -0.022 % yr^{-1}, implying that Cl-VSLS further enhances Antarctic ozone loss. This could be due to the role that chlorine plays in Antarctic stratospheric chemistry, including a coupling system with bromine [Danilin et al., 1996], and removing chlorine affects this system non-lineally. **Figure 5.8** illustrates the difference in Antarctic lower stratospheric ozone between the two SLIMCAT scenarios through time. Slices of the difference in Antarctic ozone at 50 hPa were taken in October over four years between 2007 and 2017. Here, it can be seen that Antarctic ozone depletion due to Cl-VSLS is fairly similarly structured from year to year, and increases over the four chosen years, reaching a maximum in 2017. This is due to the increasing stratospheric chlorine from Cl-VSLS over the study period.

Figure 5.8 also shows a similar representation for the Arctic Spring, using the ozone difference due to Cl-VSLS in March over the same four years. Arctic ozone loss is more subject to interannual variation than in the Antarctic. This is due to the more variable state of the Arctic polar vortex [Langematz et al., 2018]. For example, the relatively large ozone decrease in 2011 coincides with an anomalously strong Arctic polar vortex, leading to exceedingly cold temperatures, and therefore a larger number of polar stratospheric clouds to facilitate ozone depletion [Manney et al., 2011]. Also, the position of the Arctic ozone hole varies significantly amongst the years. In 2007 the majority of the depletion resides directly over the pole, however in the subsequent years of the Figure, the centre lies more towards Siberia, a latitude shift of 10-15°.

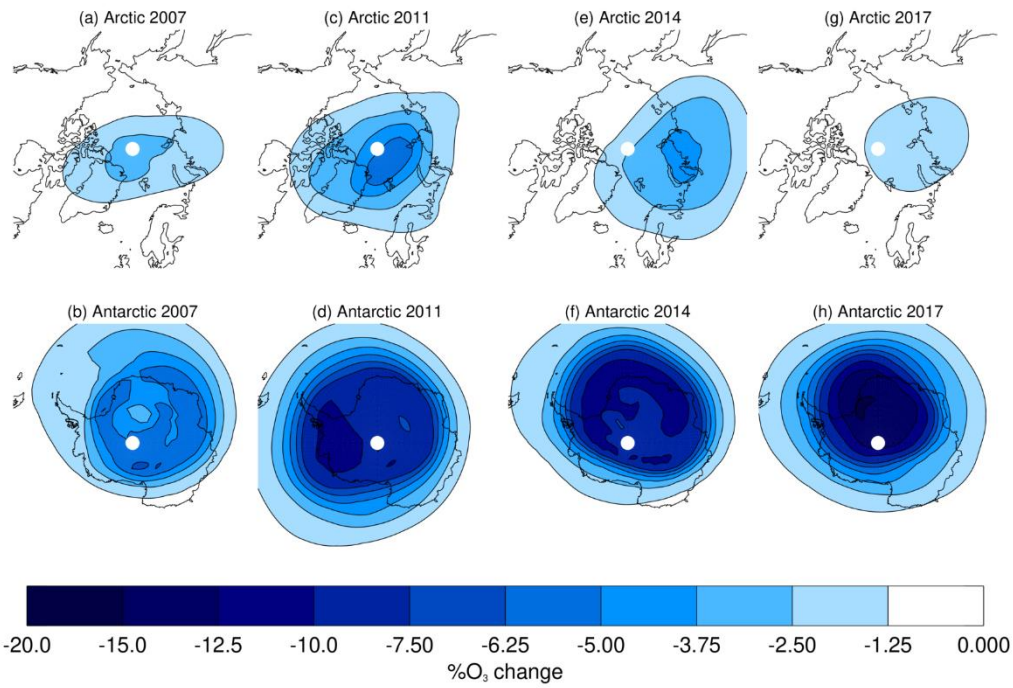

Figure 5.8. Polar spring ozone changes (%) between the two SLIMCAT VSLS scenarios, over the lower stratosphere (50 hPa) for four different years. March and October are the months chosen for Arctic and Antarctic springs, respectively.

Comparing model runs with and without Cl-VSLS is important in quantifying the extent of ozone depletion caused by Cl-VSLS. However, it is equally important to check if including Cl-VSLS chemistry leads to better agreement to observations. Ozone satellite data from ACE-FTS (Atmospheric Chemistry Experiment Fourier Transform Spectrometer) [Bernath et al., 2005; Hegglin et al., 2008] has been used to compare with SLIMCAT model output on previous occasions [Griffin et al., 2019; Singleton et al., 2007]. **Figure 5.9** compares the two SLIMCAT model outputs with ACE-FTS observations over three locations: the Arctic, in March; the Antarctic, in October; and the tropics, annually averaged. All three comparisons were performed over 2007-2017. Unfortunately, the ACE-FTS instrument does not observe ozone polewards of 70° latitude at all times [Bernath et al., 2005]. As a large proportion of the depletion of ozone caused by Cl-VSLS occurs over the poles, these comparisons are not able to take all of this impact into account. Both the available observations and model outputs are in fairly good agreement in

Figure 5.9, when taking into account the large uncertainty ranges. However, it is very difficult to distinguish between the two model outputs, due to the small percentage differences highlighted in **Table 5.9**, even in the Antarctic lower stratosphere. Generally, **Figure 5.9** suggests that the model outputs overestimate the observations towards the lower stratosphere. Because of this overestimation, including VSLS into SLIMCAT slightly increases the model performance, owing to the decreases in ozone caused by including VSLS shown in **Figure 5.7**. Conversely, in the upper stratosphere, the model outputs tend to underestimate the observations.

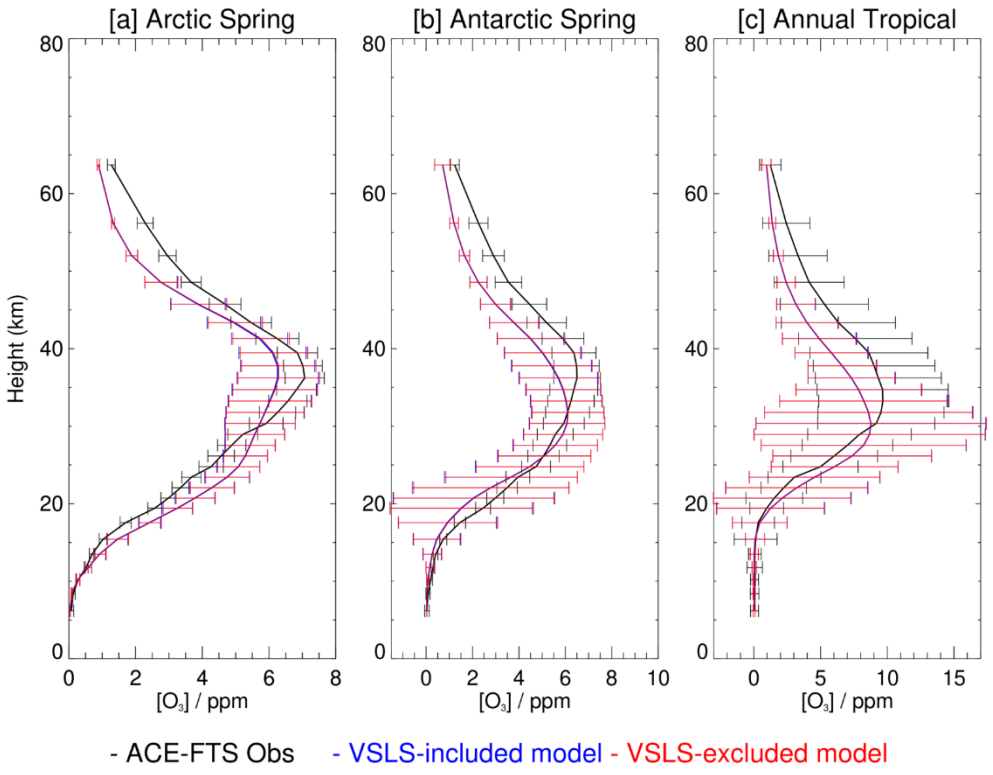

Figure 5.9. Ozone/height profiles comparing SLIMCAT model outputs with and without Cl-VSLS with ACE-FTS observations in: (a) the Arctic (60-70°N), in March; (b) the Antarctic (60-70°S), in October; (c) and the tropics (30°N - 30°S), over a whole year, all averaged over 2007-2017. In (a) and (b) the error bars represent ±2 standard deviations for each dataset. In (c) the error bars represent ±1 std. dev.

Table 5.9. Differences in ozone between a model run with Cl-VSLS included and one with Cl-VSLS excluded, expressed as (a) global zonal mean % change through the LS (lower stratosphere, 50 hPa), (b) mean % change over the Antarctic (60°S-90°S) LS, (c) mean % change over the Antarctic LS in October (d) global zonal mean % ozone change through the US (upper stratosphere, 5 hPa), (e) global mean column change (DU), (f) mean column change over the Antarctic (60°S-90°S, DU), and (g) global mean % column change.

Year	2007	2008	2009	2010	2011	2012	2013	2014	2015	2016	2017
(a): %O_3 change, LS	-0.45	-0.49	-0.44	-0.43	-0.47	-0.48	-0.48	-0.51	-0.51	-0.55	-0.56
(b): %O_3 change, Ant. LS	-0.89	-1.01	-0.89	-0.95	-1.10	-0.93	-1.04	-1.02	-1.19	-1.06	-1.19
(c): %O_3 change, Ant. LS Oct	-1.30	-2.37	-1.27	-2.63	-3.73	-1.85	-2.53	-2.17	-5.17	-2.44	-3.16
(d): %O_3 change, US	-0.32	-0.31	-0.32	-0.34	-0.33	-0.35	-0.36	-0.36	-0.38	-0.40	-0.40
(e): O_3 column, global (DU)	-0.98	-1.01	-0.96	-0.98	-1.02	-1.05	-1.05	-1.13	-1.14	-1.22	-1.23
(f): O_3 column, Ant. (DU)	-2.20	-2.35	-2.27	-2.45	-2.54	-2.75	-2.98	-2.91	-2.96	-3.03	-3.44
(g): %O_3 column, global	-0.33	-0.35	-0.33	-0.33	-0.35	-0.36	-0.36	-0.38	-0.39	-0.42	-0.41

5.4.3.2 Column Ozone Changes

A useful concept for studying ozone changes is *column* ozone. This is a measure of how much ozone is situated over a unit area and is reported in Dobson Units, where 1 DU is 0.01 mm of ozone if the vertical column of ozone was brought down to surface temperature and pressure. Natural levels of column ozone are approximately 300 DU; however, over the Antarctic during

spring, can fall down to <200 DU [Langematz et al., 2018]. **Figure 5.10(a)** depicts the modelled change in the geographical distribution of column ozone due to Cl-VSLS in 2017. **Figure 5.10(b)** shows the change in October 2017, the peak of Antarctic spring ozone loss. The column ozone changes in **Figure 5.10(a)** are fairly uniform zonally, and the three main areas of the two polar regions and the tropics can be identified. There is little annual mean tropical column ozone change due to Cl-VSLS, a relatively large Antarctic decrease (averaging -3.4 DU, minimum -3.9 DU), and smaller Arctic decreases (reaching -2.1 DU). Similarly, in **Figure 5.10(b)**, this Antarctic decrease is deepened (to a minimum of -6.9 DU) when just considering October, and the Arctic decrease is lessened (to a minimum -1.2 DU). In March, Arctic column ozone differences deepen to -5.0 DU. Globally the difference in mean column ozone between the two scenarios is -1.23 DU in 2017, or -0.41% of global total column ozone.

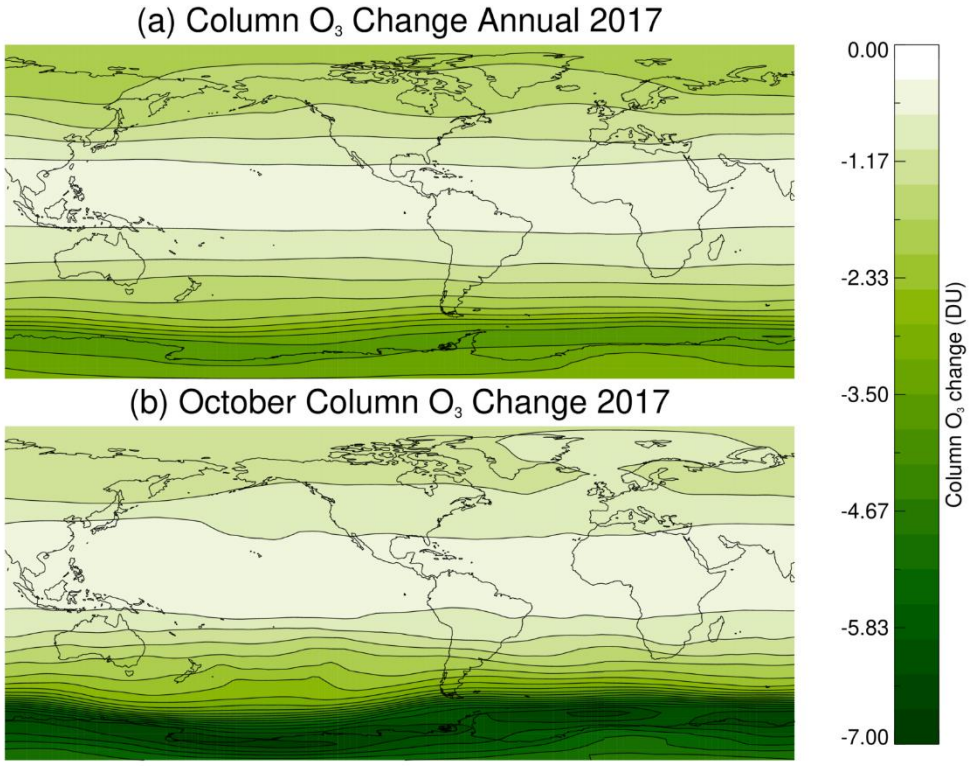

Figure 5.10. Column ozone difference (DU) between SLIMCAT model runs with Cl-VSLS and without, expressed as (a) an annual average for 2017 and (b) an October 2017 average.

The time series of column ozone change due to Cl-VSLS can also be studied (**Figure 5.11**). With increasing Cl-VSLS, it is likely that the southern hemisphere decrease will become larger year upon year, as should be the case globally. **Table 5.9** calculates the column ozone change between the two model scenarios globally, and over the Antarctic (60°S to 90°S), for each year of study. Column ozone change due to Cl-VSLS decreases at a rate of roughly -0.03 DU yr^{-1} globally, and at a rate of -0.10 DU yr^{-1} over the Antarctic. The 2018 WMO Ozone Assessment Report have assessed Antarctic ozone recovery to be occurring at a rate of about 0.5-1.0 DU yr^{-1}, between 2000 and 2020 [Langematz et al., 2018]. The -0.10 DU yr^{-1} decrease due to Cl-VSLS therefore represents a small, but not insignificant, counteraction against this recovery.

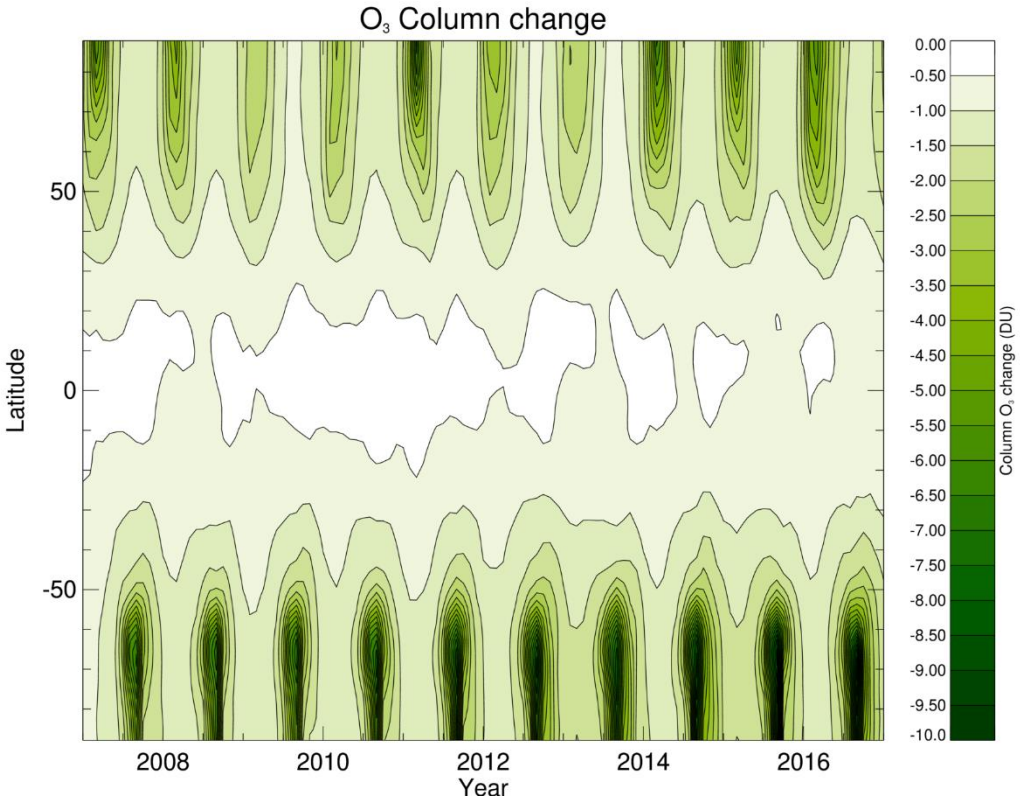

Figure 5.11. Modelled zonally averaged column ozone change (DU) between the two Cl-VSLS scenarios as a function of latitude.

Figure 5.11 plots a time series of monthly column ozone change due to Cl-VSLS as a function of latitude, which allows for the depiction of the seasonal cycle of ozone depletion. The sheer decreases in ozone during Antarctic (and Arctic) spring are fully evident here. However, the fairly small rate of change of the difference in global column ozone between the two Cl-VSLS scenarios, of -0.03 DU yr^{-1} over the 11 years, shows how difficult it is to note significant decreases from year to year, and even the -0.10 DU yr^{-1} trend over Antarctica is only a tiny fraction (1-1.5%) of the maximum extent of column ozone loss (which varies from -7.0 to -9.9 DU over the 11 years). Over the Arctic, the interannual variation seen in **Figure 5.8** is far more striking, with the 2011 Arctic ozone hole event noticeably standing out, and approaching levels of Antarctic ozone depletion [e.g. Manney et al., 2011].

5.5 Conclusions

Overall, we have quantified the impacts of transient Cl-VSLS emissions on stratospheric ozone from utilisation of a chemistry transport model, which required a new estimation of global emissions of $CHCl_3$ from 2006-2017. Our main findings are the following:

- A fully empirical estimate of global gridded $CHCl_3$ emissions, based on literature values and industrial estimates was developed. When used in the TOMCAT CTM, the emission field provides fairly good agreement with observational data, particularly at NH sites and when comparing with aircraft mission data. Global emissions of $CHCl_3$ are estimated as 355 ± 120 Gg yr^{-1} in 2006, rising to 416 ± 120 Gg yr^{-1} in 2017, with the source of this increase pertaining to increases in East Asian emissions. Natural sources, from oceans and soil, comprise 73-86% of total emissions, and there is a strong natural seasonality of emissions. Further work in refining recent industrial emission trends may help with the model underestimation of $CHCl_3$ compared with observations at Asian sites.

- Using these $CHCl_3$ emissions, in combination with literature estimates of global CH_2Cl_2 and C_2Cl_4 emissions [Claxton et al., 2020], the TOMCAT

CTM was used to track Cl-VSLS source gases and key product gases (phosgene and Cl_y) and to determine the amount of chlorine that enters the stratosphere. We estimate that total stratospheric chlorine from Cl-VSLS (CH_2Cl_2, $CHCl_3$ and C_2Cl_4) increased from 92.3 ± 8.0 ppt Cl in 2006 to 132.1 ± 8.9 ppt Cl in 2017. These values are within the estimated range from the most recent WMO Scientific Assessment of Ozone Depletion, of 89.9-141.1 ppt Cl in 2016 from the same three Cl-VSLS. We estimate that product gas injection contributes 26.6% of the total chlorine injection, with source gases accounting for the remaining 73.4%. Of the total chlorine source gas injection, CH_2Cl_2 provides 70.7% of the total and $CHCl_3$ provides 25.8%, in 2017. There are many other known Cl-VSLS, but for which accurate emission estimates are not known (e.g. $C_2H_4Cl_2$). Hence, the true contribution of Cl-VSLS to stratospheric chlorine is likely larger than modelled here.

- The SLIMCAT stratospheric model was used to quantify Cl-VSLS impacts on ozone, using the calculated tropopause chlorine injections due to CH_2Cl_2, $CHCl_3$, C_2Cl_4, and products. Two scenarios were devised, one with these stratospheric chlorine injections, and one without any Cl-VSLS sources. Global annual mean lower stratosphere ozone loss due to Cl-VSLS was found to be -0.56% in 2017, reaching -1.19% over the Antarctic (60°-90°S). For October, the peak month of lower stratosphere Antarctic ozone loss, the percentage loss of ozone in 2017 extended to -18% at its maximum, just from this consideration of Cl-VSLS. Ozone column data provided a more absolute change throughout the atmosphere, with the inclusion of Cl-VSLS leading to a loss of global ozone column of -1.23 DU in 2017, and -3.44 DU over Antarctica in the same year. The transient nature of ozone loss was also studied, with the difference in global column ozone between the two Cl-VSLS scenarios decreasing at a rate of -0.03 DU yr^{-1}.

In conclusion, rising Cl-VSLS emissions since the mid-2000s have caused a steady increase in the injection of chlorine into the stratosphere, and in turn have contributed to a decrease in lower stratospheric ozone, predominantly

over Antarctica. These ozone losses act against the ozone recovery predicted as a result of the Montreal Protocol prohibiting long-lived ozone depleting substances, and therefore it is paramount that more investigation of Cl-VSLS (e.g. identifying new compounds) and their impacts is performed. In particular, results from other models should be used to supplement this single model study.

Chapter 6

Conclusions and outlook

This thesis has generated novel information about emissions of Chlorinated Very Short-Lived Substances (Cl-VSLS) and their impacts on stratospheric ozone. Chapter 2 presented an overview of the dynamical and chemical processes that govern ozone production and loss in the atmosphere, with particular focus on chlorine chemistry. This chapter detailed the changing state of stratospheric composition as a consequence of ozone depleting substances (ODSs), and introduced the role that Cl-VSLS perform in atmospheric composition, and in stratospheric ozone destruction. Existing knowledge of Cl-VSLS emissions, uses, and abundances are described, their specific chemistry in the troposphere, and potential impacts in the stratosphere.

Chapter 3 presented an analysis of the Ozone Depletion Potential (ODP) of four major Cl-VSLS: Dichloromethane (CH_2Cl_2), chloroform ($CHCl_3$), perchloroethylene (C_2Cl_4), and ethylene dichloride ($C_2H_4Cl_2$). These four compounds are among the most abundant Cl-VSLS in the troposphere, yet for two of them, CH_2Cl_2 and $C_2H_4Cl_2$, there had been no accurate estimation of their ODPs. The ODPs of the Cl-VSLS were calculated using the TOMCAT/SLIMCAT 3-D chemical transport model (CTM). Briefly the TOMCAT model configuration was used to calculate the steady state stratospheric injection of each Cl-VSLS and CFC-11 due to a unit emission (in Tg yr^{-1}) of each from different geographical regions. These injections were then used in the SLIMCAT model configuration to investigate their impact on ozone (as per the ODP definition, see Chapter 3).

Chapter 3 derived ODPs on a regional and seasonal basis, considering five of the most significant industrial emitting regions. It was discovered that there was very little seasonal variability, and the ODPs instead greatly depended on the geographical region of emission. Emissions from Tropical Asia were found to lead to the largest ODP, due to its prime location to deep convective systems over the Maritime Continent and West Pacific. Here ODPs were between 40% and 250% greater than from other world regions, depending on the specific Cl-

VSLS. Emissions from Temperate Asia, the region thought to be central to increasing anthropogenic emissions of Cl-VSLS, led to a higher than average ODP. The ODP of $CHCl_3$ ranged from 0.0143-0.0264, which is approaching the ODP of some substances already proscribed by the Montreal Protocol, e.g. HCFC-22. The ODP of CH_2Cl_2 is 0.0097-0.0208, for C_2Cl_4 it is 0.0057-0.0198, and for $C_2H_4Cl_2$ it is 0.0029-0.0119. This novel ODP information should prove useful to scientists and policymakers looking to assess the significance of growing Cl-VSLS emissions in future years.

Chapter 4 investigated the emissions of two of the main Cl-VSLS: CH_2Cl_2, and C_2Cl_4. Previous emissions of Cl-VSLS have been poorly quantified, and with rising atmospheric CH_2Cl_2 concentrations, it is important to determine the region(s) driving this trend. For this chapter, this was performed by a technique called 'synthesis inversion'. The technique is used to optimise a gridded set of surface emissions by assimilating atmospheric observations, in conjunction with output from a global 3-D CTM that uses a prior emission estimate. This prior estimate was amalgamated from available industry estimates and literature calculations from the 1990s. The observations assimilated were from the NOAA and AGAGE surface monitoring networks, and TOMCAT was used to generate the concentration model output. The synthesis inversion was performed over a 12-year period from 2006-2017 to investigate how emissions have changed over time, in addition to any regional variability.

The inversion results show that global total CH_2Cl_2 emissions increased over the 12 years, from 637 ± 36 Gg yr^{-1} in 2006 to 1171 ± 45 Gg yr^{-1} in 2017. This was due to emission increases over Asia, which have changed from 431.3 ± 32.2 to 1044.9 ± 40.4 Gr yr^{-1}. Corollary, there were slight decreases in emissions over Europe and North America, two historically key CH_2Cl_2 producing regions whose productions have declined due to market shifts and health concerns over CH_2Cl_2 use. C_2Cl_4 emissions had been under steady decline for decades, and this chapter details that between 2007 and 2017, global emissions decreased from 140.8 ± 13.8 to 106.1 ± 12.0 Gg yr^{-1}, primarily due to decreases in Europe and North America; however, Asian emissions have remained relatively constant.

Calculated global emissions of both Cl-VSLS were compared to estimates reported in the 2018 WMO/UNEP Scientific Assessment of Ozone Depletion Report using a simpler 12-box model. These inversion results were found to lie within the uncertainty ranges. The posterior emissions were evaluated within TOMCAT by comparing model output with observations, in order to determine the success of the inversion process. As expected, the observations that were assimilated were captured well by the posterior model output, and additionally, the model output performed almost equally as well against independent observations that were 'held back' for verification. The results also included a test for the veracity of CH_2Cl_2 ocean sources, where it was concluded that there is no evidence for or against ocean emission fluxes existing as a significant source of CH_2Cl_2. Furthermore, an additional test scenario was developed to investigate the impact of adding a competing C_2Cl_4 loss reaction, with Cl. The base inversion does not include it, as tropospheric Cl concentrations are uncertain; however, this scenario calculated a 50% increase in C_2Cl_4 emissions as a result, and marginally improved performance when comparing to observations.

Chapter 5 built on the previous chapter and considered the impact that changing Cl-VSLS emissions have had on stratospheric injection of chlorine. First, a simple 12-year amalgamation of $CHCl_3$ emissions was derived from literature estimates of natural sources and Asian emissions, and industry estimates for other key $CHCl_3$ producing regions. The total derived global $CHCl_3$ emission rate was 354.8 ± 120 Gg yr^{-1} in 2006 and 416.1 ± 120 Gg yr^{-1} in 2017. These emissions were gridded and implemented in the TOMCAT CTM for evaluation, and found to perform reasonably well at reproducing available global AGAGE observations. Despite not being calculated by an inverse modelling process, the $CHCl_3$ emissions performed equally as well as for CH_2Cl_2 and C_2Cl_4 in the preceding chapter.

In Chapter 5 the TOMCAT/SLIMCAT modelling framework from Chapter 3 was then used to calculate the time-varying injections of Cl-VSLS and their products into the stratosphere, and the resulting ozone changes, from 2007 to 2017. The total stratospheric chlorine injection due to Cl-VSLS and their products was found to have increased at a rate of 4.2 ppt Cl yr^{-1} over the study period, totalling

132.1 ± 8.9 ppt Cl in 2017. For comparison, the 2018 WMO/UNEP Ozone Assessment Report estimated total stratospheric chlorine from Cl-VSLS to be 89.9-141.1 ppt Cl. The SLIMCAT model was used to calculate the ozone change resulting from the above Cl injections; i.e. comparing a scenario with Cl-VSLS and one with no Cl-VSLS. Between the two cases, lower stratosphere ozone changed by -0.56% in 2017 due to Cl-VSLS alone, expressed as a global annual mean. Over Antarctica, where the seasonal ozone hole forms, this ozone difference reached -1.19%, also as an annual mean, though a larger October change was found (-3.2% on average, but up to a -18% minimum). This chapter also calculated a difference in global mean column ozone of -1.23 DU when comparing the two scenarios in 2017, decreasing at a rate of -0.03 DU yr^{-1} between 2007 and 2017.

Overall, in this thesis I quantified ODP values for several influential Cl-VSLS, some for the first time, and showed that there is significant variation in ODP due to region of emission. I demonstrated that global emissions of CH_2Cl_2 have increased rapidly, mostly due to Asian emissions, the most important region for ozone depletion potential. The emission fields produced in this work have been successfully evaluated using a range of observations and found to accurately capture observational trends, in addition to being verified to current literature estimates. My gridded emissions represent the most up-to-date best estimate of Cl-VSLS emissions and should prove useful to other modelling groups. Finally, I have demonstrated the atmospheric impact that these uncontrolled Cl-VSLS have had on ozone to date, using the emission estimates that I had calculated. My results show that Cl-VSLS have had a significant impact on stratospheric ozone loss.

Considerations for further research

Uncontrolled emissions of Cl-VSLS are one of the main policy-relevant issues in stratospheric ozone research at present. As the atmospheric abundance of key controlled ozone depleting compounds (e.g. CFCs) declines – due to the success of the Montreal Protocol – substances that were once considered unimportant become increasingly prominent as their relative importance rises.

However, due to Cl-VSLS research only being explored in recent decades, atmospheric observations and information on emissions are limited and subject to uncertainty. Ethylene dichloride ($C_2H_4Cl_2$) and trichloroethylene (C_2HCl_3) are two Cl-VSLS often included in WMO Ozone Assessments, but with very limited emissions information and measurement data, investigations into global emissions and their impacts are not easily achievable.

There is also a large sector of compounds that we know even less about. Several very short-lived chlorocarbon compounds have been found to exist in high levels (approaching ppb levels of concentration) in urban locations, for example 1,2-dichloropropane and vinyl chloride. As well as the importance of studying urban environments on a human health basis, these large abundances of “minor” Cl-VSLS may have wider impacts on tropospheric (and potentially stratospheric) composition. These include the altering of the chlorine budget of the troposphere. The release of more Cl radicals allows for additional oxidative capacity, with consequences towards surface ozone production and air pollution.

Outside of Cl-VSLS, there are several other challenges towards ozone recovery that must be considered as part of a greater picture. Sulphate geoengineering strategies, in which sulphate aerosol precursor compounds such as SO_2 and H_2S are hypothetically injected into the stratosphere in order to increase scattering of solar radiation, have dangerous potential consequences towards stratospheric ozone chemistry. Aerosols are key sites for heterogeneous chemistry, particularly regarding polar ozone depletion, and any implemented schemes are likely to exacerbate depletion. Other threats to stratospheric ozone include increasing anthropogenic sources of N_2O, the main source of stratospheric NO_x, and rogue emissions of CFCs. These both will act to decrease the expected recovery rate of stratospheric ozone.

Despite their considerable contribution to total Cl-VSLS emissions, there is a general lack of understanding of natural emissions, and there are inadequate measurement campaigns and data to get to the bottom of the issue. Until these problems are fixed, emission inventories will always be uncertain in this regard. Another source of uncertainty has come from the distribution of industrial Cl-

VSLS emissions. Generally, it has been assumed that distributions of CH_2Cl_2 and C_2Cl_4 emissions are identical, which although is unlikely to be the case, we have no data to suggest otherwise. Another problem arises from distributions changing rapidly with time, particularly within East Asia. The ability to create accurate Cl-VSLS emissions maps at a high spatial and temporal resolution would greatly assist any future Cl-VSLS-focused impact studies, both locally and globally.

Observational data has been vital for testing the validity of the results from the synthesis inversion process. Despite fairly good global coverage from the NOAA and AGAGE networks, there were problems with some of the regions lacking any observational data. Although these regions were not thought to be significant sources of Cl-VSLS emissions (e.g. Africa, Siberia and South America), the synthesis inversion process would have a tendency of shifting emissions towards or away from these regions that have little constraint. Unfortunately, observations from aircraft campaigns are very short-term, not spatially fixed, and are therefore difficult to successfully assimilate in a synthesis inversion. A first step would be to support measurements of Cl-VSLS in poorly sampled regions (e.g. developing countries in Africa and Latin America).

Nonetheless, the development of Cl-VSLS emissions allows us to further constrain their atmospheric impacts. As more and more short- and long-term observational studies are undertaken, our understanding of Cl-VSLS can only grow. New observations can be implemented in the synthesis inversion process when available, and this will extend the yearly record of emission estimates. Additional short-term observations, particularly from aircraft campaigns, can supplement the results from the extended inversion. For Cl-VSLS such as $CHCl_3$, it may be possible that in the future enough observations exist such that a synthesis inversion process can effectively estimate regional emissions.

Higher resolution models would also greatly assist any impact studies of tropospheric Cl-VSLS. Improvements in horizontal resolution would allow for a more accurate treatment of sub-grid scale transport processes, including convection. Additionally, improvements in vertical resolution can lead to better description of boundary layer and processes occurring in the climate-relevant

near-tropopause region. High resolution regional models can be set up using boundary conditions from a global concentration output e.g. what I generated in Chapter 5. Regional models are far more able to determine local sources of emission, as well as any potential impacts Cl-VSLS have on human activity, particularly in urban environments. Consequently, it would be of significant policy interest to research how the composition of the troposphere and urban environments varies with Cl-VSLS emissions. Overall, the work of this thesis already has important policy implications towards stratospheric considerations of Cl-VSLS, and can be used in tandem with the breadth of ongoing research on this ever-expanding discipline.

Bibliography

Agency for Toxic Substances and Disease Registry. (1997). *Toxicological profile for chloroform*. Public Health Service, U.S. Department of Health and Human Services, Atlanta, GA. [online] Available at: https://www.atsdr.cdc.gov/ToxProfiles/tp6.pdf [Accessed 23/09/2020]

Andrews, S. J., Hackenberg, S. C., & Carpenter, L. J. (2015). Technical Note: A fully automated purge and trap GC-MS system for quantification of volatile organic compound (VOC) fluxes between the ocean and atmosphere, *Ocean Science*, **11**, 313-321, doi:10.5194/os-11-313-2015.

Andrews, S. J., Carpenter, L., Apel, E., Atlas, E., Donets, V., Hopkins, J. R., et al. (2016). A comparison of very short lived halocarbon (VSLS) and DMS aircraft measurements in the tropical west Pacific from CAST, ATTREX and CONTRAST, *Atmospheric Measurement Techniques*, **9**, 5213-5225. doi.10.5194/amt-9-5213-2016.

Arnold, S. R., Chipperfield, M. P., & Blitz, M. A. (2005). A three-dimensional model study of the effect of new temperature-dependent quantum yields for acetone photolysis, *Journal of Geophysical Research: Atmospheres*, **110**, doi:10.1029/2005JD005998.

Aschmann, J., Sinnhuber, B.-M., Chipperfield, M. P., & Hossaini, R. (2011). Impact of deep convection and dehydration on bromine loading in the upper troposphere and lower stratosphere, *Atmospheric Chemistry and Physics,* **11**, 2671-2687. doi:10.5194/acp-11-2671-2011.

Ashfold, M. J., Pyle, J. A., Robinson, A. D., Meneguz, E., Nadzir, M. S. M., Phang, S. M., et al. (2015). Rapid transport of East Asian pollution to the deep tropics. *Atmospheric Chemistry and Phys*ics, **15**(6), 3565-3573. doi:10.5194/acp-15-3565-2015.

Aucott, M, L., McCulloch, A., Graedel, T. E., Kleiman, G., Midgley, P., & Li, Y.-F. (1999). Anthropogenic emissions of trichloromethane (chloroform, $CHCl_3$) and chlorodifluoromethane (HCFC-22): Reactive Chlorine Emissions Inventory, *Journal of Geophysical Research: Atmospheres*, **104**, doi:10.1029/1999JD900053.

Baker, D. F., Law, R. M., Gurney, K., Rayner, P., Peylin, P., Denning, A. S., et al. (2006). TransCom 3 inversion intercomparison: Impact of transport model errors on the interannual variability of regional CO_2fluxes, 1988-2003, *Global Biogeochemical Cycles*, **20**(1), [GB1002]. doi:10.1029/2004GB002439.

Barletta, B., Meinardi, S., Simpson, I. J., Rowland, F. S., Chan, C.-Y., et al. (2006). Ambient halocarbon mixing ratios in 45 Chinese cities, *Atmospheric Environment*, **40**, 7706-7719. doi:10.1016/j.atmosenv.2006.08.039.

Bates, D. R., & Nicolet, M. (1950). The photochemistry of atmospheric water vapor, *Journal of Geophysical Research*, **55**, doi:10.1029/JZ055i003p00301.

Bergman, J. W., Jensen, E. J., Pfister, L., & Yang, Q. (2012). Seasonal differences of vertical-transport efficiency in the tropical tropopause layer: On the interplay between tropical deep convection, large-scale vertical ascent, and horizontal circulations, *Journal of Geophysical Research,* **117**(D5), D05302. doi:10.1029/2011JD016992.

Bernath, P. F., McElroy, C. T., Abrams, M. C., Boone, C. D., Butler, M., Camy-Peyret, M., et al. (2005). Atmospheric Chemistry Experiment (ACE): Mission overview, *Geophysical Research Letters*, **32**, L15S01. doi:10.1029/2005GL022386.

Bousquet, P., Yver, C., Pison, I., Li, Y. S., Fortems, A., Hauglustaine, D., et al. (2011). A three-dimensional synthesis inversion of the molecular hydrogen cycle: Sources and sinks budget and implications for the soil uptake, *Journal of Geophysical. Research*, **116**, D01302. doi:10.1029/2010JD014599.

Brewer, A. W. (1949). Evidence for a world circulation provided by the measurements of helium and water vapour distribution in the stratosphere, *Quarterly Journal of the Royal Meteorological Society*, **75**, doi:10.1002/qj.49707532603

Bridgeman, C. H., Pyle, J. A., & Shallcross, D. E. (2000). A three-dimensional model calculation of the ozone depletion potential of 1-bromopropane (1-C_3H_7Br), *Journal of Geophysical Research*, **105**, 26493-26502. doi:10.1029/2000JD900293.

Brioude, J., Portmann, R. W., Daniel, J. S., Cooper, O. R., Frost, G. J., Rosenlof, K. H., et al. (2010). Variations in ozone depletion potentials of very short-lived substances with season and emission region, *Geophysical Research Lett*ers, **37**, L19804. doi:10.1029/2010GL044856.

Brunner, D., Staehelin, J., Rogers, H. L., Köhler, M. O., Pyle, J. A., Hauglustaine, D., et al. (2003). An evaluation of the performance of chemistry transport models by comparison with research aircraft observations. Part 1: Concepts and overall model performance, *Atmospheric Chemistry and Physics*, **3**(5), 1609-1631. doi:10.5194/acp-3-1609-2003.

Burkholder, J. B., Sander, S. P., Abbatt, J., Barker, J. R., Huie, R. E., Kolb, C. E., et al. (2015). Chemical kinetics and photochemical data for use in atmospheric studies, Evaluation number 18, *JPL Publication 15-10*, Jet Propulsion Laboratory, Pasadena. [online] Available at: http://jpldataeval.jpl.nasa.gov/. [Accessed 28 August 2020]

Butchart, N. (2014). The Brewer-Dobson circulation, *Reviews of Geophysics*, **52**, doi:10.1002/2013RG000448.

Carpenter, L. J., Reimann, S., Burkholder, J. B., Clerbaux, C., Hall, B. D., Hossaini, R., Laube, J. C., & Yvon-Lewis S. A. (2014). Update on ozone-depleting substances (ODSs) and other gases of interest to the Montreal

Protocol. In Chapter 1 of *Scientific assessment of ozone depletion: 2014, global ozone research and monitoring project – Report No. 58, World Meteorological Organization*, Geneva, Switzerland.

Catoire, V., Lesclaux, R., Schneider, W. F., & Wallington, T. J. (1996). Kinetics and mechanisms of the self-reactions of CCl_3O_2 and $CHCl_2O_2$ radicals and their reactions with HO_2, *Journal or Physical Chemistry*, **100**, 14356-14371. doi:10.1021/jp960572z.

Chapman, S. (1930). A theory of upper atmospheric ozone, *Memoirs of the Royal Meteorological Society*, **3**, 103-125.

Chen, Y.-H., & Prinn, R. G. (2006). Estimation of atmospheric methane emissions between 1996 and 2001 using a three-dimensional global chemical transport model, *Journal of Geophysical Research*, **111**, D10307. doi:10.1029/2005JD006058.

Chipperfield, M. P. (2006). New version of the TOMCAT/SLIMCAT off-line chemical transport model: Intercomparison of stratospheric tracer experiments, *Quarterly Journal of the Royal Meteorological Society*, **132**(617), 1179-1203. doi:10.1256/qj.05.51.

Chipperfield, M. P., Bekki, S., Dhomse, S., Harris, N. R. P., Hassler, B., Hossaini, R., et al. (2017). Detecting recovery of the stratospheric ozone layer, *Nature*, **549**, 211-218. doi:10.1038/nature23681.

Chipperfield, M. P., Lutman, E. R., Kettleborough, J. A., Pyle, J. A., & Roche, A. E. (1997). Model studies of chlorine deactivation of formation of ClONO2 collar in the Arctic polar vortex, *Journal of Geophysical Research*, **102**, 1467-1478. doi:10.1029/96JD00442.

Chipperfield, M. P., Dhomse, S., Hossaini, R., Feng, W., Santee, M. L., Weber, M., et al. (2018). On the cause of recent variations in lower stratospheric ozone, *Geophysical Research Letters*, **45**, 5718-5726. doi:10.1029/2018GL078071.

Cho, K., Tiwari, S., Agrawal, S. B., Torres, N. L., Agrawal, M., Sarkar, A., et al. (2011). Tropospheric ozone and plants: absorption, responses, and consequences, *Reviews of Environmental Contamination and Toxicology*, **212**, 61-111. doi:10.1007/978-1-4419-8453-1_3.

Claxton, T., Hossaini, R., Wild, O., Chipperfield, M. P., & Wilson, C. (2019). On the regional and seasonal ozone depletion potential of chlorinated very short-lived substances, *Geophysical Research Letters*, **46**(10), 5489-5498. doi:10.1029/2018GL081455.

Claxton, T., Hossaini, R., Wilson, C., Montzka, S. A., Chipperfield, M. P., Wild, O., et al. (2020). A synthesis inversion to constrain global emissions of two very short lived chlorocarbons: dichloromethane, and perchloroethylene, *Journal of Geophysical Research: Atmospheres*, **125**, doi:10.1029/2019JD031818.

Crutzen, P. J. (1970). The influence of nitrogen oxides on the atmospheric ozone content, *Quarterly Journal of the Royal Meteorological Society*, **96**, doi:10.1002/qj.49709640815.

Crutzen, P. J. (1974). Photochemical reactions initiated by and influencing ozone in unpolluted tropospheric air, *Tellus*, **26**, 44-55. doi:10.1111/j.2153-3490.1974.tb01951.x.

Cunnold, D. M., Prinn, R. G., Rasmussen, R. A., Simmonds, P. G., Alyea, F. N., Cardelino, C. A., et al. (1983). The atmospheric lifetime experiment: 3. Lifetime methodology and application to three years of $CFCl_3$ data, *Journal of Geophysical Research: Oceans*, **88**, 8379-8400. doi:10.1029/JC088iC13p08379.

Cuvelier, C., Thunis, P., Vautard, R., Amann, M., Bessagnet, B., Bedogni, M., et al. (2007). CityDelta: A model intercomparison study to explore the impact of emission reductions in European cities in 2010, *Atmospheric Environment*, **41**, 189-207. doi:10.1016/j.atmosenv.2006.07.036.

Danilin, M. Y., Sze, N.-D., Ko., M. K. W., Rodriquez, J. M. & Prather, M. J. (1996). Bromine-chlorine coupling in the Antarctic ozone hole, *Geophysical Research Letters*, **23**(2), doi:10.1029/95GL03783.

Davis, S. M., Rosenlof, K. H., Hassler, B., Hurst, D. F., Read, W. G., Vömel, H., et al. (2016). The Stratospheric Water and Ozone Satellite Homogenized (SWOOSH) database: a long-term database for climate studies, *Earth System Science Data*, **8**, 461-490. doi:10.5194/essd-8-461-2016.

Dee, D., Uppala, S., Simmons, A., Berrisford, P., Poli, P., Kobayashi, S., et al. (2011). The ERA-Interim reanalysis: Configuration and performance of the data assimilation system, *Quarterly Journal of the Royal Meteorological Society*, **137**(656), 553-597. doi:10.1002/qj.828.

Dhomse, S. S., Kinnison, D., Chipperfield, M. P., Salawitch, R. J., Cionni, I., Megglin, M. I., et al. (2018). Estimates of ozone return dates from chemistry-climate model initiative simulations, *Atmospheric Chemistry and Physics*, **18**(11), 8409-8438. doi:10.5194/acp-18-8409-2018.

Dobson, G. M. B. (1956). Origin and distribution of polyatomic molecules in the atmosphere, *Proceedings of the Royal Society*, **A236**, 187-193. doi:10.1098/rspa.1956.0127.

Dobson, G. M. B. (1968). Forty years' research on atmospheric ozone at Oxford: a history, *Applied Optics*, **7**, 387-405. doi:10.1364/AO.7.000387.

ECHA (2016). *Dichloromethane; methylene chloride – substance information – ECHA*. [online] Available at: https://echa.europa.eu/substance-information/-/substanceinfo/100.000.763 [Accessed 26 August 2020]

Engel, A., Atlas, E. L., Bernath, P. F., Bönisch, H., Brown, A., Laube, J., et al. (2013). Inferred lifetimes from observed trace-gas distributions. In Chapter 4 of *Lifetimes of stratospheric ozone-depleting substances, their replacements, and related species, SPARC Report No. 6, WCRP-15/2013*. [online] Available at: https://www.sparc-climate.org/publications/sparc-reports/sparc-report-no-6/ [Accessed 26 August 2020]

Engel, A., Rigby, M., Burkholder, J. B., Fernandez, R. P., Froidevaux, L., Hall, B. D., et al. (2018). Update on ozone-depleting substances (ODSs) and other gases of interest to the Montreal Protocol. In Chapter 1 of *Scientific assessment of ozone depletion: 2018, global ozone research and monitoring project-Report No. 55, World Meteorological Organization,* Geneva, Switzerland.

Enting, I. G., Trudinger, C. M., & Francey, R. J. (1995). A synthesis inversion of the concentration and $\mu^{13}C$ of atmospheric CO_2, *Tellus B: Chemical and Physical Meteorology*, **47**, 35-52. doi:10.3402/tellusb.v47i1-2.15998.

Environmental Protection Agency. (1995). *Qs & As on ozone-depleting solvents and their substitutes*. *Report No. EPA 430/R-95-019*. [online] Available at: https://nepis.epa.gov/Exe/tiff2png.cgi/50000S6R.PNG?-r+75+-g+7+D%3A%5CZYFILES%5CINDEX%20DATA%5C95THRU99%5CTIFF%5C00000344%5C50000S6R.TIF [Accessed 26 August 2020]

Environmental Protection Agency. (2014). *TSCA work plan chemical risk assessment for methylene chloride: paint stripping use*. Document No. 740-R1-4003. Cincinnati, Ohio: United States Environmental Protection Agency. [online] Available at: https://www.epa.gov/sites/production/files/2015-09/documents/dcm_opptworkplanra_final.pdf [Accessed 26 August 2020]

European Commission (2010). Commission Regulation (EU) No 276/2010 amending Commission Regulation (EC) No 1907/2006 as regards Annex XVII of REACH (dichloromethane, lamp oils and grill lighter fluids and organostannic compounds), *Official Journal of the European Union*, **L86**, 7-12. [online] Available at: https://eur-lex.europa.eu/LexUriServ/LexUriServ.do?uri=OJ:L:2010:086:0007:0012:EN:PDF [Accessed 26 August 2020]

Eyring, V., Cionni, I., Bodeker, G. E., Charlton-Perez, A. J., Kinnison, D. E., Scinocca, J. F., et al. (2010). Multi-model assessment of stratospheric ozone return dates and ozone recovery in CCMVal-2 models, *Atmospheric Chemistry and Physics*, **10** (19), 9451-9472. doi:10.5194/acp-10-9451-2010.

Falk, S., Sinnhuber, B.-M., Krysztofiak, G., Jöckel, P., Graf, P., & Lennartz, S. T. (2017). Brominated VSLS and their influence on ozone under a changing climate, *Atmospheric Chemistry and Physics*, **17**, 11313-11329. doi:10.5194/acp-17-11313-2017.

Fang, X., Park, S., Saito, T., Tunnicliffe, R., Ganesan, A. L., Rigby, M., et al. (2019). Rapid increase in ozone-depleting chloroform emissions from China, *Nature Geoscience*, **12**, 89-93. doi:10.1038/s41561-018-0278-2.

Farman, J. C., Gardiner, B. G., & Shanklin, J. D. (1985). Large losses of total ozone in Antarctica reveal seasonal ClO_x/NO_x interaction, *Nature*, **315**, 207-210. doi:10.1038/315207a0.

Feng, Y., Bie, P., Wang, Z., Wang, L., & Zhang, J., (2019). Bottom-up anthropogenic dichloromethane emission estimates from China for the period 2005-2016 and predictions of future emissions, *Atmospheric Environment*, **186**, 241-247. doi:10.1016/j.atmosenv.2018.05.039.

Fernandez R. P., Salawitch R. J., Kinnison D. E., Lamarque J. -F., & Saiz-Lopez A. (2014). Bromine partitioning in the tropical tropopause layer: Implications for stratospheric injection, *Atmospheric Chemistry and Physics*, **14**, 13,391-13,410. doi: 10.5194/acp-14-13391-2014.

Fu, D., Boone, C. D., Bernath, P. F., Walker, K. A., Nassar, R., Manney, G. L., & McLeod, S. D. (2007). Global phosgene observations from the atmospheric chemistry experiment (ACE) mission, *Geophysical Research Letters*, **34**(17), doi:10.1029/2007GL029942.

Gettelman, A., Hoor, P., Pan, L. L., Randel, W. J., Hegglin, M. I., & Birner, T. (2011). The extratropical upper troposphere and lower stratosphere, *Reviews of Geophysics*, **49**, doi:10.1029/2011RG000355.

Gettelman, A., Lauritzen, P. H., Park, M., & Kay, J. E. (2009). Processes regulating short-lived species in the tropical tropopause layer, *Journal of Geophysical Research*, **114**, D13303. doi:10.1029/2009JD011785.

Giannakopoulos, C., Chipperfield, M. P., Law, K. S., & Pyle, J. A. (1999). Validation and intercomparison of wet and dry deposition schemes using ^{210}Pb in a global three-dimensional off-line chemical transport model, *Journal of Geophysical Research: Atmospheres*, **104**, doi:10.1029/1999JD900392.

Giannakopoulos, C., Good, P., Law, K. S., Wang, K.-Y., Akylas, E. & Koussis, A. (2004). Rainfall parameterization in an off-line chemical transport model, *Atmospheric Science Letters*, **5**, 82-88. doi:10.1002/asl.68.

Griffin, D., Walker, K. A., Wohltmann, I., Dhomse, S. S., Rex, M., Chipperfield, M. P., et al. (2019). Stratospheric ozone loss in the Arctic winters between 2005 and 2013 derived with ACE-FTS measurements, *Atmospheric Chemistry and Physics*, **19**, 577-601. doi:10.5194/acp-19-577-2019.

Gurney, K. R., Law, R. M., Denning, A. S., Rayner, P. J., Baker, D., Bousquet, P., et al. (2003). Transcom 3 CO2 Inversion Intercomparison: 1. Annual mean

control results and sensitivity to transport and prior flux information, *Tellus Series B: Chemical and Physical Meteorology*, **55**, 555-579. doi:10.1034/j.1600-0889.2003.00049.x.

Hackenberg, S. C., Andrews, S. J., Airs, R., Arnold, S. R., Bouman, H. A., Brewin, R. J. W., et al. (2017). Potential controls of isoprene in the surface ocean, *Global Biogeochemical Cycles*, **31**, 644-662. doi:10.1002/2016GB005531.

Hardacre, C., Wild, O., & Emberson, L. (2015). An evaluation of ozone dry deposition in global scale chemistry climate models, *Atmospheric Chemistry and Physics*, **15**, 6419-6436. doi:10.5194/acp-15-6419-2015.

Harris, N. R. P., Carpenter, L. J., Lee, J. D., Vaughan, G., Filus, M. T., Jones, R. L., et al. (2017). Co-ordinated Airborne Studies in the Tropics (CAST), *B. American Meteorological Society*, **98**, doi:10.1175/BAMS-D-14-00290.1.

Harris, N. R. P., Wuebbles, D. J., Daniel, J. S., Hu, J., Kuijpers, L. J. M., et al. (2014). Scenarios and information for policymakers. Chapter 5 In *Scientific assessment of ozone depletion: 2014, global ozone research and monitoring project-Report No. 55, World Meteorological Organization,* Geneva, Switzerland.

Hartley, W. N. (1880). On the probable absorption of solar radiation by atmospheric ozone, *Chemistry News*, **42**.

Hartmann, D. L., Klein Tank, A. M. G., Rusticucci, M., Alexander, L. V., Brönnimann, S., Charabi, Y. A., et al. (2013). Observations: Atmosphere and surface. In Chapter 2 of *Climate Change 2013 the Physical Science Basis: Working Group I Contribution to the Fifth Assessment Report of the Intergovernmental Panel on Climate Change*, Cambridge University Press. doi:10.1017/CBO9781107415324.008.

Hase, E., & Kitano, M. (2013). Effectiveness verification of the main three amendments in law concerning the evaluation of chemical substances and regulation of their manufacture, etc. of Japan, *Japanese Journal of Risk Analysis*, **23**, 153-163. doi:10.11447/sraj.23.153.

Hegglin, M. I., Boone, C. D., Manney, G. L., Shepherd, T. G., Walker, K. A., Bernath, P. F., et al. (2008). Validation of ACE-FTS satellite data in the upper troposphere/lower stratosphere (UTLS) using non-coincident measurements, *Atmospheric Chemistry and Physics*, **8**, 1483-1499. doi:10.5194/acp-8-1483-2008.

Hofzumahaus, A., Kraus, A., Kylling, A., & Zerefos, C. S. (2002). Solar actinic radiation (280-420 nm) in the cloud-free troposphere between ground and 12 km altitude: Measurements and model results, *Journal of Geophysical Research: Atmospheres*, **107** (D18). doi:10.1029/2001JD900142.

Holbrook, M. T. (1993). Dichloromethane. In Kroschwitz, J. I., Howe-Grant, M. (Eds.), *Kirk-Othmer encyclopedia of chemical technology*, (Vol. 16, pp. 1041-1050). New York, NY: John Wiley. ISBN:978-0471484943.

Holtslag, A., & Boville, B. (1993): Local versus nonlocal boundary-layer diffusion in a global climate model, *Journal of Climate*, **6**, 1825-1842. doi:10.1175/1520-0442(1993)006<1825:LVNBLD>2.0.CO;2.

Hosking, J. S., Russo, M. R., Braesicke, P., & Pyle, J. A. (2010). Modelling deep convection and its impacts on the tropical tropopause layer, *Atmospheric Chemistry and Physics*, **10**(22), 11175-11188. doi:10.5194/acp-10-11175-2010.

Hossaini, R., Atlas, E., Dhomse, S. S., Chipperfield, M. P., Bernath, P. F., Fernando, A. M., et al. (2019). Recent trends in stratospheric chlorine from very short-lived substances, *Journal of Geophysical Research: Atmospheres*, **124**, doi:10.1029/2018JD029400.

Hossaini, R., Chipperfield, M. P., Monge-Sanz, B. M., Richards, N. A. D., Atlas, E., & Blake, D. R. (2010). Bromoform and dibromomethane in the tropics: A 3-D model study of chemistry and transport, *Atmospheric Chemistry and Physics*, **10**, 719-735. doi:10.5194/acp-10-719-2010.

Hossaini, R., Chipperfield, M. P., Montzka, S. A., Leeson, A. A., Dhomse, S. S., & Pyle, J. A. (2017). The increasing threat to stratospheric ozone from dichloromethane, *Nature Communications*, **8**, 1-9. doi:10.1038/ncomms15962.

Hossaini, R., Chipperfield, M. P., Saiz-Lopez, A., Fernandez, R., Monks, S., Feng, W., et al. (2016). A global model of tropospheric chlorine chemistry: Organic versus inorganic sources and impact on methane oxidation, *Journal of Geophysical Research: Atmospheres*, **121**, 14,271-14,297. doi:10.1002/2016JD025756.

Hossaini, R., Chipperfield, M. P., Saiz-Lopez, A., Harrison, J. J., von Glasow, R., Sommariva, R., et al. (2015).: Growth in stratospheric chlorine from short-lived chemicals not controlled by the Montreal Protocol, *Geophysical Research Letters*, **42**, 4573-4580. doi:10.1002/2015GL063783.

Hossaini, R., Mantle, H., Chipperfield, M. P., Montzka, S. A., Hamer, P., Ziska, F., et al. (2013). Evaluation global emission inventories of biogenic bromocarbons, *Atmospheric Chemistry and Physics*, **13**, 11819-11838. doi:10.5194/acp-13-11819-2013.

Hossaini, R., Patra, P. K., Leeson, A. A., Krysztofiak, G., Abraham, N. L., Andrews, S. J., et al. (2016). A multi-model intercomparison of halogenated very short-lived substances (TransCom-VSLS): Linking oceanic emissions and tropospheric transport for a reconciled estimate of the stratospheric source gas injection of bromine, *Atmospheric Chemistry Physics,* **16**, 9163-9187. doi:10.5194/acp-16-9163-2016.

Huijnen, V., William, J., van Weele, M., van Noije, T., Krol, M., Dentener, F., et al. (2010). The global chemistry transport model TM5: Description and evaluation of the tropospheric chemistry version 3.0, *Geoscience Model Development*, **3**, 445-473. doi:10.5194/gmd-3-445-2010.

International Agency for Research on Cancer (1986). Some halogenated hydrocarbons and pesticide exposures, *IARC Monographs on the Evaluation of Carcinogenic Risks to Humans*, **41**, 1-407, Lyon, France. ISBN:978-92-832-1241-6.

International Agency for Research on Cancer (1999). Re-evaluation of some organic chemicals, hydrazine and hydrogen peroxide, *IARC Monographs on the Evaluation of Carcinogenic Risk to Humans*, **71**, 1-315, Lyon, France. ISBN:978-92-832-1571-4.

International Agency for Research on Cancer (2014). Trichloroethylene, tetrachloroethylene, and some other chlorinated agents, *IARC Monographs on the Evaluation of Carcinogenic Risk to Humans*, **106**, 219-329, Lyon, France. ISBN:978-92-832-0172-8.

International Agency for Research on Cancer (2016). Some chemicals used as solvents and in polymer manufacture, *IARC Monographs on the Evaluation of Carcinogenic Risk to Humans*, **110**, 1-243, Lyon, France. ISBN:978-92-832-0176-2.

Jacob, D. J. (1999). *Introduction to Atmospheric Chemistry*. Princeton, New Jersey: Princeton University Press. ISBN:0-691-00185-5.

Jia, J., Rozanov, A., Ladstätter-Weißenmayer, A., & Burrows, J. P. (2015). Global validation of SCIAMACHY limb ozone data (versions 2.9 and 3.0, IUP Bremen) using ozonesonde measurements, *Atmospheric Measurement Techniques*, **8**, 3369-3383. doi:10.5194/amt-8-3369-2015.

Johnson, D. G., Traub, W. A., Chance, K. V., Jucks, K. W., & Stachnik, R. A. (1995). Estimating the abundance of ClO from simultaneous remote sensing measurements of HO_2, OH and HOCl, *Geophysical Research Letters*, **22**, 1869-1871. doi:10.129/95GL01249.

Johnson, M. T. (2010). A numerical scheme to calculate temperature and salinity dependent air-water transfer velocities for any gas, *Ocean Science*, **6**(4), 913-932. doi:10.5194/os-6-913-2010.

Jones, C. E., & Carpenter, L. J. (2005). Solar photolysis of CH2I2, CH2ICl, and CH2IBr in water, saltwater, and seawater, *Environmental Science and Technology*, **39**, 6130-6137. doi:10.1021/es050563g.

Keene, W. C., Khalil, M. A. K., Erickson III, D. J., McCulloch, A., Graedel, T. E., Lobert, J. M., et al. (1999). Composite global emissions of reactive chlorine from anthropogenic and natural sources: Reactive chlorine emissions inventory, *Journal of Geophysical Research*, **104**, 8429-8440. doi:10.1029/1998JD100084.

Khalil, M. A. K., Moore, R. M., Harper, D. B., Lobert, J. M., Erickson, D. J., Koropalov, V., Sturges, W. T., & Keene W. C., (1999). Natural emissions of

chlorine-containing gases: Reactive Chlorine Emissions Inventory, *Journal of Geophysical Research*, **104**(D7), 8333-8346. doi:10.1029/1998JD100079.

Khalil, M. A. K., & Rasmussen, R. A. (1999). Atmospheric Chloroform, *Atmospheric Environment*, **33**, 1151-1158. doi:10.1016/S1352-2310(98)00233-7.

Kindler, T. P., Chameides, W. L., Wine, P. H., Cunnold, D. M., Alyea, F. N., & Franklin, J. A. (1995). The fate of atmospheric phosgene and the stratospheric chlorine loadings of its parent compounds: CCl_4, C_2Cl_4, C_2Cl_3, CH_3CHCl_3, and $CHCl_3$, *Journal of Geophysical Research*, **100**, 1235-1251. doi:10.1029/94JD02518.

Ko, M. K. W., Poulet, G., Blake, D. R., Boucher, O., Burkholder, J. H., Chin, M., et al. (2003). Very short-lived halogen and sulfur substances. Chapter 2 In *Scientific assessment of ozone depletion: 2002, global ozone research and monitoring project – Report No. 47*, *World Meteorological Organization,* Geneva, Switzerland.

Kolusu, S. R., Schlünzen, K. H., Grawe, D., & Seifert, R. (2016). Chloromethane and dichloromethane in the tropical Atlantic Ocean, *Atmospheric Environment,* **150**, 417-424. doi:10.1016/j.atmosenv.2016.11.037.

Kolusu, S. R., Schlünzen, K. H., Grawe, D., & Seifert, R. (2018). Determination of chloromethane and dichloromethane in a tropical terrestrial mangrove forest in Brazil by measurements and modelling, *Atmospheric Environment*, **173**, 185-197. doi:10.1016/j.atmosenv.2017.10.057.

Krüger, K., Tegtmeier, S., & Rex, M. (2009). Variability of residence time in the Tropical Tropopause Layer during Northern Hemisphere winter, *Atmospheric Chemistry and Physics*, **9**(18), 6717-6725. doi:10.5194/acp-9-6717-2009.

Kuhn, M., Builtjes, P. J. H., Poppe, D., Simpson, D., Stockwell, W. R., Andersson-Sköld, Y., et al. (1998). Intercomparison of the gas-phase chemistry in several chemistry and transport models, *Atmospheric Environment*, **32**, 693-709. doi:10.1016/S1352-2310(97)00329-4.

Langematz, U., Tully, M., Calvo, N., Dameris, M., de Laat, A. T J., Klekociuk, A., et al. (2018). Polar stratospheric ozone: Past, present, and future. Chapter

4 In *Scientific assessment of ozone depletion: 2018, global ozone research and monitoring project – Report No. 58, World Meteorological Organization,* Geneva, Switzerland.

Lary, D. J. (1997). Catalytic destruction of stratospheric ozone, *Journal of Geophysical Research*, **102**, 21515-21526. doi:10.1029/97JD00912.

Laube, J. C., Engel, A., Bönisch, H., Möbius, T., Worton, D. R., Sturges, W. T., et al. (2008). Contribution of very short-lived organic substances to stratospheric chlorine and bromine in the tropics - a case study, *Atmospheric Chemistry and Physics*, **8**, 7325-7334. doi:10.5194/acp-8-7325-2008.

Law, K. S., Sturges, W. T., Blake, D. R., Blake, N. J., Burkholder, J. B., Butler, J. H., et al. (2006). Halogenated very short-lived substances. Chapter 2 in *Scientific assessment of ozone depletion: 2006, global ozone research and monitoring project – Report No. 50, World Meteorological Organization*, Geneva, Switzerland.

Law, R. M., Peters, W., Rodenbeck, C., Aulagnier, C., Baker, I., Bergmann, D. J., Bousquet, P., & Brandt, J. (2008). TransCom model simulations of hourly atmospheric CO_2: Experimental overview and diurnal cycle results for 2002, *Global Biogeochemical Cycles*, **22**, GB3009. doi:10.1029/2007/GB003050.

Lawler, M. J., Sander, R., Carpenter, L. J., Lee, J. D., von Glasow, R., Sommariva, R., & Saltzman, E. S. (2011). HOCl and Cl_2 observations in marine air, *Atmospheric Chemistry and Physics*, **11**, 7617-7628. doi:10.5194/acp-11-7617-2011.

Lawson, S. J., Keywood, M. D., Galbally, I. E., Gras, J. L., Cainey, J. M., Cope, M. E., et al. (2015). Biomass burning emissions of trace gases and particles in marine air at Cape Grim, Tasmania, *Atmospheric Chemistry and Physics*, **15**, 13393-13411. doi:10.5194/acp-15-13393-2015.

Lee-Taylor, J. M., Doney, S. C., Brasseur, G. P., & Müller, J.-F. (1998). A global three-dimensional atmosphere-ocean model of methyl bromide distributions, *Journal of Geophysical Research: Atmospheres*, **103**(D13), doi:10.1029/98JD00970.

Leedham Elvidge, E. C., Oram, D. E., Laube, J. C., Baker, A. K., Montzka, S. A., Humphrey, S., O'Sullivan, D. A., & Brenninkmeijer, C. A. M. (2015). Increasing concentrations of dichloromethane, CH_2Cl_2, inferred from CARIBIC air samples collected 1998-2012, *Atmospheric Chemistry and Physics*, **15**, 1939-1958. doi:10.5194/acp-15-1939-2015.

Lefèvre, F., Brasseur, G. P., Folkins, I., Smith, A. K., & Simon, P. (1994). Chemistry of the 1991-1992 stratospheric winter: Three-dimensional model simulations, *Journal of Geophysical Research: Atmospheres*, **99**, doi:10.1029/93JD03476.

Levine, J. G., Braesicke, P., Harris, N. R. P., Savage, N. H., & Pyle, J. A. (2007). Pathways and timescales for troposphere-to-stratosphere transport via the tropical tropopause layer and their relevance for very short lived substances, *Journal of Geophysical Research: Atmospheres*, **112**, doi:10.1029/2005JD006940.

Li, M., Karu, E., Brenninkmeijer, C., Fischer, H., Lelieveld, J., & Williams, J. (2018). Tropospheric OH and stratospheric OH and Cl concentrations determined from CH_4, CH_3Cl, and SF_6 measurements, *Nature Partner Journals: Climate and Atmospheric Science*, **1**, doi:10.1038/s41612-018-0041-9.

Liang, Q., Atlas, E., Blake, D., Dorf, M., Pfeilsticker, K., & Schauffler, S. (2014). Convective transport of very short lived bromocarbons to the stratosphere, *Atmospheric Chemistry and Physics*, **14**, 5781-5792. doi:10.5194/acp-14-5781-2014.

Lieleveld, J., Gromov, S., Pozzer, A., & Taraborrelli, D. (2016). Global tropospheric hydroxyl distribution, budget and reactivity, *Atmospheric Chemistry and Physics*, **16**, 12477-12493. doi:10.5194/acp-16-12477-2016.

Liu, S. C., Trainer, M., Fehsenfeld, F. C., Parrish, D. D., Williams, E. J., Fahey, D. W., Hübler, G., & Murphy, P. C. (1987). Ozone production in the rural troposphere and the implications for regional and global ozone distributions, *Journal of Geophysical Research*, **92**, 4191-4207. doi:10.1029/JD092iD04p04191.

Lobert, J., Keene, W. C., Logan, J., & Yevich, R. (1999) Global chlorine emissions from boimass burning – Reactive Chlorine Emissions Inventory, *Journal of Geophysical Research*, **104**, 8373-8390. doi:10.1029/1998JD100077.

Lowe, D., & MacKenzie, A. R. (2008). Review of polar stratospheric cloud microphysics and chemistry, *Journal of Atmospheric and Solar-Terrestrial Physics*, **70**, doi:10.1016/j.jastp.2007.09.011.

Malley, C. S., Henze, D. K., Kuylenstierna, C. I., Vallack, H. W., Davila, Y., Anenberg, S. C., Turner, M. C., & Ashmore, M. R. (2017). Updated global estimates of respiratory mortality in adults ≥ 30 years of age attributable to long-term ozone exposure, *Environmental Health Perspectives*, **125**, doi:10.1289/EHP1390.

Manney, G. L., Santee, M. L., Rex, M., Livesey, N. J., Pitts, M. C., Veefkind, P., et al. (2011). Unprecedented Arctic ozone loss in 2011, *Nature*, **478**, 469-475. doi:10.1038/nature10556.

Matsumi, Y., & Kawasaki, M. (2003). Photolysis of atmospheric ozone in the ultraviolet region, *Chemical Reviews*, **103**, 4767-4782. doi:10.1021/cr0205255.

McCulloch, A. (2003). Chloroform in the environment: occurrence, sources, sinks and effects, *Chemosphere*, **50**, 1291-1308. doi:10.1016/S0045-6535(02)00697.5.

McCulloch, A. Aucott, M. L., Benkovitz, C. M., Graedel, T. E., Kleiman, G., & Midgley, M. (1999). Global emissions of hydrogen chloride and chloromethane from coal combustion, incineration and industrial activities: reactive chlorine emissions inventory, *Journal of Geophysical Research*, **104**, 8391-8403. doi:10.1029/1999JD900025.

McCulloch, A., & Midgley, P. M. (1996). The production and global distribution of emissions of trichloroethene, tetrachloroethene and dichloromethane over the period 1988-1992, *Atmospheric Environment*, **30**, 601-608. doi:10.1016/1352-2310(09)50032-5.

McElroy, M. B., Salawitch, R. J., Wofsy, S. C., & Logan, J. A. (1986). Reductions of Antarctic ozone due to synergistic interactions of chlorine and bromine, *Nature*, **321**, 759-762. doi:10.1038/321759a0.

McNorton, J., Wilson, C., Gloor, M., Parker, R. J., Boesch, H., Feng, W., Hossaini, R., & Chipperfield, M. P. (2018). Attribution of recent increases in atmospheric methane through 3-D inverse modelling, *Atmospheric Chemistry and Physics*, **18**, 18149-18168. doi:10.5194/acp-18-18149-2018.

McPeters, R. D., & Labow, G. J. (1996). An assessment of the accuracy of 14.5 years of Nimbus 7 TOMS version 7 ozone data by comparison with the Dobson network, *Geophysical Research Letters*, **23** (25), 3695-3698. doi:10.1029/96GL03539.

METI (2012). *Monthly report of chemical industry statistics*. Tokyo: Ministry of Economy, Trade and Industry. [online] Available at: https://www.meti.go.jp/statistics/tyo/seidou/result/gaiyo/resourceData/02_kagaku/kakuho/h2dbb201205k.pdf [Accessed 27 August 2020]

Molina, L. T., & Molina, M. J. (1987). Production of Cl_2O_2 from the self-reaction of the ClO radical, *Journal of Physical Chemistry*, **91**, 433-436. doi:10.1021/j100286a035.

Molina, M. J., & Rowland, F. S. (1974). Stratospheric sink for chlorofluoromethanes: chlorine atom-catalysed destruction of ozone, *Nature*, **249**, 810-812. doi:10.1038/249810a0.

Monks, P. S. (2005). Gas-phase radical chemistry in the troposphere, *Chemical Society Reviews*, **34**, 376-395. doi:10.1039/b307982c.

Monks, S. A., Arnold, S. R., Hollaway, M. J., Pope, R. J., Wilson, C., Feng, W., et al. (2017). The TOMCAT global chemical transport model v1.6: description of chemical mechanism and model evaluation, *Geoscientific Model Development*, **10**, 3015-3057. doi:10.5194/gmd-2016-212

Montzka, S. A., Dutton, G. S., Yu, P., Ray, E., Portmann, R. W., Daniel, J. S., et al. (2018). An unexpected and persistent increase in global emissions of ozone-depleting CFC-11, *Nature*, **557**, 413-417. doi:10.1038/s41586-018-0106-2.

Montzka, S. A., Krol, M., Dlugokencky, E., Hall, B., Jöckel, P., & Lelieveld, J. (2011). Small interannual variability of global atmospheric hydroxyl, *Science*, **331**, 67-69. doi:10.1126/science.1197640.

Montzka, S. A., Reimann, S., Engel, A., Kruger, K., O'Doherty, S., Sturges,W. T., et al. (2011). Ozone-depleting substances (ODSs) and related chemicals. In *Scientific assessment of ozone depletion: 2010, global ozone research and monitoring project-Report No.* 52*, World Meteorological Organization*, Geneva, Switzerland.

Moore, R. M. (2004). Dichloromethane in North Atlantic waters, *Journal of Geophysical Research*, **109**, C09004. doi:10.1029/2004JC002397.

Moore, R. M., Webb, M., Tokarczyk, R., & Wever, R. (1996). Bromoperoxidase and iodoperoxidase enzymes and production of halogenated methanes in marine diatom cultures, *Journal of Geophysical Research: Oceans*, **101**, doi:10.1029/96JC01248.

Mühle, J., Lueker, T. J., Su, Y., Miller, B. R., Prather, K. A., & Weiss, R. F. (2007). Trace gas and particulate emissions from the 2003 southern California wildfires, *Journal of Geophysical Research*, **112**, D03307. doi:10.1029/2006JD007350.

Mühle, J., Trudinger, C. M., Western, L.M., Rigby, M., Vollmer, M. K., Park, S. Manning, A. J., et al. (2019). Perfluorocyclobutane (PFC-318, c-C4F8) in the global atmosphere, *Atmospheric Chemistry and Physics*, **19**(15), 10335-10359. doi:10.5194/acp-19-10335-2019.

Navarro, M. A., Atlas, E. L., Saiz-Lopez, A., Rodriguez-Lloveras, X., Kinnison, D. E., Lamarque, J.-F., et al. (2015). Airborne measurements of organic bromine compounds in the Pacific tropical tropopause layer, *Proceedings of the National Academy of Sciences of the United States of America*, **112**(45), doi:10.1073/pnas.1511463112.

National Toxicology Program (2011). *Report on carcinogens, twelfth edition, dichloromethane*. Research Triangle Park, NC: National Toxicology Program, Department of Health and Human Services, Public Health Service. [online] Available at:

https://ntp.niehs.nih.gov/ntp/roc/content/profiles/dichloromethane.pdf [Accessed 27 August 2020]

O'Doherty, S., Simmonds, P. G., Cunnold, D. M., Wang, H. J., Sturrock, G. A., Fraser, P. J., et al. (2001). In situ chloroform measurements at Advanced Atmospheric Gases Experiment atmospheric research stations from 1994 to 1998, *Journal of Geophysical Research: Atmospheres*, **106**, doi:10.1029/2000JD900792.

OECD SIDS (2011). *Dichloromethane. SIDS initial assessment profile.* Paris, France: Organisation for Economic Co-operation and Development screening information dataset. [online] Available at: http://webnet.oecd.org/hpv/UI/handler.axd?id=B8EA971C-0C2C4976-8706-A9A68033DAA0 [Accessed 27 August 2020]

Ooki, A., & Yokouchi, Y. (2011). Dichloromethane in the Indian Ocean: Evidence for in-situ production in seawater, *Marine Chemistry*, **124**(1-4), 119-124. doi:10.1016/j.marchem.2011.01.001.

Oram, D. E., Ashfold, M. J., Laube, J. C., Gooch, L. J., Humphrey, S., Sturges, W. T., et al. (2017). A growing threat to the ozone layer from short-lived anthropogenic chlorocarbons, *Atmospheric Chemistry and Physics*, **17**(19), 11,929-11,941. doi:10.5194/acp-17-11929-2017.

Orbe, C., Waugh, D.W, & Newman, P. A., (2015). Air-mass origin in the tropical lower stratosphere: The influence of Asian boundary layer air, *Geophysical Research Letters*, **42** (10). 4240-4248. doi:10.1002/2015gl063937.

Orbe, C., Waugh, D. W., Newman, P. A., & Steenrod, S., (2016). The transit-time distribution from the Northern Hemisphere midlatitude surface, *Journal of Atmospheric Science*, **73**(10), 3785-3802. doi:10.1175/JAS-D-15-0289.1.

Orce, V. L., & Helbling, E. W. (1997). Latitudinal UVR-PAR measurements in Argentine, *Global and Planetary Change*, **15**(3), doi:10.1016/S0921-8181(97)00007-6.

Pan, L. L., Altas, E. L., Salawitch, R J, Honomichl, S B, Bresch, J F, Randel, W J, Apel, E C, & Hornbrook, R S., (2017). The Convective Transport of Active

Species in the Tropics (CONTRAST) experiment, *Bulletin of the American Meteorological Society*, **98**, 106-128. doi:10.1175/BAMS-D-14-00272.1.

Pandis, S. N., Wexler, A. S., & Seinfeld, J. H. (1995). Dynamics of tropospheric aerosols, *Journal of Physical Chemistry*, **99**, 9646-9659. doi:10.1021/j100024a003.

Patra, P. K., Houweling, S., Krol, M., Bousquet, P., Belikov, D., Bergmann, D., et al. (2011). TransCom model simulations of CH_4 and related species: linking transport, surface flux and chemical loss with CH_4 variability in the troposphere and lower stratosphere, *Atmospheric Chemistry and Physics*, **11**, 12813-12837. doi:10.5194/acp-11-12813-2011.

Pawson, S., Steinbrecht, W., Charlton-Perez, A. J., Fujiwara, M., Karpechko, A. Y., Petropavlovskikh, I., Urban, J. & Weber, M. (2014). Update on global ozone: Past, present, and future. Chapter 2 In *Scientific assessment of ozone depletion: 2014, global ozone research and monitoring project-Report No. 55, World Meteorological Organization,* Geneva, Switzerland.

Pétron, G., Granier, C., Khattatov, B., Lamarque, J.-F., Yudin, V., Müller, J.-F., & Gille, J. (2002). Inverse modelling of carbon monoxide surface emissions using Climate Monitoring and Diagnostics Laboratory network observations, *Journal of Geophysical Research,* **107**(D24), 4761. doi:10.1029/2001JD001305.

Pisso, I., Haynes, P. H., & Law, K. S. (2010). Emission location dependent ozone depletion potentials for very short-lived halogenated species, *Atmospheric Chemistry and Physics*, **10**, 12025-12036. doi:10.5194/acp-10-12025-2010.

Platt, U., Allan, W., & Lowe, D. (2004). Hemispheric average Cl atom concentration from $^{13}C/^{12}C$ ratios in atmospheric methane, *Atmospheric Chemistry and Physics*, **4**, 2393-2399. doi:10.5194/acp-4-2393-2004.

Portmann, R. W., Daniel, J. S., & Ravishankra, A. R. (2012). Stratospheric ozone depletion due to nitrous oxide: influence of other gases, *Philosophical Transactions of the Royal Society B*, **367**, 1256-1264. doi:10.1098/rstb.2011.0377.

Prinn, R. G., Huang, J., Weiss, R. F., Cunnold, D. M., Fraser, P. J., Simmonds, P. G., et al. (2005). Evidence for variability of atmospheric hydroxyl radicals over the past quarter century, *Geophysical Research Letters*, **32**, doi:10.1029/2004GL022228.

Prinn, R. G., Weiss, R. F., Arduini, J., Arnold, T., DeWitt, H. L., Fraser, P. J. et al. (2018). History of chemically and radiatively important atmospheric gases from the Advanced Global Atmospheric Gases Experiment (AGAGE), *Earth System Science Data Discussions*, **10**, doi:10.5194/essd-10-985-2018.

Quack, B., & Wallace, D. W. R. (2003). Air-sea flux of bromoform: Controls, rates, and implications. *Global Biogeochemical Cycles*, **17**(1), 1023. doi:10.1029/2002GB001890.

Ravishankara, A. R. (1988). Kinetics of radical reactions in the atmospheric oxidation of CH4, *Annual Review of Physical Chemistry*, **39**, 367-394. doi:10.1146/annurev.pc.39.100188.002055.

Ren, X., Olson, J. R., Crawford, J. H., Brune, W. H., Mao, J., Long, R. B., et al. (2008). HOx chemistry during INTEXT-A 2004: Observation, model calculation, and comparison with previous studies, *Journal of Geophysical Research: Atmosphere*, **113** (D5). doi:10.1029/2007JD009166.

Rigby, M., Prinn, R. G., O'Doherty, S., Montzka, S. A., McCulloch, A., Harth, C. M., et al. (2013). Re-evaluation of the lifetimes of the major CFCs and CH_3CCl_3 using atmospheric trends, *Atmospheric Chemistry and Physics*, **13**, 2691-2702. doi:10.5194/acp-13-2691-2013.

Rood, R. B., Allen, D. J., Baker, W. E., Lamich, D. J., & Kaye, J. A. (1989). The use of assimilated stratospheric data in constituent transport calculations, *Journal of Atmospheric Science*, **46**, 687-701. doi:10.1175/1520-0469(1989)046<0687:TUOASD>2.0.CO;2.

Rudolph, J., Koppmann, R., & Plass-Dülmer, C. (1996). The budgets of ethane and tetrachloroethene: Is there evidence for an impact of reactions with chlorine atoms in the troposphere?, *Atmospheric Environment*, **33**, 1887-1894. doi:10.1016/1352-2310(95)00385-1.

Saiz Lopez, A., & von Glasow, R. (2012). Reactive halogen chemistry in the troposphere, *Chemical Society Reviews*, **41**, 6448-6472. doi:10.1039/C2CS35208G.

Salawitch, R. J., Fahey, D. W., Hegglin, M. I., McBride, L. A., Tribett, W. R., & Doherty, S. J. (2018). Twenty questions and answers about the ozone layer: 2018 update, *Scientific Assessment of Ozone Depletion: 2018, global ozone research and monitoring project – Report No. 58, World Meteorological Organization,* Geneva, Switzerland.

Salawitch, R. J., Weisenstein, D. K., Kovalenko, L. J., Sioris, C. E., Wennberg, P. O., Chance, K., Ko, M. K. W., & McLinden, C. A. (2005). Sensitivity of ozone to bromine in the lower stratosphere, *Geophysical Research Letters*, **32**(5), L05811. doi:10.1029/2004GL021504.

Savage, N. H., Law, K. S., Pyle, J. A., Richter, A., Nüß, H., & Burrows, J. P. (2004). Using GOME NO2 satellite data to examine regional differences in TOMCAT model performance, *Atmospheric Chemistry and Physics*, **4**, 1895-1912. doi:10.5194/acp-4-1895-2004.

Say, D., Ganesan, A. L., Lunt, M. F., Rigby, M., O'Doherty, S., Harth, C., et al. (2019). Emissions of halocarbons from India referred through atmospheric measurements, *Atmospheric Chemistry and Physics*, **19**, 9865-9885. doi:10.5194/acp-19-9865-2019.

Schuck, T. J., Lefrancois, F., Gallmann, F., Wang, D., Jesswein, M., Hoker, J., Bonisch, H., & Engel, A. (2018). Halocarbons at Taunus Observatory, *Atmospheric Chemistry and Physics*, **18**, 16553-16569. doi:10.5194/acp-18-16553-2018.

Shao, M., Huang, D., Gu, D., Lu, S., Chang, C., & Wang, J.-L. (2011). Estimate of anthropogenic halocarbon emission based on measured ratio relative to CO in the Peal River Delta region, China, *Atmospheric Chemistry and Physics*, **11**(26), doi:10.5194/acp-11-5011-2011.

Shepherd, T. G. (2008). Dynamics, stratospheric ozone, and climate change, *Atmopshere-Ocean*, **46**(1), 117-138. doi:10.3137/ao.460106.

Sherwen, T., Schmidt, J. A., Evans, M. J., Carpenter, L. J., Großmann, K., Eastham, S. D., et al. (2016). Global impacts of tropospheric halogens (Cl, Br, I) on oxidants and composition in GEOS-Chem, *Atmospheric Chemistry and Physics*, **16**, 12239-12271. doi:10.5194/acp-16-12239-2016.

Simmonds, P. G., Manning., A. J., Cunnold, D. M., McCulloch, A., O'Doherty, S., Derwent, R. G., et al., (2006). Global trends, seasonal cycles, and European emissions of dichloromethane, trichloroethene, and tetrachloroethene from the AGAGE observations at Mace Head, Ireland, and Cape Grim, Tasmania, *Journal of Geophysical Research*, **111**, D18304. doi:10.1029/2006JD007082.

Simpson, I. J., Meinardi, S., Blake, N. J., Rowland, F. S., & Blake, D. R. (2004). Long-term decrease in the global atmospheric burden of tetrachloroethene (C_2Cl_4), *Geophysical. Research Letters*, **31**, L08108. doi:10.1029/2003GL019351.

Simpson, I. J., Akagi, S. K., Barletta, B., Blake, N. J., Choi, Y., Diskin, G. S., et al., (2011). Boreal forest fire emissions in fresh Canadian smoke plumes: C_1-C_{10} volatile organic compounds (VOCs), CO_2, CO, NO_2, NO, HCN and CH_3CN, *Atmospheric Chemistry and Physics*, **11**, 6445-6463. doi:10.5194/acp-11-6445-2011.

Singleton, C. S., Randall, C. E., Harvey, V. L., Chipperfield, M. P., Feng, W., Manney, G. L., et al. (2007). Quantifying Arctic ozone loss during the 2004-2005 winter using satellite observations and a chemical transport model, *Journal of Geophysical Research*, **112**, D07304. doi:10.1029/2006JD007463.

Sinnhuber, B.-M., Sheode, N., Sinnhuber, M., Chipperfield, M. P., & Feng, W. (2009). The contribution of anthropogenic bromine emissions to past stratospheric ozone trends: a modelling study, *Atmospheric Chemistry and Physics*, **9**, 2863-2871. doi:10.5194/acp-9-2863-2009.

Sivasakthivel, T., & Reddy, K. K. S. K. (2011). Ozone layer depletion and its effects: A review, *International Journal of Environmental Science and Development*, **2**, doi:10.7763/IJESD.2011.V2.93.Solomon, S. (1999). Stratospheric ozone depletion: A review of concepts and history, *Reviews of Geophysics*, **37**, doi:10.1029/1999RG900008.

Solomon, S., & Albritton, D. L. (1992). Time-dependent ozone depletion potentials for short- and long-term forecasts, *Nature*, **357**, 33-37. doi:10.1038/357033a0.

Solomon, S., Garcia, R., Rowland, F. S., & Wuebbles, D. J. (1986). On the depletion of Antarctic ozone, *Nature*, **321**, 755-758. doi:10.1038/321755a0.

Spivakovsky, C. M., Logan, J. A., Montzka, S. A., Balkanski, Y. J., Foreman-Fowler, M., Jones, D. B. A., et al. (2000). Three-dimensional climatological distribution of tropospheric OH: Update and evaluation, *Journal of Geophysical Research*, **105**, 8931-8980. doi:10.1029/1999JD901006.

Steinbrecht, W., Hegglin, M. I., Harris, N. R. P., & Weber, M. (2018). Is global ozone recovering?, *Comptes Rendus Geoscience*, **350**, 368-375. doi:10.1016/j.crte.2018.07.012.

Stolarski, R. S., & Cicerone, R. J. (1974). Stratospheric chlorine: a possible sink for ozone, *Canadian Journal of Chemistry*, **52**, 1610-1615. doi:10.1139/v74-233.

Sturges, W., Oram, D., Carpenter, L., Penkett, S., & Engel, A. (2000). Bromoform as a source of stratospheric bromine, *Geophysical Research Letters*, **27**(14), 2081-2084. doi:10.1029/2000GL011444.

Tarantola, A., & Valette, B. (1982). Generalized nonlinear inverse problems solved using the least squares criterion, *Reviews of Geophysics*, **20**, 219-232. doi:10.1029/RG020i002p00219.

Tegtmeier, S., Krüger, K., Quack, B., Atlas, E., Blake, D. R., Boenisch, H., et al. (2013). The contribution of oceanic methyl iodide to stratospheric iodine, *Atmospheric Chemistry and Physics*, **13**, 11869-11886. doi:10.5194/acp-13-11869-2013.

Tiedtke, M. (1989). A comprehensive mass flux scheme for cumulus parameterization in large-scale models, *Monthly Weather Review*, **117**, 1779-1800. doi:10.0.1175/1520-0493(1989)117<1779:ACMFSF>2.0.CO;2.

Trudinger, C. M., Etheridge, D. M., Sturrock, G. A., Fraser, P. J., Krummel, P. B., & McCulloch, A. (2004). Atmospheric histories of halocarbons from analysis

of Antarctic firn air: Methyl bromide, methyl chloride, chloroform and dichloromethane, *Journal of Geophysical Research*, **109**, doi:10.1029/2004JD004932.

Tsai, W. T., (2017). Fate of Chloromethanes in the Atmospheric Environment: Implications for Human Health, Ozone Formation and Depletion, and Global Warming Impacts, *Toxics*, **5**(4), 23. doi:10.3390/toxics5040023.

Tuazon, E. C., Atkinson, R., Aschmann, S. M., Goodman, M. A. & Winer, A. M. (1988). Atmospheric reactions of chloroethenes with the OH radical, *International Journal of Chemical Kinetics,* **20**, 241-265. doi:10.1002/kin.550200305.

Turner, A. J., Fung, I., Naik, V., Horowitz, L. W., & Cohen, R. C. (2018). Modulation of hydroxyl variability by ENSO in the absence of external forcing, *Proceedings of the National Academy of Sciences*, **115**, 8931-8936. doi:10.1073/pnas.1807532115.

Vautard, R., Builtjes, P. H. J., Thunis, P., Cuvelier, C., Bedogni, M., Bessagnet, B., et al. (2007). Evaluation and intercomparison of ozone and PM10 simulations by several chemistry transport models over four European cities within the CityDelta project, *Atmospheric Environment*, **41**, 173-188. doi:10.1016/j.atmosenv.2006.07.039.

von Clarmann, T. (2013). Chlorine in the stratosphere, *Atmósfera*, **26**(3), 415-458. doi:10.1016/S0187-6236(13)71086-5.

Wales, P. A., Salawitch, R. J., Nicely, J. M., Anderson, D. C., Canty, T. P., Baidar, S., et al. (2018). Stratospheric injection of brominated very short-lived substances: Aircraft observations in the Western Pacific and representation in global models. *Journal of Geophysical Research: Atmospheres,* **123**, 5690-5719. doi:10.1029/2017JD027978.

Wang, C., Shao, M., Huang, D., Lu, S., Zeng, L., Hu, M., & Zhang, Q. (2014). Estimating halocarbon emissions using measured ratio relative to tracers in China, *Atmospheric Environment*, **89**, 816-826. doi:10.1016/j.atmosenv.2014.03.025.

Wang, J. S., Kawa, S. R., Collatz, G. J., Sasakawa, M., Gatti, L. V., Machida, T., et al. (2018). A global synthesis inversion analysis of recent variable in CO_2 fluxes using GOSAT and in situ observations, *Atmospheric Chemistry and Physics*, **18**, 11097-11124. doi:10.5194/acp-18-11097-2018.

Wang, X., Jacob, D. J., Eastham, S. D., Sulprizio, M. P., Zhu, L., Chen, Q., et al. (2019). The role of chlorine in global tropospheric chemistry, *Atmospheric Chemistry and Physics*, **19**, doi:10.5194/acp-19-3981-2019.

WHO (1994). *Chloroform.* Environmental Health Criteria No. 163. Geneva: International Programme on Chemical Safety, World Health Organization.

WHO (1996). *Methylene chloride.* Environmental Health Criteria No. 164, 2nd ed. Geneva: International Programme on Chemical Safety, World Health Organization.

World Meteorological Organization (1998). Frequently asked questions about ozone In *Scientific assessment of ozone depletion: 1998, WMO global ozone research and monitoring project – Report No. 44*, Geneva, Switzerland.

World Meteorological Organization (2018). Executive Summary, *Scientific Assessment of Ozone Depletion: 2018, World Meteorological Organization, Global Ozone Research and Monitoring Project – Report No. 58,* Geneva, Switzerland.

Worton, D. R., Sturges, W. T., Schwander, J., Mulvaney, R., Barnola, J.-M., & Chappellaz J. (2006). 20th century trends and budget implications of chloroform and related tri-and dihalomethanes inferred from firn air, *Atmospheric Chemistry and Physics*, **6**, doi:10.5194/acp-6-2847-2006.

Wright, J. S., Fu, R., Fueglistaler, S., Liu, Y. S., & Zhang, Y. (2011). The influence of summertime convection over Southeast Asia on water vapor in the tropical stratosphere, *Journal of Geophysical Research*, **116**(D12), D12302. doi:10.1029/2010JD015416.

Wuebbles, D. J. (1981). *The relative efficiency of a number of halocarbons for destroying stratospheric ozone, (Report UCID-1824)*. Lawrence Livermore National Laboratory.

Wuebbles, D. J. (1983). Chlorocarbon emission scenarios: potential impact on stratospheric ozone, *Journal of Geophysical Research,* **88**, 1433-1443. doi:10.1029/JC088iC02p01433.

Wuebbles, D. J., Jain, A. K., Patten, K. O., & Connell, P. S. (1998). Evaluation of ozone depletion potentials for chlorobromomethane (CH_2C1Br) and 1-bromo propane (C_3H_7Br), *Atmospheric Environment*, **32**, 107-114. doi:10.1016/S1352-2310(97)00322-1.

Wuebbles, D. J., Patten, K. O., Wang, D., Youn, D., Martínez-Avilés, M., & Francisco, J. S., (2011). Three-dimensional model evaluation of the ozone depletion potentials for n-propyl bromide, trichloroethylene and perchloroethylene, *Atmospheric Chemistry and Physics.*, **11**, 2371-2380. doi:10.5194/acp-11-2371-2011.

Xiang, B., Patra, P. K., Montzka, S. A., Miller, S. M., Elkins, J. W., Moore, F. L., et al. (2014). Global emissions of refrigerants HCFC-22 and HFC-134a: Unforeseen seasonal contributions, *Proceeding of the National Academy of Sciences of the United States of America*, **111**, 17379-17384. doi:10.1073/pnas.1417372111.

Xiao, X. (2008). *Optimal Estimation of the Surface Fluxes of Chloromethanes Using a 3-D Global Atmospheric Chemical Transport Model* (Doctoral dissertation). Cambridge, Massachusetts, USA: Massachusetts Institute of Technology. [online] Available at: https://globalchange.mit.edu/sites/default/files/Xiao_PhD_08.pdf [Accessed 2 September 2020]

Yang, X., Cox, R. A., Warwick, N. J., Pyle, J. A., Carver, G. D., O'Connor, F. M., & Savage, N. H. (2005). Tropospheric bromine chemistry and its impacts on ozone: A model study, *Journal of Geophysical Research*, **110**, doi:10.1029/2005JD006244.

Yin, Y., Chevallier, F., Ciais, P., Broquet, G., Fortems-Cheiney, A., Pison, I., & Saunois, M. (2015). Decadal trends in global CO emissions as seen by MOPITT, *Atmospheric Chemistry and Physics,* **15**, 13433-13451. doi:10.5194/acp-15-13433-2015.

Yung, Y. L., Pinto, J. P., Watson, R. T., & Sander, S. P. (1980). Atmospheric bromine and ozone perturbations in the lower stratosphere, *Journal of the Atmospheric Sciences*, **37**, 339-353. doi:10.1175/1520-0469(1980)037<0339:ABAOPI>2.0.CO;2.

Zhao, Y., Saunois, M., Bousquet, P., Lin, X., Berchet, A., Hegglin, M. I., et al. (2019). Inter-model comparison of global hydroxyl radical (OH) distributions and their impact on atmospheric methane over the 2000-2016 period, *Atmospheric Chemistry and Physics*, **19**, 13701-13723. doi.org:10.5194/acp-19-13701-2019.

Ziska, F., Quack, B., Abrahamsson, K., Archer, S. D., Atlas, E., Bell, T., et al. (2013). Global sea-to-air flux climatology for bromoform, dibromomethane and methyl iodide. *Atmospheric Chemistry and Physics*, **13**(17), 8915-8934. doi:10.5194/acp-13-8915-2013.

Ziska, F., Quack, B., Tegtmeier, S., Stemmler, I., Krüger, K. (2017). Future emissions of marine halogenated very-short lived substances under climate change, *Journal of Atmospheric Chemistry*, **74**, 245-260. doi:10.1007/s10874-016-9355-3.